The use of china clay waste as a construction material using alkali-activated cement technology

Zografou, Adamantia

Award date:
2015

Awarding institution:
University of Bath

THE USE OF CHINA CLAY WASTE AS A CONSTRUCTION MATERIAL USING ALKALI-ACTIVATED CEMENT TECHNOLOGY

By Adamantia-Ioanna Zografou

A thesis submitted for the degree of
Doctor of Philosophy to the
University of Bath

University of Bath
Faculty of Engineering and Design
Department of Architecture and Civil Engineering

November 2015

Acknowledgements

Many thanks to BRE Trust for funding this research. Thanks also to Imerys and Aggregate Industries in Cornwall for the time, materials, valuable comments and provision of data.

The author would like to thank Professor Pete Walker for the supervision and for the opportunity he gave me when choosing me to do this PhD. Dr.Susan Bernal from the University of Sheffield is acknowledged for the invaluable input she offered during the first stages of this research.

For being able to complete this thesis, the author owns special thanks to Professor Andrew Heath, not only for the constant scientific input he offered but also for being encouraging and supportive in difficult times.

The author would like to thank Elena and David for making my life in Bath so much better. Last, many thanks to my family and especially to my mum and dad for being the greatest supporters and bringing joy in my life.

Note: The PhD topic lies in an interdisciplinary area. To ensure a successful completion, many people were contacted either for advice or practical help: Dr. John Mitchels, Mr. Harry Bone, Dr.Vasilios Bellas (University of Bristol), Prof.Ioanna Papayianni (Aristotle University of Thessaloniki), Jeremy Hooper (Imerys), professionals from Tatasteel Strip UK, SSE and Generation Aggregates, Dr. Ivana Perná (Institute of Rock Structures and Mechanics, Prague), Dr. Asel Sartbaeva, Dr. Yiannis Pontikes (KU Leuven), Dr. Fernando Pacheco-Torgal (University of Minho), not including suppliers of materials and equipment and the contribution of all the technicians.

Abstract

Every 1 t of china clay produced in the UK generates 9 t of waste material. A limited quantity of the coarser waste has beneficial use as a building stone or secondary aggregate in concrete and asphalt, but there are currently limited uses for the finest waste fraction. 'Mica' waste is a mixture of fine minerals and is one of the forms of waste with little beneficial use other than the restoration of old quarries. Looking for innovative solutions for the needs of a new Eco-town in the UK and with an aim to find new commercially viable and low environmental impact uses in construction, this PhD introduces the idea of using the china clay waste in alkali-activated binders. First, it was investigated whether the contained mica mineral could be used as an alkali-activated binder. This was done using different MAS NMR and XRD analysis, and mechanical strength tests based on European standards. The material was shown to have low reactivity and some direct trials of alkali-activation of thermally treated mica mineral produced in average weak binders. Later, three series of alkali-activated binders were studied, one based on Ground Granulated Blastfurnace Slag (GGBS), one based on Fly Ash (FA) and one based on a 50%GGBS-50%FA blend (50/50). The china clay waste was incorporated in selected optimum binders from the three series as aggregate to make mortars and concrete. Compared to control specimens, the test specimens using the china clay waste always showed lower strength. It is suggested that the high water demand of the waste is the main problem.

When the waste was used in mortars, the impact of the water declined over time, with sand waste from china clay extraction showing approximately equivalent strength to the control silica based mortar after 6 months of curing for the GGBS and 50/50 series. For the same series, mica-waste specimens gave about 50% of the strength of the control mortar on the 7th day of curing but increased to 70-80% of the control compressive strength at 6 months. In the FA series, the impact of additional water resulted in very low strengths and that series did not proceed in concrete making.

The concrete design was accompanied by an environmental analysis to ensure environmentally beneficial outcomes were obtained. Testing in compression shows a similar decreasing strength for the Portland and the alkali-activated series for increasing amounts of waste used. However, the test specimens of the GGBS series showed potential for replacing Portland control specimens. The potential for making blocks and tiles using the new concrete would be greater if the mix design is optimized. Durability testing will be required on an optimized design and final product, but initial analysis of test results and the literature indicate this is unlikely to be a concern. Not using the final product to run durability tests would lead to arbitrary conclusions. The environmental analysis shows that although the carbon emissions would be reduced using alkali-activated concrete, most of the other environmental impact categories would be affected negatively which has to be considered when making the final decision on whether to use this new material in the Eco-town or elsewhere.

List of Figures

List of Tables

List of notations

AA	Alkali-activated
AAC	Alkali-activated concrete
AAM	Alkali-activated material
MW	Mica waste
CMW	Calcined mica waste
CCS	China clay sand
SS	Standard sand
GSS	Ground standard sand
FA	Fly ash
GGBS	Ground granulated blastfurnace slag
XRF	X-ray fluorescence
XRD	X-ray diffraction
MAS NMR	Magic angle spinning spectroscopy Nuclear magnetic resonance
SEM	Scanning electron microscopy
EDX	Energy dispersive X-ray spectroscopy
GWP	Global warming potential

Table of Contents

Chapter 1: **Introduction**

This chapter introduces the waste from the production of china clay in the South West of England and reveals the reasons for investigating the potential of the china clay waste as a building material. Alternative uses considered are developed together with the drivers of the research. The aims and the structure of the thesis are presented at the end of the chapter.

1.1 Types of waste used and general information

China clay is a commercial term for kaolin, and the name was derived from its origin in China (Christie et al., 2007). Currently the operations of china clay extraction in the UK which exist in Cornwall and Devon, leave a mark in the landscape (Thurlow, 2005, BGS, 2009). A pit at the area of Cornwall is shown in Figure 1. The extraction of every tonne of china clay in the UK generates nine tonnes of by-product (Thurlow, 2005). The by-product has three main forms which are described in more detail in Chapter 3:

- Stent is coarse, unaltered granite and its diameter can reach up to 2m. It is composed of the common minerals of granite, mostly of quartz and micas.
- Coarse sand derives from the same rock. Its fragmented form is a result of weathering and mechanical crushing (Figure 2).
- "*Mica*" is the finest fraction of the waste with maximum particle size just over 0.5mm. Surprisingly with its name, this product does not comprise pure mica but it is fine sand which contains mica flakes and this is discussed in more detail later. To avoid confusion, the mica waste in this study is referred to as MW to distinct it from mica as mineral.

Quantitatively the current waste streams are comprised approximately of 50% stent, 39% sand and 11% MW (Thurlow, 2005). Less than 20% of the live feed production of stent and coarse sand is sold to commercial enterprises who use it as 'secondary aggregates'. These aggregates are used in ready-mixed concrete, in asphalt bases and binder courses, in precast concrete products and as plain aggregates for fills, capping, in hydraulically bound and unbound mixtures (WRAP, 2004). The existing applications are described in detail later in Chapter 2. The remaining 80% of the waste, together with material that is rejected from the production of secondary aggregates, is stored in stockpiles and later used for landscape restoration of old quarries. Finding new uses for stent and coarse sand would add value as a higher percentage of waste would be reused and the costs, environmental impacts and visual intrusion from the stockpiles could be minimised.

MW, which is transported as a slurry, is stored separately in MW dams (see Figure 3), as it could be unstable if placed on the stockpiles. There is currently no secondary use for the MW; therefore, this product is destined only for landscape restoration (filling in the closed quarries). The research had a special focus on this type of waste, as it was considered possible that, apart from fine aggregate, it could be used as a cementitious binder component for the reasons explained later in this chapter.

Figure 1 Littlejohn's quarry in Cornwall.

Figure 2 Coarse sand transported by conveyors to tips.

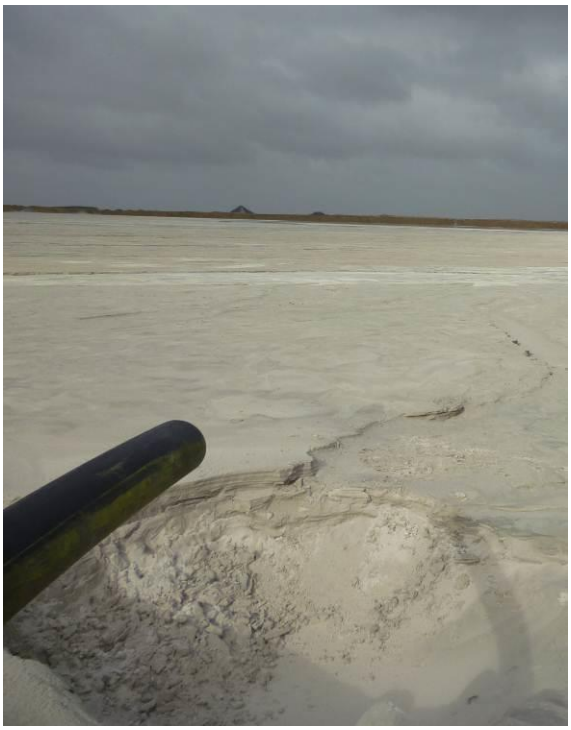

Figure 3 MW dam/ lagoon.

1.2 Background of the research

This PhD was funded by the BRE Trust and was part of the consultation provided by BRE for the construction of a new eco-town in Cornwall, as part of a government-sponsored programme for the development of new towns. The intention was to create a number of eco-towns around the UK where both the economic and environmental sustainability of the towns was of the highest possible standards.

To this direction a number of former China Clay mining sites were considered to have the potential to deliver eco-communities in accordance with Planning Policy Statement standards and stimulate transformational regeneration within the wider project area, with two sites at Par and West Carclaze/Baal likely to be the subject of planning applications. The land owner and mining company Imerys together with Orascom, a development company which has substantial experience of building sustainable communities around the world, formed Eco-bos the company which designs the project. A hybrid planning application was submitted at the end of February 2011 for the West Carclaze and Baal site (Figure 4 and 5), representing the first phase of the eco-communities project. The submission included a detailed application for a 92-home demonstrator site, but in total about 2000 homes is planned for the site. BRE provided technical support to the project and was engaged with both retrofit and new build projects, together with engendering skills and supply chain to deliver local economic benefits from the major new low carbon development (BRE, 2010a). This coincided with the BRE approaching the University of Bath in early 2011 to conduct research to assist in the development of the eco-town initiative.

"*As part of a wider regeneration and green growth vision for Cornwall the St Austell Clay Country Eco-community aims to build a thriving rural community, with a strong economy and a sustainable restored environment, using restructuring and land restoration of disused clay extraction sites."* (ECO-DEVELOPMENTGROUP, 2012). In other words, the project was intended to take advantage of all possible local sources including local construction materials, human resources and skills, and use them in the construction phase.

Currently progress with the Cornwall the eco-town project has halted (BBC, 2012), but this research should provide the technical knowledge to enable the development of sustainable construction materials using local waste materials when the project does eventually commence.

Figure 4 Pilot scheme – the first 50 houses to be built.(BRE, 2010b)

Figure 5 West Carclaze & Baal (BRE, 2010b)

1.3 Development of the research focus

As this research derives from the needs of the Cornish Eco-town which is also intended to be the immediate area for applying the new use of the china clay waste, the focus of the research had to comply with the eco-community values and therefore, seek innovative, low impact applications in construction. It should be added that the new uses could also be the region near to the eco-town market. A broader, national market is considered less likely due to high transportation costs, a problem that already sets barriers to the current sale of the secondary aggregates (Thurlow, 2005). The existing applications for secondary aggregate deriving from china clay pits do not make full use of the stent and coarse sand (less than 20% sold as mentioned in section 1.1). Also as the MW has no current market value, there is scope for innovative research and development with this material so that the environmental impact of the eoc-town could be reduced to the minimum possible.

The ideal new application would comply with the following requirements:

- Use large quantities of waste in order to minimise the need to stockpile or landfill.
- Show potential for the MW stream which currently has no use other than backfilling old pits.
- Have consistent performance, although the input waste has variation in mineralogical composition.
- Apply to the Cornish Eco-town (i.e. low environmental impact), to Cornwall and elsewhere in the UK (i.e. cost effective). High levels of processing of the waste before use and high energy processes after manufacture would negatively affect both cost and environmental impact, but may still outweigh the costs and environmental impacts of alternatives.

Using the list above, the criteria in Table 1 were selected to assess potential new applications. Based on discussions with industry experts, this list summarises feasible applications for the waste in the construction industry (other than the current uses), and provides a comparison between them. The potential uses considered were in mineral wool insulation products, in Portland cement (PC) based blocks, tiles and in-situ concrete, and use of all waste in in alkali activated (AA) based blocks, tiles and in-situ concrete. The table also presents an assessesment whether the contribution of a given material is positive, negative or equivalent to the current state-of-art for the different displayed criteria, and if the degree of uncertainty in the judgement made.

Mineral wool, specifically stone wool, is produced when an aluminosilicate rock, often basalt, is melted together with limestone, dolomite or blast furnace slag and then followed by the processing stages of fiberisation, binder application, curing and cooling and product finishing. The raw material is usually coarse (particle diameter larger than 50mm) and may also contain recycled materials or product waste in lumps or briquette form (EIPPCB, 2012). Although basalt and decomposed granite (china clay waste) have

different mineralogical composition (Allaby, 2008), mineral wool could be a possible application as the different waste forms do have different alumina to silica ratios (see Chapter 3) which could enable the waste streams to be blended to produce the desired aluminosilicate ratio. If this approach could be used, then there is potential for the fine MW stream to be used. However, as the goal of insulation is to produce a light-weight product, only small amounts of material will be used which is contrary to the goals listed above. Based on data in the Inventory of Carbon and Energy (Hammond and Jones, 2008) for a wall with two 15mm layers of render/plaster, two layers of 100mm dense concrete block and 130mm of mineral wool cavity insulation (able to meet the current minimum thermal requirements for a house wall in England), only 1.2% of the wall mass will be in the insulation, but approximately 88% of the mass will be in the concrete blocks.

Moreover, the process of producing mineral wool insulation consumes high amount of energy (EIPPCB, 2012), although this could be recovered by reduced energy consumption in the building post occupancy. A report (Flury and Frischknecht, 2012) based on the Ecoinvent (Kellenberger et al., 2007) , life cycle analysis (LCA) database for building materials and processes used in Chapter 6, and advances in the basalt mining industry estimated that 1 kg of rock wool causes 1.01kg CO_2-eq greenhouse gas emissions. Therefore the global warming potential of rock wool is higher than the global warming potential of "unspecified cement", 0.773kg CO_2-eq (see Table 29 and Chapter 6 for details). Moreover, basalt mining and supply used to contribute more than 40% (Flury and Frischknecht, 2012) to the total environmental performance of rock wool but according to the reassessment of Flury and Frischknecht (2012) it has only little contribution. Therefore replacement with MW would not result to major saving in carbon emissions and that, in general, despite the environmental advantage that arises from the reuse of the waste streams, the impact of the mineral wool technology would still be high.

Portland cement concrete applications could be subdivided into mass concreting applications (in-situ concrete) and precast concrete elements (including blocks and tiles). As mentioned earlier, stent and sand are currently used for these applications but the use of MW is currently excluded due to the reasons mentioned in section 2.6.2. Any innovation in applications with Portland cement would rely on using minimum amount of Portland cement in the mixture, in combination with other supplementary cementing materials such as pulverised fly ash and granulated blast furnace slag.

As the coarser secondary aggregates generally meet the requirements for standard aggregates (see section 2.2), there is little scope for innovation as the optimization of concrete mixes with "standard" aggregates has been optimized over many years (Purnell and Black, 2012). Ways of processing the aggregates before use could be considered and compared to those for conventional aggregates, but this is unlikely to result in significant savings as the environmental impact of the aggregates used in concrete is very small when compared to those of other components (Purnell and Black, 2012). Assuming that MW could be used effectively in some way in Portland cement applications, due to its small particle size it would be more likely to be used in unreinforced uses such as concrete blocks, rather than in mass, reinforced load-bearing concrete that generally has

higher demand in strength and for normal mixes the small particle size of aggregate is limited (Teychenné et al., 1997). This is largely because a high fines content in concrete can lead to decreased strengths (Kwan et al., 2014) which is undesirable as an increased binder content would be required for comparable strength, thereby increasing environmental impacts and costs. In terms of environmental impact, it is shown that partial replacement of Portland cement with pulverised fly ash and granulated blast furnace slag can cause significant decrease of the global warming potential for given compressive strength (Yang et al., 2014) with Habert et al. (2011) estimating up to a 50% decrease in CO_2 emissions. However, it is not sure to what extent the demands of energy for prior processing of the waste would counteract this advantage.

Table 1 Potential new applications of china clay waste.

Potential use	**Large amount of material?**	**Potential for MW?**	**Consistent product possible?**	**Potential reduced environmental impact than alternatives?**	**Potential lower cost than alternatives?**
Mineral wool insulation	-	+?	0	0?	0?
PC based blocks/tiles	+	+?	0?	0?	0
In-situ PC based concrete	+	0	-	0?	0
AA based blocks/tiles	+	+?	0?	+?	0?
In-situ AA based concrete	+	0	-	+?	0?
+ = likely to be beneficial 0 = likely to be similar to current technology - = likely to be worse than current technology ? = high degree of uncertainty					

Alkali-activated materials (AAMs) are considered a promising alternative to Portland cement as studies claim it offers up to 70% lower CO_2 emissions (Weil, 2009) (see section 2.4.6), thereby potentially meeting the eco-town requirement for a use with lower environmental impact than current options . The advantage of this technology is that it is based on aluminosilicates and is clinker-free (Davidovits, 2011) as it is largely due to the production of clinker for Portland mixes that the carbon emissions are high (IPCC, 2014) (see section 1.4). Moreover, the fact that aggregates that cannot be used in Portland

cement with the fear of causing local expansion and breakage through alkali-silica reaction, have no restriction to be used in alkali-activated composites (Concrete Institution of Australia, 2011). The presence of aluminosilicates in the china clay waste (see sections 2.1 and 2.5), triggers interest as whether the waste is compatible with this novel form of binder and this concept is explained in section 2.6). As a result of the low carbon emissions of AAMs compared to PC and assuming minimal prior processing of the waste, the contribution of this alternative to the environment is considered positive as noted in Table 1. The logic behind evaluating the use of AA based blocks/tiles and in-situ AA based concrete as for the first three criteria of Table 1 is the same as with the Portland equivalent uses.

While there are numerous other binders which could be used instead of Portland cement in low impact concretes (Gartner, 2004), AAMs are the only potential binder which could utilize the aluminosilicate chemistry of the waste (see Chapters 2 and 3) and potentially produce products which are cost competitive but with lower environmental impact than the currently used Portland cement binders. Based on the Intergovernmental Panel on Climate Change (IPCC) report available at the start of this research (Solomon, 2007), only AAMs and high fly-ash / ground granulated blastfurnace slag (GGBS) content Portland cement blends were considered viable alternatives for minimizing the CO_2 emissions from cement manufacture. In the UK context, it is not currently feasible to use very high fly ash or GGBS contents with Portland cement as there are limited supplies of these materials (Heath et al., 2013). The drivers for more sustaibale cements are discussed more later.

Aggregates deriving from the china clay waste is exempt from the Aggregates Levy (WRAP, 2004) as a measure to favour its reuse. The price of the tax is £2/tonne of aggregate (HMRevenue&Customs, 2015) for 2015/16 (reviewed annually), therefore the savings would be small but they apply to all the listed uses in Table 1. It is not easy to estimate the cost of prior processing of the waste where it applies, as there is not set works it this stage of investigation but again it is assumed that it is not important compared to the overall cost of the technology. Some authors (Davidovits, 1993; Gartner, 2004; McLellan et al., 2011) have stated that depending of the scale, some areas could have cost advantage for production of AAM rather than Portland cement. Moreover, a comparison of cost between CEM I and AA cement concrete in (BFTinternational, 2011) based on prices of 2007, gave high variation in the values due to uncertainties and varying information about the basic mixes considered. The minimum cost of the AA mixes was lower than the minimum cost of CEM I concrete and the maximum cost was higher. Hence there is uncertainty in whether the AAM would have lower cost than Portland cement and in Table 1 it is considered that is likely to be as the current technology.

Based on the above, it was decided that AAM is the most favourable technology to reuse the waste. Because this technology has not been commercially implemented in the UK there is a high level of uncertainty in magnitude of the environmental benefits and the final costs, but experience in Australia has shown that commercial implementation can result in comparable costs but lower environmental impact than with PC based

alternatives (McLellan et al., 2011). While this does provide confidence in the potential benefits, the Australian situation is different to the UK as there is an excess of low cost fly-ash available in Australia (McLellan et al., 2011), while the fly ash supply is becoming increasingly limited in the UK and temperatures are lower which is important for curing of these materials (see Chapter 2). Furthermore, the use of alkaline solution (high pH) (Davidovits, 2011) raises safety issues and from that point of view, manufacturing of alkali-activated products in a plant would be preferable as the environment is more controllable. Although there are current applications of AAM in building and civil infrastructure which are described in Shi et al. (2006) and Provis and van Deventer (2014), the area of AAM is quite recent in terms of research. Also there is limited long-term (20+years) durability data, while the current standards which are designed for Portland cement are not always suitable to characterise geopolymers (Duxson et al., 2007c, Heath et al., 2013). Under this perspective and technical difficulties, the low risk applications as blocks and tiles which incorporate reversibility and low cost of replacement are the most feasible solution that meets all the requirements for this PhD project, and more details on this potential application are provided in the following chapters.

1.4 Aims and objectives

Based on the requirements for the eco-town, the consultation with industry experts and an analysis of potential uses an overall aim and specific objectives for this study were formulated. The overall aim of this research was to investigate possible new and innovative uses for waste from the china clay mining operations in the construction industry. This was focused in the area immediately surrounding the proposed eco-town development and was intended that this fundamental research could be used for the development of sustainable building products for the eco-town and elsewhere in the UK. It would offer an engineering solution to the problem of waste accumulation in the South-West and the environmental impact of construction product manufacture. The results of this PhD will help achieve an economically and environmentally sustainable eco-town in Cornwall.

As indicated in section 1.3, the most appropriate new applications are in the development of materials which could be used in alkali-activated blocks and roof tiles. To fulfil this aim, a number of specific objectives were formulated:

- Determine whether the china clay waste could be used as a binder component in alkali-activated blocks. As this is likely to be the highest value application, this aspect was considered first.
- Determine whether the fine fraction of the waste is suitable for use as a filler of aggregate replacement in alkali-activated binders
- Determine whether all waste streams (MW, sand and stent) could be used in alkali-activated block or roof tiles.

- Quantify the embodied environmental impacts from production of the blocks and determine whether the proposed use does provide environmental benefits in line with the eco-town philosophy.

1.5 Thesis structure

Having introduced the waste and the objectives of this study, Chapter 2 provides a brief review of the literature relating to alkali-activated cement technology. Additional information from the scientific literature is included in later chapters where specific aspects are discussed in depth. There is no distinct section for methodology as the experimental work which starts in Chapter 3 and is completed in Chapter 6 is specific to the particular aspect under investigation. Therefore each chapter contains a section describing the relevant methodology and is based on the information in the previous chapter. Chapter 3 contains a description of the forms of waste and other materials used in the study. This includes their chemical, physical, microstructural and compositional characterisation. Chapter 4 deals with the formulation and characterisation of binders based on the waste and other materials while in Chapter 5 the equivalent mortars using standard and waste sands are described. A Portland cement series was used as a control so that the impact of the different fillers on compressive strength with different binders could be assessed. Chapter 6 describes the use of the waste in concrete: a concrete design is set to highlight the impact of the different forms of the waste on properties with both Portland and alkali activated binders. Issues related to durability are addressed in this chapter. The same chapter includes the environmental impact of the produced concrete. The conclusions and potential applications are presented in Chapter 7 together with suggestions for future work. In the Annex additional information is presented.

Chapter 2: **Literature Review**

This chapter starts with a review of technical information on the waste: geological formation, places and processes for china clay extraction, quantities of china clay production and waste generation as well as current uses of the waste. It should be noted that a detailed review on the potentials of the waste as aggregate and as binder is presented towards the end of the chapter, after presenting the alkali activated cement technology in section 2.4, as some of the potential uses were on this type of binders therefore, in the meanwhile, the science behind the applications should be clear. The framework of this thesis is set by environmental drivers which are discussed in section 2.3 together with a brief review of state-of-art methods and cement technologies which contribute to that direction. The containing minerals of the waste are presented in 2.5 and there is special focus on mineralogical information for kaolinite and mica for reasons which will be explained. Section 2.6 is focused on aggregate uses in research for the kaolin waste as a whole (section 2.6.1) and its constituent minerals (section 2.6.2). Section 2.7 looks at the binder potentials of a) the kaolin waste as whole, b) kaolin and other pozzolan in Portland cement, c) the same minerals in alkali-activated cement technology and d) micaceous minerals in alkali-activated cement technology.

2.1 China clay extraction and processing in the UK

The UK was the sixth largest global kaolin producer in 2009, with almost all extraction of refined kaolin (or China Clay) in the Cornwall/Devon area. Annual UK kaolin extraction reduced considerably between 2005 and 2009 (from 1.9 to 1.1 million tonnes) because of the high cost of UK extraction, while the fifth largest global producer in 2009, Iran, increased production from 0.5 to 1.2 million tonnes over the same period (BGS, 2011). The size of UK reserves is not published because of the commercial nature of this information, but it has been estimated that more than 50 year's capacity is available using current technology (BGS, 2011). UK china clay production peaked in 1988 at nearly 2.8 million tonnes, with the major uses as paper fillers and ceramics. Deposits exist in many other places in the world (France, Germany, Spain, parts of the USA, Russia, Greece, Hungary, Iceland, Italy, Mexico and Turkey). The UK deposits of kaolin clay are of economically viable size and of high quality.

Visits to mining operations together with discussions with R&D staff and other professionals involved with mining operations were conducted during the initial stages of the project. The extraction pits that were visited belong to Imerys Minerals Ltd, one of the two major kaolin producers in the UK. The other is Sibelco UK Ltd, it has operations only in Devon and is owned by SCR Sibelco of Belgium. It should be noted however that Imerys Minerals Ltd is by far the largest producer accounting for over 77% of the total output, with operations in both Cornwall and Devon. It is a subsidiary of the Imerys

Group of France, the world's largest kaolin producer with major operations in the USA, the Amazon Basin and elsewhere in the world and with about 25% of the world market. (BGS, 2009)

Kaolin extraction in the UK starts in areas where kaolinisation of granite has occurred as they are primary deposits, meaning the clay is found at the site where it was formed (BGS, 2009). Other areas, including the Amazon basin, contain secondary deposits where kaolin has been formed elsewhere and deposited through alluvial processes resulting in a higher purity deposit and less waste from extraction and processing.

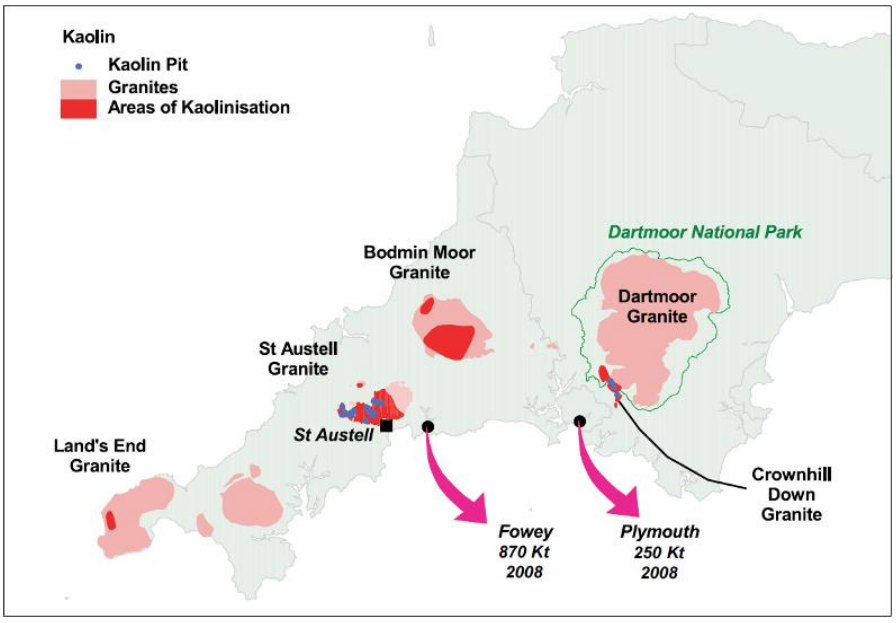

Figure 6 Areas of kaolinised granite in the South West (after BGS (2009))

Granite is rich in quartz and feldspar and while the quartz is consistent in chemical and mineralogical form, the feldspar can be a silicate of alumina with potash (K_2O), soda (Na_2O) or lime (CaO) (Minerals Zone, 2012). In the South West of the UK, the granites with extensive kaolinisation have feldspar with higher soda content than potash content. China clay, which has kaolinite as its main constituent, is formed through a complex sequence of events. Soon after the granite was formed, it was attacked successively by steam, boron, fluorine and tin vapour, these acting on the alkali content of the feldspar. Additional weathering took place later as water entered cracks from the surface which combined initial hydrothermal weathering, leading to kaolinisation (BGS, 2009). Permeable fracture and vein systems through which the kaolinising fluids circulated, is related to regions of commercial kaolinisation. These regions are "*funnel or trough-like in form narrowing downwards but the merging of funnels gives more extensive zones of kaolinisation*" (Figure 7). Kaolinisation may extend to depths of over 250m, although 100m is more typical (BGS, 2009).

Extraction starts with the removal of the overburden layer. When the desired decomposed granite is reached, it is broken up by water jets (Figure 9) which result in a

mixture of clay and sand in suspension running to a low point in the pit. Intact and unaltered rock (called stent) accumulates at the foot of the washing face and is taken out of the pit using shovel loader and dumpers. Smaller stones which run down the pit are separated by vibrating screens or rotating trommels. This sand is separated by bucket wheel classifiers (Figure 13), placed on vibrating screens to drain further water and finally drops onto a system of conveyor belts, which either take it to tips, to a sand grading plant or to a stockpile where it is loaded into dumpers for tipping. At the same time, the wash is pumped continuously into a circular, tapered pipe, the hydrocyclone or hydroclone (Figure 12). This process divides the feed into particles coarser than 50μm (0.05millimeters) and particles finer than 50μm. At this size there is an almost complete separation between china clay and other minerals, such as micaceous minerals and fine quartz sand. The coarse underflow (>50μm) (Figure 11) is pumped to MW lagoons. The finer particles are mainly china clay and are pumped to refining plants (Figure 14-15) for removal of fine mica and further sorting to produce the grades of clay required by different industries. MW from hydrocyclones and subsequent refining stages is suspended in water and as mentioned before, it could cause instability if placed on sand tips which is why it is placed in lagoons which are typically old mines. In lagoons, the MW settles leaving a layer of clean water on the surface which is pumped away for reuse. The flat surfaces of lagoons can be restored to agriculture by seeding and careful management. (Thurlow, 2005), but because of the uncompacted placement, they are not generally suitable for building over. Forms of the waste are presented in Figure 8.

As mentioned in section 1.1, the ratio of waste to china clay is 9:1. A survey in 2005 (Smith et al., 2005) assessed the aggregates that have potential to be used as secondary aggregate, taking into account old stockpiles and the currently produced waste (as the mean value of the period 2001-2004). The results show that the potential sand and stent arisings by live-feed operations reach more than 5.7Mt/year. This is a significant potential source of aggregates, considering approximately 50Mt of sand and aggregate is used annually for construction in the UK (ONS, 2014). The arisings considered in Smith et al. (2005) did not include material used in restoration and the value would be even greater if all the accessible and recoverable waste, not just what can be used as secondary aggregates was considered. As the MW stream was not considered as an aggregate with reuse options, this was not included. As a result, only stent and sand was quantified. Because of transport costs and emissions, the use of the china clay waste is unlikely to be the best financial or environmental solution for all regions in the UK. The existing reuse options are discussed in the following section.

As a last remark regarding the geology and applications deriving from granite in Cornwall it is noted that it has elevated levels of radon. However, in the South-West aggregates which derive from that rock are currently used in concrete. Most radon problems are associated with constructing over the granite which requires radon barriers and/or specialist ventilation systems to be installed for buildings (HealthProtectionAgency, 2009).

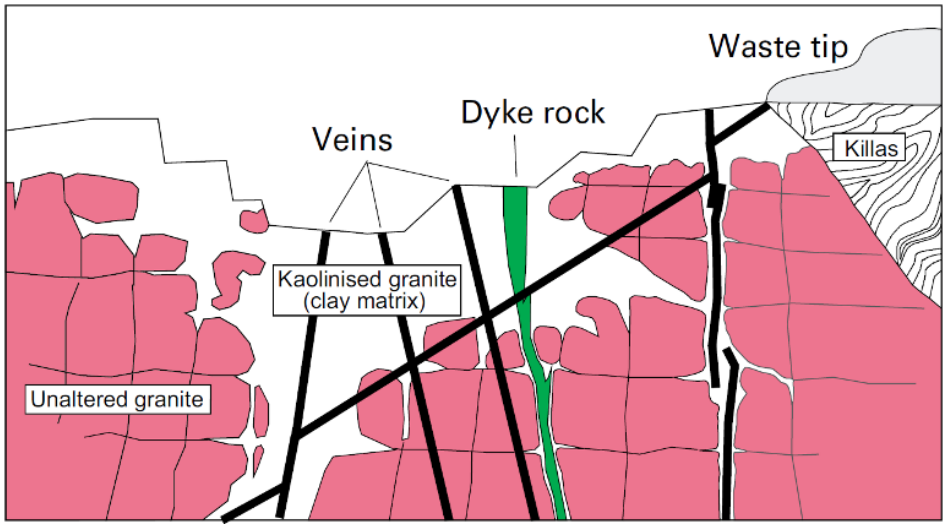

Figure 7 Kaolinised region in cross-section (BGS, 2009)

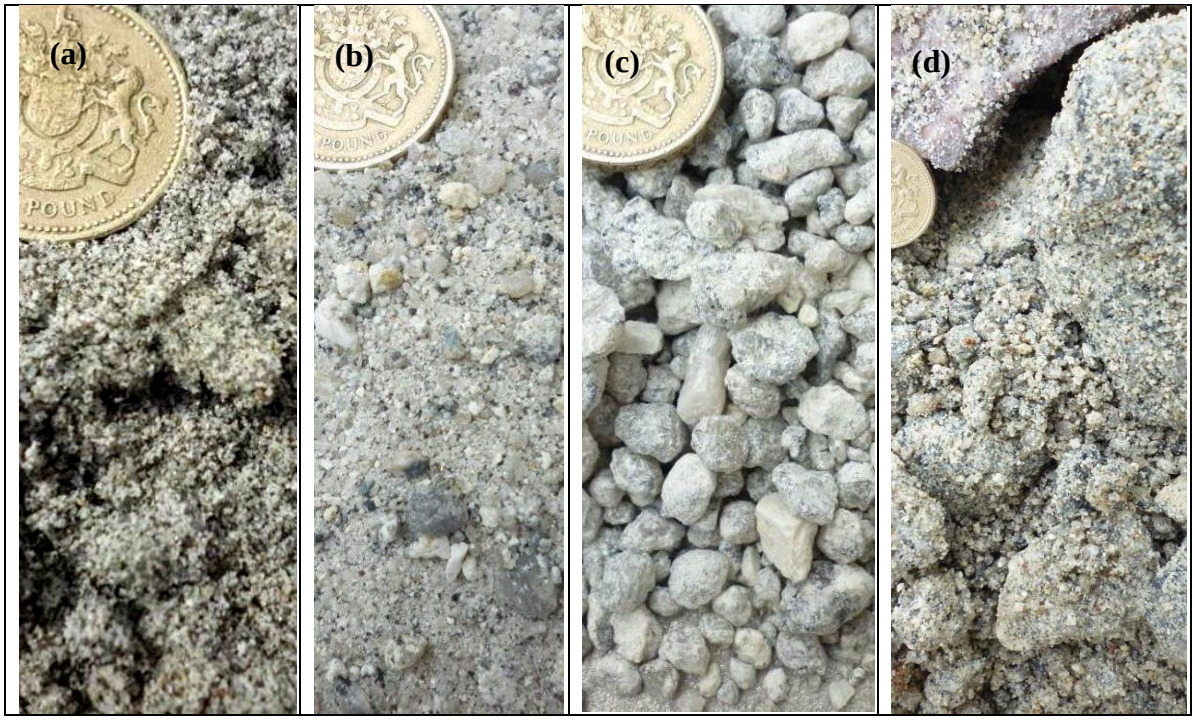

Figure 8 Forms of by-product: a) MW, b) coarse sand 0/4, c) gravel 2/10, d) stent.

Figure 9 Water jets to break down the granite releasing clay, sand and stones.

Figure 10 The wash runs to a low point in the pit and is pumped up to be processed.

Figure 11 MW suspended in water, running out of the hydrocyclones.

Figure 12 Hydrocyclones – Removal of mica and fine quartz.

Figure 13 Bucket wheel classifiers, 6meters in diameter– Removal of sand.

Figure 14 Refiners - Filtering overfloating organic pieces.

Figure 15 Refiners – On the left: Nozzle centrifuges to make clay with particular specifications.

2.2 Current uses of the by-product

From late 1800s till 1950s concrete structures in Cornwall and parts of Devon built using mining waste from presented the mundic issue. The waste together with good aggregate, contained minerals such as pyrite, or “fools gold” from where the term “mundic” comes, and other metallic sulphides associated with the tin and other metal ore. (Forde and Institution of Civil, 2009) The oxidation of the sulphide mineral and the products from the reaction of pyrite, cause local expansion, breakage and lower the strength of concrete. However, nowadays, the part of china clay waste which is sold as secondary aggregate is free from such components (seen in Table 10 in Chapter 3 and from the detailed chemical analysis for stent and china clay sand in the Annex A.1) it is

seen that the total sulphur content is minimum (<0.1% with sulphur not even detected in the chemical analysis).

Nowadays, large rocks find use as armour stone, rocks placed to minimise the effects of wave action in coastal defence schemes, and just over 0.5Mt of sand from china clay workings is sold annually and is widely used in Cornwall and Devon (Thurlow, 2005). There would be greatly increased sales of this sand if the cost of transport to more distant markets could be reduced. Sand costumers include ready-mixed concrete makers and the manufacturers of concrete products such as paving slabs and kerbs (Thurlow, 2005).

About 70% of aggregates used in Cornwall for road construction are derived from china clay pits. In particular, based upon the Specification for Highway Works, Volume 1 and the Design Manual for Roads and Bridges (Highways Agency, 2004), china clay sand can be recycled into:

- Bitumen bound materials – china clay sand asphalt base is specified in Clause 946 of the Specification for Highway Works (Highways Agency, 2004) and may be used in a variety of base course, binder course mixtures and surface layers.
- Concrete – may contain stent or/and china clay sand as the coarse/fine aggregate.
- Pipe bedding – may use china clay sand.
- Hydraulically bound mixtures (HBM) for sub-base and base – china clay sand may be used as part of the fine aggregate within HBMs.
- Unbound mixtures for sub-base - may use china clay sand where the grading permits.
- Capping – may contain china clay sand or stent
- Embankments and fill – china clay sand and stent are generally suitable for construction of embankments and as bulk fill

As transportation is a major issue that often sets barriers to the use of china clay by-product, most of its use takes place locally, in the county of Cornwall (WRAP, 2012). The construction of A30 Bodmin to Indian Queens dual carriageway is one of the largest road projects in the UK using secondary aggregates. It was constructed using eight hundred thousand tonnes of by-product and it includes 11.5km of carriageway, new junctions and side roads. (Highways Agency, 2008)

It should be noted that china clay sand, because of its manufacturing process, does not require much modification to conform to BS EN 12620 Grade 0/4 (MP) and is naturally very clean with a low silt content as a result of the processing, and is therefore easy to use in concrete (WRAP, 2004). In addition, concrete formed using stent or china clay sand can conform to BS 8500 and BS EN 206-1 (Marsh, 2007, Marsh, 2006). Other benefits of china clay sand is that it is abundant as mentioned in section 2.1, cheap and largely chemically inert, immune to alkali-silica reaction (ASR) and the thaumasite form of sulphate attack (TSA) as it is actually granite (WRAP, 2004).

The only issue that causes some discomfort with manufacturers is the higher water content in concrete mixes compared with many other natural aggregates. This is because of the mica mineral in the granite which can split into very thin flakes because of its perfect cleavage parallel to the basal plane of the mica crystal, thus increasing the surface area of the fine aggregate causing higher water demand. Higher cement content would compensate for that increase in water for given concrete strength. To avoid this situation, the china clay sand is often blended with high quality sand (either from land deposits or washed marine sand). The blending in the correct designed ratios of sand needs careful monitoring, therefore there is an extra cost which, however, can be offset by the low cost of the material, which is available locally and is exempt from the Aggregates Levy (WRAP, 2004).

Figure 16 Completed building at One Coleman Street, London (Marsh, 2007)

Stent has been used as secondary aggregate in concrete for buildings: Foundations for the Aquatic Centre, Handball Arena and the main Stadium of London 2012 Olympics used concrete containing more than 30 per cent recycled materials, including aggregates from china clay waste (Olympic Delivery Authority (ODA), 2009). For One Coleman Street (Figure 16) in the City of London china clay stent was used as coarse aggregate in concrete (Marsh, 2007). In this case 100% of the primary aggregate was replaced by stent in pile-caps, floor slabs and structural frame. No difficulties were reported at plant and on site regarding the use of stent. Other secondary aggregates had also been considered (slate waste, waste glass, incinerator waste, recycled aggregate, sewage sludge ash, shredded tyres, bottle cork waste periwinkle shells) including china clay sand which was noticed to increase the cement demand, therefore it was decided not to be used in the construction of the building (Marsh, 2007). The publication by Marsh (2007) provides four mix designs of compressive strength class of C32/40 and C28/40. The content of stent is constant in all of them (1000kg/m^3) while the cementitious material is between 350-420kg/m^3, including 35-40% fly ash (by binder mass). It is useful to consider these Portland cement concrete mix designs when the design of equivalent AA cement concrete mixes is presented in Chapter 6. This also shows the current feasible maximum transport distance

which, in both the London Olympic and One Coleman Street cases, involved rail as the primary transport mode.

2.3 The drivers for more sustainable cement

While there are a number of impacts from construction, the latest report of the Intergovernmental Panel on Climate Change (IPCC) (IPCC, 2014) offers a detailed insight to the problem of the high carbon emissions from the cement industry and refers to probable mitigation measures. The carbon emissions from the cement industry are related to fuel combustion (calcination of limestone, clay and sand to 1450°C) and to the calcination reaction. Asia is leading the way in global cement production. To understand the large scale of the problem, the context is given in numbers from the IPCC report:

- Emissions from industry comprise 30% of the total UK Greenhouse Gas (GHG) emissions and 44% of the CO_2 emissions from industry are due to the production of iron, steel and non-metallic minerals (mainly cement).
- 1.352Gt of CO_2 were emitted in 2010 from only the cement-forming reactions (not including the cement energy-related direct emissions) while another source (Boden 2013) stated a slightly higher number of 1.65Gt CO_2 in 2010.
- 50% of the total CO_2 emissions are due to the calcination reaction, 40% is related to fuel emissions and 10% to transport and grinding. A decrease in demand, including material efficiency, would reduce the emissions from the calcination reaction while the fuel emissions could be limited by use of alternative- to-carbon fuel (such as fossil or biomass wastes) and improvements in energy and material efficiency.

The efficiency of the Portland cement industry could be enhanced if alternative fuels were employed, if there was higher energy efficiency in terms of waste heat recovery, if CO_2 is captured and stored, or if there was further substitution of cement by supplementary cementitious materials (Habert, 2013). Cement additions such as blast furnace slag, fly ash, limestone and natural or artificial pozzolans reduce to an extent the use of clinker and suggest an example of material efficiency. Modern facilities are highly energy efficient (Gartner, 2004) and the inclusion of blast furnace slag, fly ash and silica fume, without including metakaolin and other pozzolans, in cement can bring up to 20% CO_2 reduction compared to non-blended Portland concrete (Yang et al., 2014). Another example of efficiency is the use of higher-strength concrete which would reduce the quantity needed. For example, CO_2 savings of 40% have been reported on specific projects using "*ultra-high-strength*" concretes (IPCC, 2014).

There are alternative cements that have potential to reduce the CO_2 emissions of the cement industry. Gartner (2004) finds the most promising technology to be cements partly based on calcium sulfates, mainly calcium sulfoaluminate-belite/ferrite cement used in China, and cements based on pozzolans. The last category includes alkali-activated and magnesia cements. The only type that actually makes use of the

aluminosilicate nature of the raw constituent is the alkali-activated binder which is the reason that they were preferred in this study. Research is ongoing for all the given alternative cement types though for some technologies there are products commercially available, for example Aether™ a belite–calcium sulphoaluminate–ferrite (BCSAF) type of cement by Lafarge (Gartner and Macphee, 2011), E-crete and Earth Friendly Concrete which are alkali activated binders by Zeobond.com and Wagner.com.au, and all show reduction of carbon emissions. Limitations that Gartner (2004) names for magnesia cements is their slow reaction with pozzolans, high carbon emissions related to the conversion of magnesite in MgO and insufficient deposits.

Alkali-activated binders make use of activators with high embodied energy and can sometimes need elevated temperature for curing and difficulty in obtaining sufficient setting times and for these reasons Gartner has expressed the concern that only precast AAC applications could have good potential to replace Portland cement, which further justifies the initial decision in this study to target precast applications. However recent advances in alkali-activated technology have minimized and sometimes eliminated the need for elevated temperature curing, as described in subsection 2.4.3.3. Also, Gartner (2004) noticed that currently none of the alternative cements could compete the low cost of Portland cement but the difference could rely on combination of low CO_2 emisions and good performance and durability. Further comparison between the above mentioned types of cement and more can be found in Gartner and Macphee (2011).

2.4 Alkali activated cement technology

The concept of alkali activation of aluminosilicates started in the 1940s but Davidovits was the first to use the term geopolymer in 1978, referring to amorphous to semi-amorphous three-dimensional aluminosilicate materials (Davidovits, 1991, Van Jaarsveld et al., 1999). The term "alkali-activated materials" includes a greater range of binders compared to geopolymers (van Deventer et al., 2010) and the difference will be explained in section 2.4.2 together with an introduction to the mechanism of the reactions (in 2.4.1) which lead to formation of hardened binder and the main products. At the end of this section the latest developments will be detailed in a range of topics relevant to this study.

In the technology of alkali-activation (including geopolymers) the addition of an alkaline activator to an aluminosilicate precursor leads to insoluble, strong hardened binders. The main sources used in AAMs are GGBS, FA and metakaolin (Provis and Bernal, 2014). However, any other fine material that contains significant amounts of silicon and/or aluminum held in an amorphous phase can be used as a binder precursor (Concrete Institution of Australia, 2011). Such material include calcined clays (Wang et al., 2005, Liew et al., 2011), rice husk ash (Kim et al., 2014) and calcined muscovite-rich waste (Pacheco-Torgal et al., 2010). The latter is of interest in this research and will be discussed in detail. It should be mentioned that addition of Portland cement in small quantities acts as an accelerator (calcium effect) (Concrete Institution of Australia, 2011) but is not commonly referred to in papers where GGBS is more commonly used.

The most widely available and economical caustic alkalis and alkali salts used as activators are NaOH, Na_2CO_3, $Na_2O\cdot nSiO_2$ and Na_2SO_4 although other caustic alkalis and alkali salts can be used too. Potassium equivalent substances have been used in studies but they have higher cost and also they are less available (Shi et al., 2006). The production of sodium carbonate, as well as the production of sodium silicate which results from melting sodium carbonate and sand, can be energy intensive. Therefore high concentration of these activators can increase the carbon emissions of the resulted binder. The above processes are further explained in 2.4.6.

The advantages of AAC technology include:

- excellent mechanical properties (Duxson et al., 2007c, Yang et al., 2012b, Marjanović et al., 2015, Shi and Fernández-Jiménez, 2006),
- excellent fire resistance of geopolymers (but not all AAC) (Palomo et al., 1992, Davidovits and Davidovics, 1988)
- the immobilization of heavy metals (Pacheco-Torgal et al., 2010, Ahmari and Zhang, 2013a, Shi and Fernández-Jiménez, 2006)
- good resistance to chemical attack (Pacheco-Torgal et al., 2012)
- excellent resistance to freeze-thaw (Cai et al., 2013, Sun and Wu, 2013)
- lower carbon emissions (McLellan et al., 2011, Stengel, 2009)

On the other hand disadvantages include:

- Reported poor resistance to carbonation for precursors of high Ca content in accelerated carbonation tests (discussed in section 2.4.5). However, the absence of tests designed for AAC technology induces barriers and doubts regarding the interpretation of results from accelerated carbonation testing (Van Deventer et al., 2012, Bernal et al., 2012b).
- High alkalinity of the fresh mixes is a concern for handling of cement and concrete (Part et al., 2015).
- The difficulty in scaling up from lab to large scale site projects (Van Deventer et al., 2012)
- Inconsistency related to the various properties of the by-products used as precursor (Part et al., 2015). A way to comply with variations in performance without major controlling of the raw products is to target significantly higher strength than needed (Concrete Institution of Australia, 2011).
- Narrowing of the potential applications and increasing the energy demand due to heat curing where it is needed (Part et al., 2015).

Despite the difficulties, there are applications in building and civil infrastructure which are described in (Shi et al., 2006) and Provis and van Deventer (2014) and initial uses indicate promising field performance.

2.4.1 Reaction mechanism

There are a number of recent reviews in the AAC technology (Provis and Bernal, 2014, Part et al., 2015) but the hydration details have been summarized in previews papers (Duxson et al., 2007b, Pacheco-Torgal et al., 2012). A brief overview of the reaction mechanism is presented here. It should be noted that the term hydration is not correct for geopolymers as they do not chemically bind water as Portland cement does (Gartner, 2004). Note also that the term "slag" is used in the following as a short form of blast furnace slag (BFS) or ground blast furnace slag (GGBS).

Contact of the aluminosilicate source with alkaline solution provides silicate and aluminate in the mix by dissolution (Xu and Van Deventer, 2000). The aluminosilicate, which can serve as a precursor of geopolymers, needs to have silicate and aluminate in its structure readily soluble (Van Jaarsveld et al., 1997). Regarding the aluminium, when it is in the four coordination (AlO^{-4} group), it creates a negative charge which can be balanced by alkali cations (usually Na^{+} and/or K^{+}) (Duxson et al., 2007b). In other words, four coordination aluminum groups are enabled to react with the activator. Xu and Van Deventer (2000) interpreting the statement of Van Jaarsveld et al. (1997) regarding the need for Al in soluble form, referred not only to Al in four but also in five coordination. The coordination of aluminum in the raw material is of interest, it is the difference between calcined clays (clay after the dehydroxylation) and the original unheated clays (Pacheco-Torgal et al., 2008) which makes calcined clays reactive (Heller-Kallai and Lapides, 2007, Sabir et al., 2001) and this topic will be further discussed in section 2.5.

Based on the model of Glukhovsky (1959) and later advances, Duxson et al. (2007b) presented an extended, modified model to describe geopolymerisation. According to this model, first, the activator causes the hydrolysis of the amorphous aluminosilite precursor and as a result, silicate and aluminate are dissolved (monomers). At high pH the process results in a supersaturated aluminosilicate aqueous phase which will later be condensed and form "*large networks*" with simultaneous elimination of water. Here lies a great difference between Portland systems and geopolymers: the water in the geopolymerisation process is a medium for the reaction and will reside within pores in the gel (Duxson et al., 2007b).

Figure 17 shows the components that will be formed in polymerisation. What is called "sialate" is actually aluminosilicate oxide. The Si and Al in the network of sialates, are tetrahedral anions ($[SiO_4]^{4-}$ and $[AlO_4]^{5-}$) sharing oxygens (Davidovits, 2011). As mentioned above, the negative charge of AlO^{+3} in four coordination will compensate by presence of positive ions. The alkalis in the mix have a role in dissolution and polycondensation therefore the activator used is of importance (Duxson et al., 2007b). Systems with slow response, far from equilibrium, may never form gel. For well-formed binders, the gel will later keep changing, making more connections in its network that leads to a three-dimensional, highly crossed-linked network (Duxson et al., 2007). The empirical formula of "polysialate" (Davidovits (2005), is cited in Pacheco-Torgal et al. (2008)):

$$M_n[-(SiO_2)_z\text{-}AlO_2]_n \cdot H_2O$$

where M is the alkali cation (usually Na or K), n the degree of polymerization and z is 1,2,3, understood to be related to sialate, sialate-siloxo and sialate-disiloxo.

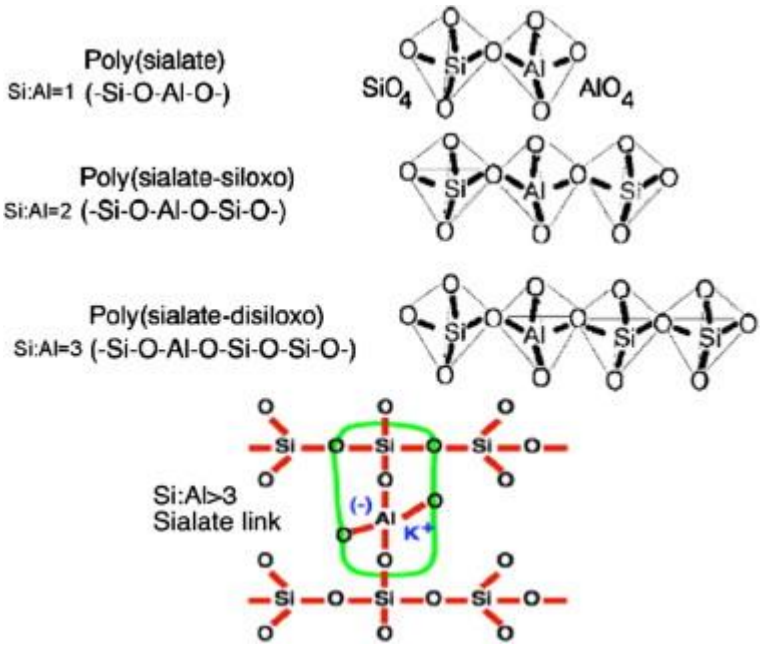

Figure 17 Sialate, compounds of geopolymers according to Davidovits (After Davidovits (2005) cited in Pacheco-Torgal et al. (2008))

The reaction of the aluminate and silicate of source material with silicate solution in highly alkaline conditions can be written as described below (Xu and Van Deventer (2000) based on the formulas of Van Jaarsveld et al. (1997)):

$$n(Si_2O_5,Al_2O_2) + 2nSiO_2 + 4nH_2O + NaOH \text{ or } (KOH) \rightarrow Na^+,K^+ + n(OH)_3\text{-}Si\text{-}O\text{-}Al^-\text{-}O\text{-}Si\text{-}(OH)_3$$

(Si-Al materials)

$(OH)_2$

(Geopolymer precursor)

$$n(OH)_3\text{-}Si\text{-}O\text{-}Al^-\text{-}O\text{-}Si\text{-}(OH)_3 + NaOH \text{ or } (KOH) \rightarrow (Na^+,K^+)\text{-}(\text{-}Si\text{-}O\text{-}Al^-\text{-}O\text{-}Si\text{-}O\text{-}) + 4nH_2O$$

$(OH)_2$

(Geopolymer backbone)

Geopolymers have completely different reaction process than pozzolanic cement which depends on availability of calcium to form calcium–silica-hydrates (C-S-H), and without the need for calcium, geopolymers harden using polycondensation of Al and Si (van Jaarsveld et al., 2002). When adding a material rich in Al, Si and Ca such as slag in an alkali-activated binder geopolymer, (blend-based geopolymer) the dissolution of Ca from the slag results. The solubility of Ca is low at high pH (Phair et al., 2000) but in the mix the dissolved Ca will react with the hydroxide groups and decrease the pH (Yang et

al., 2012b). Because of the decrease in pH, a decrease in the Al and Si dissolution from the aluminosilicate source will follow (Duxson et al., 2007b). As a result slag lowers the degree of geopolymerisation and leads to short-range chemical ordering which is good for pore size and strength of (blend-based) geopolymers (Yang et al., 2012b). As a result the presence of Ca in the aluminosilicate source is so significant that alkali-activation of slag (slag only) has different main products than an aluminosilicate poor in Ca.

2.4.2 Difference between AAM and geopolymers and their related products

The classification and according terminology is based on the Ca content in the binder that leads to different main phases in the product (van Deventer et al., 2010). The different terms used are presented graphically in Figure 18 based on the Ca and Al content compared together with PC and sulpho-aluminate cements. In spite of this guidance on terminology, many continue to use the term "geopolymer" to represent alkali-activated materials, regardless of calcium content (Duxson et al., 2007, Davidovits, 2011).

Alkali activated materials

AAM is the largest and broadest category where any classic aluminosilicate-rich precursors (slag, natural pozzolan, fly ash or bottom ash) can be used, while the alkaline component can be any that can rise the pH to accelerate the dissolution of the precursor (alkali hydroxides, carbonates, sulphates, aluminates or oxides) (van Deventer et al., 2010). Precursors lower in Ca and higher in Al would form "Inorganic polymer" binders. Activation of slags using silicate, hydroxide or carbonate would also fall in this category (unlike using sulphate). In this study no further reference will be made to inorganic polymers. Only the terms of geopolymer and AAM will be used to avoid complication.

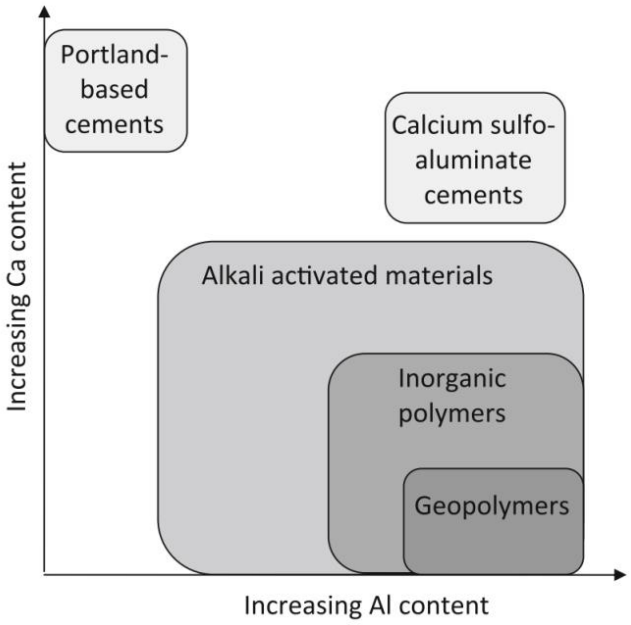

Figure 18 Classification of alkali-activated types of cement, PC and sulfo-aluminate cements (after van Deventer et al. (2010)). Darker areas represented increased alkali content.

High-in-calcium binder systems that fall in the alkali-activated material category are defined as a system having a ratio of Ca/(Si+Al) about 1 (Provis and Bernal, 2014) with AA slag (AAS) being the typical case. AAS has characteristic green colour, the intensity and the extent of the colour depends *o*n the rate of oxidation and a number of other parameters as the amount of slag used, curing conditions and porosity of the concrete surfaces (Brice et al., 2012). The main products of AAS is calcium silicate hydrate with some amount of aluminium incorporated (C-A-S-H) (Wang et al., 1995, Brough and Atkinson, 2002, Myers et al., 2013) low in Ca/Si and with a chain structure (Shi and Fernández-Jiménez, 2006). Calcium has been found to enhance durability by reducing permeability, which is related to the structurally bound hydrates in C-A-S-H and observed in samples with ≥50% slag (Provis et al., 2012). Slag-based binders activated using NaOH compared to activation using sodium silicate have slightly sharper XRD patterns as a consequence of their more ordered nanostructure and they have higher Ca/(Si+Al), although the exact composition of the hardened binder will depend on the chemical composition of the slag (Fernández-Jiménez et al., 2003). XRD peaks of uncarbonated AAS samples have been identified as dicalcium silicate hydrate ($Ca_2SiO_4 \cdot 3H_2O$) and other minerals of C-S-H like tobermorite and hillebrandite (Bernal et al., 2012b). In the first stages of carbonation the XRD can show Ca and C containing phases as vaterite and calcite while presence of calcite at early stage may of samples be due to small degree of carbonation of the fresh cement, during mixing (Bernal et al., 2012b). However, Ismail et al. (2013a) detected aragonite in alkali-activated GGBS specimens after 40days curing, using XRD. Aragonite is a more stable metastable phase of calcium carbonate and 40days would be considered too early for natural carbonation to occur. Therefore it is not clear if the detection of vaterite and aragonite indicates carbonation rather than being part of the reaction process.

Apart from the C-A-S-H gel there are secondary phases which may be aluminium and/or magnesium rich products as hydrotalcite and/or zeolites like gismondine (Bernal et al., 2013, Ismail et al., 2013a). The presence of hydrotalcite after hydration is related to the amount of MgO and Mg-containing phases like akermanite in slag before activation (Haha et al., 2011). Alumino-ferrite-mono (AFm) phases have also been detected mainly using EDX (not always detectable by XRD), detected in between C-S-H structure, in the nanoscale (Bernal et al., 2013) and in the form of stratlingite (Haha et al., 2012). No $Ca(OH)_2$ is formed in AAS (Shi and Fernández-Jiménez, 2006). Of course based on the chemistry of the source slag, the secondary products that authors detect vary.

Table 2 summarises atomic ratios of AAS which have been activated using NaOH only (where only the Na_2O% per 100g of slag or NaOH molarity is mentioned) or sodium silicate/+NaOH (where Ms=molar ratio of SiO_2/Na_2O is given). As the nature of the raw material plays important role (Duxson et al., 2007b), the main oxides of the used slag is displayed. Depending on the focus of the research, authors have used different types of slag (Haha et al., 2012, Bernal et al., 2014), while others use one slag and different alkaline solutions (Puertas et al., 2004, Gebregziabiher et al., 2015). As seen, some

authors express their results by giving a range of values, and some give an average value. Authors who present a range of values, usually plot them. A characteristic type of plot for AAS is shown in Figure 19 where the inclined lines are related to Mg-containing phases (hydrotalcite-like) and the intercept on the Al/Si axis indicate the Al in C-S-H. The maximum reported value for Al incorporation in C-S-H is 0.33 (Richardson et al., 1993) and depends to bridging positions occupied by Al in the chain-structure (Haha et al., 2012). Interestingly it has been reported that while the Al/Si increases for increasing Al_2O_3 content in the slag, the Ca/Si ratio is not affected neither by the "hydration" time nor the Al_2O_3 content of slag (Haha et al., 2011, Haha et al., 2012). The fact that the Mg/Si in the matrix can be higher than the Mg/Si of the undissolved slag particles was attributed by Brough and Atkinson (2002) to removal of Si and, in a lower rate, removal of Al and Ca from the slag particles. In Figure 19, Mg/Al=1.3 is considered low for a hydrotalcite-like phase but it is attributed to the very low Mg/Al measured in the A14 and A17 unhydrated slags used and indicated recrystallisation. Brough and Atkinson (2002) found in AAS that the Mg possibly in hydrotalcite-like phases was intermixed in the matrix in size lower than the interaction volume of the microanalysis probe. Over time clearer formations of Mg could be seen although they were still mixed with the outer product and/or unreacted slag. After one year the Mg/Al was 2.3 (in the expected range for hydrotalcite).

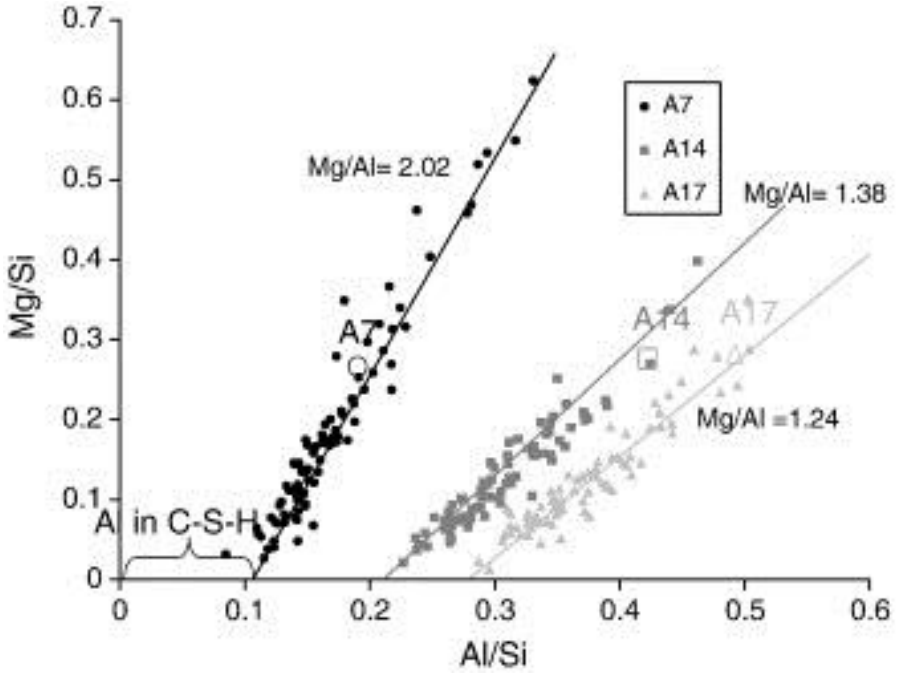

Figure 19 Plot of atomic Mg/Si to Al/Si ratios of three slags of different Al_2O_3 content after curing for 180days (from Haha et al. (2012). The inclined lines are related to presence of hydrotalcite-like phase (of different Mg/Al ratios). The intercepts (0.11, 0.21, 0.27, for zero Mg content) on the Al/Si axis are related to the Al incorporation in the C-S-H.

In Table 2, apart from one study (Brough and Atkinson, 2002), most of the studies show relatively constant atomic Ca/Si ratio, largely between 0.70 and just over 1.00. The Al/Si is largely between 0.20-0.50. Ratios Ca/Si and Al/Si are lower for use of silicate rather than NaOH only which is due to the higher silicate content in the solution. To present the results in a comparable way, maybe some atomic ratios and the alkalinity of the activators have been calculated rather than clearly given in papers. Explanations and some comments are given on the Table, while some more information is given in 2.4.3.1 where discussing about the importance of different oxides for slags.

In Table 2, it is seen that Puertas et al. (2004) refers to two shades of grey in their EDX analysis. The darker areas include what is called "inner product" by Brough and Atkinson (2002) or "hydration rims" by Haha et al. (2012), a slim area around the undissolved slag particles. This area has high Mg content. As Brough and Atkinson (2002) mentioned, Mg does not migrate out the inner product region as in OPC or blended cements and can be used as a marker for the inner product hydrates. These regions are very narrow and of relatively coarse porosity in microstructure for hydration using NaOH while clearly less porous (filing capacity of the hydrates) for using sodium silicate (Haha et al., 2012).

A Ca-containing system that does not involve slag was patented by Davidovits et al. (2012) and uses natural resources rich in iron oxides and in ferro-kaolinite. After treating the raw material at 600-850°C, the iron oxides are transformed from goethite FeO(OH) and magnetite Fe_3O_4 are transformed to hematite Fe_2O_3 and the ferro-kaolinite becomes ferro-metakaolin. The raw material was ground to 10-25μm and it was mixed with a Ca-containing activator to form a binder that would probably be characterised as inorganic polymer. The key in this type of binder is that Fe atoms substitute some of the Al atoms to form a ferro-aluminosilicate polymer. The reached strength for curing, covered, at 20°C was 30-40MPa on day 7 and 75-90MPa on day 28.

Geopolymers

Based on Figure 18 geopolymers are the narrowest subset and comprise almost exclusively aluminosilicate to form as primary binding phase a gel similar to zeolites but rather amorphous (Davidovits, 2011). To develop this amorphous gel structure, rather than the C-S-H-like chain structure in AAS, the calcium content of the raw aluminosilicate material has to be low and therefore characteristic precursors are FA (Fly ash which has CaO content <5% is preferred (Concrete Institution of Australia, 2011)) and calcined clays like metakaolin (van Deventer et al., 2010). The gel is N-A-S-(H) and the parenthesis is often used to remind that water is not a major structural component as C-A-S-H gel (Allen et al., 2007, Provis and Bernal, 2014, Ismail et al., 2013a). The N-A-S-(H) gel has Si and Al in four coordination. The presence of amorphous gel is shown in XRD patterns a halo (Heah et al., 2013b, Criado et al., 2007) or increased background as other authors (e.g. Pacheco Torgal et al. (2005b) refer to it. The halo of the gel is at about 25–40° 2θ, slightly shifted to the right compared to the halo of the raw aluminosilicate material (Heah et al., 2013b, Criado et al., 2007).

Table 2 Atomic ratios of AAS based on literature.

	Main oxides of the chemical composition of slag				**Atomic ratios in products** (unless otherwise specified)						
Reference	**SiO_2**	**Al_2O_3**	**CaO**	**MgO**	**Al/Si**	**Ca/Si**	**Al/Ca**	**max Mg/Si (*)**	**Mg/Al in Mg-rich phases**	**Activator**	**Comments**
Brough 2002	35.44	13.04	40.19	7.94	0.20-0.50	0.40-1.30		0.7		< 5.9% Na_2O, Ms= 2	Scattered Ca/Si . Al/Ca cannot be calculated from the figures given.
Puertas 2004	35.5	12.15	41.45	8.34	0.43	0.92	0.48	0.61		4% Na_2O	Refers to dark grey area of the BSE image. Activator/slag=0.5.
	35.5	12.15	41.45	8.34	0.39	0.91	0.44	0.47		4% Na_2O	Refers to clear grey area of the BSE image. Activator/slag=0.5.
	35.5	12.15	41.45	8.34	0.33	0.77	0.45	0.55		4% Na_2O, Ms=1.5	Refers to dark grey area of the BSE image. Activator/slag=0.5.
	35.5	12.15	41.45	8.34	0.25	0.78	0.33	0.30		4% Na_2O, Ms=1.5	Refers to clear grey area of the BSE image. Activator/slag=0.5.
Yang 2012b	33.28	17.47	35.59	8.10	0.17	1.02	0.17			Ms= 1.4 (?)	Na-3.07, Al-4.80, Si-13.96, Ca-14.22
Haha 2012	41.60	7.00	39.10	7.20	0.12 (**)	0.88 (**)	0.14 (**)	n/g	2.02	3% Na_2O	180days. w/b=0.40. Molar Ca/Si ratio in all slags of this study is 1.01, while molar Mg/Al=1.29 (for slag of 7% Al_2O_3),0.6 (14%), 0.49(~17%). To the decreasing Mg/Al of slags and/or poor in Mg hydrotalcite is attributed the decreasing Mg/Al of the results.
	41.60	7.00	39.10	7.20	0.11 (**)	0.79 (**)	0.14 (**)	0.65	2.02	3% Na_2O+2.8% SiO_2	
	38.20	14.10	36.00	6.60	0.24 (**)	0.89 (**)	0.27 (**)	n/g	1.58	3% Na_2O	
	38.20	14.10	36.00	6.60	0.21 (**)	0.77 (**)	0.27 (**)	0.42	1.38	3% Na_2O+2.8% SiO_2	
	37.20	16.70	35.00	6.40	0.30 (**)	0.89 (**)	0.34 (**)	n/g	1.27	3% Na_2O	
	37.20	16.70	35.00	6.40	0.27 (**)	0.80 (**)	0.34 (**)	0.29	1.24	3% Na_2O+2.8% SiO_2	
Bernal 2014	31.62	14.65	42.86	1.17	0.40-0.50	0.70-1.10	~ (0.36-0.64)	0.10	0.11<< Shows there is Mg incorporated in C-A-S-H instead of forming hydrotalcite.	4.1% Na_2O, Ms=1.00	180days. w/b=0.40. Values taken from figures given in the paper. Where "~" the ratio has been calculated.
	32.25	13.29	42.33	5.21	0.28-0.40	0.90-1.30	~ (0.25-0.33)	0.35	~ 2.11	4.1% Na_2O, Ms=1.00	
	34.11	12.38	40.21	7.44	0.30-0.40	0.65-0.90	~ (0.36-0.64)	0.40	~ 2.05	4.1% Na_2O, Ms=1.00	
Gebregziabiher 2015	36.00	10.50	39.80	7.93	0.37	1.12				NaOH 5M	Solution/slag=0.50
	36.00	10.50	39.80	7.93	0.31	1.16				NaOH 8M	
	36.00	10.50	39.80	7.93	0.31	1.39				NaOH 12M	
	36.00	10.50	39.80	7.93	~0.38 (***)	~ 0.69(***)				2.5% Na_2O, Ms=1.50	
	36.00	10.50	39.80	7.93	~0.54 (***)	~ 0.86(***)				2.5% Na_2O, Ms=2.50	

Where modulus of activator, Ms is the molar SiO_2/Na_2O. Where A% Na_2O, means A grams per 100g of slag

(*) theoritically this ratio goes down to zero. Practically it can go close to zero (but not exact zero) where it corresponds to low in Mg phases.

(**) Understood to be the atomic ratios in C-A-S-H where there is minimum or zero presence of Mg (where "max Mg/Si" ~ 0). Therefore it is selected values.

(***) Calculated from given EDX patterns, therefore based on ratios of intensity for the major peaks on the elements of interest. Not actual atomic ratios.

(?) In this study three Ms values are used (1.2 ,1.4 and 2.0). It is not clearly stated for which Ms the EDS analysis was conducted (probably for Ms=1.4).

~ Calculated.

n/g : Not given

Table 3 Atomic ratios of FA-based geopolymers based on literature.

	Main oxides of the chemical composition of FA				Atomic ratios in products				
Reference	SiO_2	Al_2O_3	CaO	Fe_2O_3	Si/Al	Na/Si	Na/Al	Activator	Comments
Fernandez-Jimenez 2005	53.09	24.8	2.44	8.01	1.62-2.17		0.25-1.29	8.68% Na_2O	ª Reactive SiO_2 in the FA was 50.44 (not all the 53.09)
	53.09	24.8	2.44	8.01	2.24-3.35		0.84-1.63	7.74% Na_2O, Ms~1.3	
	53.09	24.8	2.44	8.01	1.90-2.80		1.24-8.04	8.68% Na_2O, 6% CO_3^{2-}	Trona and Nahcolite detected
Yang 2012b	53.00	30.58	4.57	3.81	4.04	~0.24	~0.92	Ms=1.4 (?)	Specifically the atomic ratios measured are: Na-2.08, Al-2.26, Si-8.84
Winnefeld 2010	56.00	25.00	1.90	8.70	~ 4.6	~ 0.09		5.2% Na_2O, Ms=1.0	ª w/b=0.27-0.64 to achieve some flowability to cast. Curing for 24h at 20°C and RH 95% and then 24h at elevated temperature.
	56.00	25.00	1.90	8.70	~ 3.6	~ 0.13		7.3% Na_2O, Ms=1.0	
	56.00	25.00	1.90	8.70	~ 3.4	~ 0.14		9.4% Na_2O, Ms=1.0	
	10.00	5.60	36.00	16.00	strong scattering			7.3% Na_2O, Ms=1.0	Poor dissolution, formation of hydrogarnet and thenardite instead of N-A-S-H
Komljenovic 2010	51.74	21.36	11.34	8.80	2.64	1.98	4.47	10% Na_2O, Ms=0.52	ª Samples cured at 20C for 24h and then 55°C for 6days.
	51.74	21.36	11.34	8.80	3.16	0.26	0.86	10% Na_2O, Ms=1.55	

Where modulus of activator, Ms is the molar SiO_2/Na_2O. Where A% Na_2O, means A grams per 100g of FA.

ª Conditions applying to all the samples of a given reference.

(?) In this study three Ms values are used (1.2 ,1.4 and 2.0). It is not clearly stated for which Ms the EDS analysis was conducted (probably for Ms=1.4).

~ Calculated.

Table 4 Atomic ratios of AA blends of FA/slag based on literature.

	FA/slag mass ratio	Main oxides of the chemical composition of FA/slag blend				Atomic ratios in products					
		SiO_2 (**)	Al_2O_3 (**)	CaO (**)	MgO (**)	Al/Si	Ca/Si	Al/Ca	max Mg/Si (*)	**Activator**	**Comments**
Yang 2012b	60/40	45.112	25.336	16.978	3.99	0.17	0.45	0.85		Ms=1.4 (?)	Specifically the atomic ratios measured are: Na-0.78, Al-2.24, Si-13.40
	20/80	37.224	20.092	29.386	6.73	0.17	0.84	0.40		Ms=1.4 (?)	Specifically the atomic ratios measured are: Na-2.13, Al-2.12, Si-12.49
Bernal 2013	50/50	48.35	19.3	21.3	3.15	0.39-0.41	0.9-1.1		0.19	4% Na_2O, Ms=1.0	Refers to uncarbonate samples
	50/50	48.35	19.3	21.3	3.15	0.3	0.65-0.86		0.16	4% Na_2O, Ms=1.0	Refers to carbonated samples

Where modulus of activator, Ms is the molar SiO_2/Na_2O. Where A% Na_2O, means A grams per 100g of the blend.

(*) theoritically this ratio goes down to zero. Practically it can go close to zero (but not exact zero) where it corresponds to low in Mg phases.

(**) Calculated based on the FA/slag mass ratios and the chemical compositions of the two components.

(?) In this study three Ms values are used (1.2 ,1.4 and 2.0). It is not clearly stated for which Ms the EDS analysis was conducted (probably for Ms=1.4).

A common observation in FA geopolymers is that the crystalline phases of FA remained after the alkali activation which has been observed by several authors (Criado et al., 2007, Fernández-Jiménez and Palomo, 2003, Rees, 2007). There is also formation of zeolites as secondary products of activation. Criado et al. (2007) used FA of chemical composition SiO_2 53.09% (but reactive SiO_2=50.44%), Al_2O_3 24.80%, Fe_2O_3 8.01%, MgO 2.44%, and for use of alkaline solutions of slightly varying Na_2O content (equal to 7.72-8.41% of the solution) and increasing modulus Ms (0-1.17). Where Ms is the molar ratio SiO_2/Na_2O. Note that FA of the same composition has been used in a previous study by Fernández-Jiménez and Palomo (2005) (Table 3), although in that study the samples cured at 85°C for only 20h while Criado et al. (2007) used 85°C at >90% relative humidity till testing. For mixing solution/FA=0.4 and the mentioned curing conditions, Criado et al. (2007) detected in XRD the presence of chabazite-Na $NaAlSi_2O_6 \cdot 3H_2O$, hydroxysodalite $Na_4Al_3Si_3O_{12}OH$, zeolite Y $Na_{1.88}Al_2Si_{4.8}O_{13.54} \cdot 9H_2O$ and P $Na_{3.6}Al_{3.6}Si_{12.4}O_{32} \cdot 12H_2O$, depending on the Si/Al ratio (from 1 for hydroxysodalite to 3.4 for Si/Al=3.4). Hydroxydalite can also appear in kaolin-based geopolymers (Davidovits, 2011). The presence of zeolites (peaks in XRD) in Criado et al. (2007) was more obvious over time (related to the elevated temperature – samples in the oven till testing) which is also confirmed by Oh et al. (2010). Apart from long times of curing developing zeolites in expense of the gel formation, increasing the curing temperature and/or water content also increases the crystallinity (Provis and Bernal, 2014). Hydrotalcite may also be formed for high in Ca FA (as in AAS) while hydroxycancrinite, levyne, franzinite nahcolite ($NaHCO_3$), natrite (Na_2CO_3) and albite ($NaAlSi_3O_8$) are other zeolites detected for use of sodium-based solutions (Oh et al., 2010, De Vargas et al., 2011).

It should be noted that there are also some authors who did not observe any zeolites (Palomo et al., 1999, Bernal et al., 2013). As Rees (2007) states that could be because the crystal is smaller than 8nm or a peak is less than 3% by weight of the crystal present. Rees (2007) also mentions that for samples of the same Na/Al ratio and different Ms, the XRD patterns will have the same location of peaks but different intensities. Generally, activation using silicates of molar ratio SiO_2/M_2O between 1-2 compared to activation using NaOH, tends to less crystallising, leads to matrix of higher homogeneity in microstructure, higher compressive strength and lower porosity (Criado et al., 2007, Lloyd et al., 2009, Fernández-Jiménez et al., 2005, De Vargas et al., 2011). Higher modulus of the alkaline solution would, first, lower the pH and consequently lower the degree of reaction but also, it would increase the viscosity of the mix and limit the free diffusion of components. Generally the composition of the hardened binders is difficult to systematically study as the matrices are heterogeneous from the nanometers scale to centimeters and include many phases some of which might change over time (Provis and Bernal, 2014).

FA is the most used raw material in geopolymer binders and as it is considered representative of the geopolymer category and Table 3 summarises atomic ratios for FA-based geopolymers which have been activated using NaOH only or sodium silicate/+NaOH/+carbonate. Si/Al is the most representative ratio from this category and

ranges considerably, mainly in the range of 2.0-4.0. Generally higher Si/Al ratios are related to higher compressive strength and excessive addition of alkalis could lower the Si/Al ratio (because of hindering dissolution) but also increase the Na/Si and Na/Al ratios, revealing formation of zeolites and/or precipitation of sodium silicate (Komljenović et al., 2010). When the percentage of atomic Si detected by EDX is increased, Al also increases but at a lower rate (Komljenović et al., 2010). Activation using NaOH forms geopolymers of lower Si/Al than activation using sodium silicate, again, as in AAS, due to the presence of more silicate in the mix (Fernández-Jiménez and Palomo, 2005). For constant Ms the Na/Si increases with increasing Na_2O (Winnefeld et al., 2010). Also Table 4 refers to blends of FA/slag (in different mass ratios) and the authors provide the same atomic ratios that are of interest for slag (Bernal et al., 2013, Yang et al., 2012b).

2.4.3 Important parameters for the alkali-activation

There is a very recent overview of parameters which affect geopolymer concrete by Part et al. (2015). According to this review the most important parameters are:

- the chemical composition of the precursor
- the alkaline activator, in the sense that they are the base for the chemical composition of the product, and
- the curing regime

They all have an effect on the mechanical, microstructural properties of the final product and therefore its durability. As there are many factors of importance and in reviews many of these details can be found, this section will only briefly review the role of chemistry and curing.

2.4.3.1 Design of mixes by tailoring chemistry

Formation of geopolymers and AAC are based on tailoring the alkaline activators to specific precursors (Van Deventer et al., 2012), meaning it is not a simple parametric analysis design. The "*Recommended practice on GP Concrete*" (Concrete Institution of Australia, 2011) suggests all geopolymeric pastes to be described in four ratios:

(1) The "*Fluids: Binder ratio by mass" where* "*fluids*" are everything that can be included in the alkaline solution, total water, sodium/potasium silicate and sodium/potassium hydroxide. A high ratio will increase workability, but will reduce the quality of fresh geopolymer.

(2) Another related factor is the H_2O:Na_2O mass ratio, meaning the concentration of the activator solution which determines the degree of dissolution. Low H_2O:Na_2O ratio,

therefore high concentration leads to robust geopolymers while very high H_2O:Na_2O ratios form zeolites instead of geopolymers.

(3) Atomic Si:Al ratio and

(4) Mass ratio of SiO_2:Na_2O. It is noted that Si dissolution correlates with strength and is related to reactivity in aluminosilicates (Xu and Van Deventer, 2000, He et al., 2000) which is discussed later.

It has been well known that the type of alkaline activator has the most important effect on the flexural and compressive strength of the alkali-activated binders, with the blend of sodium silicate and sodium hydroxide giving the strongest mixes (Fernández-Jiménez et al., 1999). Likewise, Duran Atiş et al. (2009) tried three alkaline activators, sodium hydroxide, sodium silicate and sodium carbonate, to activate slag and the compressive and flexural strengths were highest for $SiO_2 \cdot nNa_2O$> Na_2CO_3> NaOH. Use of NaOH only results in higher permeability (Shi, 1996) compared to activation using sodium silicate, and sometimes in efflorescence as often the reaction is still not fully complete when the binder hardens so that alkali-rich solution resides in pores (Najafi Kani et al., 2012).

The alkali content in a mix has been found to be the second most important factor for strength development, after the type of activator (Fernández-Jiménez et al., 1999). It is shown that generally an increase in the alkali content of the activator leads to improved compressive strength (Wang et al., 2005). For metakaolin activated by NaOH 4-12M solution and sodium silicate of Ms=3.3 (the two solutions in constant mass ratio 4.15:1) the mix gave compressive strength 40MPa for NaOH 6M but 65M for NaOH 10M and 12M, although for 12M there was no further significant strength increase, but there is a cost and environmental impact increase. The trends for flexural strength and apparent density were similar to that of the compressive strength. The results were attributed to higher dissolution at high concentration of NaOH. The same outcome was observed for kaolin activation by Heah et al. (2013b) who also suggested that excessive content of alkalis (14M NaOH in their case) was not beneficial for the binder and this was included when referring to the tables of atomic ratios. For this reason the Na_2O content of the activator will be stated in the following chapters when referring to the composition of binders.

Related to the concentration of the activator is also the fact that for high strength the water to binder ratio in geopolymers and AAM has to be low (van Jaarsveld et al., 2002, Concrete Institution of Australia, 2011). Water plays a role in dissolution and polycondensation. As in zeolites, higher water content leads to formation of larger crystals for geopolymers based on FA. Areas of pseudocrystallinity increase in size for higher H_2O/SiO_2 molar ratio leading to a decrease in the specific area of the sample (van Jaarsveld et al., 2002). Low water content in concrete usually implies the use of solid NaOH and dry aggregates (or of controlled moisture) (Concrete Institution of Australia, 2011). Figure 20 shows the extent of decrease in strength that takes place for binders of different FA/slag ratios (100:0, 25:75, 50:50, 75:25, 0:100) by Marjanović et al. (2015).

Blends of precursors may lead to improved properties of fresh and hardened cement products. FA/slag of 25:100 had equal or higher (up to 10MPa) compressive strength than AAS (FA/slag 0:100) for high alkali concentration (10% Na_2O) and various Ms. The binders containing more than 50% FA had lower strength. This is expected as FA and metakaolin need higher alkalinity than slag (Ismail et al., 2013b, Bernal et al., 2012a). Ismail et al. (2013b) used activator of Ms=1 and 8% Na_2O content for blends of slag above 50% and 12% for blends of less than 50% slag content to activate mortar and concrete based on FA/slag blends. Ismail et al. (2013b) found little decrease for 25:100 FA/slag mortar compared to 0:100 based binder (<10% difference), but slightly higher compressive strength for the equivalent concrete samples (<5% difference). It should be noticed that their 50:50 concrete samples had the same strength as 0:100 FA/slag-based samples, although in mortars the strength after 28 days was 35% lower. Chi and Huang (2013) found that 50:50 is the optimum for both Na_2O contents used, 4% and 6%, and during all the ages of testing. The second best was FA/slag 30:70 and then 0:100. The Ms of the alkaline solutions used was 1.0. Yang et al. (2012b) activated FA/slag and found the mass ratio that leads to the highest compressive strength is 20:80. The second best was FA/slag 40:60 close to the strength of 100% slag. Therefore the above studies agree that 50/50 FA/slag suggests the maximum percentage of FA incorporation in the blend which can provide binder of similar strength to binder based on 100% slag. The incorporation of high FA content is of interest due to the shortage of slag (section 1.3).

Apart from the FA/slag mass ratios, the authors used different solutions of Ms=1.2, 1.4, 2.0 of increasing alkalinity and the compressive strength had increasing trend from Ms=1.2 to 1.4 but decreased significantly for Ms=2.0 (strength lower than that using Ms=1.2). The increase from Ms=1.2 to 1.4 is because of the higher dissolution caused by the higher alkalinity while the decrease of strength for Ms=2.0 was attributed to excessive alkalinity and dissolution which does not cause though even reaction degree. The pastes in this study had w/b=0.42, were demoulded after 24h in sealed bags and then put at 50C for 48h, before finally being left at room temperature till testing. It should be noted that for given level of slag content in the blend, the differences between pastes activated using the three Ms values had no obvious difference in XRD analysis. Therefore the differences of the matrices are not of crystalline or semi-crystalline nature which is detected efficiently by XRD.

Other than blends of FA/slag, Ren et al. (2014) in an effort to design a mix which incorporates aluminum sludge to improve mine waste geopolymers, observed which ratios Si/Al and Na/Al (instead of giving the mass SiO_2:Na_2O ratio suggested by the Australian Concrete Institution) give the optimum design. Figure 21 and 22 show the graphs the authors composed based on work of other researchers. These graphs do not include ratios from GGBS-based AAM which have different mechanism of activation. The citations that Ren et al. (2014) used can be find in their paper and are not listed here. It is understood that these results are based on calculations of design in the overall mix and are not the actual compositional values (which can be found by EDX). The Si/Al ratio shows variation but

most of the values are close to 2.0. The Na/Al ratio on the other hand is in the range of 1.0-1.3. Si/Al ratio equal to 2:1 is also stated in the "*Recommended practice on GP Concrete*" for low calcium systems and by Duxson et al. (2005) as the optimum ratio. Bernal et al. (2012a) activated slag with up to 20% substitution by metakaolin and expressed the results in relation to the overall SiO_2/Al_2O_3 ratio in the mix. Three values were used: SiO_2/Al_2O_3 equal to 3.6, 4.0 and 4.4 (atomic Si/Al ratio of 3.18:1, 3.53:1, 3.89:1 by stoichiometry). As the Na_2O/SiO_2 ratio in the mix was designed constant at 0.25, the increasing SiO_2/Al_2O_3 led to increasing amount of Na_2O, higher for each increasing the slag substitution level. It was found that 10% of slag substitution of slag to metakaolin resulted in higher strength but 20% of substitution did not much further contribute to strength with maximum strength do not exceeding 80MPa for any mix.

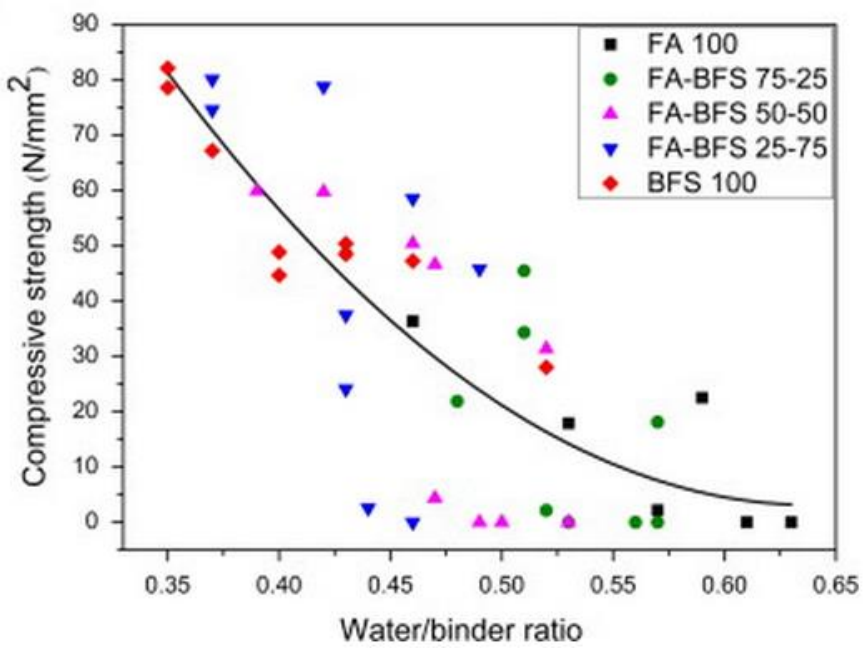

Figure 20 Effect of water/binder ratio for AAC mortars based on blend of FA/slag. (from Marjanović et al. (2015))

Duxson et al. (2007c) has stated that based on aluminosilicate precursors with Si/Al< 1.0 or >5.0, dissolution in water of the formed geopolymer might occur. This is also related to the high Na/Al ratio and presence of alkali in the geopolymer structure, therefore they suggested that the precursor to have 1 < Si/Al < 5 and a Na/Al ratio close to 1.0. With that in mind, Ahmari and Zhang (2013b) used Si/Al of 7.76 and a Na/Al of 0.86 and 1.73 in two samples of mine tailings-based geopolymer bricks. The sample of Na/Al=1.73, the furthest from 1.0, indeed significantly lost strength after immersion in water.

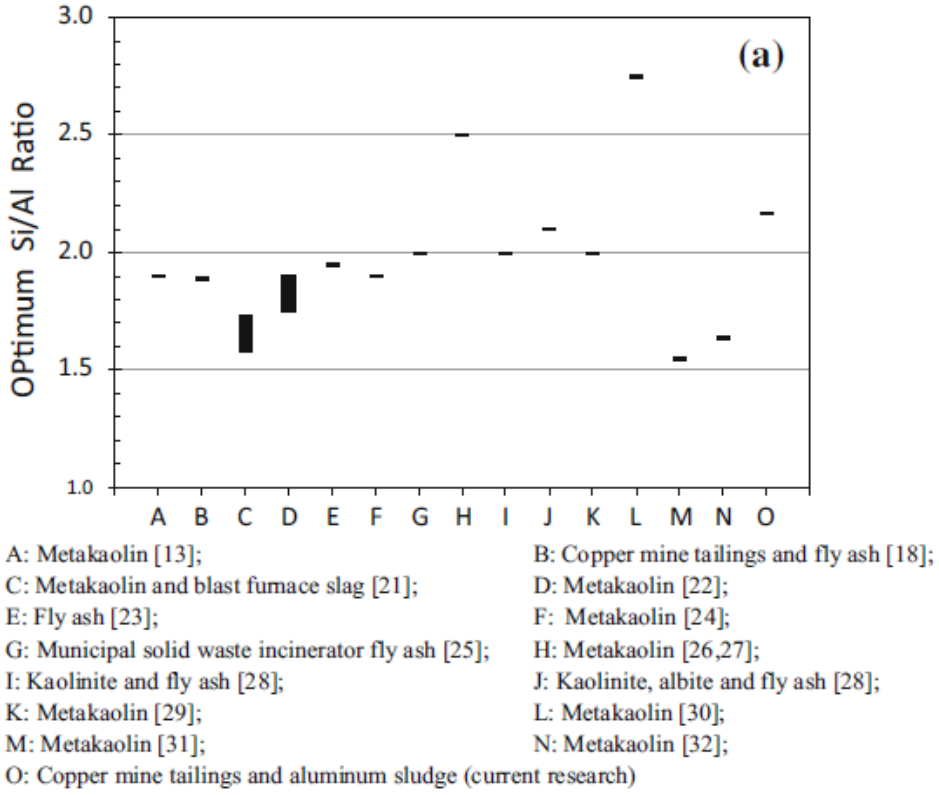

Figure 21 Si/Al ratios in optimum designs from different researchers studying geopolymers. (from Ren et al. (2014))

As all the ratios mentioned largely derive from the precursor, it is important to know which oxides are related to specific properties. For example in AAS, a high content of MgO is beneficial. Haha et al. (2011) observed that alkali-activated GGBS using sodium silicate would reach higher compressive strength for higher MgO content. That was related to the enhanced coarse porosity of the matrix which derived from a higher amount of formed hydrotalcite. Both Haha et al. (2011) and Bernal et al. (2014) (see Table 2) have stated that higher MgO content reduces the incorporation of Al in the C-A-S-H and Bernal et al experimentally showed that formation of hydrotalcite enhances the resistance in natural carbonation as it acts as an internal CO_2 sorbent. In Bernal et al. (2014) hydrotalcite was identifying for MgO>5% while for at MgO<5% gismondine was detected instead.

The low content of iron(III) oxide is also a good indication of a reactive GGBS as the iron rich phases of minerals, as hematite, magnetite, magnemite do not contribute to gel formation. In the case where slag is added in the mix or the fly ash has relatively high calcium content, hydrate phases will form by the reaction of calcium with aluminum and silicon, in addition to the aluminosilicate gel discussed above. The hydrates are similar to Portland/slag blends and slag-based alkali activated binders (Puertas et al., 2014).

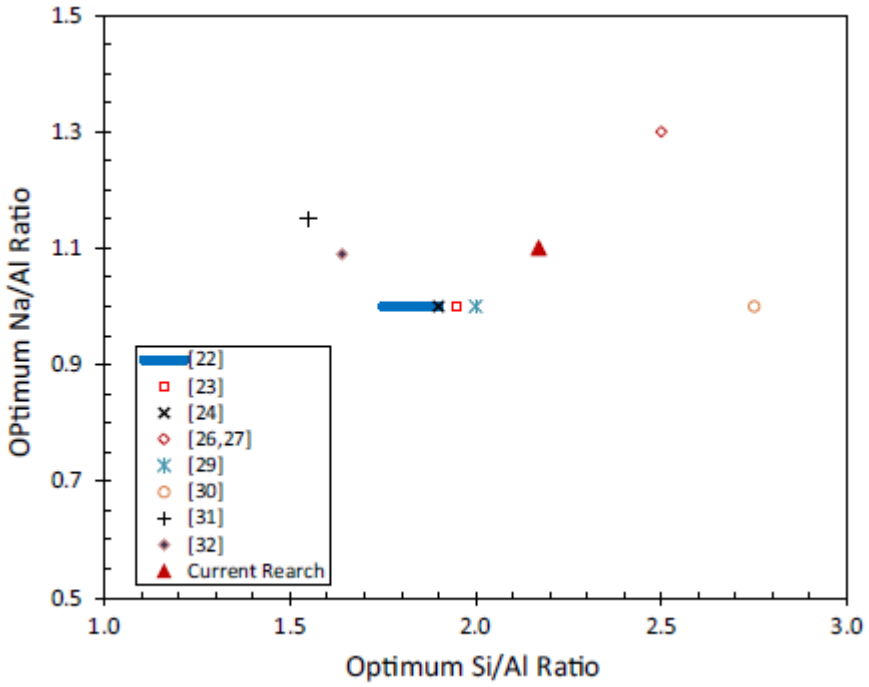

Figure 22 Na/Al vs Si/Al ratios in optimum designs from different researchers studying geopolymers. (from Ren et al. (2014))

Haha et al. (2012) (see Table 2) investigated the role of Al_2O_3 of raw slag in alkali activation. Three types of slag were used of Al_2O_3 content about 7%,14% and 17%. They found that higher Al_2O_3 decreased the Mg/Al ratio of hydrotalcite in the products and led to higher incorporation of Al in C-A-S-H. For Al_2O_3 17%, strätlingite was formed in dispense of hydrotalcite. Moreover, higher Al_2O_3 content delayed the hydration resulting in lower early compressive strength but had no impact on the 28day (or later) to the extent of hydration, volume of hydrates or strength. Generally, the different Al_2O_3 content of slag was found not to alter the microstructure of the final product in terms of porosity and amount of unreacted slag particles by the end of 1 year. The atomic Ca/Si ratios of the product phases for various ages, were not affected by the Al_2O_3 content. It should be mentioned that the molar Ca/Si in the three types of slag was the same, equal to 1.01. The EDX results were collected at 7, 90, 180 and 360 days but for the same samples, the age did not significantly affect the results of Ca/Si and Al/Si atomic ratios for either activation using NaOH or sodium silicate. On the contrary the Mg/Al atomic ratio had a decreasing trend over time in slags of high Al_2O_3 content and for activation using both, sodium silicate or NaOH (see Figure 19). The atomic ratios for the different slags, on day 180, can be seen in Table 2. It is seen that activation using sodium silicate or NaOH have small differences in atomic Si/Al, Ca/Si and Mg/Al and almost no difference in Al/Ca, however it is very important that the systems

involve slags of the same molar Ca/Si and the same alkalinity (Na_2O content). Bernal et al. (2014) also found same range of atomic Ca/Si for all ages of samples analysed in EDX.

2.4.3.2 Setting times

It is found in slag-based AAC mixes that prolonged mixing enhances later properties (enhances strength and reduces shrinkage without altering the the mineralogical and chemical composition of the products) of the hardened material (Palacios and Puertas, 2011), however the mixing time will also depend on the setting time of the binder. Studies have shown that AAS may have very short times of setting (initial setting even less than 30minutes) and which is also associated with drying shrinkage (Duran Atiş et al., 2009). It should be noted that different batches of precursor may show different setting properties with Brough and Atkinson (2002) reporting differences in the setting time of slag even within a batch. The setting time and mechanical strength of alkali-activated slag for three types of activator have been studied by Fernández-Jiménez and Puertas (2003) who concluded that the pH is important for the initial dissolution of slag, that silicon anions in the solution accelerate the setting time and anions from Na_2CO_3 solution delay the setting time. This is confirmed by Duran Atiş et al. (2009), Table 5, where activation of slag using "LSS", liquid sodium silicate, had much shorter setting times than use of "SC", sodium carbonate. The same study also shows that for constant alkaline content (8% Na_2O), increasing the Ms slightly increases the initial setting times and has the opposite result on the final setting times. Taking into account the effect of Ms on PC, it is seen that the Ms definitely decreased the final setting times. Increasing the alkaline content from 4%-8% Na_2O (use of "SH", sodium hydroxide) clearly resulted in decrease of the setting times.

Regarding FA, Hardjito et al. (2008) in a study of low calcium fly ash measured the setting times for different temperature of curing: at 60°C the initial and final setting times were 230 and 270minutes respectively, at 70°C was 177 and 240, at 80°C was 129 and 165min, therefore for increasing temperature the setting times were shorter and there was significant time between initial and final setting time. The paste would not harden for at least one day. On the contrary, a blend of coal fly ash and metakaolin (Wang and Cheng, 2003) set quickly, with 60 and 65min initial and final setting time at 60°C. The paste of Wang and Cheng (2003) could also set at the ambient temperature, with 7 and 9.5hours initial and final setting time. However, this is due to the inclusion of metakaolin which may set at room temperature reaching though lower strength than for curing at elevated temperatures (Mohsen and Mostafa (2010), see 2.7.3). The non-setting or long time for hardening of geopolymers is the reason that heat curing is broadly used (Ahmari and Zhang, 2013b, Wang et al., 2005, Marjanović et al., 2015). A study on high-in-calcium FA geopolymers (Chindaprasirt et al., 2012) tried to control the setting time by adjusting the overall SiO_2/Al_2O_3 ratio of the mix, in the range 2.87–4.79. The activation took place using a 10M NaOH solution and the SiO_2 content was adjusted by adding RHA (not sodium silicate). It was shown that the higher the

addition of SiO_2 was in the activator the quicker was the setting. The initial setting time for increasing SiO_2 content was 60 to 20min and the final time 100 to 40min.

Table 5 Initial and final setting times for activation of PC and slag using different activators (after Duran Atiş et al. (2009))

Binder	Activator Type	Concentration	Initial Setting (min)	Final Setting (min)
PC	-	-	200	315
	Liquid Sodium silicate (LSS)	4% Na, Ms=0.75	26	127
	LSS	4% Na, Ms=1.00	15	70
	LSS	4% Na, Ms=1.25	24	58
	LSS	4% Na, Ms=1.50	35	54
	LSS	6% Na, Ms=0.75	22	77
	LSS	6% Na, Ms=1.00	28	65
	LSS	6% Na, Ms=1.25	33	55
	LSS	6% Na, Ms=1.50	35	50
Slag	Liquid Sodium silicate (LSS)	8% Na, Ms=0.75	19	63
	LSS	8% Na, Ms=1.00	15	60
	LSS	8% Na, Ms=1.25	24	56
	LSS	8% Na, Ms=1.50	31	47
	Sodium Hydroxyde (SH)	4% Na	21	59
	SH	6% Na	9	34
	SH	8% Na	4	28
	Sodium Carbonate (SC)	4% Na	190	306
	SC	6% Na	180	294
	SC	8% Na	170	288

In Marjanović et al. (2015), Ms=1.0 and 1.5 and Na_2O equal to 7% and 10% was monitored for the setting time. The pastes were based on FA/slag: 100/0, 50/50, 25/75 and 0/100. Interestingly, the FA geopolymer set quicker than the AAS for most of the activator combinations used and the setting times of pastes which were based on FA/slag blends would fall in between. However, although the pastes are said to cure at 95°C before imaging in SEM, it is not clear if the monitoring indeed took place in the oven as it is also mentioned that the test was according to SRPS EN 196-3 using the Vicat needle where there is no provision for such curing conditions. For most of the pastes monitored, the initial and setting times was more than 60minutes and less than 350minutes (about 6hours). The authors reported that the alkali concentration is of major importance for setting time as for 10% Na_2O

the setting times were much longer than for use of 7% Na_2O. This shows opposite trend for increasing Na_2O compared to Duran Atiş et al. (2009) which is likely due to the complexity of Si and Al dissolution for the different alkali contents that were used, especially after taking into account that Marjanović et al. (2015) used inconsistent water/binder ratios (the mixes measured for setting time are included in Figure 20). Also this contradiction is also an example showing the importance of using a range of formulations of alkaline solutions before concluding to the optimum binder as different aluminosilicate sources may respond differently to the conditions used. Regarding the Ms, the results did not show a specific trend: the setting time mostly decreased for increasing Ms, when Na_2O was 10%, while for Na_2O 7% the setting time remained mostly unchanged. Considering the studies mentioned studies (Chindaprasirt et al., 2012, Marjanović et al., 2015, Duran Atiş et al., 2009), increasing the Ms rather accelerates the setting time however there are variations.

Moreover, in Marjanović et al. (2015), regarding the different FA/slag ratios used, delay occurred in the setting times for higher content of slag and for most of the activators used. This is in contrast to Jang et al. (2014) who also studied blends of slag/FA but found that higher content of slag leads to shorter setting times (with 30% substitution of FA by slag leading to up to 85% decrease of the initial and final setting time). However in Jang et al. (2014) the setting times have been measured for mixes which involve superplasticizers (more details will be given later) so this could have created implications.

2.4.3.3 Curing

AAS hardens at ambient temperature while low calcium geopolymers usually need heat to set as mentioned above. In both cases authors often report keeping the relative humidity high to avoid quick evaporation of water from the samples. This practice is reported for binders and mortars but seems not to be significant for concrete which may be due to the size of the samples, as for small samples usually used for binders all variation in temperature and relative humidity of curing may have impact on the mechanical properties. Generally, curing has been reported to be a parameter affecting the properties of AAS but is less important than the tailoring of the chemistry according to Fernández-Jiménez et al. (1999). Therefore the focus here is on the more complicated curing of geopolymers.

The maximum temperature for geopolymer formation is 90°C (Duxson et al., 2007a, Davidovits, 2011). Temperatures of curing higher that 90°C have been investigated by authors (Heah et al., 2011a, Mohsen and Mostafa, 2010) but as expected they destroy the amorphous content of the product. Davidovits (2011) states that polycondensation at 50°C requires about 4hours, at 85°C about 1.5hours and at 95°C about 0.5hours. However scientists use various durations for heating: Ren et al. (2014) cured their AS+mine waste geopolymer specimens at 90°C for 7days. The samples were already demoulded when put in the oven, which was possible as they had been first pressed in small cylindrical moulds (33.4mm diameter, 72.5mm height) using 0.5MPa for 1min. Similar was the way that Ahmari

and Zhang (2013b) cured their bricks, (pressed, demoulded, at 90°C for 7days uncovered) but first left for 6hours at room temperature. Wang et al. (2005) used 65 °C for 10 h.

Table 6 Example of strength development for curing in the oven with and without keeping the relative humidity high for a matrix containing fly ash with compositional variables: clay (kaolinite) content= 15% (mass), water/fly ash (mass)=0.31, M_2O/SiO_2=1.14, Al_2O_3/SiO_2=0.57 and K as alkali metal activator. (After van Jaarsveld et al. (2002))

	Temperature (°C)					
Time (h)	30	50	70	30 B	50 B	70 B
6	6	-	14	19	-	28
12	15	26	34	7	22	21
24	20	12	33	19	24	29
48	19	-	28	21	-	15
Average (12/24 h samples)	17	19	34	13	23	25

Samples were cured in an oven, open to the atmosphere except for samples denoted by "B" which were cured in sealed plastic bags under the same conditions. Compressive strength values in MPa.

There are authors who stated that prolonged curing, more than a few hours, at high temperature does not further contribute to strength and that there should be remaining water in the structure because it prevents cracking while extensive duration of heating dehydrates the samples, breaks the gel-structure without leading to a semi-crystalline matrix and causes shrinkage. (van Jaarsveld et al., 2002) Curing the fly ash/kaolinite geopolymers in sealed bags, keeping the relative humidity high, did not improve the compressive strength in all cases (Table 6) However, prolonged curing is not necessarily detrimental, Criado et al. (2007) oven cured the specimens at 85°C using a relative humidity >90% for 8 h, 7, 28, 60, 90 or 180 days and the compressive strength was gradually developed from 20-40MPa to 70-90MPa (several mixes). The difference between van Jaarsveld et al. (2002) and Criado et al. (2007) is probably because the use of bag under high temperatures might not be enough to keep the relative humidity high and constant.

2.4.4 Superplasticizers

The need to keep the water content to a minimum while having a workable mix has led to investigation of suitable plasticizing admixtures and superplasticizers. According to BS EN 934-2:2009+A1:2012 admixture is a material added in ≤5% by mass of dry cement during

mixing to affect the properties of the fresh and hardened mix. The majority of admixtures refers to water reducing/flow increasing. Van Deventer et al. (2012) underlined the importance to develop a whole set of new admixtures for the geopolymer system, as most of the various admixtures used to control slump, air dispersion, water retention, and other properties of the OPC system are less effective in the geopolymer system and the existing range of commercially available superplasticisers, developed specifically to suit the complex series of chemical reactions in the OPC system, are usually not effective in the geopolymer system. It has been stated that commercial SPs are attacked by the alkaline solution (Concrete Institution of Australia, 2011, Nematollahi and Sanjayan, 2014b) and on this basis the Concrete Institution of Australia (2011) suggests that some SP can work if added with some water to the solids to disperse the precursor particles before adding the activator in the mix. A review by Nematollahi and Sanjayan (2014b) is enlightening regarding the effectiveness of superplasticizers (SP) in AAS and FA-based geopolymer. It is also extensively compared to the review of Part et al. (2015) on this topic. Publications on AA slag and FA geopolymers were reviewed and showed variation of results which were sometimes contradictory. This was attributed to the variation of several conditions including nature of precursor, nature and concentration of activator, type of SP and dosage, curing conditions.

Regarding AA slags, there are studies reported where vinyl copolymer and polyacrylate copolymer (Puertas et al., 2003), melamine-based SP (Wang et al., 2009), lignosulphates and naphthalene (N) based SP (Douglas and Brandstetr, 1990) did not have any effect of workability. A common issue about the use of SP in slags is that the strength may decrease (Wang et al., 2009, Bakharev et al., 2000). According to Puertas et al. (2003) who performed a calorimetric study for systems activated by NaOH+silicate, it was found the decrease in strength that vinyl copolymer caused is related to the delaying in the activation process that it caused. Based on work (Palacios and Puertas, 2005, Palacios and Puertas, 2004) where naphthalene (N) based SP improved the workability, compressive and flexure strength and delayed the setting times for activation using NaOH solution only, Nematollahi and Sanjayan (2014b) suggest N based SP to be the most efficient for the specific type of activation (slag+NaOH). That was attributed to the fact that only N-based SP is chemically stable in NaOH. One of the most recent studies on the use of SP in AAS (Palacios et al., 2009) used 0.005M and 2.57M NaOH (pH equal to 11.7 and 13.6 respectively) and found that the rheological properties, yield stress and plastic viscosity, were dependent on the pH. That could be explained by Kashani et al. (2014) who found that the yield stress of AAS is rapidly increased for higher reaction rates, hence higher for activation using NaOH, especially at high concentration, rather than silicates. In Palacios et al. (2009), N-based SP was able to affect these properties at high pH (13.6). However, the adsorption of N-based SP and vinyl copolymer, independently of the pH, was 3-10 times lower than in PC mixes. Pan et al. (2014) found a way to increase adsorption. They tested aminosulphonate (AS) based superplasticizer in AAS activated by NaOH and found that use of YP-3 retarder increases the

adsorbed AS and leads to improved rheological properties. There was no testing of strength though. Therefore although the understanding is growing, in practice, for activation of slags using both sodium silicate and NaOH there is not yet a proven efficient SP.

Regarding FA geopolymers, Nematollahi and Sanjayan (2014b) concluded that among vinyl copolymer, polyacrylate copolymer, polycarboxylate and N based SP, the most efficient is modified polycarboxylate for activation using sodium silicate+NaOH. In contrast with the AA slag where it is a common problem reported, decrease of strength is not often reported; Kong and Sanjayan (2010) reported up to ~50% decrease in strength for use of polycarboxylate and ~20% for N based SP (KOH+silicate being the activator) while Hardjito et al. (2005) reported decrease for use of naphthalene sulphonate superplasticizer when the content was higher than 2%. For ≤2% the workability was improved without causing decrease in strength. Another type of superplasticizer, a polycarboxylic-ether hyperplasticizer was also tried but this type did not show any significant difference in the workability of the fresh fly ash-based geopolymer concrete and increased costs.

A study not found in recent reviews (Laskar and Bhattacharjee, 2013) tried polycarboxylic-ether-based superplasticizer and lignin-based plasticizer in FA-based geopolymer concrete. The authors found 4 M to be a critical molar value for NaOH with lower molar causing a decrease in yield stress and plastic viscosity and increase in slump and lignin-based SP being the most efficient in altering workability. For NaOH greater than 4M both admixtures had an adverse effect on yield stress, plastic viscosity and slump. Not based on the molarity of the NaOH activator, but based on the type of activators of approximately the same pH, is the study of Nematollahi and Sanjayan (2014a) who investigated the effect of six SPs in a FA geopolymer. The pH of the two activators used, NaOH (8M) and a mix of NaOH (8M)+sodium silicate, was 13.32-13.36. Two N-based SP, one melamine and three modified polycarboxylate admixtures were used as 1% by mass of class F FA. All samples were cured at 60°C for 24h and tested in compression on day 3 as the authors considered that the strength would not develop further and that was equivalent of the 28day strength for PC. The results showed that for activation using only NaOH, the N-based SP greatly improved the workability (136% based on the mini slump test) without having an effect on the compressive strength comparing to samples without SP. For activation using only NaOH+sodium silicate, the melamine-based SP decreased the workability but all the other SPs increased it. However, all of them reduced the strength. The authors suggest that the three polycarboxylate SPs were the most effective as they caused 39-45% increase in slump and 16-29% decrease in strength while the other three SPs cause worse combination, less than 10% increase of workability and about 50% reduction of strength. But having some decrease in strength for the "most efficient SP" automatically makes it not ideal.

Jang et al. (2014) studied blends of slag/FA activated by NaOH(4M)+silicate, cured at ambient conditions. 0-4% of polycarboxylate-based and naphthalene-based superplasticizers was added in the mixes. In this study the polycarboxylate-based SP was proved to be better

than the N-based, as it delayed the setting time without affecting much the heat of hydration and was better in improving the workability. It is worth noting that the products after addition of SP were not observed different in SEM/EDS. The results of compressive strength were complicated, with the polycarboxylate-based superplasticizer increasing and decreasing the strength depending on the ratio of slag/FA in the blend and without a smooth trend over time (adverse effect observed for 50/50 slag/FA after 7 days of curing).

SPs are used in studies which have other main focus and therefore might be not very detailed about the effect on workability and strength compared to mixes without SP. For example Pacheco-Torgal (2008,a) used SP, without giving details on its type, for some of their tungsten mine waste+lime mortars. For up to 2% SP by mass of binder the compressive strength of the mortars increased by up to about 35% on day 28. The percentage was higher at earlier ages where the mortar without SP had slower development of strength. The workability could not be measured because of technical issues related to the high viscosity of sodium silicate in the mix. However, the increase in strength was attributed to better packing and lower porosity in mixes with SP and also to delay in setting time leading to higher amount of Si and Al ions. Another study which uses SP in AAM other than based on slag or FA, is by Pacheco-Torgal et al. (2011). Investigations are based on activation of metakaolin using NaOH of 10-16M and 1-3% of SP content. The SP is supplied by "MAISOL - FPR" but again, no additional information was supplied. The results showed that increasing molarity decreases the workability (highest workability at 10M) but positive results are shown for using SP (significant differences only for 3% of SP). Mixes of 16M were not affected by the addition of SP. Another aspect of this study is the substitution of metakaolin with 5 and 10% of $Ca(OH)_2$. For addition of $Ca(OH)_2$ the trends of workability for increasing molarity of NaOH and increasing SP content remained the same but for 10% $Ca(OH)_2$ the response of workability to increasing SP was much greater. Characteristically, mix of 10% $Ca(OH)_2$ and 3% SP almost doubled workability and had the same compressive (tested till day 28) and flexural strength levels. For addition of $Ca(OH)_2$ even the mixes of 16M increased their workability when SP was added. The compressive strength for given value of $Ca(OH)_2$, did not show significant changes depending on the SP content. It is noticed that both these studies by Pacheco and colleagues present very good results compared to the problems that other authors faced when investigating other AAM (based on slag and FA) as shown above and maybe that could be attributed to the reaction of lime to SPs, similar to the case of OPC.

Although there are some SPs indicated which may be not ideal, but suitable for AAC technology, it was considered that this study should not rely on such admixtures as there are significant advances to be made in this topic.

2.4.5 Durability

The targeted uses of concrete roofing tiles and concrete blocks have prerequisites of performance described in BS EN 490:2011 and EN 771-3:2011 respectively. In these standards water permeability and resistance to freeze-thaw are the required tests for durability. Although testing the resistance to carbonation is not included in the standards above, it is discussed here as it is related to loss of strength and increased permeability (Forde and Institution of Civil, 2009). Other aspects of durability, related to concrete reinforcement or special conditions as fire resistance and chemical resistance, are beyond the scope of this study.

Pacheco-Torgal et al. (2012) reviewed studies on freeze-thaw, carbonation, shrinkage resistance and other aspects of durability such as alkali–silica reaction, acid attack and fire/heat resistance. All the papers reported regarding resistance in freeze-thaw either based on slag, FA or blends, showed improved performance and where compared to PC based mixes. The latest studies in this area confirm this outcome. Sun and Wu (2013) mixed mortars based on FA activated by an alternative silicate based on silica fume, NaOH and distilled water. The samples cured at 75°C for 12h and then left at room temperature. OPC samples were used as control samples. After 300 freeze-thaw cycles according to ASTM C666 there was -1.4% mass loss for the PC sample and 0.17 mass gain for the geopolymer mortar while the loss of compressive strength was 20% and 5% respectively. Loss in dynamic modulus was 8.4% and 6.8%. In this study the PC had low aggregate content of sand/cement equal to 1.2 and W/C = 0.38, supposedly equivalent to the geopolymer mix. The results were improved for both PC and geopolymer when 2% by mass air entraining agent was used. The fact that some air voids in samples enhance the freeze-thaw resistance, this time in AAS concrete, is also stated by Cai et al. (2013). The freeze-thaw testing (according to ASTM C666) was conducted for slag activated using NaOH+silicate solution and showed excellent resistance. Based on this test models were developed to predict performance. Three factors were important, the slag content, the solution/slag ratio and to a lesser degree, the "sand ratio" (not indicated in the research but probably meaning sand to total aggregate ratio). An increase in the slag content for constant other two factors was positive for the frost resistant coefficient, while an increase in the solution/slag and sand ratio had an adverse impact and decreased the coefficient. This study noted that the software developed provided a good fit for the given raw materials, but for different compositions it should be revised. The good performance of AAS in freeze-thaw is attributed to the low water permeability offered by the low in Ca/Si ratio C-A-S-H gel, which subsequently prevents saturated freezing of concrete, and also to the absence of "mass $Ca(OH)_2$" as in PC.

The N-A-S-(H) type of gel has lower filling capacity than C-A-S-H gels which is the reason that the low water permeability of the AAS is observed (Bernal et al., 2012a, Provis and Bernal, 2014). Concrete of AA blend of slag and up to 20% metakaolin was tested by Bernal et al. (2012a) in total porosity and absorption according to ASTM C642-06 (includes

a stage of drying at 100 °C for 24 h) and capillary sorptivity based on EMPA-SIA 162/1. The concrete had in total 400kg/m^3 slag+metakaolin and was cured at relative humidity 90% at 25±5 °C. In this study there is no comparison with OPC but the results showed that all the durability aspects were suitable for high performance concrete without being clear how the performance of high performance concrete is defined. Densification of the pores and pore refinement was observed over time which was more evident for use of slag only (without metakaolin). Addition of metakaolin and higher concentrations of activator (NaOH+silicate) reduced the water sorptivity. However, the capillary when associated to the permeable pores did not show a specific trend for increasing concentration of activator and metakaolin addition. This was attributed to "interaction and competition" of gel aging and gel composition (Bernal et al., 2012a). The presence of aggregates made more complex the understanding of the capillary pore system. Bernal et al. (2011) also compared silicate-activated slag concrete to Portland concrete in terms of water absorption and capillary sorptivity among other properties. The mixes were designed for Portland cement and slag equal to 300, 400 and 500kg/m^3, meaning the binder content of the AAC including the solid part of the activator (5% Na_2O per 100 g slag, Ms=2.4) was higher. For the same level of binder content and w/b=0.42, the PC samples had 10-20MPa lower strength than AAS. The results showed that the water permeability and capillary sorptivity of the AAS concrete was lower to the equivalent of PC, with the difference becoming significant for increasing content of binder.

FA of class F has also shown low sorptivity absorption (Law et al., 2014) for activator NaOH+silicate of Ms equal to 1.00 and 1.25, while for Ms=0.75 the sorptivity values were higher. That is probably related to the homogeneity of the microstructure when the soluble silica in the mix is high and the consequently, less porous microstructure. As Law et al. (2014) noted, it is due to the higher rate of reaction. Bleeding of the geopolymer concrete was observed which led to higher initial absorption and non-linearity of the early data compared to OPC and blended cement. Chi and Huang (2013) using a blend of FA/slag in mortars, reported less water absorption than OPC mortars, regardless of the ratio FA/slag and the Na_2O content (4%, 6%) of the activator. The design of mortars was based on ASTM C192 and 528kg/m^3 precursor.

In contrast to the papers cited above, Ismail et al. (2013b) found higher water absorption in AA concrete compared to OPC. In this study slag/FA blends (from 100% slag to 100% FA) were activated using sodium silicate of Ms=1.0 and mixed mortars of w/b=0.4, total binder to sand by mass 1:2.75 and cured in sealed bags at 30°C and concrete which had w/b such to reach 60±10MPa and 400kg/m^3 of slag+FA. The gravel used in the concrete had water absorption 1.1% and sand 0.9%. As mentioned in previously the activator used was 8% for blends of slag above 50% and higher for blend of less than 50% content. Then the sorptivity testing and measuring of the volume of permeable voids (according to ASTM C642) started. Part of the testing demands drying and the drying conditions were decided to

be 60°C for AA mortars and 100°C for AA concrete until reaching constant weight. Control mortar and concrete samples of PC (360kg/m^3 of cement) were dried at 100°C.

The results of Ismail et al. (2013b) showed that the capillary absorption coefficient is higher than OPC in almost all cases, for mortar and concrete and the addition of FA worsened the absorption (and slightly the mechanical strength of mortar). The capillary absorption coefficient increases over time (a trend which cannot be confirmed by Bernal et al. (2011) who reported only the 28^{th} day capillary sorptivity) while for PC it decreases over time. For the given condition the volume of permeable voids was 8-16% for AAC mortar while 10% for PC mortar and 14-16% for AAC concrete while about 13% for OPC concrete. Therefore the differences were small, however taking into account the difference in binder content of AAC and OPC (400-360kg/m^3) revealed that the porosity is higher for AAM. The authors concluded that the drying described in the Standards for OPC is not suitable for AAM, especially for the dense C-A-S-H gel where cracks can occur during drying, affecting the capillary suction. Moreover, it is important to consider that the OPC control mortars used in Chi and Huang (2013) this study had very low strength (20MPa) compared to the strength of AAM (60-120MPa) while Ismail et al. (2013b) compared the durability of OPC and AAM concrete of comparable strength (no greater than 5MPa difference for concrete and for mortars, referring to OPC and AAM of slag content >50%). That means that designing equivalent in terms of material quantity, mixes of OPC and AAM may lead to superior strength and other superior properties for AAM, but when comparing equivalent in terms of strength OPC and AAM then we may have different results. However, this assumption does not fully agree with the results of Bernal et al. (2011) who reported superiority of AAS over PC while relatively small differences in strength.

By comparing the case of slag with addition of metakaolin (Bernal et al., 2012a) and FA (Ismail et al., 2013b), independently of the performance of equivalent OPC mixes, it is seen that the addition of metakaolin was positive while addition of FA was mostly negative in mechanical properties and water absorption. Therefore one implies that coexistence of (C-N)-A-S-H is favourable, while the other implies C-A-S-H only is the best. However, these studies are not easily comparable as the levels of substitution were different and so are the materials used. Last, it is worth noting that no issues were reported for drying samples at 100°C by Bernal et al. (2012a) in contrast with Ismail et al. (2013b). The work of Law et al. (2014) is based on FA, therefore it is considered normal that there was no problem with heat, as removing not chemically connected water from N-A-S-(H) is not as damaging (Ismail et al., 2013a).

Data from existing buildings using AA slag show good durability (up to approximately 8mm carbonation depth) (Xu et al., 2008). Generally, the good stability of aged structures so far show that natural carbonation is not a problem for AAM but authors who compared AA slag and OPC using accelerated carbonation test (Bakharev et al., 2001, Bernal et al., 2012b, Puertas et al., 2006) report lower resistance in carbonation. Specifically, Puertas et al. (2006)

observed decalcification of the gel and found differences depending on the type of activator used. For use of sodium silicate there was loss of cohesion, increase of porosity and small, subsequent decrease in strength (14%), while for use of NaOH there was increase in strength attributed to formation of large amount of calcium carbonate in the pores which reduced the porosity. Observation in NMR (Bernal et al., 2013) showed that decalcification of the C-A-S-H gel leads to cross-linking and losing of the chain-character (extensive damage in the silicate structure in contrast to natural carbonation) at high level of CO_2 exposure. This happens because increasing CO_2 level of exposure changes the pH of the pore solution of the gel and changes of carbonate to bicarbonate. It had been observed earlier (Bernal et al., 2012b) that accelerated carbonation, a test made to simulated natural carbonation for PC, underestimates significantly the service life of AAM and is not adequate for the carbonation mechanism of AAS, however later (Bernal et al., 2013), a 1% was suggested to be the limit for accelerated carbonation test. It should be also mentioned that higher amount of binder paste in concrete can lead to a carbonation depth equal to that of OPC, with 400kg/m^3 of slag in AAS being a good compromise of durability and economy while 500kg/m^3 had superior mechanical properties and durability than equivalent OPC mixes (Bernal et al., 2011).

Blends of precursor target to better durability, however, in terms of carbonation, addition of metakaolin in slag decreased its resistance (Bernal et al., 2012a). Using accelerated carbonation, concrete samples were exposed in CO_2 concentration of 3.0 ± 0.2% at 20°C and 65% relative humidity, left in these conditions up to 1000h. Then the depth of carbonation was measured using 1% phenolphthalein in alcohol. The results showed up to 40% carbonation depth for 0% metakaolin and up to 60% depth for 20% metakaolin addition. There was also decrease in compressive strength after carbonation, up to 40% and 70% for 0% and 20% metakaolin addition respectively.

C-A-S-H and N-A-S-H behave differently in carbonation. The later carbonates mainly by forming alkali bicarbonate salts from the pore solution leaving the nanoscale of the gel unchanged after exposure to CO_2, observed by TGA and NMR (Bernal et al., 2013). Therefore it is understood that the test of accelerated carbonation is not a problem for FA-geopolymers, unless a blend of FA/slag is used where the C-A-S-H deriving from slag would have the issues mentioned above. The above provide a good explanation for the study of Sufian Badar et al. (2014) who studied three types of FA (1.97, 5.00, 12.93 % CaO content). The authors found that the low Ca content is crucial to have concrete resistant in the environment of 5% CO_2, 24±5 °C and RH 65±5% that they used (for 450 days) as the high in CaO FA, highly corroded carbon steel rods casted in the samples. There was loss of the splitting tensile strength, 4%, 17% and 34% respectively to the increasing CaO content of FA. The activator/binder ratio was 0.5. It should be mentioned that 489 kg/m^3 binder content was used which should be enough to provide a robust concrete mix. Given of the problems in testing carbonation, Ul Haq et al. (2014) tried a new method, mixing AA mortar adding sodium bicarbonate ($NaHCO_3$) and by its decomposition during curing (65°C for 24 h and later 150°C for two hours) CO_2 was produced. The results showed that ≤4% of $NaHCO_3$

should be used as excess leads to cracks and delay of the geopolymerisation. Carbonated samples with adequate amount of $NaHCO_3$ showed higher compressive strength than the samples without $NaHCO_3$. Curing at 150°C is too high for formation of amorphous phases (geopolymer) based on subsection 2.4.3.3, however in the XRD patterns presented there can be a hump attributed to the glassy phase. The chemical composition of the FA used is not given so the CaO content here is not known to compare with the study of Sufian Badar et al. (2014). If this method is indeed valid then useful observations can be made in the future for AAM.

2.4.6 Environmental assessment of AAC technology

There have been several studies recently investigating the environmental advantage of geopolymers over OPC (Habert et al., 2011, McLellan et al., 2011, Stengel, 2009, McGuire, 2012, Yang et al., 2013). Determining the environmental impact of products and materials is not an exact science as interpretation of data, boundaries for analysis and uncertainty in future processes can have a significant effect on outcomes.

While the German Federal Environment Agency (UBA) and many other bodies recognize global warming potential (generally presented as CO_2 equivalent) as the most important impact (Schmitz et al., 1999) more emphasis is given from researchers to evaluation of the direct carbon emissions which may not include additional greenhouse gas emissions. According to Davidovits (2011), 0.180 metric tons of CO_2 is generated for 1metric ton of geopolymeric cement which is less than one fifth of the carbon emissions of Portland cement. McLellan et al. (2011),Weil (2009) and Stengel (2009) have also evaluated the carbon emissions of geopolymers compared to OPC and their results are in favour of geopolymer cement. However the difference between the two types of cement varies with Weil (2009) estimating 70% reduction for AA fly ash concrete compared to OPC and McLellan et al. (2011) a 44-64% lower for Australian AA fly ash product. The location is important as it is related to transport as together with the energy source and design of the concrete mixes, transport can have a large effect on the calculations of carbon emissions (McLellan et al., 2011). Recently, Yang et al. (2013) used a methodology suggested by Damineli et al. (2010) to estimate the efficiency of 34 GGBS mixes activated with $Ca(OH)_2$ and a small amount of sodium silicate or sodium carbonate (1-2%), 3 fly ash-based and 1 metakaolin based mix activated with NaOH versus OPC mixes and OPC+FA or/and GGBS. According to the methodology followed there are two values of interest: the "*CO_2 intensity*" (C_i) and the "*binder intensity*" (B_i) which are calculated as:

$$B_i = B/f_c$$

$$C_i = C_e/f_c$$

where f_c is the concrete compressive strength (in MPa), B is the binder content in $1m^3$ of concrete (in kg/m^3) and C_e is the corresponding emissions of the design mix (in kg/m^3). The binder intensity is used as a criterion as it is the binder in OPC concrete that mainly causes

carbon emissions (Damineli et al., 2010, Gartner, 2004). The calculation was based on the Korean and Japanese life cycle inventory (LCI) databases (Yang et al., 2013). The results showed that CO_2 emissions of AA concrete varies between 55-75% compared to OPC, and the difference is about 20% less (Yang et al., 2014, Yang et al., 2013) compared to OPC plus supplementary cementitious materials (SCM). Because of the methodology used, it was possible to observe that the intensities B_i and C_i tend to decrease (positive change) when the compressive strength of concrete increases. That would add further value to the already reduced quantity of high-strength concrete needed in an actual project if appropriate. However, it should be noted that the difference of 55-75% was calculated based on a large range of OPC samples but the extremely limited data on AAM mentioned above, which does not include many alkaline solutions and many common precursors.

Not all authors agree with the alleged high carbon reductions offered by AA cement technology (Habert et al., 2011, Turner and Collins, 2013). Habert et al. (2011) used this database to conduct a Life Cycle Analysis (LCA) to estimate the environmental footprint of geopolymer concrete and OPC. Interestingly, this study showed that while geopolymer concrete can offer a 45% reduction in CO_2 emissions compared to 100% Portland cement concrete, recent advances in Portland cement technology can reach 50% reduction in CO_2. To confirm the 50% reduction that Habert suggested for use of Portland+SCM which the study of Yang et al. (2014) addressed. The author statistically processed results from 9209 concrete mixes of OPC and OPC+SCM and as mentioned in section 2.3, found 20% difference in carbon emissions for the same strength class. However, this 20% refers to comparison of medium values and looking at Figure 23 it is seen in red lines. However, comparing the extremes shows about 66% difference in CO_2 intensity for the same class of strength (i.e. 50MPa in this case). That means that the 50% estimated by Habert et al. (2011) is possible, but the potential limited future supply of fly ash and GGBS in the UK could limit the benefits of mixes with a high SCM content (Heath et al., 2013). Turner and Collins (2013) calculated only a 9% reduction for FA-based geopolymer concrete (320kg CO_2-e/m^3) compared to 100% OPC concrete (354kg CO_2-e/m^3), not including SCM as in Habert et al. (2011). The calculations which led to such unfavourable results included emissions from mining, treatment and transport of raw materials, expenditure related to activator manufacturing and curing at 60°C for 24hours. The study had as target concrete of 40MPa compressive strength and used values from the "Australian National Greenhouse Accounts (NGAs) Factors" as input values of GWP, and also values calculated based on audits of manufacturing outputs of Australian companies for the activators (NaOH and sodium silicate). The estimated 1.514kg CO_2-e per kg sodium silicate and 1.915kg CO_2-e per kg NaOH are higher than the equivalent values used by Habert et al. (2011) and presumably they do not correspond to the UK market which is covered by European databases used by Habert, and like Kostick (2011).

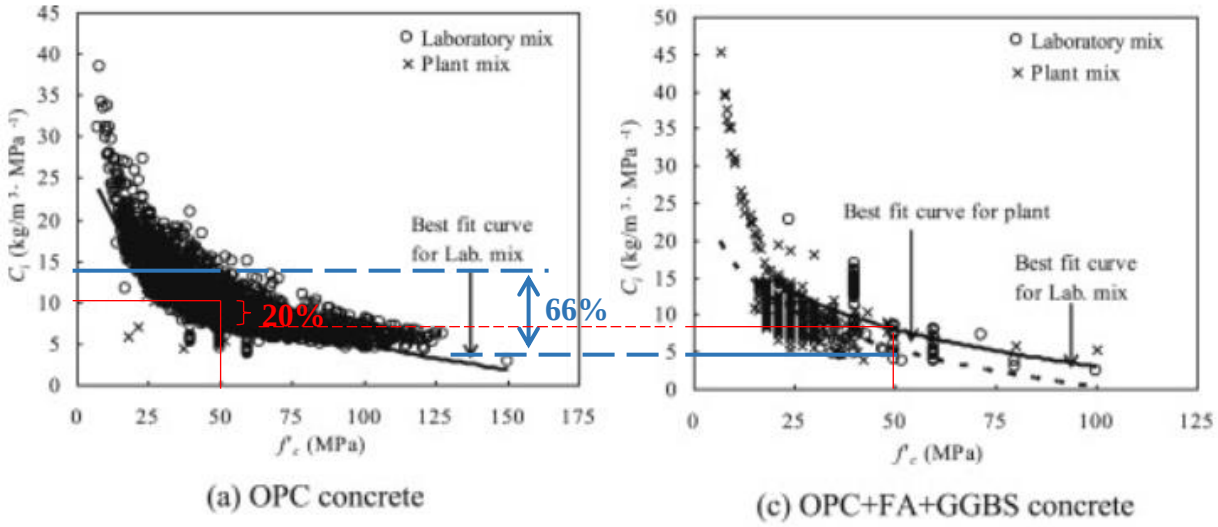

Figure 23 Reduction of carbon emission of OPC by including GGBS and FA (after Yang et al. (2014))

Apart from the global warming potential, there are other nine important environmental categories, namely abiotic depletion, acidification, eutrofication, ozone layer depletion, photochemical oxidation, human toxicity, fresh water aquatic, marine aquatic and terrestrial ecotoxicity, explained in Goedkoop et al. (2008). Input values for all the ten categories are provided in the Ecoinvent database (Kellenberger and Althaus, 2003). Providing this set of environmental categories is according to the CML (Center of Environmental Science of Leiden University) method. It should be noted that the use of a single number calculated from a weighted sum of different values, such as Eco-indictor 99 or BRE Ecopoints, can be subjective and therefore misleading when used for construction materials (Zabalza Bribián et al., 2011). The work by Habert et al. (2011) between AAM and Portland of the latest technology noted the lower global warming potential for geopolymer concrete mentioned earlier, but a higher impact of geopolymer concrete in the other nine environmental categories, with human toxicity and aquatic ecotoxicity showing the highest increases. They indicated further research was needed into the impacts of both geopolymer and PC based concretes across all categories.

A shortcoming in Habert et al. (2011) is that when calculating the emissions of geopolymer concrete they used the worst case scenario sodium silicate in terms of CO_2 emissions ("*sodium silicate, furnace liquor, 37% in H_2O*" of Ms=3.3) (McGuire, 2012), assigning 70% of the estimated geopolymer cement emissions to sodium silicate production while the production of NaOH powder was less significant (0.2%). Sodium silicates are produced by melting sand and sodium carbonate at 1350-1450°C, followed by dissolution at 140-160°C presence of steam pressure. On the other hand sodium carbonate can derive from nature or be synthetic. The Solvay process is the main manufacturing process and it is as well

energy intensive (Shi et al., 2006). Therefore, sodium silicate has carbon emissions which vary significantly depending on the way of producing (McGuire, 2012). In the Ecoinvent database this is shown by increasing values of environmental impact for "*Sodium silicate, hydrothermal liquor, 48% in H_2O*" of Ms=2.0, "*sodium silicate, furnace liquor, 37% in H_2O*" of Ms=3.3 and "*sodium silicate, spray powder 80%"* of Ms=2.0 (where extra energy is spent to dry the silicate) respectively where values are taken by Fawer et al. (1999). That is the reason that many scientists underline the importance of alkaline solution content and concentration when assessing the environmental impact (Gartner, 2004, McLellan et al., 2011). According to revised calculations on emissions based on the 2011 European sodium silicate data (Kostick, 2011) instead of the data of Fawer et al. (1999), data used in Ecoinvent and by Habert et al. (2011), the alternative ways of sodium silicate production have up to 80% reduced carbon emissions (126kg CO_2/m^3 for the worst case scenario and 22kg CO_2/m^3 for the best case scenario). Another shortcoming is that although the LCA studies of Habert et al. (2011) and Stengel (2009) attribute a percent of emissions to heat curing, that is optional and many geopolymer mixes cure at ambient temperature as is the case for the concretes investigated as part of this research.

More recently there was a positive development with Mellado et al. (2014) using an alternative type of sodium silicate produced by refluxing rice husk ash in NaOH. For this new formula the carbon emissions were reduced by 50% compared to geopolymers using commercial sodium silicate. The compressive strength decreased by about 25% (from 59.7 to 44.1MPa). Taking that reduction into account the difference in terms of Ci ratio is 22.6%.

It is generally observed that GGBS-based AAM have lower GWP than FA-based and metakaolin-based geopolymers have the highest GWP (Habert et al., 2011, Yang et al., 2013) which is because of the lower concentration of activator needed and also in the case of metakaolin, energy is consumed during extraction, refining and calcination. Moreover, the outcomes of GWP for AAM based on by-products, FA and GGBS, vary and can be calculated in three ways (Habert et al., 2011):

- "*No allocation*" is as if they are considered waste, therefore they do not share the impact for production of iron and coal respectively. In Chen et al. (2010) these values are not zero because there are still actions required for their processing such as grinding in the case of GGBS, drying and packaging, which incorporate some environmental impact. This methodology is questionable in a situation where all GGBS produced in the UK is currently used and where all FA is likely to be used in the near future.
- "*Economic allocation*" attributes part of the impact of iron and coal production to slag and FA based on the prices of the materials. While this approach can be considered the most reasonable of the three, it has the disadvantage of constantly varying prices for electricity, steel, FA and GGBS affecting the outcomes.

- "*Mass allocation*" attributes part of the impact of iron and coal production to slag and FA based on the produced masses. This approach is questionable, particularly for FA production as electricity does not have mass.

2.4.7 Summary of AAC literature

Based on the literature reviewed, the following summary information is relevant for use of AAMs in the target application of concrete blocks and roof tiles:

1. There are numerous advantages (including low embodied CO_2) of using AAMs instead of PC based binders, but also a number of potential shortcoming which need to be investigated further, and in particular the issue of scaling up binder based research to larger scale applications.
2. A wide range of aluminosilicate powders have potential to be used as AAM precursors
3. The Na_2O content as well as the ratios of Na_2O:Si:Al in the mix and the precursor are the key chemical parameters for mixes. The quantity of Si and Al in the amorphous form is critical.
4. For low Ca content mixes heat curing is required, but if a higher Ca precursor is used (most commonly GGBS), no heat curing is required which would be beneficial for the applications considered. The addition of Ca has secondary benefits for the microstructure of the material.
5. Superplasticisers are unlikely to provide a consistent improvement in workability for wet AAM mixes.
6. Samples should be moist when cured otherwise they show a strength decrease.
7. AAMs generally show improved free-thaw resistance and reduced water permeability compared with equivalent PC based mixes (relevant for the applications being considered). Accelerated carbonation testing is unlikely to yield accurate results with AAMs, but this is not directly relevant to the applications being considered.

2.5 Mineralogical aspects for Constituent Minerals of CCW

Tests for this research on the quantitative composition of china clay waste are presented in Chapter 3. All the forms of the waste derive from the same original type of rock as explained in section 2.1 and therefore all forms of the waste all contain quartz, feldspar, schorl, mica mineral and some kaolinite. The kaolinite present is the material which was not possible to cost-effectively regain during the processing described previously in section 2.1. Table 7

summarises information regarding the minerals present in the china clay waste; chemical composition, optical properties, colour and diaphaneity, and physical properties (density, hardness, melting point) provide a context for the discussion in later section, helping the identification of the different minerals in the waste under an optical microscope, in scanning electron microscopy (SEM) and when discussing thermal processing. All the information in the table is taken from the American Mineralogist Crystal Structure Database (Downs and Hall-Wallace, 2003), apart from the melting points which are from Wypych (2010).

Quartz (SiO_2) and feldspars are common minerals (Allaby, 2008). As explained in section 2.1, the areas of kaolinisation have feldspar of soda content higher than its potash content, therefore the types of feldspars present in the waste can be K-feldspar ($KAlSi_3O_8$) and albite ($NaAlSi_3O_8$) which can weather to form kaolinite. While the K-feldspars have different polymorphs, microcline, orthoclase and sanidine, orthoclase is the common feldspar in granites (Wypych, 2010). Schorl ($NaFe^{2+}{}_3Al_6(BO_3)_3Si_6O_{18}(OH)_4$) belongs to the tourmaline group. Quartz, feldspar and mica are inert (not active) phases according to (Massazza, 2003) while kaolinite can be heated (calcined) to form a pozzolan for Portland cement. It is noted that "pozzolan" in Portland cement technology is the inorganic aluminosilicate, glassy (called "active phase") to a great extent, which hardens in water when reacting to calcium hydroxide (added lime or clinker) and pozzolanic activity is measured based on the maximum amount of lime consumed and rate at which the consumption occurs (Massazza, 2003). As shown previously, geopolymerisation is not a calcium-based system but relies on the glassy content in aluminosilicates (including pozzolans) to react with alkaline solutions. Understanding the changes which occur to the crystal structure of kaolin during heating that lead to the formation of reactive metakaolin is of interest and it is presented in the following section. Although the mica minerals are considered inert in the literature, changes in the crystal structure of mica are also described to compare with the case of kaolinite.

Table 7 General properties of minerals under study (selected information from Downs and Hall-Wallace (2003) and Wypych (2010)).

Quartz		**Chemical formula:** SiO_2 with traces of other elements	**Mineral Category:** Silicate mineral. Cleavage indistinct	**Density:** 2.65	**Hardness:** 7	**Melting point (°C):** 1500-1700
		Diaphaneity: Transparent to nearly opaque.	**Colour:** Colorless, white; from chemical or particulate inclusions, rose-pink to rose-red, yellow to yellowish brown, green, blue, bluish violet, brown to black; zoned or mottled.			
Potassium Feldspar (orthoclase)		**Chemical formula:** $KAlSi_3O_8$	**Mineral Category:** Silicate mineral. Cleavages intersect at 90°	**Density:** 2.55-2.63	**Hardness:** 6-6.5	**Melting point (°C):** 1200-1450
		Diaphaneity: Transparent to translucent.	**Colour:** Colorless, white, gray, pale yellow,flesh-red, green; colorless in thin section; may exhibit opalescence or schiller iridescence.			
Kaolinite		**Chemical formula:** $Al_2Si_2O_5(OH)_4$	**Mineral Category:** Phyllosilicate with imperfect basal cleavage	**Density:** 2.61-2.68	**Hardness:** 2-2.5	**Melting point (°C):** 1800
		Diaphaneity: Transparent to translucent as single crystals.	**Colour:** White to tan, be variously colored by impurities.			
Micas	**(muscovite)**	**Chemical formula:** $KAl_2(Si_3Al)O_{10}(OH, F)_2$	**Mineral Category:** Phyllosilicate with near perfect basal cleavage	**Density:** 2.77-2.88	**Hardness:** 2.5-4	**Melting point (°C):** 1320
		Diaphaneity: Transparent to translucent	**Colour:** Colorless, gray, brown, green, yellow, rose-red; commonly colorless in thin section, but may be pale yellow, green, red-brown.			
	(biotite)	**Chemical formula:** $K(Mg, Fe^{2+})_3(Al,Fe^{3+})Si_3O_{10}(OH, F)_2$	**Mineral Category:** Phyllosilicate with near perfect basal cleavage	**Density:** 2.7-3.3	**Hardness:** 2.5-3	
		Diaphaneity: Semitransparent	**Colour:** Dark green, brown, black, reddish brown, light yellow, grayish yellow, brownish green, brown; yellow to reddish brown in thin section.			
	(zinnwaldite)	**Chemical formula:** $KLiFe^{2+}Al(AlSi_3)O_{10}(F,OH)_2$	**Mineral Category:** Phyllosilicate with near perfect basal cleavage	**Density:** 2.90-3.02	**Hardness:** 2.5-4	
		Diaphaneity: Transparent to translucent	**Colour:** Gray-brown, yellow-brown, pale violet,dark green, color zoning common; colorless to light brown in thin section.			
Schorl		**Chemical formula:** $NaFe^{2+}{}_3\ Al_6(BO_3)_3Si_6O_{18}(OH)_4$	**Mineral Category:** Cyclosilicates. Indistinct cleavage	**Density:** 3.18-3.22	**Hardness:** 7	
		Diaphaneity: Transparent to nearly opaque.	**Colour:** Black, brownish black, bluish black; in thin section, bluish yellow.			

2.5.1 Kaolinite and thermal activation to metakaolin

China clay primarily contains kaolinite and is used mainly in two industries: the paper industry, both as filler and finishing, and in the ceramics industry. These two uses account for up to 80% of the UK china clay sales (BGS, 2009). There are several other uses, referred to as speciality applications, which include metakaolin for the building and construction industry, paint applications, rubber applications, glass fibre, cable insulations, filler in plastics, speciality films, pharmaceutical applications, cosmetic applications and other minor industrial applications (Minerals Zone, 2012) There are a vast number of studies on the use of metakaolin as additive in Portland cement systems (Rashad, 2015, Sabir et al., 2001, He et al., 1994), as a successful precursor in geopolymers (Arellano-Aguilar et al., 2014, Hounsi et al., 2013, Rashad, 2013) and in AAM cements based on slag/metakaolin (Bernal et al., 2012a), based on fly ash/metakaolin (Zhang et al., 2014) or Portland systems with many additives including a combination of limestone, fly ash and metakaolin (Vance et al., 2013). However it has to be noted that in alkali activated technology even uncalcined kaolin has potentials (Heah et al., 2011b) which is discussed later, after presenting the latest advances in alkali-activated cement systems.

Kaolinite ($Al_4Si_4O_{10}(OH)_8$) is a 1:1 dioctahedral phyllosilicate mineral. An ideally layered kaolinite structure is shown in Figure 24 by Sperinck et al. (2011). The structure has tetrahedra of SiO_4 forming sheets by sharing some of their oxygen atoms and while other oxygen atoms in the c-axis are shared with aluminium with 6-coordination (octahedral). The aluminate and silicate are firmly tied by ion-covalent bonds. The bonds of the hydroxyls on the AlO_6 tetrahedra are much weaker and are connected to the non-shared silicate oxygen atoms. It is assumed that during dehydroxylation the water leaves first from the inter-layer shown in Figure 24 (Sperinck et al., 2011).

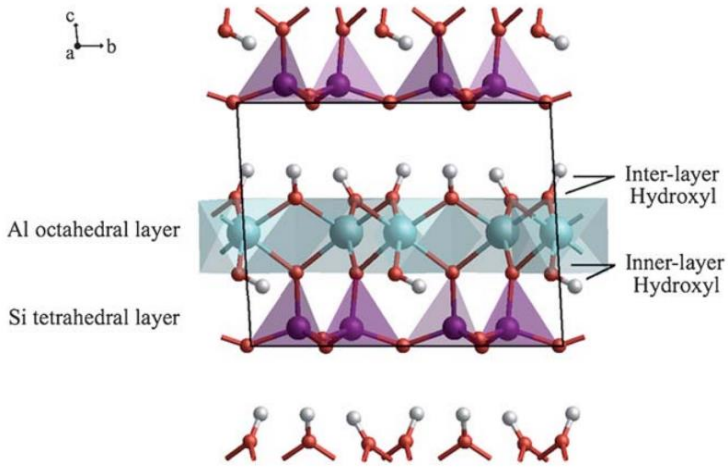

Figure 24 Ideal layered structure of kaolinite (After Sperinck et al. (2011))

Many studies on the thermal transformation of kaolinite have been conducted using solid-state Nuclear Magnetic Resonance (NMR) (MacKenzie et al., 1985a, Meinhold et al., 1985b, Watanabe et al., 1987, Slade and Davies, 1989). These studies have made known that metakaolin which is formed at ~600°C has structural differences to the original kaolin as a result of the thermal treatment. Generally, the difference in metakaolin ($Al_2Si_2O_7$) which makes it reactive is that during the dehydroxylation, Al changes from predominantly Al(6) to predominantly Al(4) and Al(5) coordination and the ordered crystal structure becomes amorphous while Si remains in 4-fold coordination. The dehydroxylation is described by the following equation (Sperinck et al., 2011):

$$Al_4Si_4O_{10}(OH)_8 \xrightarrow{600\ ^\circ C} 2Al_2Si_2O_7 + 4H_2O$$

However, it is seen that the temperatures of transformation have a range and may slightly vary between different kaolin sources. There is also variation regarding the exact amount of Al(4) and the presence or absence of Al(6) in metakaolin: Watanabe et al. (1987) showed that kaolinite started forming into metakaolin at ~600°C but the maximum Al(4):Al(6) ratio was observed at 841°C. At higher temperatures, the Al(6) increased at the expense of the Al(4). Generally after the formation of metakaolin there are two more stages of transformation at higher temperatures: the formation of spinel and free silica (not bound with aluminium) and at even higher temperature the formation of mullite and remaining amorphous silica which according to Meinhold et al. (1985b) could possibly form cristobalite (SiO_2). These higher temperature crystalline mineral phases are undesirable in pozzolans as they have lower reactivity than the metakaolin and require higher temperatures and therefore ore energy from processing. In Watanabe et al. (1987) and Meinhold et al. (1985b) crystallization of the metakaolin occurred at ~980°C, with the formation of spinel and, later, mullite ($A1_6Si_2O_{13}$). Al(5) was not detected although may have existed at an intermediate stage. Slade and Davies (1989) showed little or no peak (at low spin rate) for Al(6) at 800°C, detecting mainly Al(4). Sperinck et al. (2011) has a peak at 978° attributed cubic spinel and amorphous silica while mullite which is thermodynamically a stable phase, is shown over 1100°C. The difference in temperatures is related to the degree of structural order in the sample, with kaolinite of low degree of order starting forming Al(4) and Al(5) at lower temperature (~500°C) than kaolinite of high order (Rocha and Klinowski, 1990). Sperinck et al. (2011) presented the dehydroxylation process using molecular dynamics. In this study it is confirmed that metakaolin does not lose the 1:1 sheet structure of kaolin although the distance between the sheets is shortened and there is buckling with simultaneous loss of the crystallinity (stated also by White et al. (2010)). In Figure 25 is the model of the kaolinite structure from the unheated state to the 100% of the dehydration process complete. It was noted that above 80% the dehydroxylation does not cause major changes as there is not enough space for Al to rearrange and that the final phase had 74% Al(4), 21% Al(5), less than 2% Al(3) and 3% Al(6). The presence of Al(5) and Al(3) was attributed as well to the physical restrain of Al to be converted in more stable forms. A new observation was that Al forms clusters which provides an explanation for why a pure metakaolin sample subject to XRD analysis shows some peaks that are often interpreted as an impurity in the

original sample. However this study is in contrast with previous work (White et al., 2010) which used density functional theory (DFT) and concluded that metakaolin had 66% Al(4), 31% Al(5) and 3% Al(3) therefore no presence of Al(6). The same research team confirmed their results providing more evidence using synchrotron X-ray absorption near-edge spectroscopy (XANES) (White et al., 2011) As a conclusion, metakaolin has aluminium mainly in 4-fold coordination but also contains Al(5), Al(3) and possibly some Al(6). Crystallization occurs at a range of temperatures, ≥841°C. This information is important as calcination of the MW is considered in later chapters, as it is important to know at which temperatures metakaolin from the leftover kaolinite in the waste would be present and potentially reactive.

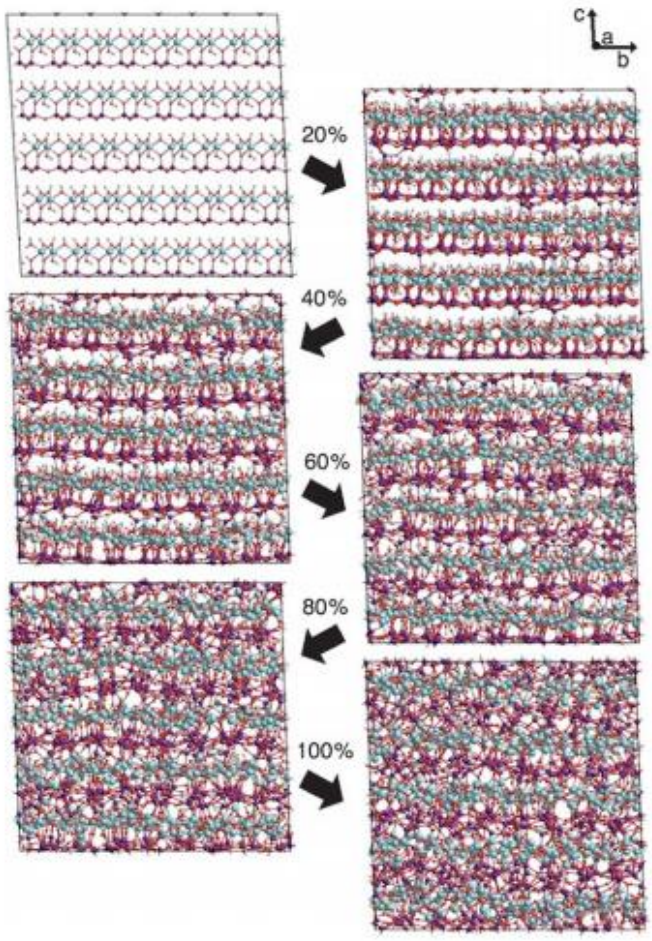

Figure 25 The changes in structure that occur in different stages of dehydroxylation of kaolinite (After Sperinck et al. (2011))

In metakaolin, Al(4) is observed at s chemical shift of 65 to 70 ppm and Al(6) near 0ppm. A small peak at 35ppm is explained that is also probably related to Al(4). Mullite is attributed to peaks at 46-48ppm (Meinhold et al., 1985b). The same values are used by other authors, with Slade and Davies (1989) and Watanabe et al. (1987) detecting Al(6) at a range of values from -3 till about 12ppm, while Al(4) is in the range of 40-60ppm

with 46-48ppm representing the Al(4) in mullite. It is noted that the presence of mullite in 27Al is mainly shown by the Al(6):Al(4) ratio increase (Slade and Davies, 1989). Another technical issue related to the solid-state NMR is the loss of signal at some temperatures after heating of kaolin. Meinhold et al. (1985b) observed initial signal loss of 90% (at 650°C) which partly recovered at temperatures above 970°C. The reason is assumed to be the defects and distortion of Al in sites which are not octahedral or tetrahedral and not detectable. Even when mullite, a crystalline phase is formed, the distortion was too high and the signal intensity for 27Al detection was still low leading to difficulties in interpretation.

2.5.2 Mica and structural changes at elevated temperatures

Mica is used for a family of phyllosilicate minerals with 2:1 atomic structure (Allaby, 2008). The mica mineral in Cornwall comprises mainly muscovite with biotite and there is presence of zinnwaldite (see Chapter 3). As it is the dominant mineral, the focus of this is muscovite. Out the three minerals, muscovite is the most important commercially. Its main use is in electronics as a thermal insulant while in ground form it has additional use in mica insulation bricks, fibre cement, roofing materials, coatings, paints, plastic, rubber, shades and other special uses taking advantage of the various properties of muscovite. These properties include a high thermal/fire resistance (leading also to prevention of cracks and dimensional stability), platy shape of thin particles (related also with noise reduction) and glittering effect (MineralsZone, 2014, Imerys, 2012).

Muscovite and biotite are common micas in nature (Allaby, 2008). Zinnwaldite is a lithium mica of $KLiFe^{+2}Al(AlSi_3)O_{10}(F,OH)_2$ chemical formula, while biotite is $K(Mg,Fe^{+2})_3(AlFe^{+3})Si_3O_{10}(F,OH)_2$ (Downs and Hall-Wallace, 2003). The chemical formula of muscovite is $KAl_2(Si_3Al)O_{10}(F,OH)_2$ (Downs and Hall-Wallace, 2003) or an ideal structure could be written $KAl_2(Si_3Al)O_{10}(OH)_2$ after Bailey (1984). When compared to the kaolin structure presented earlier, it can be noted that muscovite has a higher Si:Al ratio and that the hydroxyl group is a smaller fraction of the mineral mass.

The crystal structure of muscovite is shown in Figure 26 by McKeown et al. (1999). It is composed of a dioctahedral sheet, Al^{+3} in 6-coordination with 1/3 of the octahedral sites vacant, between two tetrahedral sheets where silicon atoms comprise the 75% of the tetrahedral sites and 25% is substituted by aluminium, noted as T2 and T1 in Figure 26 (McKeown et al., 1999). The aluminium in the dioctahedral sheet might be substituted (impurity), usually by Fe (Imerys, 2012). The substitute of aluminium creates a negative charge which is balanced by the presence of potassium cations in the interlayer area (Bailey, 1984, Imerys, 2012). The extraction of the K cations is not normally possible in natural conditions due to the strength of chemical bonds between K and the tetrahedral layers and due to the steric effect. This results in the high chemical and weathering resistance of muscovite (Imerys, 2012). Each of the octahedral aluminimum (Al(6)) has two OH groups (McKeown et al., 1999).

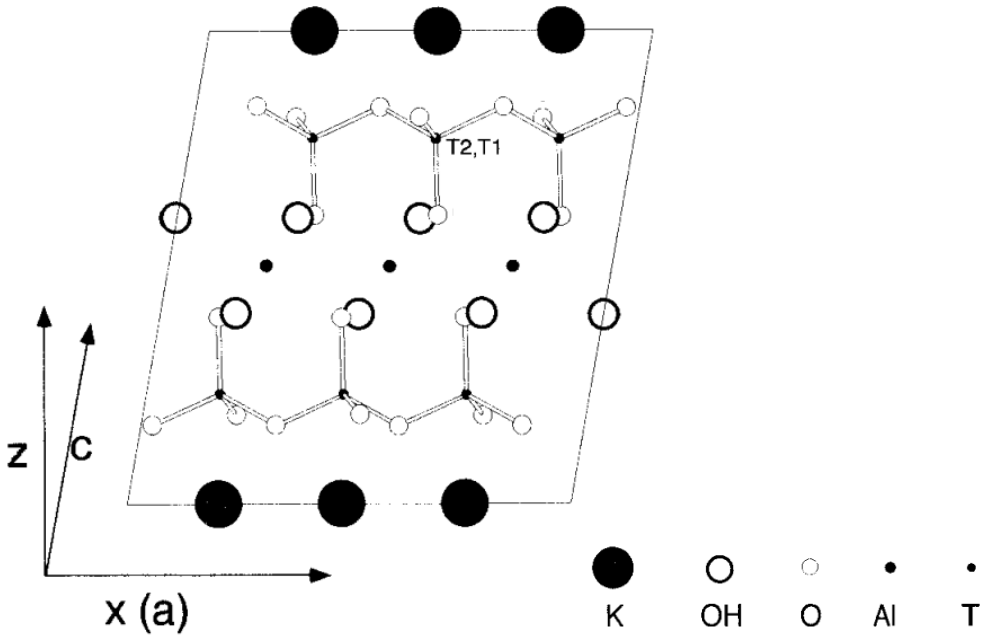

Figure 26 Crystal structure of muscovite (by McKeown et al. (1999))

In engineering studies clay sized particles are considered to have an average particle dimension ≤2μm, while the mica flakes in the waste are definitely larger and can be seen by visual observation. Because of their flaky shape, the concept of average particle size is not necessarily meaningful but the particle shape does provide a high surface area per unit volume. The weathering of muscovite or feldspar eventually results in another phyllosilicate mineral, illite, which is clay-sized (Allaby, 2008). Regarding the reactivity of muscovite, Zhang and Bailey (1998a) studied its basal surfaces, steps and edges and using $PbCl_2$ solution demonstrated that $PbCl_2$ precipitates are formed preferably on the edges of freshly cleaved muscovite. This reactivity was attributed to "*terminal Al-$OH_{1/2+}$ or Al-$OH_{1/2-}$ groups on these crystalline surfaces, which favor adsorption of Pb^{2+} ions*". That means that the edges of naturally weathered muscovite as it occurs in MW would not be as reactive with $PbCl_2$ as the freshly cleaved surfaces. Kuwahara (2008) studied muscovite under alkaline conditions and concluded that dissolution takes place only at the edges. Oelkers et al. (2008) studied the dissolution rates of Al and Si for muscovite for ranging pH=1-10.3, having first ground the mineral to particle size of 50-100μm and cleaned it ultrasonically in methanol. At basic conditions (pH=9, T=150°C) the dissolution of Si and Al was relatively fast in the beginning but it was then reduced, reaching a steady state of solution concentration (no more dissolution). Generally it was observed that the dissolution is limited by Al and Si present (already dissolved or added) in the solution at basic conditions and only by Al under acid conditions. This provides an explanation why muscovite is more resistant in sedimentary basins than alkali feldspar and other minerals that have their dissolution rate independent of aqueous Si presence. In addition, the results of Oelkers et al. (2008) show dissolution to be higher towards the extremes (pH near 1 and 10) but very interesting and maybe related to the effect of using sodium silicates in AAM as discussed later, is the evidence that the dissolution under

some conditions may range significantly for the same pH. That led the authors to the conclusion that changing the Al and/or Si in the solution may be of greater effect than changing the pH. As Zhang and Bailey (1998a) and Kuwahara (2008), Oelkers et al. (2008) also suggest that the dissolution of muscovite is much faster at the edges rather than from the basal planes, as in SEM there were no features of dissolution (as etches) on the surfaces and there was only rounding of the edges detected. These observations are based on unheated muscovite and may therefore not be applicable to the heated muscovite.

Muscovite dehydroxylates when calcined as happens in the case of kaolin-metakaolin and there are many studies on its dehydroxylation using XRD and thermal analysis (Mazzucato et al., 1999, Guggenheim et al., 1987, Gridi-Bennadji and Blanchart, 2007, Mackenzie et al., 1987) but there is limited work using solid-state NMR analysis after calcining (Mackenzie et al., 1987). At low temperatures, there may be small loss of mass, of 1% in the case of Guggenheim et al. (1987) due to water absorbed by the surface. Later the hydroxyls condense followed by "water diffusion through and along the layers" (Mazzucato et al., 1999, Gridi-Bennadji and Blanchart, 2007). Two hydroxyls form a water molecule:

$$KAl_2(Si_3Al)O_{10}(OH)_2 \rightarrow H_2O + KAl_2(Si_3Al)O_{11}$$

As the water molecules move out of the crystal structure, there is distortion, loss of K and layer expansion which leads to exfoliation (Gridi-Bennadji and Blanchart, 2007, Rodriguez-Navarro et al., 2003). From the TGA and DTA graphs of Gridi-Bennadji and Blanchart (2007) it is seen that there is constant loss of weight during dehydroxylation, with 4.7% of mass loss till 980°C although most of the hydroxyl groups are removed below 850°C. It is explained that there is a broad temperature range for the completion of the dehydroxylation which is associated to the non-homogeneous character of the process. In their study, the dilatation of muscovite was measured and it is shown that it depends on the heating rate, but generally the total, final exfoliation for all the heating rates was approximately the same (about 60%) and took place rapidly at temperatures above 600 and below 850°C. Regarding the coordination of Al in the muscovite structure, Mackenzie et al. (1987) who studied two types of muscovite with 2.43% and 4.59% iron content respectively found that the detectable Al(6) before dehydroxylation is underestimated as Al adjacent to Fe broadened the signal beyond detection. The signal further decreased on dehydroxylation (950°C) because of the transition to undetectable Al(5). At 950°C the 27Al spectra showed a proportion of tetrahedral aluminium which had identical shift to the raw material and therefore it was suggested that it represents the initial Al(4) layer which remained relatively unchanged by dehydroxylation. While Mackenzie et al. (1987) refers to dehydroxylation as an homogenous process, Guggenheim et al. (1987) describes it as non-homogeneous, as Gridi-Bennadji and Blanchart (2007), and concluded that the Al-OH bonds are weaker when the neighboring aluminum sites are in 6-fold compared to when neighboring with Al(5), which means that in an intermediate state of dehydroxylation (partial) the remaining Al-OH bonds get stronger and therefore lost in higher temperature. A study where muscovite was ground

by sonication showed that for fine particle size, the formation of new phases takes place earlier, at lower temperatures (Pérez-Rodríguez et al., 2006). The untreated samples lost weight between 650-920°C.

At higher temperatures new phases are formed including mullite ($Al_6Si_2O_{13}$), sillimanite (Al_2SiO_5), corundum (Al_2O_3, belongs to hematite group), cubic γ-Al_2O_3, spinel ($MgAl_2O_4$), K-feldspar and/or leucite ($KAlSi_2O_6$) together with an amorphous phase (Mazzucato et al., 1999, Barlow and Manning, 1999, Devineau et al., 2006). There are not strictly set temperatures where these changes take place (Barlow and Manning, 1999). Regarding the glass formation, Rodriguez-Navarro et al. (2003) studied the growth of mullite after the breakdown of muscovite using transmission energy microscopy (TEM), and did not observe melting after 3hours at 800°C. The first "boxes" of melt occurred at 900°C which led to the nucleation of nanocrystals of mullite within the muscovite particle. Therefore, melting, leading to more stable mullite phases, starts before full dehydroxylation which is important when considering the use of muscovite as a pozzolan or precursor in AAMs. At this first stage of melting, the melt is rich in Si and has less Al compared to the "host" muscovite which is attributed to the favourable incorporation of Al in the surrounded mullite crystals. The melt also contains Na and K but again in lower concentration than dehydroxylated muscovite.

Firing *T*	Qtz	Phy	Hem	Mul	Fs
Raw material	*	*	‡	nd	‡
700 °C	*	*	nd	nd	‡
800 °C	*	†	‡	nd	‡
900 °C	*	†	‡	nd	‡
1000 °C	*	nd	‡	‡	‡
1100 °C	*	nd	‡	†	‡

Notes: nd = not detected; phy = phyllosilicates, mainly Ms and Ill with traces of Kao and smectite. Mineral symbols after Kretz (1983).
* Very abundant.
† Abundant.
‡ Scarce.

Figure 27 Phases detected by XRD by Rodriguez-Navarro et al. (2003).

The texture of mullite is interesting at later stages as its crystals grow in the next stages: at first they grow in specific orientation with regard to the basal planes of muscovite, then the crystals coarsen at approximately 1000°C but keep their orientation and at the last stage the muscovite is replaced with mullite fibres and bubbles formed by dehydroxylated water moving out of the mineral. At this last stage the previously oriented crystals can show random orientation due to the high rate of formation and further growing of the crystals during cooling. The temperature that melting and mullite formation initiated is about 100°C lower than the expected temperature based on the equilibrium phase diagram of constituent oxides of muscovite, a fact attributed to the water released during dehydroxylation and presence of K,Na, Mg and Fe in the melt. In backscattered electron images the partially dehydroxylated muscovite is shown brighter

than the melt/mullite areas which are darker. Mackenzie et al. (1987) identified at the dehydroxylation temperature formation of a feldspar-like phase and spinel. Due to the feldspar-like phase, in solid-state NMR the chemical shift of the tetrahedral Al site decreased. Unexpectedly, at 1100°C and above, the octahedral site could no longer be detected suggesting that iron was preferentially incorporated in specific, new phases of mullite or corundum.

2.6 China clay waste and mineral components as aggregate

2.6.1 Reuse of kaolin mining waste as an aggregate

Research on the reuse of kaolin mining waste as an aggregate has been conducted in the following areas:

Concrete

Where the silt content of the waste is low, the uses focus on primary aggregate replacement: In Lavangare et al. (2014) china clay sand replaced 0-50% of river sand in concrete as fine aggregate. The maximum particle size of china clay sand and river sand was 4.75mm. The water absorption for both types of sand was reported as 0.5%, their surface smooth and the china clay sand used was slightly finer than the river sand (fineness modulus 2.7 compared to 3.1). In this study as shown in section 3.1.1 the water absorption of china clay sand is higher (1.1%) and the maximum particle size 6.3mm. For a mix design with water cement ratio of 0.44 and cement:sand:coarse aggregate about 1:1.5:2.7, the results based on Indian standards showed enhancement of the mechanical performance for concrete with up to 30% of river sand substitution: the compressive strength reached 31 to 37MPa, the tensile splitting strength had a 15% increase and the flexural strength an 8% increase which is a modest difference in absolute values. China clay waste from the UK has been used in bulk concreting applications as mentioned in section 2.2, but also in dry-mix sprayed concrete (Henderson and Asbridge, 2006). Mixes included china clay waste sand from two pits, while some mixes included metakaolin and silica fume. Metakaolin was found to improve the durability, which was assessed by petrographical observation, and spraying performance of the mix. Some mixes incorporated mica and fibres in order to investigate their effect in ductility. The mica inclusion (only a 5% mica waste inclusion) did not enhance the compressive strength of the mixes but interestingly, showed some increased ductility.

Asphalt

Another publication (Nema et al., 2014) on the reuse of china clay sand in semi-dense bituminous concrete is based on the Marshall test, a test for bitumen, which does not include testing in compression. Although the conclusions were positive, showing lower bitumen binder content for the use of china clay compared to stone dust for equivalent performance (a small 0.5% difference), it is observed that the reported values of bulk density of the china clay sand samples are all lower than the stone dust, for all tested binder contents.

Resin products

Pilot projects also sought new, innovative uses. One of these projects was conducted by a private company, Ecobond, which used the MW stream in addition of 10% resin, heated to 100-200^{o}C, to create roofing tiles. The tiles produced met all the required product standards. The final product when tested in freeze-thaw showed no defects after 100 cycles and had consistent water absorption less than 5%. In terms of colour, dyes could be used but that would add to the cost and processing (Ecobond, 2007). However, no product was finally, commercially, released.

Clay products

Another effort was made by "Clayworks" a Cornish manufacturer, and provider of services and products in unfired clay, to use china clay waste fines in clay based plasters and renders. Clay plasters typically have high silt content, with comparatively low clay and sand contents. Currently materials used in the UK are imported from Germany. However, the trial failed and china clay by-product could not provide an appropriate finish in clay renders. (pers.com.Weismann (2011))

2.6.2 Performance of constituent minerals in china clay waste as aggregates in mortar and concrete

In 2.6.1 previous research on the use of the whole of china clay waste as aggregate was presented. In this section the use of constituent minerals of the waste, quartz, feldspar and mica mineral, as aggregates in cementitious products are reviewed. Schorl is not given any attention in papers on concrete science, probably because schorl only comprises a small component in natural aggregates rather than as a major phase of an aggregate. Together with mineralogy, other aspects which contribute to mechanical properties of concrete are presented.

Important factors in developing concrete blocks and tiles

For commercial applications, the aggregates used in concrete in Europe have to comply with BS EN 12620:2002+A1:2008 and BS EN 1097-6:2013. De Larrard and Belloc (1999) stated that aggregates affect compressive strength of concrete in three ways. One is the packing density which leads to a maximum paste thickness, described as the mean distance between two adjacent coarse aggregate particles. Another factor is the bonding in the interfacial transition zone (ITZ) between past and aggregate and third is the called ceiling effect which is a restraint in concrete strength caused by the strength of the aggregate. The packing density relies on the concrete mix and the BRE guide for concrete mixes (Teychenné et al., 1997) is an example of a guide for designing normal Portland concrete mixes, taking into account a number of parameters as the targeted compressive strength, the desired water to cement ratio and slump class, the maximum particle of coarse aggregate used. Although there are standards for mixing concrete blocks and concrete tiles (BS EN 490:2011, BS EN 771-3), there is not a specific design mix implied because these are highly porous and the volumetric mix design methods used in the BRE guide and other methods are not applicable. Limited and recent publications

show some reference mixes for concrete blocks and tiles (Huang et al., 2013, Zhan and Poon, 2015, Borges et al., 2014, Arellano-Aguilar et al., 2014, Burciaga-Díaz et al., 2013) but commercial manufacturers typically optimize mixes using their own in-house methods.

Aggregate mineralogy has some contribution on the ceiling effect. In Portland cement mixes it has been shown that the type of coarse aggregate does not play an important role in normal strength concrete (40-60MPa using water/cement ratio equal to 0.55 and 0.44) but it induces significant differences in high strength concrete (80-100MPa using water/cement ratio equal to 0.26) (Wu et al., 2001) However, even in high strength concrete, concrete using quartzitic aggregate of more than 200MPa rock strength showed about the same compressive strength and split tensile strength with concrete using granitic aggregate of 150MPa rock strength.

Granitic aggregates are of concern to engineers when used in Portland cement because of the potential for alkali-aggregate reaction (AAR), where an expanded gel develops after the silica in the aggregate reacts with alkalis in the pore solution, causing local cracks (De Paiva Gomes Neto et al., 2014). Leemann and Holzer (2005) studied two complex Swiss aggregates in regard to their potential for alkali-aggregate reaction in alkali-activated binders. The aggregates, that contained several minerals, were polished and embedded in an alkaline solution (2M NaOH solution at 38°C in a calibrated heater without stirring). The results showed that quartz in the aggregates dissolves more readily than micas or feldspars. Feldspars were shown to dissolve more readily than micas and are a common source for alkali ions. In an earlier study it was shown that the presence of detrital mica and clay in sandstone appears to enhance the solubility of quartz due to the release of alkali ions. (Broekmans, 2002) This would not be an issue for AAC where very high alkali concentrations are used in the activators as mentioned earlier. Makani (2014) examined aggregates of different characteristics (size, texture, quality, mineralogy, shape) and concluded that it is positive for the compressive strength to have high quartz to feldspar ratio. It was also noted that the feldspars are related to the presence of mica minerals and furthermore, the strength is negatively affected by the degree of weathering of feldspars. The composition of the china clay sand as presented in Chapter 3 is similar to the aggregate that Makani (2014) calls "siliceous aggregate" (quartz > 50%), not to their "granite" aggregate (feldspar close to 50%). For the siliceous aggregate the total and closed porosity was higher than for the granite which led to higher water absorption (1.1-1.2%) as water suction depends on open porosity and the higher the interconnection and size of the pores, the higher the water absorption. The water absorption affects the mix workability and humidity (and associated curing) inside concrete. Because of the high quartzitic content, the china clay sand and stent are expected to have acceptable performance as aggregate in concrete, although it is expected to have relatively high water absorption. This is unsurprising considering it is already extensively used in this manner.

The mineralogy also has some effect on the strength of the ITZ in geopolymers and Portland cement based concrete. Backscattered electron imaging has been found to be the

best approach to observe the ITZ according to Scrivener and Gartner (1987) (cited in Hussin and Poole (2011)). Borges et al. (2014) used this method to observe the ITZ between geopolymer matrix and quartz or glass as aggregates. It was decided to investigate glass as an aggregate as the amorphous silica from its particles would possibly react with the alkali matrix and improve the bond in the ITZ and increase the mechanical strength of the concrete. The compressive strength using quartz was insignificantly higher than for use of glass (maximum 44 and 42MPa respectively) but the flexural strength was significantly higher (maximum 7 and 3.4MPa). The porosity was also lower when using quartz aggregate. These differences were attributed to the elongated shape of the glass particles which may indicate potential problems with the flat mica mineral particles which may also break easily (fail in flexure). However, in the backscattered images, the sample of glass aggregate appears denser than the sample of quartz aggregate which affects the maximum paste thickness. In terms of bonding between binder and aggregate, it was observed that for quartz the interface is continuous and not very porous while the interface with glass showed a thin area of darker gray than the binder, visible for x50 times magnification (scale of 2mm) and more clear in higher magnifications (x100 and x500). This layer exists (or is visible) only on some particles. Although no EDS was conducted on those areas, the authors concluded that the observed layer is a gel that could be similar to ASR-gel although there have been no reports of detrimental ASR expansion in geopolymers free of Ca. The decrease in mechanical strength and increase in porosity was attributed to this possibly weaker layer. Isabella et al. (2005), in a preliminary analysis proved that there is relation between the surface area and the development of strength of a geopolymer. The optimum surface area, the rate of water loss from the interfacial bonding zone as well as the packing density of the aggregate were suggested to be important parameters.

The role of mica in PC mortar and concrete

The increase in water demand and the consequent increase in cement to provide comparable strength has already been reported already as the reason that MW, as a material which contains mica mineral particles, is not used in Portland cement applications. In Lea's chemistry of cement and concrete (Sims and Brown, 2003) muscovite and biotite micas are described to have disadvantageous effects when used in fine aggregate. This is because when mica occurs in flakes in fine aggregates, it increased the water demand and has negative effect on strength and durability of concrete (Sims and Brown, 2003). Dewar (1963) studied granite-derived sands from southwest England and reported that for a typical concrete mix the compressive strength might be decreased up to 5% for presence of 1% by weight muscovite mica in the total aggregate.

A study by Fookes and Revie (1982) (cited in Sims and Brown (2003))demonstrated the impact of mica on strength, workability and w/c ratio in Portland cement concrete; for mixes of constant workability, the compressive strength reduces by approximately 45% on the 28th day if 6% of total aggregate –an equivalent of 18% in fine aggregate- is replaced by mica minerals. It should be added that according to Fookes (1980) apart from the effect on strength, muscovite and biotite may be deleterious in the long term for

concrete because of chemical agents produced during the hydration of cement which alter the mica to other forms, but the author did not provide more details. This previous work did not distinguish between the effect of changing particle size distribution and the effect of adding mica mineral, and this was also only focused on using mica mineral in PC based concretes.

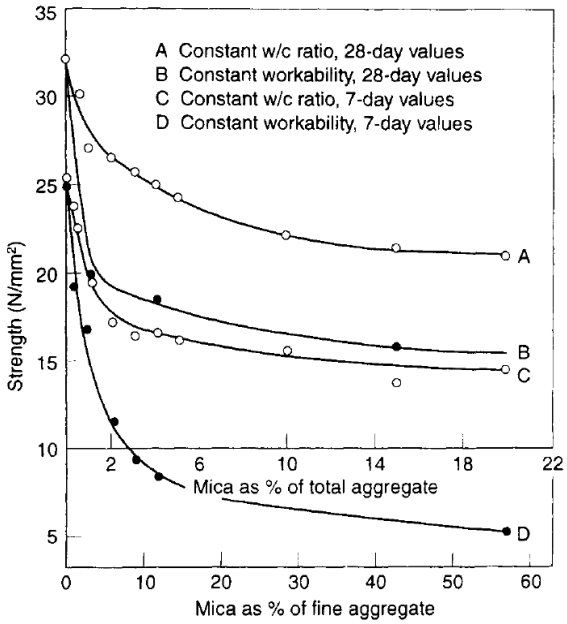

Figure 28 Compressive strength of concrete for different content of muscovite mica as aggregate, for constant water/cement ratio or workability. (Fookes and Revie (1982))

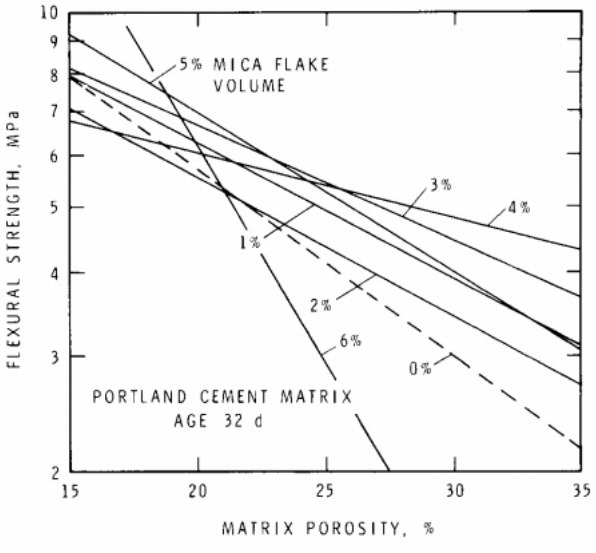

Figure 29 Flexural strength of Portland cement paste reinforced with mica flakes versus porosity. (Beaudoin (1983))

Beaudoin (1983) studied phlogopite type of mica as an alternative of glass fibre in fibre-reinforced cement, an application where good flexural strength and fracture toughness is required. Again, this author noted lower compressive strengths for any addition of mica, but the flexural strength and fracture toughness in some cases could be enhanced depending on porosity, but there was no clear relationship between flexural strength / fracture toughness and mica addition. In concrete roof tile manufacture, one of the applications considered for this research, the flexural strength and fracture toughness are important for final product performance. In Figure 29, the flexural strength is shown for 0-6% mica flakes per unit volume versus porosity, showing that for example, for 30% matrix porosity 4% mica would increase the flexural strength from 3 to 5MPa. This is important for concrete block applications where the blocks have much higher porosity than conventional structural concretes, indicating up to 5% mica flakes may actually increase flexural strength. Surface area, pore size distribution and non-evaporable water content were also affected by the use of mica. Stone powder rich in mica was used in mortar and concrete (Li, 2012, Xing et al., 2014) not only reduced the compressive

strength but also the workability, tensile strength and increased the mass and strength loss after 50 cycles of freeze-thaw and water demand. Finally, Li (2012) observed by SEM that the mica particles would worsen defects, including by spreading micro-cracks.

From the above, it is understood that MW has potential to be used as a fine aggregate in mortars, but based on this previous work it is expected to lead to a decrease in strength which may result in a higher cement content and corresponding greater environmental impact in order to achieve comparable performance to more conventional mortar sands. Based on Figure 28 a 9% mica mineral content, about the amount of mica in the MW, could cause up to 50% decrease in 28day compressive strength for constant workability, but this could be due to the different particle size distribution of the MW compared to the conventional sands. This current work has attempted to quantify the effect of particle size distribution as well as mica content on the performance of both PC and alkali-activated binder mortars with the reasons for choosing alkali-activated binders described earlier. Based on the description of PC and alkali-activated binders presented earlier, the impact of the MW on PC and alkali-activated binders may be different for two main reasons:

- Portland cement based mortars require water for hardening reactions, while alkali-activated geopolymers require water for dissolution but can produce water during hardening (Duxson et al., 2007a). As noted earlier, the addition of mica affects the water demand of the mix which could therefore affect the hardening of the different binders in different ways.
- Micas are aluminosilicate minerals which could affect the Al:Si ratio in the alkali-activated materials and thereby affect their strength (Davidovits, 2011). If used as an aggregate, the micas will not be converted to a dehydroxylated state through calcination, but there could still be some dissolution of micas under alkali conditions and this is affected by temperature, dissolved Al and pH. (Oelkers et al., 2008)

2.7 China clay waste and mineral components as binder

2.7.1 Reuse of kaolin mining waste as a binder component

Numerous research studies using kaolin mining waste in building materials have been conducted and the applications vary according to the origin of the waste. Kaolin mining and processing waste from secondary deposits in Brazil has kaolinite as the major constituent (Maia et al., 2014) and investigations have focussed on calcining the waste to produce reactive metakaolin and silica (Maia et al., 2014, Angelica, 2006) and to produce zeolites (Hildebrando et al., 2014, Maia et al., 2011), AA blocks (Gomes et al., 2012), ceramics, mullite bodies and bricks (Menezes et al., 2009a, Menezes et al., 2009b, Menezes et al., 2008a, Menezes et al., 2005, Menezes et al., 2008b) and concrete applications including self-compacting concrete (Azeredo and Diniz, 2013). Waste from Canada but also high in kaolinite content has been used by other researchers (Lotfy et al., 2015) as partial substitution of cement without prior processing of the waste, while

"kaolin sand" which is a mixed mineral deposit with low purity kaolin (36% of kaolinite) was calcined and used in a similar manner to partly replace cement in concrete (Kuliffayová et al., 2012).

Of these studies, the one with properties closest to the UK waste was by Lotfy et al. (2015) which used kaolin waste equivalent to MW in fineness, which was dried, milled in a ball mill and sieved using a 150μm sieve. The waste consisted of kaolinite, mica and quartz. The mix design was based in 400 kg/m^3 binder content, 0.40 water to binder ratio, use of superplastisizer, 45% sand and 55% coarse aggregate and 0-25% substitution of cement with the processed waste. Their results showed that up to 10% replacement of cement did not negatively affect the porosity and water absorption of the samples while the higher the kaolin waste content the higher was the chloride ion penetration resistance. The use of kaolin waste also reduced the drying shrinkage which may be because part of the waste was acting as an inert filler. However, in terms of workability use of waste had negative effect in that additional water was required to achieve comparable flow, and the compressive strength ranged close to the value of the control mix (of 48.6MPa on day 56), reaching 48.5-51.3MPa. The equivalent results for splitting and flexural tensile strength were comparable to the control mix, without following a particular trend for increasing waste content.

The work of Kuliffayová et al. (2012) with a higher kaolinite content than in the UK waste showed that replacement of Portland cement with 5-15 wt% metakaolin deriving from kaolin sand heated at 650°C for 1h, showed up to 24% increase in compressive strength on day 28 and 46% on day 90 compared to the control samples (0% cement substitution). The increase in strength was attributed to pozzolanic activity, consumption of the produced $Ca(OH)_2$ by the burnt kaolin sand to produce a gel like product and improving the microstructure and pore structure. This strength increase is higher than that noted by Lotfy et al. (2015) and a similar level to that noted by Siddique and Klaus (2009) for pure metakaolin with Portland cement.

Gomes et al. (2012) tried to alkali activate coarse and fine kaolin waste using calcium hydroxide and separately, sodium silicate. Although the coarse waste contained 26% kaolinite, it did not develop sufficient strength to enable reliable measurement. The fine waste developed strength only after calcining at 750°C for 2h, and milling was suggested to improve the strength as it refines the mica flakes and therefore reduces the potential breaking points of its layers. The compressive strength on day 7 reached less than 10MPa using calcium hydroxide as the activator. When using sodium silicate as the activator and extensive milling of the waste after calcining (60000 rotations), the strength reached 40MPa. However, it is understood that the fine kaolin waste the authors used contains kaolinite as a major mineral, unlike the UK situation. This higher content of kaolinite in the waste from Brazil is most likely due to the different geological environment (a secondary or sedimentary deposit instead of the primary UK deposits) and the different processes used. In the UK what is called the "*clay matrix*", the material under the overburden that goes for refining contains a variable amount of kaolinite but is typically in the range of 10-25%. (BGS, 2009) Therefore, the performance that Gomes et al

reached would not be possible if using the same processing for the MW. Based on the details of the previous research using kaolin mining waste as a supplementary cementing material (SCM), the concentration of the kaolinite in the waste appears to be the key factor in the effective use of the waste as a binder component. In the cases discussed above, the kaolinite content of the waste was much higher than in the UK situation (typically below 10%, as shown in Chapter 3), indicating the option of use of the UK waste as a SCM may not be available.

2.7.2 Kaolinite, metakaolin and other natural/blended pozzolans in Portland cement systems

Metakaolin is valuable additive in Portland cement and its effect has been studied by many scientists (Khan et al., 2014, Shafiq et al., 2015, Sabir et al., 2001). Metakaolin in Portland cement consumes calcium hydroxide to an extent generating calcium silicate hydrate (C-S-H) and calcium aluminate hydrate (C-A-H), but pH does not drop below 12.5 (Khan et al., 2014). He et al. (1994) confirmed these products, specifically indicating C-S-H or tobermorite ($C_5S_6H_9$), gehlenite hydrate (C_2ASH_8), calcium aluminate monosulphate (C_4ASH_x) and calcium aluminate hydrate (C_4AH_{13}), in mortars using unheated and calcined kaolin at 550, 650, 800, 950°C for 100minutes at different intensities in XRD. Furthermore they found amorphous gel phase in all samples. After treating at 950°C, a fibrous C-S-H was detected using SEM.

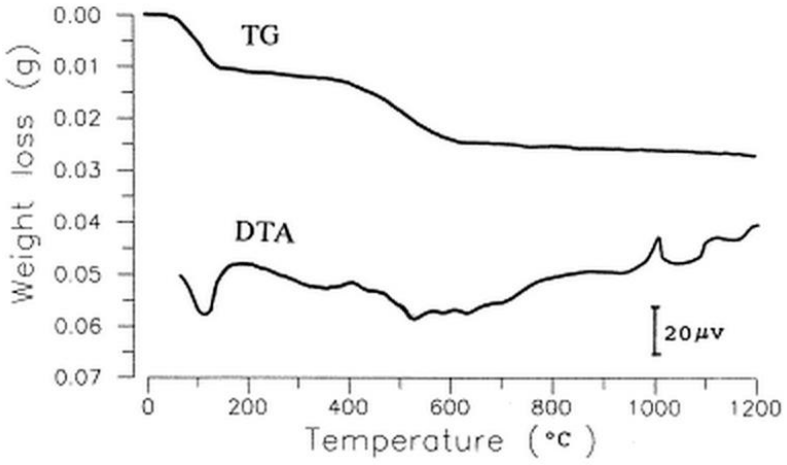

Figure 30 TGA and DTA patterns of synthetic mixed layer illite/smectite. Heating rate: 10°C/min. Sample weight: 0.169 g.

Khan et al. (2014) reviewed results on the use of various additives in cement and categorized metakaolin as “chemically active admixture” together with silica fume while other additives such as FA, GGBS and rice husk ash were categorized as “microfiller mineral admixtures” which work in different ways in cement. The first category is proved to improve the cohesiveness while increasing the water demand which can be adapted by using a superplasticizer, increasing the heat of hydration, decreasing the setting times. Metakaolin was the most reactive in the Chapelle test, with silica fume, fly ash and GGBS following in that order. Moreover it was noted that the small particle size and high specific area favours denser concrete microstructure and impermeability. Shvarzman et al.

(2003) (cited by Khan et al. (2014)) resulted that when adding metakaolin in a mix, if the amorphous content is less than 20% then it is considered inert, while an adequate amorphous content would enhance the performance in the activity index test (discussed in later chapter) without though an increase in amorphous content above 55%.

Detailed work on concrete mixes by Shafiq et al. (2015) on investigating optimum temperatures and the duration of calcination, showed optimum results in compression when up to 15% kaolin was used with 3 hours heating at 800°C with compressive strength of Portland cement based pastes reaching up to 100MPa. One hour intervals were used and it is noted that there was an increase in compressive strength recorded after day 28 when metakaolin was added, while the OPC had insignificant improvement from day 28 to 90. This trend is not confirmed for the PC mortars in Figure 31 which contain various clays.

The mortars of He et al. (1994) also showed their best performance after calcining at 800°C. However the increase in strength for calcining between 550 and 800°C was not significant and to serve environmental scopes, it was suggested to use the calcined kaolin at 550°C. At 950°C there was a reduction in the reaction rate but the strength is comparable to the strength at 650 and 800°C despite the appearance of mullite which reduces the amorphous material measured as the background in XRD. This is compatible with the NMR and structural characterisation by Watanabe et al. (1987) and Meinhold et al. (1985b), although 950°C is low temperature for formation of mullite according to Sperinck et al. (2011), noted in section 2.5.1. Use of unheated kaolin reduced the strength compared to the control 100% Portland cement mortars. The study of He et al. (1994) is included in Figure 31 (kaolinite heated at 800°C and unheated).

He et al. (2000) investigated the pozzolanic activity of a synthetic mixed layer mica/smectite raw material which was both unheated and calcined. What they referred to as a mica was found to be illite based on the powder XRD analysis. Smectite is also a phyllosilicate clay mineral and is highly expansive (Allaby, 2008). This study yielded interesting results and is described in detail as illite is related to muscovite to some extent. The TGA showed 6% weight loss due to the interlayer and absorbed water (60-160°C) loss, 9% loss during dehydroxylation (360-670°C) and the DTA showed two events (at 1000 and 1100°C) attributed to appearance of new phases (Figure 30). Based on the TGA the material was heated to 560°C (dehydroxylation had started), 960°C (before recrystallization, maximum glass content), 760°C (intermediate temperature). Sintering and agglomeration occurred at the highest temperature. The XRD at 560°C showed a hardly detectable background increase which is attributed to amorphous phases which common after calcination of crystalline phyllosilicates (He et al., 1994). At 760°C the background increased but the crystalline phases at 560 and 760°C remain the same indicating that the glass content developed in rims and the surfaces of the particles. Heating to 960°C shows even higher background and peaks for γ-Al_2O_3.

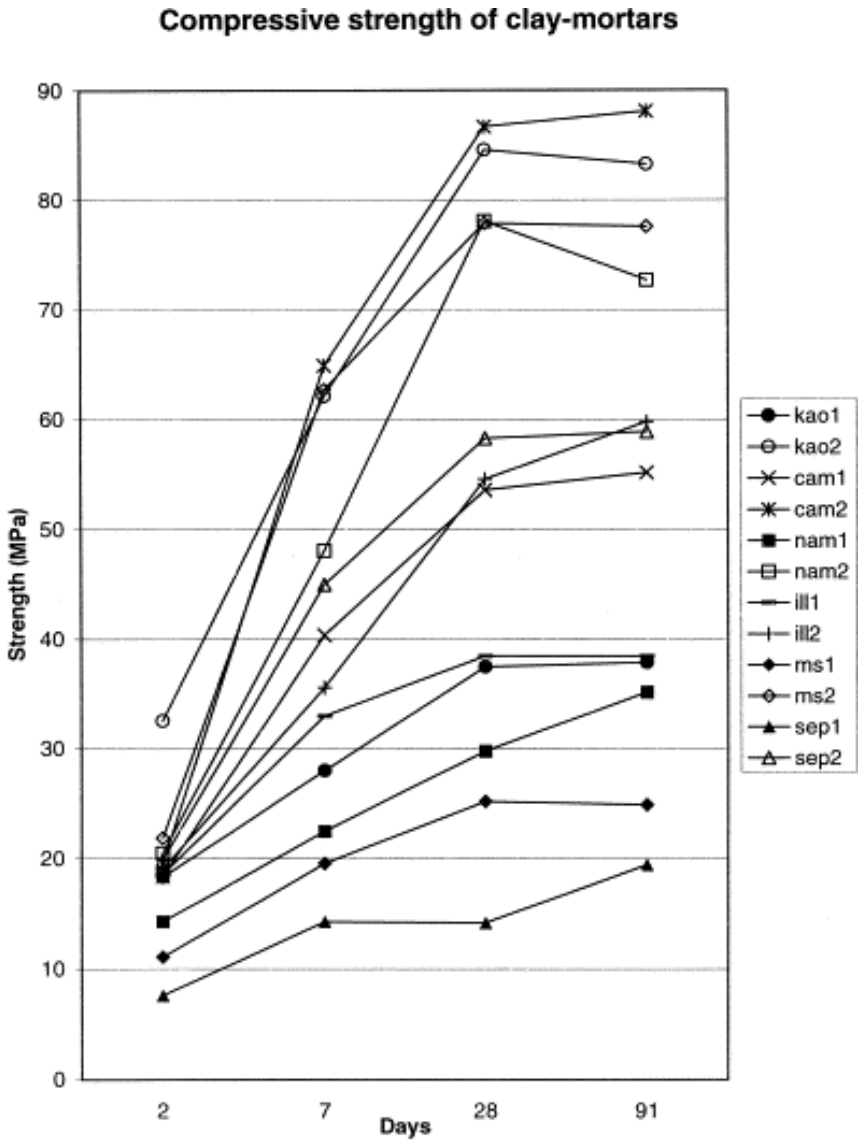

Figure 31 Effect of clays unheated (1) and heated to the optimal temperature (2), on compressive strength of mortars. Where: kao - kaolinite, cam - Ca-montmorillonite, ill - illite, ms - mixed-layer mica/smectite, nam - Na-smectite, sep - sepiolite. (from He et al. (2000))

Using NaOH (alkaline) and HCl (acid) solutions the solubility of Al and Si was investigated based on the concept of that the amount of Si and Al soluble in an alkali liquid can be an indication of pozzolanic activity as they would react with the pore solution of cement (Surana and Joshi, 1990, Massazza, 2003). The results show that an increasing amount of Si is released with increasing temperature (within the limits investigated) but the Al content is increased until 760°C and then dropped completely at 960°C due to the formation of γ-Al_2O_3 which is assumed to decrease the amorphous content in the calcine. However, the results of compressive strength of cement mortar samples of similar workability using the unheated and calcined mica/smectite showed a different trend, which rather correlates with the Si but not Al solubility. In addition there was a collapse of the mica/smectite structure as shown by XRD. There was an unsatisfactory pozzolanic index (indicating low pozzolanic behavior) for the unheated

material, double the strength for calcination at 560 and 760°C and an additional 60% increase for use of the 960°C calcine. In that perspective, it is understood that the measurement of Si and Al solubility is not necessarily indicative of the actual pozzolanic index of a material and in the next chapters the investigation of pozzolanic activity is focused on compressive strength. Moreover, Mehta (Mehta, 1987, Mehta, 1984) has shown that compressive strength is the most important factor when assessing pozzolanity.

It is noticed that based on the provided data in He et al. (2000), the w/c ratio for the unheated material when used in cement mortar was more than 1.0 and the value drops to 0.7 for a similar workability mix calcined at 560°C, with further slight decreases in w/c ratio for use with calcines at 760°C and 960°C. This behaviour is related to the loss of expansion with water during dehydroxylation and is probably one of the reasons for strength gain when using the calcines. As muscovite is not expansive and as it exfoliates during dehydration, the behaviour of the MW after heating is probably very different but no references to work on this could be found.

Figure 31 shows the effect of many types of clay to the compressive strength of PC. This figure is outcome of a series of studies on the listed clays, where the same experimental processes were followed. It is noted that kaolinite and Ca-montmorillonite when heated to optimal temperatures reach top strength. It is also of interest that the heated mica/smectite sample which was discussed above reached better strength than heated illite. It should be noted that in a book, Habert (2013) while referring to heated pozzolans, clearly stated that muscovite and phlogopite micas do not show pozzolanic activity but without giving reference or further information, therefore more investigation was needed.

2.7.3 Kaolinite, metakaolin and other natural/blended pozzolans as binder components in AAC technology

Regarding the use of natural pozzolans in geopolymeric cement, the most commonly used one is metakaolin. As it reaches high performance (Liew et al., 2011) its formulation into geopolymer was of interest: Davidovits (2011) presents MK-based geopolymer mixes with SiO_2/Al_2O_3=3.5-4 and Na_2O/SiO_2= 0.25-0.28 as overall molar ratios (from activator+precursor). Mohsen and Mostafa (2010) who used calcined kaolin measured compressive strengths of 20MPa at room temperature (curing for 3days) and about 28MPa at 75°C(curing for 1day) when using NaOH only while for use of sodium silicate the strength for the equivalent curing conditions was up to 60 and 70MPa. The potentials of unheated and heated kaolin have been summarised by Liew et al. (2011) but there are also publications specifically on the use of unheated kaolin in geopolymeric cement (Heah et al., 2013b, Heah et al., 2011b, Heah et al., 2013a, Heah et al., 2011a) showing that even the unheated material has potential for use in construction. However kaolin-based geopolymers without presence of other aluminosilicates form weak matrices according to Xu and Van Deventer (2002). Heah et al. (2013b) activated the kaolin using solution of NaOH of 6,10,12 and 14M together with sodium silicate in mass ratio of sodium silicate/NaOH equal to 0.24. That led to four mix combinations that all had molar SiO_2/Al_2O_3 ratios equal to 3.28 and Na_2O/SiO_2 decreasing from 0.28 (for 6M NaOH) to

0.53 (for 14M NaOH). Therefore the values used are close to the values recommended by Davidovits (2011) indicated above. As the XRD patterns from the research by Heah et al. show unreacted kaolin, the above ratios are the mix ratios and not the actual ratios in the reacted mix. The authors found atomic ratio Si/Al equal to 1.44 for kaolin particles and 1.53 for the geopolymeric product using EDX. Heah et al. (2013b) used kaolin/activator equal to 0.8, which sounds low (too much activator), and cured their samples at 80°C for 1, 2 or 3 days and tested them in compression. The results were low in the first 2 days (1-2MPa) but improved on day 3, with the combination of NaOH of 6 and 12M giving the best results of about 4.7 and 5.7MPa respectively. The same trend followed the measured bulk density. The fact that the trend was not smoothly increasing for increasing molarity of the NaOH as the authors were expecting was interpreted as related to the water content and regarding the mix of 14M which dropped the compressive strength, it was assumed that there was excess in Na_2O in the mix which weakened the hardened structure. No samples on day 2 and 3 dissolved in water and had no cracks. It is understood that when investigating the reactivity of a material, authors preferred using hydroxide rather than a combination with sodium silicate as the molar ratio of Na_2O/SiO_2 as mentioned earlier induces complexity. However, the strength would be higher for use of sodium silicate/hydroxide combinations.

van Jaarsveld et al. (2002) studied blends of fly ash/kaolin and used sodium and potassium based solutions of hydroxide and silicates for activation. The potassium based activators gave products with slightly higher compressive strength with a maximum 11.4MPa for 21% clay content and molar ratio of K_2O/SiO_2=1.05 on day 14. The equivalent value for use of Na_2O was 10.6MPa. The molar ratio K_2O/SiO_2=1.05 was understood to correspond to the solution, not overall from precursor and solution, as that would lead to excessive content of K_2O (estimating about 100g of K_2O for 100g of 79% fly ash plus 21% kaolinite without including silicate solution). In this publication, it was not clear what amount of M_2O (where M is Na or K) was used for the mixes. However, it is clearly shown that there is an optimum kaolin content, about 21%, above which the particles of kaolinite are only partially reacted and the remaining unreacted particles weaken the matrix. After calcining the kaolin at various temperatures, the performance highly improved. For 1 hour at 600°C and using K_2O/SiO_2=1.14, the compressive strength was 54MPa and for 900°C it was only 8MPa indicating the reactive metakaolin had transformed to more stable mineral phases as noted earlier. Calcining for 6, 12 and 24 hours were also tried but the maximum of 54MPa was not exceeded.

Bernal et al. (2012a) used GGBS/metakaolin(MK)-based mixes with solutions of variable SiO_2/Na_2O molar ratio for geopolymer concretes, so that the overall (activator+precursor) Na_2O/SiO_2=0.25 and SiO_2/Al_2O_3 was 3.6, 4.0, 4.4. These ratios are not representative of the microstructure of the binder due to incomplete dissolution but provide an initial target activator concentration. For increasing substitution of GGBS with MK, the Na_2O content of the mixes had to be increased in order to reach equivalent, high strengths. For the series based on GGBS only, the molar ratios of SiO_2/Al_2O_3=3.6 (which resulted in SiO_2/Na_2O molar ratio of the activator equal to 0.25) gave the lowest compressive strength (~18MPa on day 7 to ~30MPa on day 180) while SiO_2/Al_2O_3=4.4

(which resulted in SiO_2/Na_2O of the activator approx. 1.0) gave the highest strength (40-75MPa). For 20% MK and 80% GGBS, SiO_2/Al_2O_3=3.6 (resulted in SiO_2/Na_2O of the activator equal to approx.1.0) gave lower results (45-60MPa) compared to the mix of SiO_2/Al_2O_3=4.4 (SiO_2/Na_2O of the activator=1.5, 40-75MPa). It should be noted that the indicated strength values refer to concrete and they could vary for a binder alone.

2.7.4 Micaceous materials and associated minerals as binder components in AAC technology

It has not been possible to find publications on the use of calcined muscovite in Portland cement as a pozzolan, potentially replacing metakaolin. Limited previous work by a single research group has indicated it may be possible to use mica-rich mixed minerals in alkali-activated binders (Pacheco-Torgal, 2008,a, Pacheco-Torgal et al., 2008,b, Pacheco-Torgal et al., 2008,d, Pacheco-Torgal, 2008,c). It was therefore decided that the initial focus would be on these novel materials which have potential to use large quantities of the waste and provide technical and environmental benefits as described earlier.

Various phyllosilicate minerals have been studied and some have shown potential in geopolymeric binders. Xu and Van Deventer (2000) underlined the necessity to optimise the concentration of the alkaline solution for each mineral type, as this can have a large impact on cost and environmental impact. In this previous study, which records the dissolution of Al and Si and the performance of sixteen minerals in geopolymeric formations, it was concluded that dissolution does not necessarily imply higher strength as noted by He et al. (2000). The dissolution of Al and Si was measured for 2, 5, and 10 M of NaOH and KOH solutions and it was higher for the use of NaOH and generally followed an increasing trend for increasing alkaline concentration. Despite NaOH resulting in the highest dissolution, it was the use of KOH which achieved the higher compressive strengths. The only micaceous mineral that was used in this study, an illite, showed average dissolution but low compressive strength compared to the other minerals (7.1MPa and 5.8MPa for use of KOH and NaOH respectively, when the maximum strength reached was 18.9MPa for stilbite and use of KOH). Buchwald et al. (2009) studied the use of thermally treated illite/smectite clay as a raw material for geopolymer binders. The samples intended to be tested in compression were activated using a 6M NaOH solution, cured first at room temperature and later at elevated temperatures and high relative humidity. The maximum compressive strength of the binder was 13MPa and it was achieved for using the illite/smectite clay calcined at 850°C and 950°C.

Numerous publications (Pacheco Torgal et al., 2005a, Pacheco-Torgal, 2008,a, Pacheco-Torgal et al., 2008,b, Pacheco-Torgal, 2008,c, Pacheco-Torgal et al., 2008,d, Pacheco Torgal et al., 2005b) investigated a tungsten mine waste mud (TMWM) rich in muscovite and quartz and produced a binder and mortar with good mechanical and physical properties. Based on that evidence, a material of similar mineralogical composition named mica concentrate was specially produced for the needs for this PhD, in order to investigate the pozzolanity of the mica mineral in the MW as described later. Information on the mica concentrate is given in section 3.1.2 including also comparisons

with the material used by Pacheco et al. The XRD pattern of the thermally treated tungsten mine waste can be seen in Figure 33 but there is no quantitative mineralogical composition found in the mentioned above publications. In Table 8 the chemical composition of the waste is displayed. The Blaine fineness of TMWM is 357m^2/kg. After calcination at 950°C for two hours, a 12% of muscovite remained based on the main peak area measurements.

Assuming that muscovite is the only phase in TMWM containing Al_2O_3, although impurities could exist (many peaks in XRD), and based on the Table 5, muscovite is 43.4% of the TMWM. This is an indication as Table 5 displays the ideal composition of unheated muscovite. Further calculations based on the remaining SiO_2, show that quartz would be a 33.9%. Therefore, a 22.7% in TMWM cannot be attributed to either quartz or muscovite (see calculations in the Annex A.5).

In the above series of publications the mud was calcined at 950°C and mixed and different content of calcium hydroxide ($Ca(OH)_2$), alkaline solution, water, aggregates and, in some mixes, superplasticizer to produce binders and mortars (Pacheco-Torgal et al., 2008,b, Pacheco-Torgal et al., 2008,d). Specifically, in Pacheco-Torgal et al. (2008,b) the authors demonstrated that 10% lime gives the best results in compression and mixes using more than that percentage (up to 22.5% lime) showed a decrease in strength after 14 days of curing. Three reasons were assumed possible for causing the decrease: the developing of a porous phase, shrinkage and subsequent cracking and formation of a gel similar to that of alkali-silica reaction (ASR). The idea started based on blends of metakaolin/slag, where a 20% content of slag is equivalent to 8.6% $Ca(OH)_2$ and higher content of 40% slag would correspond to 17% $Ca(OH)_2$. The mixes were produced using sodium silicate ($Na_2O.nSiO_2$) and very high molar ratios of sodium hydroxide (NaOH) of between 6 and 24M which raises safety, cost and environmental impact concerns. It was stated that above a 6:1 mass ratio of sodium silicate to sodium hydroxide the mixes were too viscous to be mixed (while viscosity was already high from ratios of 3:1 and above, equivalent to Ms=1.5-1.9 depending on the molarity of the sodium hydroxide) and that NaOH of 24M was the highest concentration that could produce a fully dissolved solution. For the optimum of activator based on 2.5:1 sodium silicate to sodium hydroxide and 24M NaOH, the Ms is 1.17 (or 1.05 based on calculations in this study, see Annex). All samples were cured at room temperature. The activator of 24M gave the highest compressive strength for mortars, up to 70MPa on day 28, and a modest paste strength of less than 30MPa at 28 days. At this level of activator and lime concentration, it is unlikely that there will be environmental advantage over PC binders and this will be discussed in Chapter 6.

Specifically, the breakdown of the binder composition can be found in Pacheco-Torgal et al. (2008,d): the binder composition was 10g $Ca(OH)_2$ and 90g mine waste, while the activator had 28.57g NaOH solution and 71.43g Na_2SiO_3 solution. Based on the materials used by Pacheco-Torgal et al. (2008,d) and after calculations which can be seen in the Annex, it is found that Pacheco et al use an activator with 19.59g Na_2O. The optimum water to binder ratio for mortars was about 0.5 and there was a decrease in strength for

higher ratios. The aggregate to binder ratio was 1:1 in Pacheco-Torgal et al. (2008,b) and 0.5-1.5:1 in Pacheco-Torgal et al. (2008,d), which is low compared to the standard 3:1 in British Standards for mortars (BS EN 196-1:2005). The authors found these ratios convenient as higher content of aggregate would need extra water which would drop the strength. Finally, the development of such high strength is attributed to the use of calcium hydroxide and nucleation centers by the iron oxide in the mine waste. The iron content of the tungsten mud mine waste is higher than the equivalent in the mica concentrate therefore that might cause a different mechanical behaviour. It is expected that calcium silicate hydrates (C-S-H) to be formed by the reaction of the sodium silicate reacting with the lime and this product was indeed identified in SEM studies in another publication of the same study (Pacheco-Torgal et al., 2008,d). Binders and mortars with 0% $Ca(OH)_2$ were not mixed/presented.

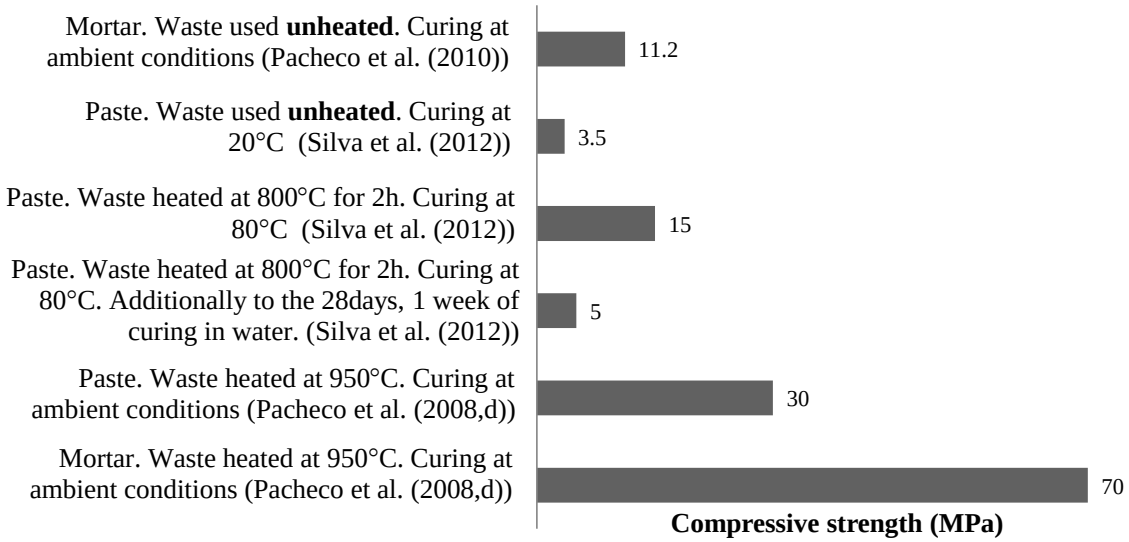

Figure 32 Panasqueira waste activated using solutions of sodium hydroxide and sodium silicate: Compressive strength after 28days of curing after Pacheco-Torgal et al. (2008,d) and Silva et al. (2012).

Pacheco-Torgal et al. (2010) studied the durability of the mortars described above comparing with OPC concrete. In abrasion resistance (mass loss measured after 1000 rotations in Los Angeles abrasion apparatus) the TMWM performed better than the OPC mixes while in acid resistance TMWM free of limestone aggregates showed low loss of mass. The performance is attributed to the low water absorption of the TMWM samples and the low content of Ca which would generate soluble substances. Interestingly, in this paper results using the raw unheated material in AA mortars are presented, showing about 11.2MPa compressive strength on day 28 while using the heated waste has about 39.6MPa on day 28, justifying the reasons the raw material was calcined. Apart from the low performance, for using unheated TMWM there is efflorescence reported in the final product caused by the reaction of unreacted sodium ions with atmospheric CO_2 forming $Na(CO)_3$. In this paper the activator is initially stated to contain 16M NaOH but later in the text they refer to 24M NaOH, which is assumed to be incorrect. Based on the previous

publications, 24M is the actual concentration of NaOH used. Even using such concentrated components in the activator, the leaching results for water contamination in this paper were found to be lower than that required values in the Portuguese Standard for irrigation water.

Waste material from the same source, Panasqueira in Portugal, was used by Silva et al (Silva et al., 2010, Silva et al., 2012). Their results were very different but they refer to different formulation: the raw material was calcined at 800°C for 2hours, the activator used was sodium hydroxide of 10M and sodium silicate (its specific chemical composition was not given) and lime was not added. Specimens that cured at 20°C and ambient relative humidity, disintegrated after immersion in water after 7days of curing. Specimens cured at 130°C in dry conditions, which is too high as 90°C is mentioned as maximum temperature for developing geopolymer gel (Davidovits, 2011, Duxson et al., 2007a) did not disintegrate. Samples intended to be tested in compression were cured at 80°C and, interestingly, samples (24MPa compressive strength on day 63) would lose their strength after immersion in water (6MPa after 1week in water). In Figure 32 the results of the 28d are presented graphically. The problems were attributed to deficient geopolymeric reaction , likely caused by insufficient concentration of NaOH to amount of reactive calcined or amorphous phases present (Silva et al., 2012). Some additional water added in the mixes and the dry conditions of curing were also suggested as a possible obstruction for the reaction. This indicates that the AAM produced by Pacheco-Torgal et al show good performance entirely due to the inclusion of lime, indicating the strength gain may be due to the C-S-H gel formed rather than a geopolymeric reaction.

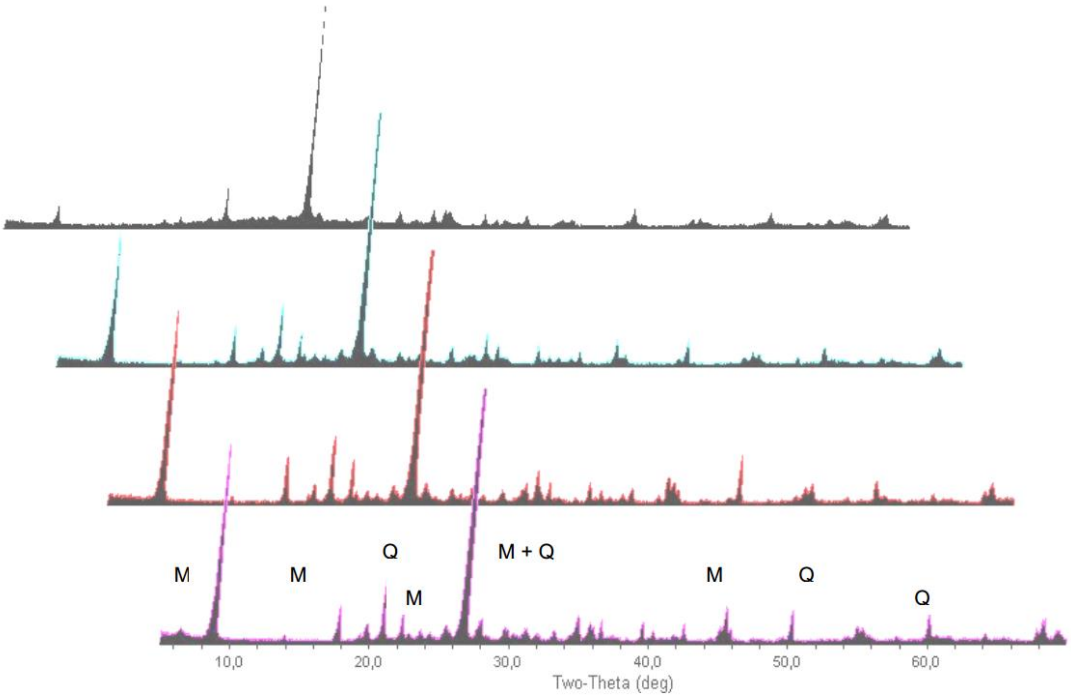

Figure 33 XRD patterns of tungsten mine waste from Panasqueira, Portugal, treated at 650,750,850,950°C. (after Pacheco Torgal et al. (2005b))

Ahmari and Zhang (2013a) used another material, copper mine tailings, to make bricks and used 15M NaOH, pressure of 0-35MPa, 8-18% water content (keeping the concentration of NaOH steady at 15M, mixing for 10min) and 90°C curing temperature. The copper mine waste in XRD showed crystalline phases of quartz, albite, sanidine and gypsum and some amorphous content (background at 2θ about 28°). Its particle size was ≤1mm. Therefore the mineralogical analysis is different to the mica concentrate but its particle size is close to the particle size of the MW. The mixes were reported to be "semi-dry to semi-paste" which is surprising for such low moisture contents (8-18%). The highest compressive strength achieved was about 35MPa on day 7 (test at dry conditions). It was reached for low pressure together with the maximum used water content (18%). The forming pressure was effective only for the lowest water content values. However, bricks that had strength of 27.8MPa, after four months in solutions of pH=4 and 7 decreased to 6 and 6.9MPa respectively. Pacheco-Torgal et al. (2014) referred to the outcome of Silva et al and Ahmari and Zhang (2013a), suggesting that it is the addition of lime that improves the durability.

Table 8 Chemical composition of tungsten mine waste (TMWM) (after Pacheco-Torgal et al. (2008,d), Pacheco Torgal et al. (2005b)) and copper mine waste and supplementary materials (by Ahmari and Zhang (2013b) and Ren et al. (2014)) .

Sample details	**Al_2O_3** (wt%)	**SiO_2** (wt%)	**Fe_2O_3** (wt%)	**TiO_2** (wt%)	**K_2O** (wt%)	**CaO** (wt%)	**MgO** (wt%)	**Na_2O** (wt%)	**SO_4/ SO_3/SO_2** (wt%)	**As** (wt%)	**Minor oxides/ LOI** (wt%)
TMWM	16.66	53.48	12.33	1.39	7.65	-	1.27	0.62	3.10	1.28	2.22
*Copper Mine T.	7.08 (14.1)	64.80 (55.9)	4.33 (3.07)	-	3.30 (3.9)	7.52 (2.27)	4.06 (1.78)	0.90 (3.02)	1.66 (2.2)	-	6.39 (13.8)
CKD	3.90	11.00	2.00	-	0.60	42.0	3.60	-		-	36.90
AS	31.70	1.50	2.68	0.01	0.08	0.20	4.03	6.44	13.3	-	40.06

* Material used by Ahmari and Zhang (2013b), values in parenthesis refer to the material used by Ren et al. (2014)

Later, Ahmari and Zhang (2013b) added cement kiln dust (CKD), a by-product of the Portland cement industry which is rich in Ca, and with only 10% addition needed to reduce the loss of strength after embedding samples in water. Ren et al. (2014) used aluminum sludge (AS), a waste product, to improve the performance of the geopolymeric bricks without testing them wet to check the durability. Both tested the compressive

strength only after 7days curing and in the case of Ahmari and Zhang (2013b), after keeping half of the samples in water for 7days. By examining the XRD traces, the CKD seems more crystalline than the rather amorphous AS. While the CKD has high content of CaO and Ahmari and Zhang (2013b) suggested that the formation of $Ca(CO)_3$ and generally incorporation of Ca in the matrix is beneficial, the AS had practically no CaO and the improvement of the strength was attributed to the available amorphous alumina and finding the optimum Si/Al and Na/Al ratios (see subsection 2.4.3.1 and Figure 21 and 21). The chemical composition of the copper mine tailings, CKD and AS is shown in Table 8. The waste used in the work of Ahmari and Zhang (2013b) and Ren et al. (2014) is from the same place (Tucson, Arizona) however, as shown in Table 8, the chemical composition varies which is expected for different batches of waste. In the table, the waste from Ahmari and Zhang (2013b) is the values out of parenthesis and the values from Ren et al. (2014) are in brackets. Depending on the molar ratios used for the mix design Ren et al. (2014) proved that addition of 20% AS can provide 0-60% more strength of the binder of 0% AS content.

From the these previous studies it is understood that a fine form of material containing mica mineral, as the MW, has potential for use in alkali activated binders, but that the performance of this binder would be very dependent on the activator concentration and Ca content of the mix. None of these presented studies investigated the environmental impact of the binders and in particular the increased activator concentrations which may limit their application as a low impact binder replacement.

Together with successful case studies, it is equally valuable to learn from unsuccessful applications. Pyrophyllite (with impurities of quartz, kaolinite and illite) was used by MacKenzie et al. (2008) to produced geopolymers after calcining at 800C for up to 24h but did not result in a viable product. Pyrophyllite ($Al_2Si_4O_{10}(OH)_2$) is not a mica but belongs to the 2:1 layer lattice aluminosilicates (MacKenzie et al., 1985b) therefore it has similar structure to the mica mineral in the china clay waste. The difference with muscovite relies on the fact that pyrophyllite does not contain alkali metal ions as interlayer, which is a charge balancing mechanism as explained before, therefore the tetrahedral sheets of Si show no substitution by Al (which would cause charge) (MacKenzie et al., 1985b). Pyrophylite dehydroxylates in similar temperature range as muscovite, at 550-900°C and its dehydroxylate has also Al in five-coordination. At higher temperatures, the dehydroxylate is destroyed and mullite and cristoballite are formed instead (MacKenzie et al., 1985b).

In MacKenzie et al. (2008) the mix had SiO_2/Al_2O_3=4.6 and Na_2O/SiO_2= 0.37 with reference to unheated pyrophyllite. The authors mixed 1.5g of pyrophyllite with 3g of alkaline solution (it is calculated that the solution contained about 0.43g of Na_2O, which is equivalent to the very high content of 28% Na_2O for 100g of pyrophyllite). According to this mixing composition, more than 2g of water (2.4g is calculated) correspond to 1.5g of pyrophyllite. That sounds high as water to binder ratio and could have a negative effect in geopolymerisation, however, depending on the fineness of pyrophyllite (which is not given) and unheated/calcined state, maybe the need for high amount of water was

necessary. The samples were cured wrapped in plastic film, heated at 60°C for 24h and then, after removing the plastic film, dried for 24h more at 60°C.

The observations of their study were based on XRD analysis for the raw material and NMR for both raw material and final product. Although the 27Al NMR showed the initially octahedral sites of the raw material being converted to tetrahedral for the calcined material at 800°C and even almost disappearance of the octahedral Al peak, the XRD pattern of the calcined material showed many peaks of high intensity. Also, looking at the XRD pattern of the calcined pyrophyllite, no increased background can be detected compared to the XRD pattern of the unheated material. Although no tests for compressive strength were performed, the conclusion that 800°C-pyrophyllite-based geopolymer is not viable was based on its NMR analysis which showed that the 27Al and 29Si spectras were similar to the spectra of pyrophyllite at 800°C; the 27Al spectra showed absence of octahedral sites which is positive, but the 29Si spectra had three peaks (at -87, -90, -101) instead of a broad peak centered at about 90ppm if to be considered well developed geopolymer. The reason for the non-reactivity of pyrophyllite despite its dehydroxylation was attributed to the 2:1 lattice which does not allow access to the tetrahedral Al as the Si layer works as a barrier.

In the same study of MacKenzie et al. (2008), grinding of pyrophyllite was also used as a way to increase reactivity. Ball milling for 20h, ball milling for 60h and vibro-milling for 15min was tried. The latest two were successful in disrupting the 2:1 layer lattice and produced semi-amorphous products (shown in their XRD patterns by presence halos). It should be mentioned that the 27Al of the raw, ground materials included octahedral (at about 4ppm), tetrahedral (at 52-70 ppm) resonances and fivefold coordinated Al (at about 30ppm), in contrast to the dehydroxylate. A shortlisting of this study is that the physical characteristics of the raw material are not sufficiently presented: It is not known what the particle distribution of pyrophyllite was initially and what the particle distribution was after milling for 20h, 60h and vibromilling and/or what the surface area of the samples was. Regarding muscovite, the minimum particle size that can be achieved is less than 53μm for micronized mica, 95-45microns for wet ground mica and 1.2mm-0.15mm for dry ground mica (Pérez-Maqueda et al., 2004). Before considering methods for reducing the particle size of muscovite, it should be noted that sonication results in reduced particle size but does not affect the Al and Si coordination (observation based on NMR analysis) (Pérez-Maqueda et al., 2004) while grinding generally leads to amorphisation (observation based on MacKenzie et al. (2008) and Sánchez-Soto et al. (2000)).

2.8 Summary

From the information presented above, it is possible to use the coarser fractions of the waste (stent and sand) as a replacement aggregate for concrete or asphalt, without any need to modify existing standards. The biggest limitation on potential use as an aggregate appears to be transport costs as the local market is already using large quantities of these

materials, but these uses are limited to high-profile specialist applications using rail transport outside of the Devon / Cornwall area.

The potential use of china clay mining waste as a binder component is largely related to waste streams with a higher kaolinite content than is present in the UK waste stream. These previous studies have focused on use with Portland cement, and one referred to alkali-activated binders (Gomes et al., 2012). It is understood that there is potential for alkali activation to enable the use of waste with a lower kaolinite content in binder applications, and this is discussed in more detail later. In none of the previous applications with Portland cement was the environmental impact of using the waste discussed in detail.

Based on the information in the literature which is presented above, the choice of using the china clay waste in AAC (a) covers the requirement for good performance and relatively good durability; (b) shows flexibility for curing conditions and setting times as precast applications are targeted; (c) takes advantage of the aluminosilicate nature of the waste which could show chemical bonding in the interfacial transition zone between aggregate-binder or ideally, could result in a geopolymer binder; (d) has good potentials to reduce carbon emissions but this will depend to the amount and the concentration of the alkaline solution for the designed mixes.

Chapter 3: **Materials and Materials Characterisation**

Several tests were conducted for the characterisation of the waste* and other materials used in the study as a starting point. The aggregates (stent, sand, MW) were characterized in terms of mineralogical (XRD) and chemical (XRF) composition, particle distribution, water absorption and apparent relative density as required in BS EN 12620:2002+A1:2008. For the secondary aggregates which were supplied by industry (stent and sand) all the properties were known and given. The chemical composition was given for materials used in the manufacturing of alkali-activated binders and the XRD analysis was conducted where applicable. Concentrated mica, a material specially produced for the scope of the PhD, was included in most of these analyses. The concept of thermally treated wastes/materials in binders has been explained in chapter 2 and applied to concentrated mica and MW in this chapter. The mineralogical and chemical analyses were of crucial importance given the complicated nature of alkali-activated binders where the design of composition is based on chemistry and the composition of the raw materials. It is noted that the waste and all the materials which are by-products have varying consistency, therefore the results presented are indicative based on a large sample collected at the start of the research. The microstructure of aggregates and finer material used as precursor in AAM is presented using SEM. An optical microscope was used where it considered useful. The last part of this chapter focuses on the reactivity of the waste as it was of special interest for the future uses: a thermogravimetric analysis, Solid state-NMR, XRD and a European Standard in pozzolanic index were all used to achieve that scope.

3.1 Materials used, composition and properties

3.1.1 Waste

MW from the Littlejohns MW dam in Cornwall (Imerys) was used in an investigation of pozzolanic properties after calcining (section 3.3) and it was used as aggregate in AAM (Chapters 5 and 6). MW had apparent relative density 2.71Mg/m^3 and water absorption 1.5%, values measured in the lab according to BS EN 1097-6:2013, clause 9.

Sand 0/4 (in this study also called CCS 0/4 from China Clay Sand) and stent 4/10 supplied by the Aggregate Industries (one of the enterprises that uses secondary aggregates in concrete and asphalt) were used in concrete (Chapter 6) while the CCS 0/4 was also sieved following the particle size distribution of standard sand and used as such in mortars (CCS, Chapter 5). Tests common for aggregate characterization and results of those tests on CCS 0/4 and stent, are provided in the Annex A.1. These tables were supplied by Aggregate Industries and include the apparent relative density and water absorption tests according to BS EN 1097-6:2013. For stent the values of apparent relative density and water absorption was 2.67Mg/m^3 and 1.3% respectively, while for CCS 0/4 it was 2.68Mg/m^3 and 1.1%. It should be mentioned that all forms of the waste

* Where "waste" meaning all three types of the china clay waste, unless otherwise indicated.

used in this study were used dry, after reaching constant mass in the oven. For stent, the drying temperature used was 105°C while the finer materials which were also investigated as binders, like MW and mica concentrate (described in the next section), oven set at 65°C was used.

Mineralogical and Chemical composition

The chemical and mineralogical analyses for the above waste forms were conducted in the laboratories of Imerys in Cornwall and are presented in Table 9 and Table 10. These results are indicative based on a large sample collected at the start of the research project. As part of the standard processes at the plant the chemical and mineralogical composition is tested at different times and discussions with Imerys indicated these results are representative of the waste streams. Because of the commercially sensitive nature of the information, the range of available properties is not presented here. This was not considered a limiting factor as the standard quality control procedures in the plant have been demonstrated to be able to supply consistent products should this be necessary for the new uses investigated here.

Table 9 Mineralogical Analysis–XRD (wt%). Analysis conducted by Imerys in Cornwall.

Sample details	**Kaolinite** (wt%)	**Mica** (wt%)	**Quartz** (wt%)	**Feldspar** (wt%)	**Schorl** (wt%)	**Montmorillonite** (wt%)
CCS 0/4	4	9	58	21	8*	---
MW	8	9	50	22	11*	---
Fines after washing Stent	32	19	8	18	5	18
Mica concentrate	17	74	9	---	---	---

*estimated

Information about the constituent minerals of the waste, quartz, feldspar, kaolinite, micas and schorl, seen in Table 9, has been presented earlier in section 2.5 and their chemical compositions and properties were listed in Table 7. Regarding the family of micas, personal communication with research staff from Imery's (Jeremy Hooper, pers. comm., 16th May 2013) confirmed that the mica mineral in Cornwall comprises mainly muscovite with biotite and there is presence of zinnwaldite. Table 9 and Table 10 were checked for consistency with the help of Table 7 and it was found that they are quite accurate (see Annex A.5). Slight variation is attributed to the fact that mica was assumed to be 100% muscovite (while as mentioned above biotite and zinnwaldite could be present) and that the XRD is often only accurate to 3% and requires some manual

interpretation (Hillier, 2000) while oxide analysis using XRF is considerably more accurate.

Fines - a powder leftover after washing stent and mica concentrate was used only in mineralogical and chemical analyses, but is not used further in this study. The mineralogical analysis ran on this material (Table 9) showed much higher content of kaolinite and higher content of mica mineral than in CCS 0/4 and MW. This is because very fine particles, as kaolinite and some small particles of mica mineral, stick on the surface of coarse aggregate without this being depicted in the particle distribution of stent (Figure 34). This observation is important when using stent in concrete (Chapter 6) and it comprises a difference between stent and primary aggregate.

Table 10 Chemical Analysis – XRF (wt%). Analysis conducted by Imerys in Cornwall.

Sample details	**Al_2O_3** (wt%)	**SiO_2** (wt%)	**Fe_2O_3** (wt%)	**TiO_2** (wt%)	**K_2O** (wt%)	**CaO** (wt%)	**MgO** (wt%)	**Na_2O** (wt%)	**LOI** (wt%)
CCS 0/4	9.2	84.3	1.58	0.14	3.11	0.05	0.23	0.32	1.03
MW	10.95	81.23	1.89	0.22	3.21	0.05	0.32	0.29	1.79
Fines after washing Stent	26.95	56.9	1.99	0.18	4.76	0.65	0.79	0.62	6.9
Mica concentrate	30.8	51.59	2.31	0.74	5.45	0.01	1.13	0.03	7.89

Particle size distribution

Figure 35 presents the distribution of the particle size of aggregates used to make concrete, including the MW, CCS 0/4 (as given by the Aggregate Industries) and stent. Figure 34 displays the CCS as used in mortar, meaning sieved and recombined to the particle size distribution of standard sand. According to BS 1377-2:1990, MW was wet sieved and the hydrometer test was used for the finer portion. The distribution of the other two samples was given by Aggregate Industries who also supplied the material. It should be noted that as CCS and stent are broadly used as secondary aggregate, their distribution can be changed but it always conforms to BS EN 12620:2002+A1:2008 before sale.

As MW is the output of hydrocyclone processing, it is consistent in terms of particle size. Approximately 92% was within the range of 0.06-0.5mm particle size and it can therefore be considered a fine to medium sand. This left 8% of silt and clay. However, cross checking with the XRF analysis revealed some inconsistency: Table 2 shows 8% of kaolinite in MW and 9% mica mineral. This difference between clay sized particles and clay minerals indicates there is some agglomeration of kaolin and presence of larger sized

mica flakes. The abundance of these larger particles may limit the reactivity of the waste without some form of processing (e.g. milling).

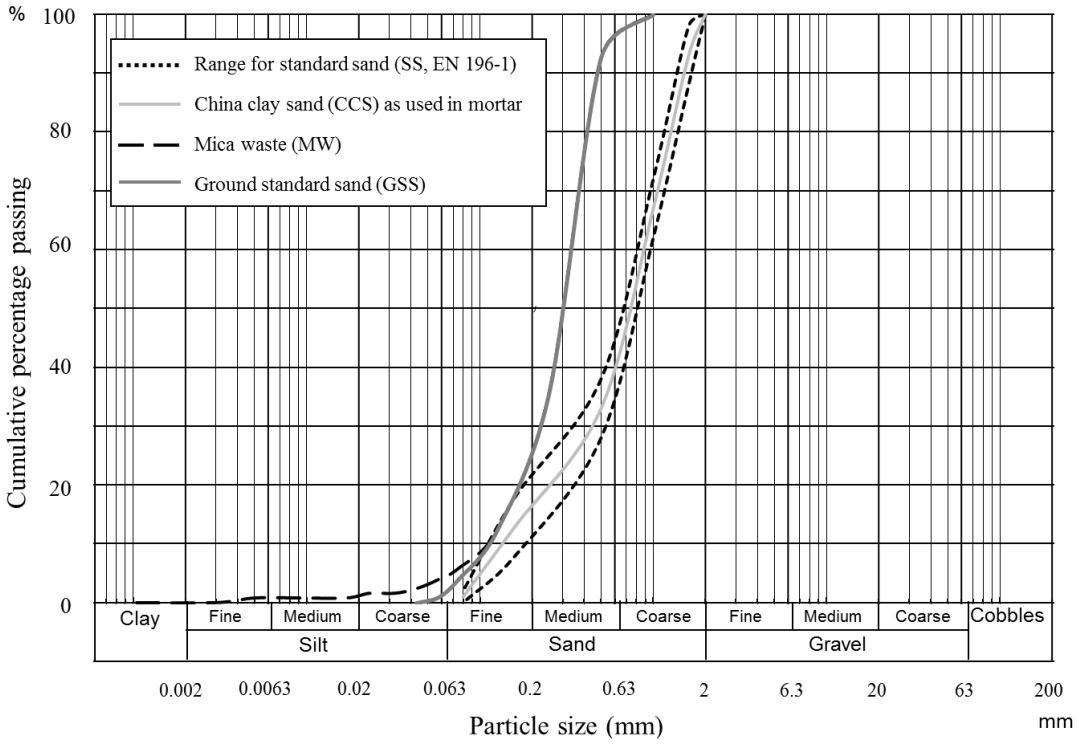

Figure 34 Distribution of the sands used in the mortar mixes.

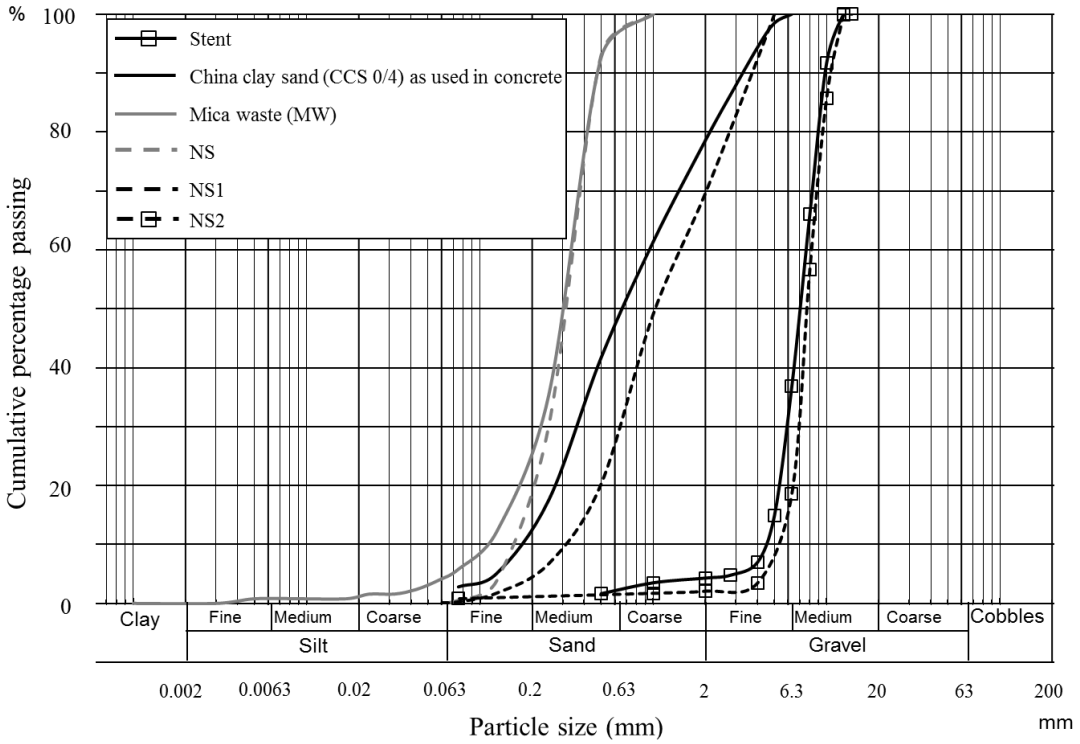

Figure 35 Distribution of the sands used in the concrete mixes.

Thermogravimetric analysis (TGA)

A thermal analysis can provide an insight into the composition of a material. Figure 36 shows the mass loss for the MW during heating to 1000°C with a rate of 10°C/min using a Q500 thermogravimetric analyser manufactured by TA instruments (University of Bristol). The test ran in nitrogen gas to minimize oxide reactions.

The TGA showed that till 1000°C there is low loss of mass which is due to the dehydroxylation of kaolinite at 450-650°C (Watanabe et al., 1987) and the dehydroxylation of muscovite as the major micaceous mineral, issues discussed in 2.5.2. The loss was low, less than 6%, which is justified based on the mineralogical analysis of MW (Table 9) which shows small content in mica mineral (9%) and kaolinite (8%). The dehydroxylation seems to be largely completed at 950°C which is consistent with the work by Pacheco-Torgal et al. (2008,b).

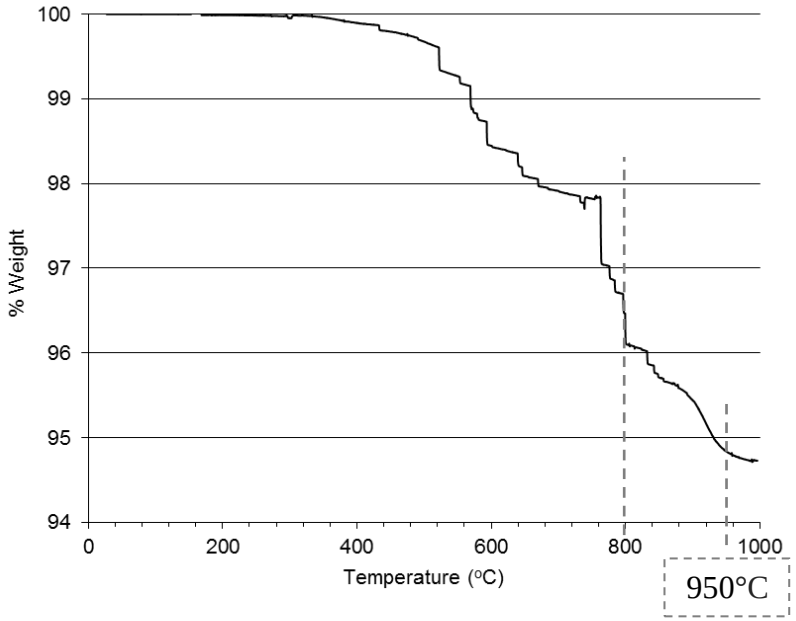

Figure 36 TGA curve of MW, 10°C/min under air flow.

For technical reasons (risk of damaging the crucible) the temperature only reached 1000°C and although at that temperature the curve appears to flatten, the thermogravimetric analysis from Mackenzie et al. (1987) referring to two types of muscovite (see section 2.5.2) is displayed in Figure 37 as an example to what to expect at higher temperatures, although more detail has been given in 2.5.2. As it can be seen that the difference between 950-1200°C on the loss of mass in that case was about 0.5%, indicating stopping at 1000°C did not adversely affect the outcomes. Therefore it is considered that the muscovite in the MW has largely completed its dehydroxylation at 950°C. It is noticed that at 800°C, the dehydroxylation is ongoing for the MW, while for the purer-in-muscovite samples of Mackenzie et al. (1987) (no kaolinite impurity), the dehydration has just started. These outcomes will be used in sections 3.3 and 4.2, in the thermal treatment of the waste.

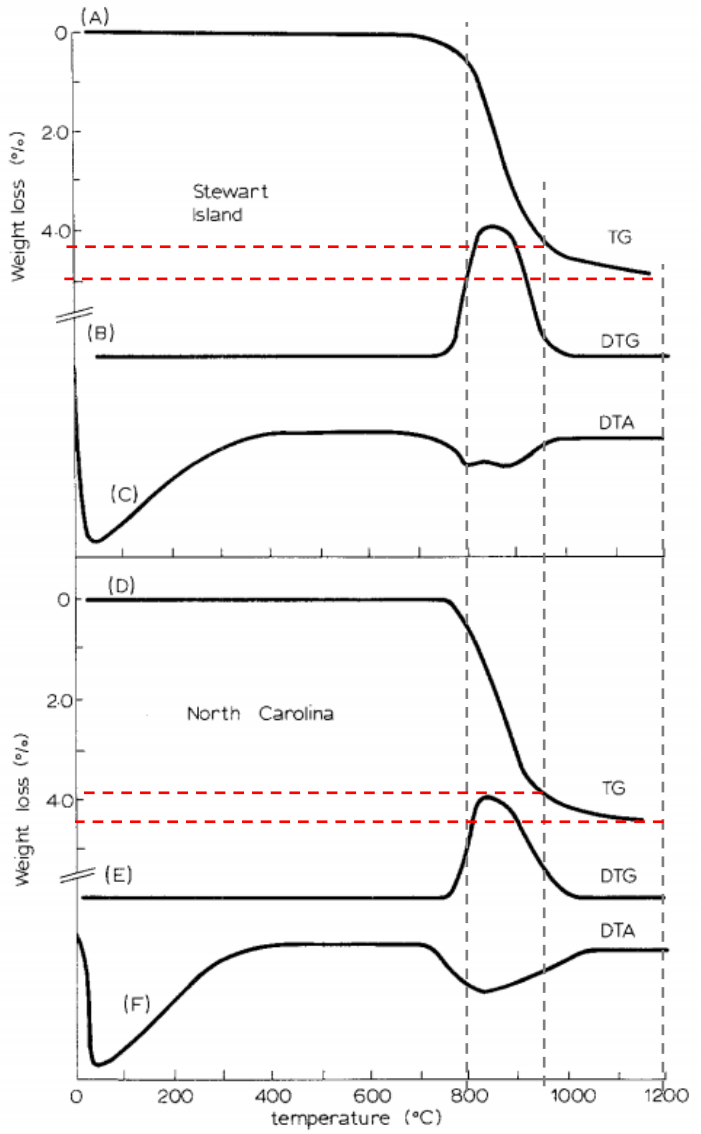

Figure 37 TGA curves of two muscovite samples from Mackenzie et al. (1987).

3.1.2 Mica concentrate

Mica concentrate is a mica mineral rich material deriving from the MW. It was produced by Imerys in Cornwall for the scope of this research in order to determine whether the mica minerals present in the waste stream could be used for the development of binders. Through froth floatation the physical separation of mica mineral particles was achieved. The physical separation method used could not achieve complete purity of mica minerals and some kaolinite and quartz remained. Mica concentrate is like powder, micronized, with all of it passing a 500μm sieve, 95.2% passing a 125μm sieve and 71.7% passing a 63μm sieve. Its mineralogical and chemical analyses are presented in Table 9 and Table 10.

3.1.3 Standard Sand (SS) and Ground Standard Sand (GSS)

Clause 5.1 EN standard 196-1 specifies that a standard sand for production of mortars contains at least 98% silica and has a particle size distribution with maximum 2% passing the 0.08mm sieve (Figure 34). This standard sand will be referred as SS in this study. The apparent particle density and water absorption of SS were measured according to BS EN 1097-6:2013, clause 9 (pyknometer method for aggregate particles passing the 4 mm test sieve and retained on the 0,063 mm test sieve – therefore only the amount of MW which was >63μm was tested), and they were 2.62Mg/m^3 and 0.5% respectively. Ground Standard Sand (GSS) was produced in the lab, using standard sand as raw material, sieved to follow the particle size distribution of MW (for fractions >63μm) as shown in Figure 34.

3.1.4 Primary aggregate for concrete

Primary aggregates that were used in concrete for comparison, were: regular coarse aggregate, Mendip rock (NS2), Marlborough sand (NS1) and quartzitic builders sand (NS). Their particle size distribution is similar to stent, CCS 0/4 and MW respectively and is shown in Figure 35.

3.1.5 FA

Cemex 450-S was the type of Fly Ash (FA) used in the tests and its chemical composition is shown in Table 11. The chemical analysis was provided directly by the supplier. An XRD analysis (Figure 38) showed distinct peaks for quartz, mullite and hematite in addition to the amorphous materials. As shown, because of the presence of these crystalline impurities, the peak signal intensity is much higher than for the GGBS. In Cemex website it's described as: "*a controlled fineness fly ash used as a Type II cement addition adding extensive concrete benefits including improved water / binder ratio (compared to Portland cement concretes of the same workability), reduced permeability, low chloride ingress, improved rheology and sulfate resistance.*"(CEMEX, 2012) Images of the raw FA using the SEM are shown in Figure 38.

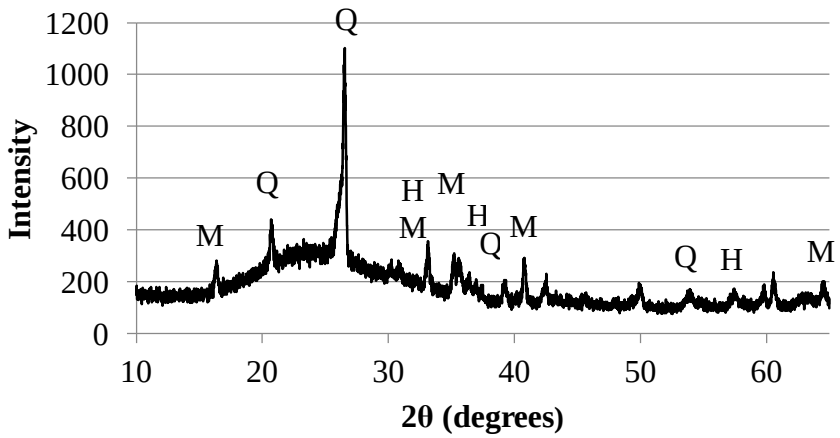

Figure 38 XRD pattern of FA (Q: quartz, H: hematite, M: mullite)

3.1.6 GGBS

Ground Granulated Blastfurnace Slag (GGBS) was provided by the Hanson Heidelberg cement group from the Port Talbot works. It had 401m^2/kg fineness. Its chemical analysis is shown in Table 11. The supplied GGBS had high content of magnesium monoxide, 8.47%, higher than the equivalent content in publications listed in Table 2. As discussed in subsection 2.4.3.1, this is considered beneficial, related to hydrotalcite and less Al incorporation in C-A-S-H, enhanced coarse porosity therefore higher compressive strength and enhanced resistance in natural carbonation. The low content of iron(III) oxide, 0.28% in Table 11, is also a good indication of a reactive GGBS (also discussed in subsection 2.4.3.1) therefore taking into account Figure 39 and Table 11 this GGBS was expected to perform well as precursor in alkali activated binders. Images of the raw GGBS using the SEM are shown in Figure 42.

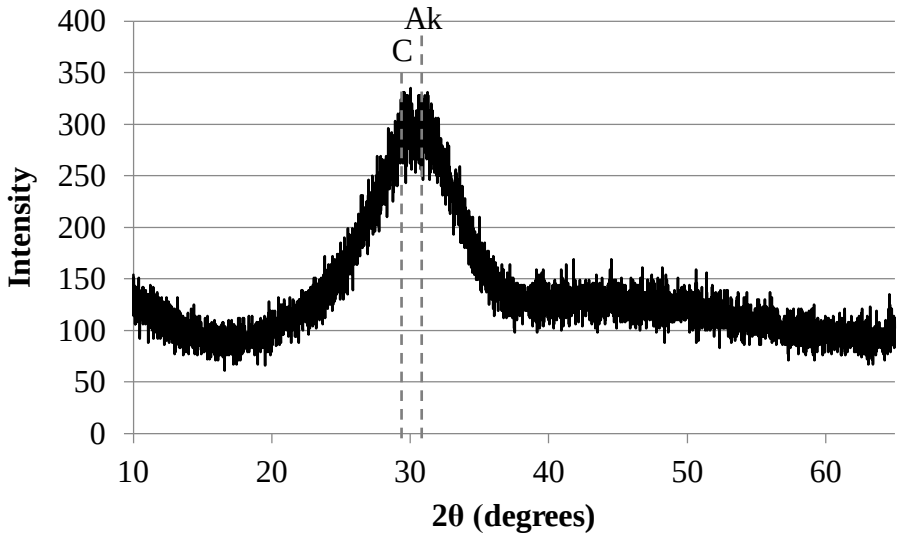

Figure 39 XRD pattern of GGBS. Hint of akermanite (Ak) and calcite (C).

In the XRD pattern (Figure 39), the halo and the absence of distinct peaks which would correspond to impurities indicate it was highly amorphous, unlike the Fly Ash which showed distinct peaks (Figure 38). In Figure 39, although there is no distinct peak, there is a hint of calcite (main peak at 2θ=29.4°) and akermanite (main peak at 2θ=31.2°). The identification has been based on powder diffraction files used by Bernal et al. (2014). It is noticed that the XRD pattern of this study is very similar to the XRD pattern of raw GGBS from Australia in Bernal et al. (2014) (the second listed slag of Bernal et al. (2014) in Table 2) although their chemical compositions (Table 2 and Table 11) are not particularly similar (only Al_2O_3 content the same, ~13%) which shows the complexity of working with by-products.

Table 11 Chemical analysis of precursors.

Constituents (wt%)	**GGBS**	**FA**
SiO_2	35.15	49
Al_2O_3	13.07	23.5
Fe_2O_3	0.28	8.7
CaO	39.6	2.4
MgO	8.47	1.4
SO_3	0.17	0.8
Na_2O	0.14	3.06
K_2O	0.51	0.87
TiO_2	0.66	-
MnO	0.44	-
P_2O_5	-	1.1
LOI	0.97	4.4

3.1.7 Sodium Silicate and Sodium Hydroxide

Only sodium silicate and sodium hydroxide were used for geopolymer activators for this research. The sodium silicate ($Na_2O{\cdot}nSiO_2$) used for the research was supplied by Tennants Distribution Ltd. It was in solid (spray-dried powder) form and comprised Na_2O, SiO_2 and H_2O at 27.05, 53.5 and 19.45 wt% respectively.

Two types of Sodium Hydroxide (NaOH) were used: One is dry NaOH pellets supplied by Sigma-Aldrich (used for mortars) and the other was NaOH solution, 50% in water, again supplied by Sigma-Aldrich (used for concrete). Dry NaOH and the $Na_2O{\cdot}nSiO_2$ were mixed separately with distilled water and cooled to ambient temperature before use.

3.1.8 Portland Cement

Portland cement mortars were produced for comparison. In order to achieve high strength, comparable to the strength of the alkali-activated cement mortars, CEM I 52.5N by Cemex was used. This is a free of mineral additives Portland cement, chosen in order to minimise the effect of mineral additives. According to BS EN 197-1:2011, 'N' is for ordinary early strength and 52.5 is the strength class: on the 28^{th} day the compressive strength of the mortar (mixed as described in BS EN 196-1:2005, beam moulds) should be higher than 52.5MPa.

3.1.9 Calcium hydroxide

Calcium hydroxide (hydrated lime) was supplied by Sigma-Aldrich. It was in the form of powder and had ≥95% purity.

3.2 Macro and Microstructure

The following images refer to MW, calcined MW (MW heated at 950°C and 1100°C, discussed in Chapter 4), mica concentrate, standard sand, FA and GGBS. The materials were adhered to SEM stubs using carbon tape and the samples were imaged in JEOL SEM6480LV analyser or a Leica M205 C optical microscope with an incorporated Leica DFC425 camera. Not all samples were viewed under both the SEM and optical microscopes. Most of the SEM images here have 100 times magnification so that the sizes will be comparable. After having presented the mineral categories and optical properties (colour and diaphaneity) of minerals in the MW in Table 7, the following can be noted from the images:

- Muscovite and zinnwaldite are easy to detect under optical microscope (Figure 40) due to their iridescent properties while biotite is hard to see due to the black background of the carbon tape (under SEM, the carbon tape shows at the background with characteristic circles, Figure 41).
- As noted from particle size distribution and the XRD analysis, the MW had a finer particle size distribution than the mainly quartzitic standard sand and contained mica minerals (Figure 41, identified by the characteristic flat plate structure and near perfect basal cleavage).
- The mica concentrate is micronized with 71.7% passing the 63 micron sieve as mentioned in section 4.1.2. Due to that the special features of the minerals were not easily detected, but it is still possible to see some layered structures (mica and/or kaolinite, Figure 41).

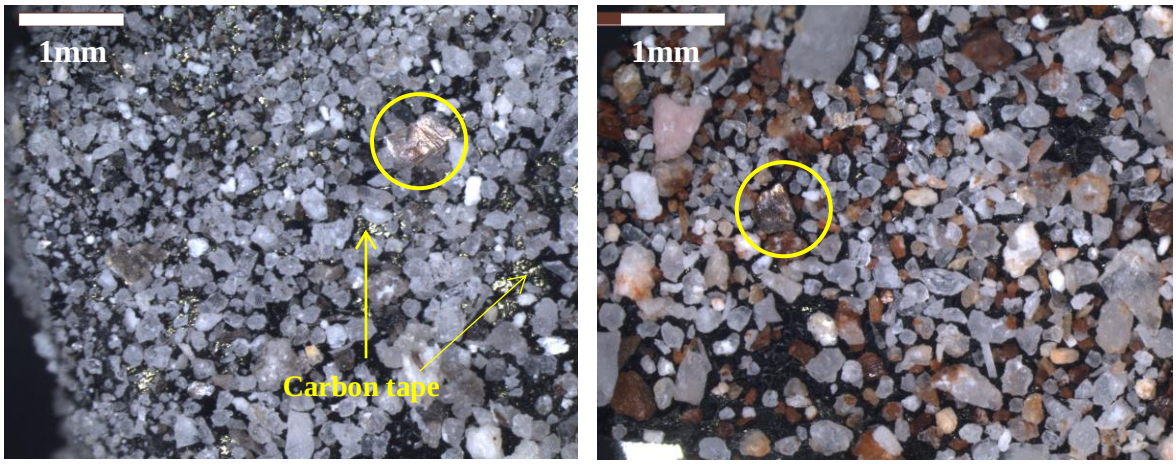

Figure 40 MW (left) and Calcined MW (right) under optical microscope. Mica mineral particles pointed in circles.

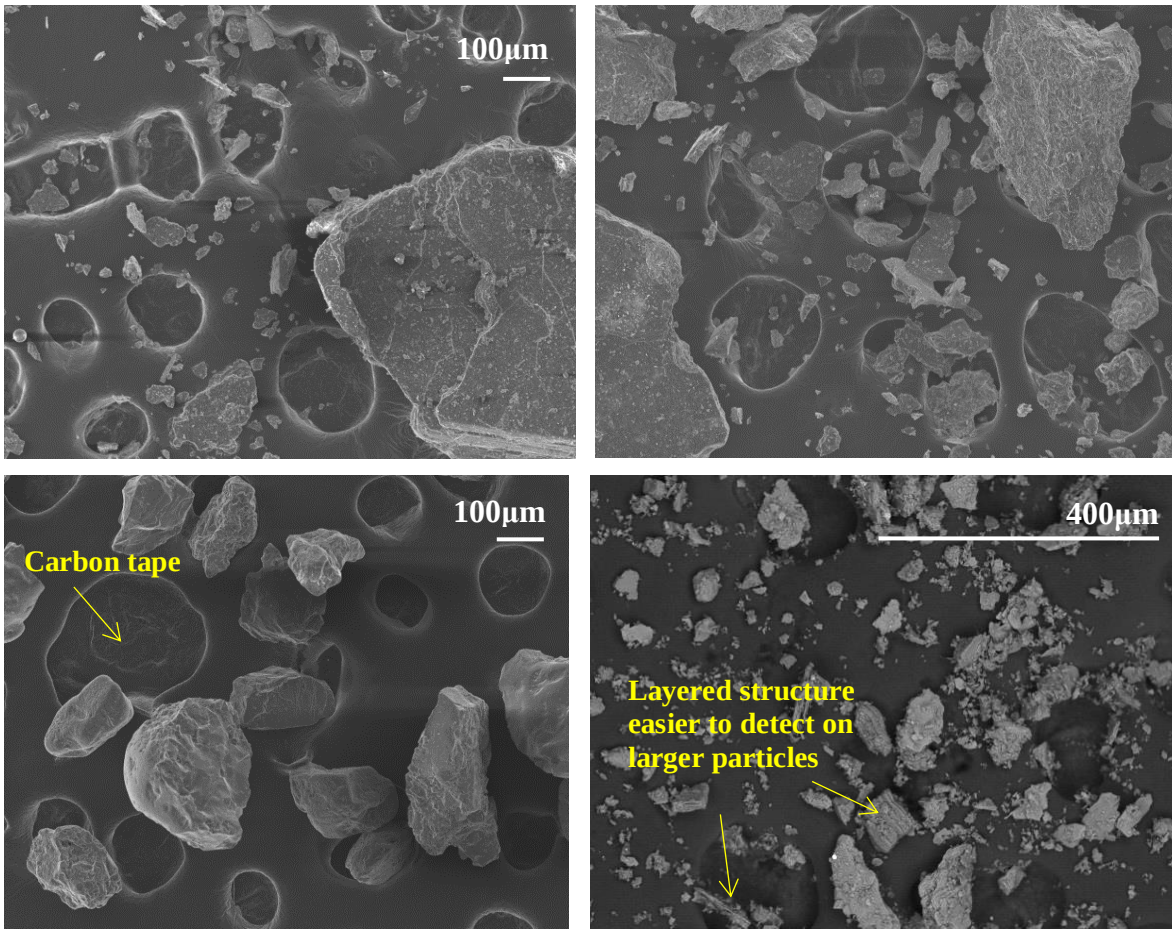

Figure 41 Secondary electron imaging (SEI) for mica (top left) and calcined mica (top right), *fines* of standard sand (bottom left) and mica concentrate (bottom right). (Setting: WD 15, Spot size 45, Acc. Volt. 10kV)

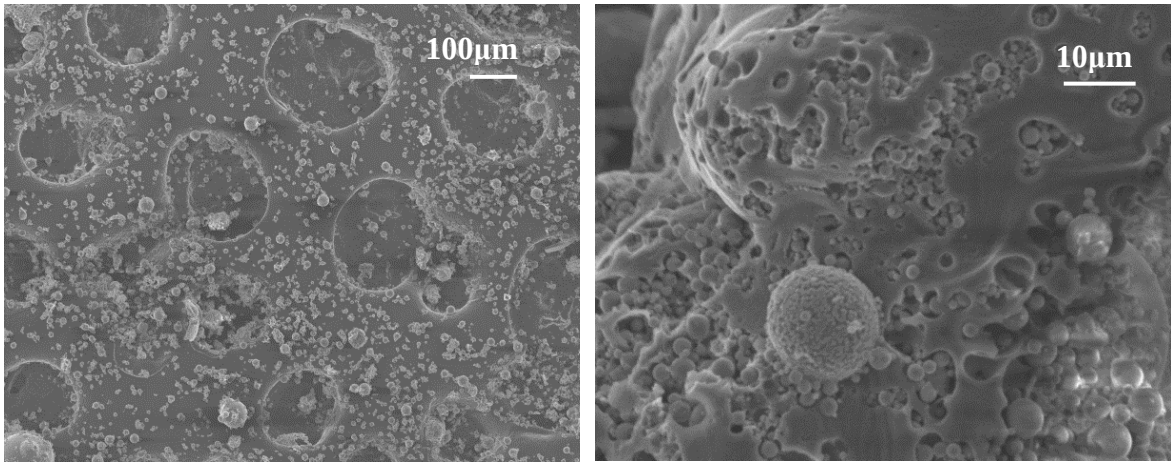

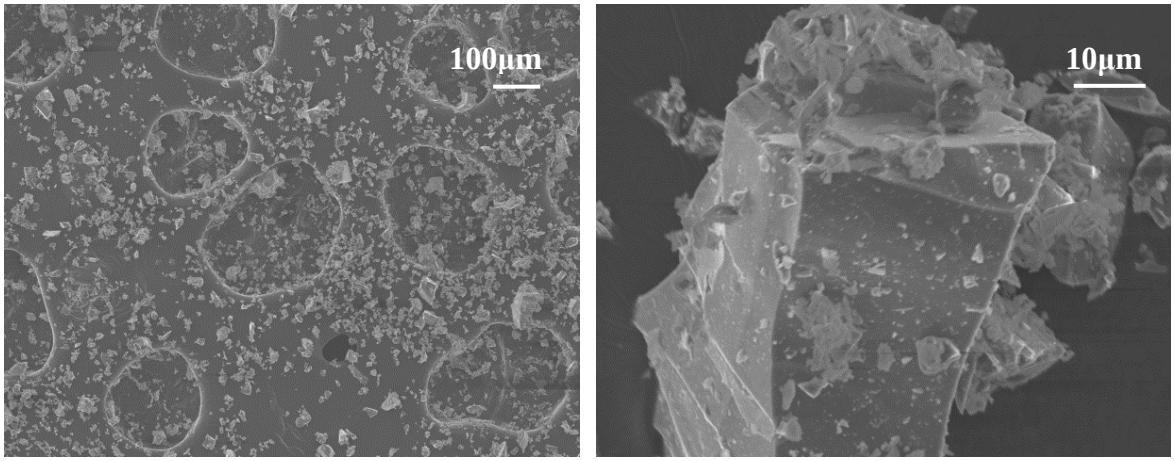

Figure 42 Secondary electron imaging (SEI) for FA (on the previous page) and GGBS (this page).

3.3 Reactivity

As mentioned in Chapter 1, the use of MW or a processed form of it in binders could be a potentially suitable, high value application. For this to be successful it needed to react with alkali activators for geopolymer binder formation, or with PC to form a blended PC based binder.

As explained in sections 2.5.1, 2.7.2 and 2.7.3., thermal treatment of kaolin varies the reactivity of aluminum in the mineral crystal and for a range of temperature leads to a reactive material. For this suitable range of temperature Al changes from predominantly Al(6) to predominantly Al(4) and Al(5) coordination and the ordered crystal structure becomes amorphous (see 2.5.1). Taking the case of kaolin dehydroxylation to metakaolin as example, it was investigated if the same principle applies to muscovite. In section 2.5.2 unheated muscovite was shown to be nonreactive crystalline mineral but at temperature till 920-980°C (depending on fineness) it was seen that muscovite dehydroxylates as well, leading to presence of some glassy content and conversion of Al(6) to Al(5). The use of the mica concentrate allowed focus on the mica minerals of the waste.

The potential reactivity was assessed using two types of analyses: the first looked at the structure of the raw and thermally treated waste (mica concentrate in this case) using solid-state Nuclear Magnetic Resonance (NMR) spectroscopy and it was necessary to find if muscovite has the potentials to react as shown in 2.4.1. The second method was indirect measurement based on compressive strength. The first part of the investigation into compressive strength (following the BS EN 450-1:2012) is presented in this chapter. Because of the lack of a standard and the complexity for geopolymer mix design, the effect of the waste on the compressive strength of geopolymer based mixes is presented in the following chapters.

Alternatives were also considered for measuring reactivity but not selected: BS EN 196-5:2011 (pozzolanic test for cement) relies on the Ca ions released from an under study cement, therefore it was not an appropriate method for testing aluminosilicates poor

in CaO. Moreover, following the BS EN 450-1:2012 was considered better than applying the Frattini test which is found to be an accurate measurement of the calcium hydroxide consumption by pozzolanic reaction (Donatello et al., 2010, Tironi et al., 2013) or any other method of direct measuring of the calcium hydroxide consumption (see 2.7.2). This is because an indirect strength measurement shows the applied contribution of a pozzolan in PC (Tironi et al., 2013) and is more representative of the reactivity based on the observations of authors in section 2.7.2.

3.3.1 XRD analysis

Three samples were tested using XRD: mica concentrate unheated and mica concentrate heated at 950°C and 1100°C for 3hours. At 1100°C the minerals sintered and a ball mill was used for 2 days. There was care taken to have the same maximum particle size, thus only material passing a 63μm sieve was taken for XRD analysis. The analysis ran using a diffractometer BRUKER AXS D8 Advance, equipped with a Vantec-1 detector, using CuKα radiation. The scanning rate was 0.016° intervals, step time was 2sec and limits were 5° to 45°. The identification of peaks was done based on the online American Mineralogist Crystal Structure database (Downs and Hall-Wallace, 2003).

The XRD patterns are displayed in Figure 43. The unheated sample has many peaks which represent kaolinite, mica and quartz, consistent with the mineralogical breakdown in Table 9. The quartz remained intact in all the samples as expected at temperatures well below the melting point (Table 7). There is slightly increased background 950°C and at 1100°C, between 15° to 40° 2θ. There is not increased background detected in the unheated sample. Some of the peaks of muscovite (2θ about 17.9°, 27° and 36.2°) at 950°C are slightly shifted to the left compared to the unheated sample. This is in accordance to muscovite peaks at elevated temperatures (up to 650°C, muscovite from Panasqueira) found in the online American Mineralogist Crystal Structure database, referring to a paper by Guggenheim et al. (1987), and shows that the mineral is still present but there are changes in its crystal structure.

The patterns at elevated temperatures are in accordance to the expected mineral phases based on Watanabe et al. (1987) and Mackenzie et al. (1987) (see section 2.5.2): kaolinite is not detected at elevated temperatures. Muscovite remains present at 950°C although it shows changes in its structure (smaller peaks, slight shift in some peaks compared to the unheated sample). At 1100°C muscovite disappears and mullite shows instead. On top of that, the slightly increased background for temperature ≥950°C confirms the presence of amorphous phases, discussed at 2.5.1 and 2.5.2 According to the discussion in 2.5.2 at temperatures higher than approximately 840°C amorphous phases should be attributed to muscovite. At lower temperature (mica concentrate at 800°C will be used in 4.2) amorphous phases should be attributed to both muscovite and metakaolin from the leftover kaolinite in mica concentrate.

The peaks for mica concentrate at 950°C have the same 2θ with the peaks of calcined at 950°C tungsten mine waste (Pacheco Torgal et al., 2005b, Pacheco Torgal et al., 2005a) which, as mentioned in 2.7.4, has been used successfully as alkali-activated binder

(only one peak at 2θ=22° is not confirmed but minerals from different locations can vary). The XRD patterns of that material, for a range of temperature, was presented in Figure 33. While the author reported only 12% of the initial amount of muscovite remaining at 950°C, here a 33% was remaining at that temperature. This was assessed based on the height of the main peak of muscovite at 2θ about 9° (Figure 43). Nevertheless, regarding the reactivity of mica concentrate, it is considered encouraging that the current XRD analysis of this study showed amorphous phases at 950°C and 1100°C, but the finding had to be crosschecked with further investigation and it was necessary to understand whether that amount of amorphous phases was enough to deliver a robust AA binder (see section 4.2).

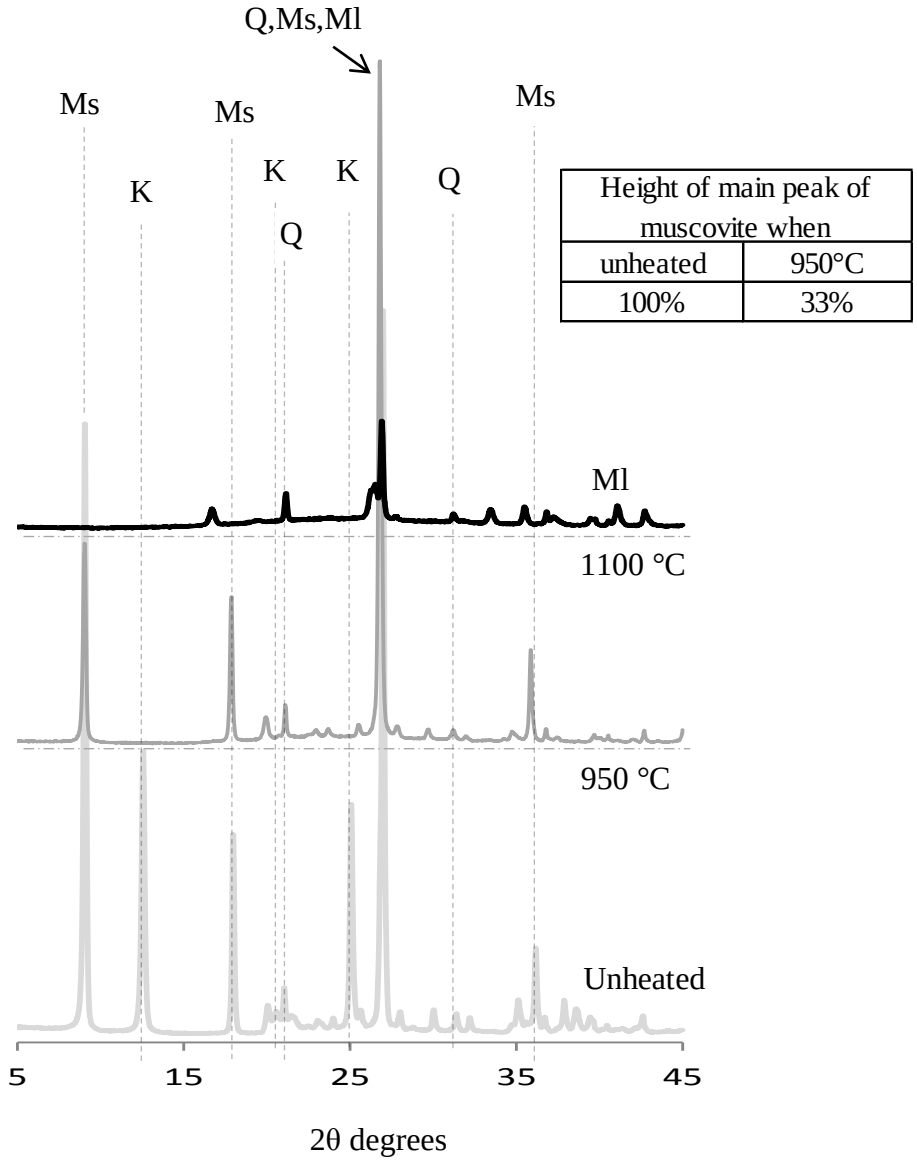

Figure 43 XRD pattern of the Concentrate, unheated and at elevated temperatures. (Q: quartz, K: Kaolinite, Ml: mullite, Ms: muscovite)

3.3.2 NMR analysis

Mica concentrate was used for this analysis as the mica mineral was in high concentration and would give clearer results than if the entire waste stream was used. Three samples were tested: mica concentrate, mica concentrate calcined at 950°C for 3h and mica concentrate calcined at 1100°C for 3h. The University of Bath does not own equipment for solid-state NMR analysis and the 27Al Solid State NMR spectra were obtained at the EPSRC funded UK National Solid-state NMR Service at Durham. The instrument used is a Varian VNMRS spectrometer with a 9.4Tesla magnet. The magic-angle spinning probes had 4mm rotor size.

The NMR spectra are shown in Figure 44 along with data from the literature (studies discussed in 2.5.1 and 2.5.2) for both muscovite and kaolin. It should be noted that according to the oxide analysis (Table 2), the mica concentrate contains 2.31% Fe_2O_3. This iron oxide can affect the NMR analysis but it was determined that the low percentage present should not alter the conclusions.

The spectrum from the mica concentrate shows two main centrebands: octahedrally coordinated aluminium (Al(6)) at 0.5 ppm and tetrahedrally coordinated aluminium (Al(4)) at 68 ppm. There is possibly a hint of a third, small signal around 20 ppm (5-coordinate species – Al(5)), not clearly visible in Figure 44. The remaining lines are spinning sidebands arising from the satellite transitions. After heating to 950°C there is lower overall signal intensity. The loss of signal is according to Meinhold et al. (1985a) and indicates presence of high number of Al sites that are neither octahedral nor tetrahedral which broadens the signal from quadrupolar 27Al beyond detection.

The spectra for the mica concentrate calcined at 950°C is plotted with the original trace factored up ten times as the signal strength varied with calcination temperature which could cause difficulties in comparison. The signal from the tetrahedrally coordinated species is now the most intense. The trend continues further with the 1100°C sample. This spectra is magnified five times the original to allow easy comparison. After calcining at 1100°C there is some retrieval of the signal compared to the sample calcined at 950°C. This is also in accordance to the findings of Meinhold et al. (1985a) who observed initial signal loss of 90% which partly recovered at temperatures above 970°C.

There is a difference in the MAS NMR spectra of this study and the work of Mackenzie et al. (1987): The Al(4) found in Mackenzie et al. (1987) was attributed to the initial Al(4) in the raw material, based on the fact that the raw material had exactly the same chemical shift with muscovite at 950°C. However, in this study the chemical shift is different between the two states without being clear if this is because of the impurity of the mica concentrate in kaolinite (notice that the peaks for kaolinite by Watanabe et al. (1987) have slight differences at different temperatures). Given that the detection of Al(5) here is beyond detection and that the presence of Al(4) in the spectra is not clearly only due to initial Al(4) in the sample, is not conclusive that mica concentrate could exhibit some pozzolanic activity as with metakaolin (kaolinite calcined between 600°C to 840°C). However it can be said that the Al(4) peak at 950°C corresponds to the muscovite in the material as kaolinite at that temperature has mainly Al(6). Whether the detected

Al(4) and the undetected but existing according to literature Al(5), is enough to join the geopolymeric reactions will be seen later.

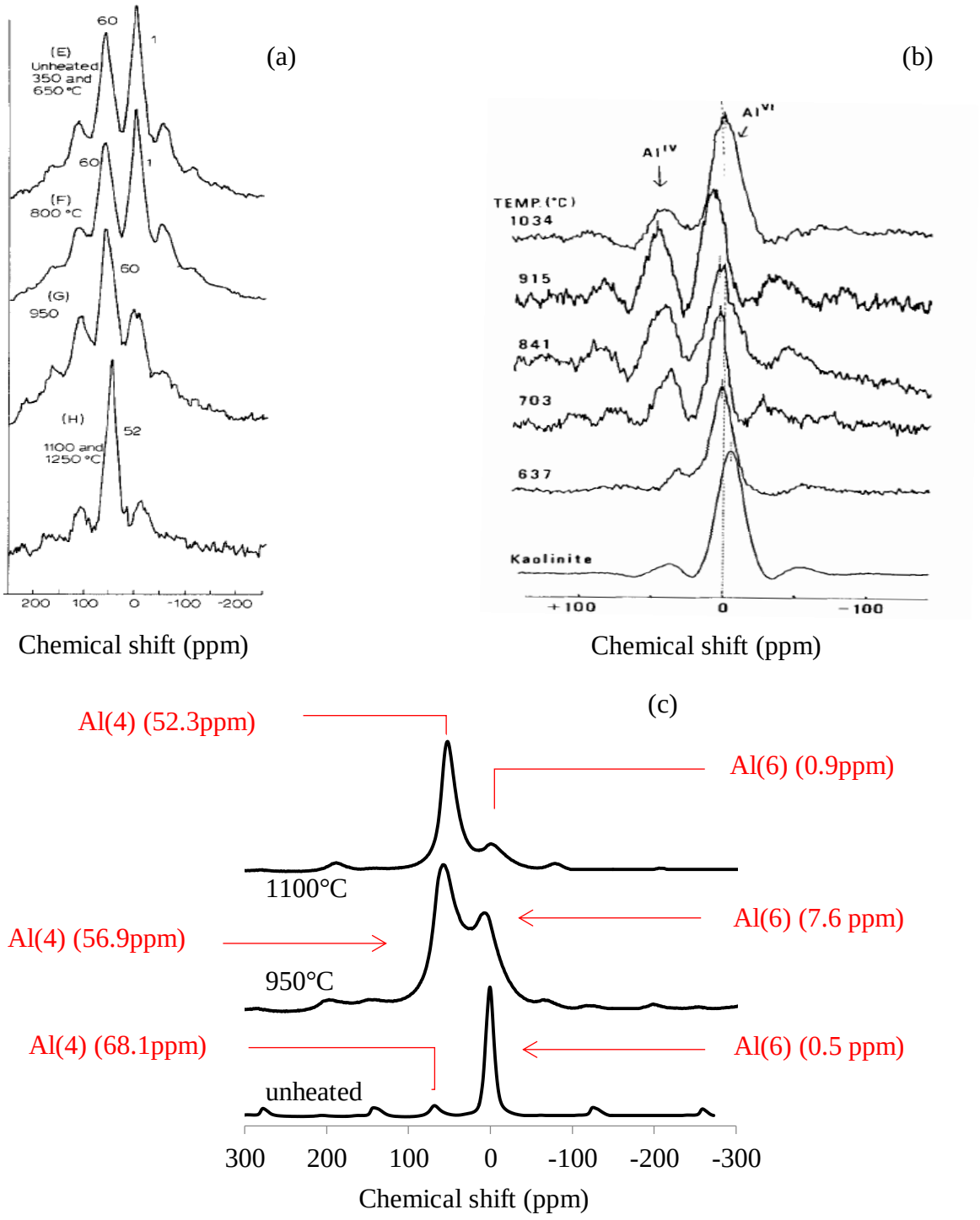

Figure 44 27Al Solid state NMR spectra of:

a. North Carolina muscovite heated to various temperatures. Source: Mackenzie et al. (1987)
b. original and heated kaolinites. Source: Watanabe et al. (1987), fig.4.
c. mica concentrate at different temperatures. (this study)

3.3.3 European standard on Pozzolanic activity

BS EN 450-1:2012 defines the method to assess the pozzolanic activity of fly ash. The same principle has been previously applied to assess the pozzolanic activity of other materials: coal bottom ash (Cheriaf et al., 1999), glass powders (Shi et al., 2005), silica fume and sand (Agarwal, 2006, Donatello et al., 2010), metakaolin and incinerated sewage sludge ash (Donatello et al., 2010).

In this study, BS EN 450-1:2012 was used to define the pozzolanic index of the waste even though this test is only directly applicable to PC based mixes which gain strength through hydration. Control samples comprised 450±2g CEM I, 1350±5g standard sand and 225±1g water. The test samples had 75% CEM I and 25% pozzolan. The materials used as potential pozzolan were MW and mica concentrate unheated and heated at different temperatures and different times. Based on the TGA results it was determined that calcining at 950°C would be most likely to favour pozzolanic properties and geopolymerisation. According to the standard, the activity index (AI) is:

AI = strength of test mortar/strength of control mortar

If AI≥75% on the 7th day and AI≥85% on the 90th day then the test material considered to have pozzolanic properties. Three prismatic samples were used for each mix. Mixing, curing and testing were conducted according to BS EN 196-1.

As the calcined mica concentrate does change to a predominantly Al (4) coordination once calcined and since there are studies where the calcined mica mineral was successfully developed in alkali-activated binders as mentioned in section 2.4.1, further investigation was needed to determine whether the mica mineral in the waste could be used in geopolymers.

Table 12 Activity index (AI) of the test samples according to BS EN 450-1:2012.

Test pozzolanas	**AI**	
	7d	**90d**
Unheated MW	67.9%	74.5%
MW at 950°C for 1.5h	58.5%	63.1%
MW at 950°C for 3h	61.4%	63.1%
MW at 1000°C for 3h	71.5%	72.3%
Unheated concentrate	59.7%	58.7%
Concentrate at 950°C for 3h	*79.0%	*88.8%
Concentrate at 1000°C for 3h	*77.3%	*89.0%
Concentrate at 1100°C for 3h	*76.6%	*87.7%

* indicates where minimum criteria exceeded

Table 12 shows that the heated MW failed the criteria but calcined mica concentrate was considered to have some pozzolanic properties which indicated it can be used to increase the strength of binders. Regarding the temperature of calcining, the samples

displayed pozzolanic behaviour at 950°C which generally slightly dropped at higher temperatures. Considering that the metakaolin in these temperatures is transformed into unreactive spinel and later mullite, it is suggested that the improved compressive strength was due to mica or due to effects related to particle physics (the calcine absorbs more water from the mix, leaving the binder with a lower cement:free water ratio and resulting in better strength) It is unlikely that the small particles provided additional nucleation sites which increased strength as the uncalcined form did not provide these same strength increases. Moreover, it was noted that prolonged calcining of MW made no difference as it largely comprises nonreactive minerals.

Chapter 4: **Development of binders using mica concentrate and other common AA binders**

With regard to the environmental benefits of alkali-activated cement technology (section 2.4.6), this chapter focuses on the performance of various alkali-activated binders:

- pastes based on mica concentrate which is of the highest interest in this chapter.
- pastes based on GGBS (GGBS series), used as it is the most representative case of alkali-activated material (section 2.4.2).
- pastes based on FA (FA series), used as being the most common raw material in geopolymer binders (section 2.4.2).
- A series of binders based on a blend of 50/50 FA/slag (50/50 series) which as shown in subsection 2.4.3.1 suggests the best compromise between slag content and strength.

Various authors (Puertas et al., 2004, Gebregziabiher et al., 2015, Yang et al., 2012b, Winnefeld et al., 2010, Haha et al., 2012) (see 2.4.2) have been involved with the chemical formulation of AAC based on GGBS and/or FA. However, as discussed in sections 2.4.2 and 2.4.3, by-products such as slag and FA can have different properties from batch to batch and the activator has to be tailored for the specific batch of aluminosilicate. Therefore, while the investigation on the formulation and characterisation of alkali-activated binders based on GGBS and/or FA was not novel in its own right, it was a necessary step to take in order later to develop mortar and concrete. Finding whether heated mica concentrate could form a robust binder was a novel idea which started from the discussion in section 2.7.4. The composition of the paste was based on the formulation of alkaline activator for metakaolin and blended aluminosicates (section 2.7.3) and tungsten mine waste (section 2.7.4).

4.1 Methodology

4.1.1 Mixing and testing

Solutions of sodium silicate and NaOH were prepared separately in glass beakers under a fume hood by mixing the solid substance (given in section 3.1.7) with part of the added water (W). The solutions were left to cool to room temperature before mixing (usually left overnight) as the solution increases in temperature (higher than 50°C for the concentrations used) as a result of the exothermic dissolution process. The cooling was required as high temperatures speed up the chemical reactions with the precursors and could affect the results.

For Portland cement based binders the binder quantity is typically the cement content, and the water / cement (or binder) ratio is related to the water added to the mix. For geopolymers this is more complex as the activator solution contains some dissolved solids and some liquid. For NaOH (solid) in particular this is complicated as 2NaOH dissolves to Na_2O+H_2O. Therefore, when referring to the composition of the alkali-activated binders, the following equations apply unless otherwise stated. In these equations, the Binder (B) includes the anhydrous part of the activator and the Total Water in the mix (W_t), used to calculate the Water to Binder ratio, includes the water part of the activator:

$$\textbf{Binder (B)} = \text{Precursor} + 77.48\%NaOH + 80.55\%Na_2SiO_3 \text{ (all in g)}$$

Total Water in the binder **(W_t)** = Water added+water in activator = B* [(W_t/B)ratio] (in g)
Where water in the activator = $22.52\%NaOH+ 19.45\%Na_2SiO_3$

$$\textbf{Water added (W)} = W_t - 22.52\%NaOH - 19.45\%Na_2SiO_3 \text{ (in g)}$$

$$\textbf{Ms} = SiO_2/Na_2O \text{ (in mol)}$$

4.1.1.1 Mixing for the GGBS, FA and 50/50 series

A small mortar mixer in accordance with BS EN 196-1:2005 (Automix Controls model 65-L0006/AM) was used in the preparation of the binders. The mixing process was:

- Place the two solutions (sodium silicate and NaOH) in the bowl and mixer at slow speed for 30seconds.
- Without stopping add the precursor (GGBS/FA). Stop the mixing process after 1:15 and using a spatula scrape the walls of the mixer allowing all the material to be properly mixed.
- After manual mixing continue at high speed for a further When finished switch on the mixer in high speed. Stop when the timer shows 7:15.

This mixing sequence was shown to be successful in trial mixes. The mixing was longer than for standard mortars in BS EN 196-1:2005 but as discussed in section 2.4.3.2 prolonged mixing could enhance properties of the hardened product.

Small cylindrical plastic moulds of 18mm diameter and 36mm height were used. The internal surface of the moulds was lubricated using Vaseline. Casting took place immediately after mixing. The samples were compacted using 3 blows per layer in 4 layers using a glass rod whenever the paste was not completely fluid. The GGBS and FA based samples had different curing conditions and will be described in the following sections.

The Vicat test was used to determine the setting times of the pastes. BS EN 196-3:2005+A1:2008 describes specific mixing times and curing processes for Portland cement binders. Here the test was conducted following the mixing times above and the

special curing conditions of each series. 400g of precursor were used for the Vicat test (instead of 500g of cement that the Standard suggests).

Three samples of each mix were tested on days 7 and 28 in compression. The compression machine used was a 100kN Dartec Universal Testing Machine (fig. Figure 45) and the rate of loading was 0.5mm/min. All the specimens were capped using dental paste on both at the top and the bottom to ensure the load was evenly distributed. It should be noted that dental paste has high compressive strength (>70MPa) and may have had an impact on specimens of that small dimensions, but as the samples had a 2:1 aspect ratio which minimises the end effects and the results were consistent, this was not considered to influence the outcomes of the testing.

Figure 45 100kN Dartec Universal Testing Machine, used for the tests in compression.

4.1.1.2 Mixing for the mica concentrate geopolymer investigation

The same equipment (moulds, machine for compression, mixer) was used for making samples using mica concentrate. The mixing followed the same process: sodium hydroxide and where applicable sodium silicate solutions, were prepared separately and left to cool to room temperature. Then the solutions were put in the mixer and blended in slow speed for 30seconds. Time was given again to let the mix cool if needed. Then the mica concentrate (heated or unheated, according to the mix design table) was added and mixed for 5 to 7 minutes. The reason that this series of binders was mixed for less time than the GGBS, FA, 50/50 series was due to the quick setting which occurred for some of

the mixes. Some mixes, noted in table Table 14, were cured at 80-85°C for 1hour and 40min, sealed in bags while most of the mixes were cured at 85°C for 5hours, wrapped in cling film. According to section 2.4.3.3, curing at 80-85°C for 1h and 40min is enough for geopolymerisation to occur, while longer durations have variable results on strength. In this study it was decided to cure samples for 5h as shorter periods was noticed to be not sufficient for all mixes. After removing the samples from the oven, they were left to cool and then demoulded and placed in a large Tupperware at 20°C and about 90% relative humidity.

Triplicates were tested after 7 and 28 days of curing. It was of interest to see the strength development on the 28 day which is the standard period for PC materials, although testing only after 7days curing is enough for most studies on natural-aluminosilicate-based geopolymers (see Ahmari and Zhang (2013a), Buchwald et al. (2009) and Pacheco-Torgal et al. (2008,d). The latter developed a paste which had 7day compression strength equal to approximately 83% of the 28day compressive strength).

The samples after testing in compression would be left in water (both after 7 and 28days) for visual observation. All the samples would be lightly rubbed (by hand) before being thrown away. Samples which disintegrated in water on their own or after rubbing were noted as "soluble".

4.1.2 Characterisation using analytical methods

These analyses applied only to the GGBS, FA and 50/50 series. The strongest of the three samples that were tested in compression for each mix were collected and sent for XRD and SEM/EDX analyses.

Arresting hydration and carbonation

Contact with air and moisture can result in hydration and carbonation which causes changes to some binders. This needs to be avoided while storing samples for later analytical analysis. In this study, samples of the GGBS and FA series were stored after the 28 days until being analysed in SEM/EDS and XRD. The 50/50 series were taken for analysis right after the 28 days, therefore they were not treated first.

The solvent replacement method using acetone was used to arrest ageing. It has been shown by Ismail et al. (2013a) that acetone is the most suitable method to remove free water from the slag-based and blend of FA/slag-based binders that were examined as it preserves the "*structural features of the binding gels and the pore network*". In contrast, vacuum drying or oven drying at 60°C caused structural changes for slag-based samples and only "*some degree of pore collapse*" for the FA/slag based samples, difference which is attributed to the form of water binding in the different types of product.

From a review of the solvent exchange procedure by Zhang and Scherer (2011), it is evident that different times for embedment and solution-to-sample volume ratios can be used as long as it is ensured that the organic liquid used has replaced all pore water. In this study compatible plastic, air tight containers were used filled with at least five times the volume of the sample in acetone. Acetone was changed three times (left for 24 hours

then changed and then changed again after another 24 hours) to ensure all cavities and pores had been filled, thereby preventing infiltration with water and CO_2.

Preparation of samples for imaging

Cross-sections were prepared using epothin epoxy resin and polished to be analysed in SEM/EDX. Samples were first cut using a diamond blade using the Struers Accutom at 1000rpm. As part of a standard process they were placed under vacuum and later were placed in the prepared epothin epoxy resin which makes use of 5 parts of resin to 1.95 parts of hardener (by weight). The samples were put under 200kPa pressure and left overnight to cure. As mentioned earlier, the use of vacuum drying can alter the structure but it is not possible to effectively epoxy saturate samples without this, and this should be considered in mind when viewing the relevant images.

Finally they were ground and polished using four series of sand paper of increasing particle size fineness and three series of fine polishing (0.04μm colloidal silicone was the finest polishing component used). The ready resin stubs were kept in vacuum desiccator until being tested. Before starting the imaging a line was drawn from bottom to top on the stubs using silver paint in order to increase the conductance.

4.2 Investigation on the potentials of mica concentrate as geopolymer precursor

4.2.1 Parameters selection

Table 13 and 15 present the composition of the trial mixes. Some of the samples are shown in Figure 46. The mica concentrate was used in four states: unheated, calcined at 800°C for 3h, calcined at 950°C for 3h and at 1100°C. These calcining temperatures were chosen after considering the information on the dehydroxylation of kaolin and muscovite (subsections 2.5.1), the studies of Silva et al. (2012), Pacheco-Torgal et al. (2008,d) and MacKenzie et al. (2008) (section 2.7.4) and the TGA of MW in Figure 37. At 800°C the dehydration of muscovite is ongoing while there is possibly still metakaolin derived from the 17% kaolin content in mica concentrate (Table 9). It is not certain if there is melt from muscovite at this temperature as Rodriguez-Navarro et al. (2003) (section 2.5.2) first found melt on their muscovite sample at 900°C. However, mica concentrate is in the micron scale and therefore it is expected to show new phases at lower temperatures (Pérez-Rodríguez et al. (2006), section 2.5.2). 950°C represents the temperature the closest to full dehydroxylation of muscovite and no presence of metakaolin and 1100°C represents a rich-in-mullite material which is probably unreactive. However, it was of interest to observe if even at the rich-in-mullite state there was still melt from sintering which could contribute to geopolymerisation. That idea was also based on the study by He et al. (1994) who, as discussed in section 2.7.1, achieved in PC system the same strength for either using metakaolin at 800°C or higher temperature where mullite had appeared as pozzolan.

There were two types of activators used to activate the mica concentrate:

- One consisted of NaOH only. As seen in section 2.7.4 NaOH solutions are used often by authors when investigating the reactivity of a material under study (Xu and Van Deventer, 2000, Buchwald et al., 2009, Ahmari and Zhang, 2013a, Heah et al., 2013b) despite the relatively low performance that would be expected. In the lab, NaOH solutions of 6M, 10M and 50% in water solution, were made and added in the aluminosilicate (plus $Ca(OH)_2$ where included) in the ratio of "solution to aluminosilicate (plus $Ca(OH)_2$)" equal to 0.57. This amount was chosen because in trials it was enough to give pastes with some workability. For the given amount and concentration of the activator, the alkalinity of the mix was 9g, 13g, 22g of Na_2O (see Table 13). There was also another NaOH solution designed to target 15g of Na_2O. The pastes were semi-dry to semi-paste.
- The other consisted of NaOH and sodium silicate. The Ms used was 1.00 and 0.25. Ms equal to 1.00 was of interest first because it is close to the value of 1.05-1.17 used by Pacheco, see 2.7.4 section. Moreover, it was suitable for formulating the calcined mica concentrate as if it was metakaolin, according to calculations which can in seen in Annex A.2. The calculations targeted a mix with overall molar ratios Na_2O/SiO_2=0.28, SiO_2/Al_2O_3=4, H_2O/Na_2O=17 (in the range of David 2011 and Heah 2013b, section 2.7.3), and resulted that the activator would need to have 22.7g Na_2O which is close to the used value of 19.59g Na_2O. The W_t/B, calculated as shown in the equations above, was 0.43 (as in Pacheco, see calculations in Annex A.2) for the mixes with 19.59g Na_2O and 0.40 for the other mixes of Table 14.

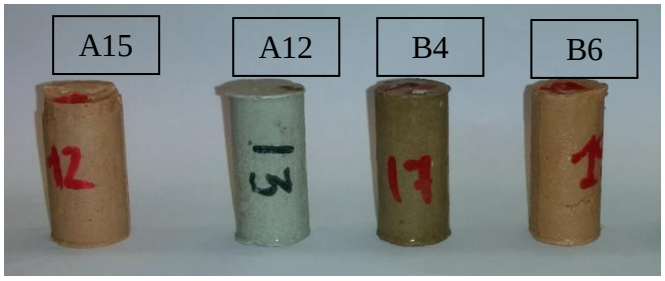

Figure 46 Samples of binder based on unheated and heated mica concentrate (named based on the names in the compositional tables)

Figure 47 Mixes that do not contain $Ca(OH)_2$ were soluble in water. Here, samples A2 and A3 in water, unstable after rubbing.

Table 13 Composition of mixes which were activated using NaOH only and their compressive strength on day 7 and 28. Cured at 85°C for 5h in cling film and after demoulding were kept at 20°C and about 90% RH. Different Na_2O – Ms – $Ca(OH)_2$ combinations are separated using a line.

Mix	Mica concentrate heated at (in °C)	Na_2O (g)	Ms	Solution/ (mica conc.+ $Ca(OH)_2$)	Mica concentrate (g)	$Ca(OH)_2$ (g)	Na_2SiO_3 powder (g)	NaOH pellets (g)	Distilled water (g)	Compressive strength (in MPa) 7d	28d	Comments
A1	unheated	22	0	0.57	100	-	-	28.3	28.3	0.0	0.0	the activator forms a 50% NaOH solution. Soluble.
A2	unheated	9	0	0.57	100	-	-	11.3	45.3	0.3	0.3	the activator forms a 6M NaOH solution. Soluble.
A3	950	9	0	0.57	100	-	-	11.3	45.3	0.3	0.4	the activator forms a 6M NaOH solution. Soluble.
A4	1100	9	0	0.57	100	-	-	11.3	45.3	0.5	0.5	the activator forms a 6M NaOH solution. Soluble.
A5	unheated	9	0	0.57	90	10	-	11.3	45.3	1.4	1.6	the activator forms a 6M NaOH solution
A6	800	9	0	0.57	90	10	-	11.3	45.3	7.2	7.2	the activator forms a 6M NaOH solution
A7	950	9	0	0.57	90	10	-	11.3	45.3	8.3	8.0	the activator forms a 6M NaOH solution
A8	1100	9	0	0.57	90	10	-	11.3	45.3	8.6	9.1	the activator forms a 6M NaOH solution
A9	unheated	13	0	0.57	90	10	-	17.0	39.7	2.4	2.3	the activator forms a 10M NaOH solution
A10	950	13	0	0.57	90	10	-	17.0	39.7	4.8	4.7	the activator forms a 10M NaOH solution
A11	800	15	0	0.56	90	10	-	18.9	37.6	7.4	6.1	
A12	unheated	9	0	0.57	80	20	-	11.3	45.3	1.6	1.7	the activator forms a 6M NaOH solution
A13	800	9	0	0.57	80	20	-	11.3	45.3	6.9	6.2	the activator forms a 6M NaOH solution
A14	950	9	0	0.57	80	20	-	11.3	45.3	12.5	8.7	the activator forms a 6M NaOH solution
A15	1100	9	0	0.57	80	20	-	11.3	45.3	3.7	3.5	the activator forms a 6M NaOH solution

Table 14 Composition of mixes which were activated using NaOH+sodium silicate and their compressive strength on day 7 and 28. Cured at 85°C for 5h in cling film and then at 20°C and RH about 90%, unless otherwise stated (different conditions highlighted in grey). Different Na_2O – Ms combinations are separated using a line.

Mix	Mica concentrate heated at (in °C)	Na_2O (g)	Ms	W_t/B	Mica concentrate (g)	$Ca(OH)_2$ (g)	Na_2SiO_3 powder (g)	NaOH pellets (g)	Distilled water (g)	Compressive strength (in MPa) 7d	28d	Comments
B1	950	13	0.25	0.40	100	0	5.9	14.7	42.0	no sample available	no sample available	Starts being workable after 6min of mixing. Loses workability in 25min. Cured at 80-85C for 1h and 40min. Did not harden.
B2	950	13	0.25	0.40	90	10	5.9	14.7	42.0	3.2	7.0	Workable. In 30min starts losing workability. Cured at at 80-85C for 1h and 40min.
B3	950	13	0.25	0.40	80	20	5.9	14.7	42.0	5.7	19.0	Workable and smooth paste. After 30min it is still workable. Cured at 80-85C for 1h and 40min.
B4	800	14	0.25	0.45	80	20	6.6	16.3	48.5	9.4	10.5	
B5	950	14	0.25	0.45	80	20	6.6	16.3	48.5	3.7	9.7	
B6	1100	14	0.25	0.45	80	20	6.6	16.3	48.5	2.1	4.9	
B7	950	9	1	0.40	90	10	4.1	10.2	41.4	6.9	no sample available	Setting within minutes, though placed in oven after setting at 80-85C for 1h and 40min.
B8	950	19.6	1	0.43	100	0	37.1	12.3	50.6	-	-	Setting within minutes. Soluble. Salts.
B9	950	19.6	1	0.43	90	10	37.1	12.3	50.6	5.5	no sample available	Mixed for 2min. Setting withing minutes, even the same mix for extra water. Not soluble but breaks easily by hand after embedding in water. Salts.

The mineralogy of TMWM (used by Pacheco-Torgal et al. (2008,d) and presented in section 2.7.4) is similar to the mineralogical composition of mica concentrate (Table 9), although according to 3.3.1 the TMWM has more quartz and less muscovite than the mica concentrate. While the calcined TMWM had 12% of muscovite remaining compared to the unheated state, the equivalent percentage for the mica concentrate is 33%. This difference was balanced by the higher content of muscovite in the mica concentrate. Another difference between the TMWM and mica concentrate is that the TMWM has a much higher Fe content. As the two materials have similarities, calcined mica concentrate was activated trying to reach a type of binder similar to Pacheco-Torgal et al. (2008,d). Therefore, $Ca(OH)_2$ was incorporated in many of the mixes. The content used was 10% and 20% substitution of the aluminosilicate.

4.2.2 Results and discussion

The results showed that the compressive strength was generally low. There were also mixes which did not harden or set too quickly to complete casting. Looking at the comments in Table 13 and Table 14, the mixes which do not contain hydrated lime are soluble, either when activated using NaOH or NaOH+sodium silicate (Figure 47). All mixes prepared using solutions of Ms=1.00 lost workability within minutes. Mixes with Ms=0.25 were workable for longer but it was observed that they could not set at ambient conditions as in Pacheco-Torgal et al. (2008,d).

Mix B9 in Table 14 (10% $Ca(OH)_2$, 19.59g Na_2O, Ms=1.00) was based on the optimum binder by Pacheco-Torgal et al. (2008,d). Although there were concerns regarding the environmental benefit from such a high-in-alkalis-solution, the mix design was repeated in lab and mixed with the calcined precursor without reaching a successful final product. These samples were not soluble but after placing in water they would easily fail under manual pressure which brings in mind the case of Silva et al. (2012). Another problem when repeating the formulation by Pacheco-Torgal et al. (2008,d) was that the 24M NaOH solution when mixed in the lab, did not reach full dissolution. It can be noted that Pacheco-Torgal et al. (2008,b) had stated that 24M was the maximum concentration where full dissolution was reached (section 2.7.4). It should be noted though that the total activator (containing 24M NaOH and sodium silicate dissolved in water) was a highly concentrated but dissolved solution. The alkaline solutions although they were used at room temperature (cooled), increased the temperature when mixed with each other. Although time was given to let the mixed activator to cool, once it was added to the aluminosilicate it would again, increase the temperature of the mix (exothermic reaction). This could not be avoided for such a concentrated activator.

The mixes without inclusion of $Ca(OH)_2$ were soluble. Some trials, designed based on Davidovits (2011) therefore for with 0%$Ca(OH)_2$ (calculations in the annex), showed that after prolong oven curing the specimens are not necessarily soluble but remain weak. These trials are not shown in Table 13-14. It is considered that the product obtained using mica concentrate was even weaker than the product of Silva et al. (2012) as they had soluble samples only for curing at 20°C and not for curing at 80°C (where only decrease

in strength was observed). Moreover, the reported compressive strengths in Silva et al. (2012) where no $Ca(OH)_2$ was used, were comparable to the strength of calcined mica concentrate+$Ca(OH)_2$ before putting their samples in water. It is therefore understood that the material from Panasqueira and mica concentrate from Cornwall are not as similar as initially assumed. And although the XRD of TMWM in Figure 33 shows mica, a quantitative mineralogical analysis would be useful to understand where the different performance between mica concentrate and TMWM can be attributed. However based on mixes B1, B8, A3, A4 from this study, dehydroxylated/or higher temperature calcined muscovite in alkaline solution is not reactive in its own right.

The explanation Silva et al. (2012) provided for their results was deficient geopolymerisation due to insufficient concentration of NaOH to amount of reactive calcined or amorphous phases present. This is not considered to be the case here because calcine at 950°C was also used, therefore a more complete dehydroxylated state was achieved. It is likely that the reason that the TMWM was successfully activated (while mica concentrate not) is because of an interaction between the dehydroxylated muscovite and another component in the TMWM. A component of interest could be Fe with regard to the patent of Davidovits (Davidovits et al., 2012), however as mentioned in 2.4.2, the patent is based on ferro-kaolinite and iron in the raw material has to be transformable in hematite. Moreover, it is noted that impurities of feldspar, muscovite, biotite and quartz in the raw material used in the patent, were stated to remain in the XRD patterns after activation, meaning they did not react. But it is the muscovite that is not anymore detected in the XRD (has been transformed in amorphous phase) that is of interest for joining a geopolymeric reaction. This was not investigated further as there is limited Fe in the Cornwall waste (1.89% Fe_2O_3 compared with 12.33% in the waste used by Pacheco-Torgal). In any case, practical issues regarding the formulation that Pacheco-Torgal et al. (2008,d) used (full dissolution of 24M, use of $Ms \geq 1$ while having enough time before setting) still raise questions.

Moreover the particle size of mica concentrate (see particle size distribution at section 4.1.2) is in the scale of microns and that was expected to favour dissolution as in the case of pyrophyllite (section 2.7.4). That expectation was reasonable considering also the findings of authors in section 2.5.2, who observed that unheated muscovite dissolves faster at the edges of the particle. Based on that finding and assuming that calcined muscovite is reactive compared to the unheated state, the belief that the micronized, featureless mica concentrate as shown in Figure 41 would have good chances to be susceptible in dissolution in alkaline solution was enhanced. However, this is not confirmed by the results.

Even for inclusion of 10% $Ca(OH)_2$ the mixes using 6M NaOH reach 7-9MPa for all the calcines (800°C, 950°C, 1100°C), while use of 10M NaOH decreased the strength of the calcine of 950°C. This could indicate lower dissolution for use of higher alkalinity, surprising considering that materials like mica concentrate would need high alkalinity to have geopolymer reaction (sections 2.7.3 and 2.7.4). It is important to point out that indeed a reaction does take place for calcining the mica concentrate, otherwise the

unheated mica for the set $Ca(OH)_2$ content and NaOH concentration would have the equal strength (for example samples A5-A8, A9-A10, A12-A15). In contrast the unheated material did not exceed 2.5MPa for any of the formulations used. Moreover, it is seen that the reaction which occurs for calcining the mica concentrate, it is in relation with the presence of $Ca(OH)_2$. That could explain why the investigation of reactivity based on the BS EN 450-1:2012 (section 4.3.3) showed pozzolanic activity in mica concentrate (because there is $Ca(OH)_2$ in PC systems).

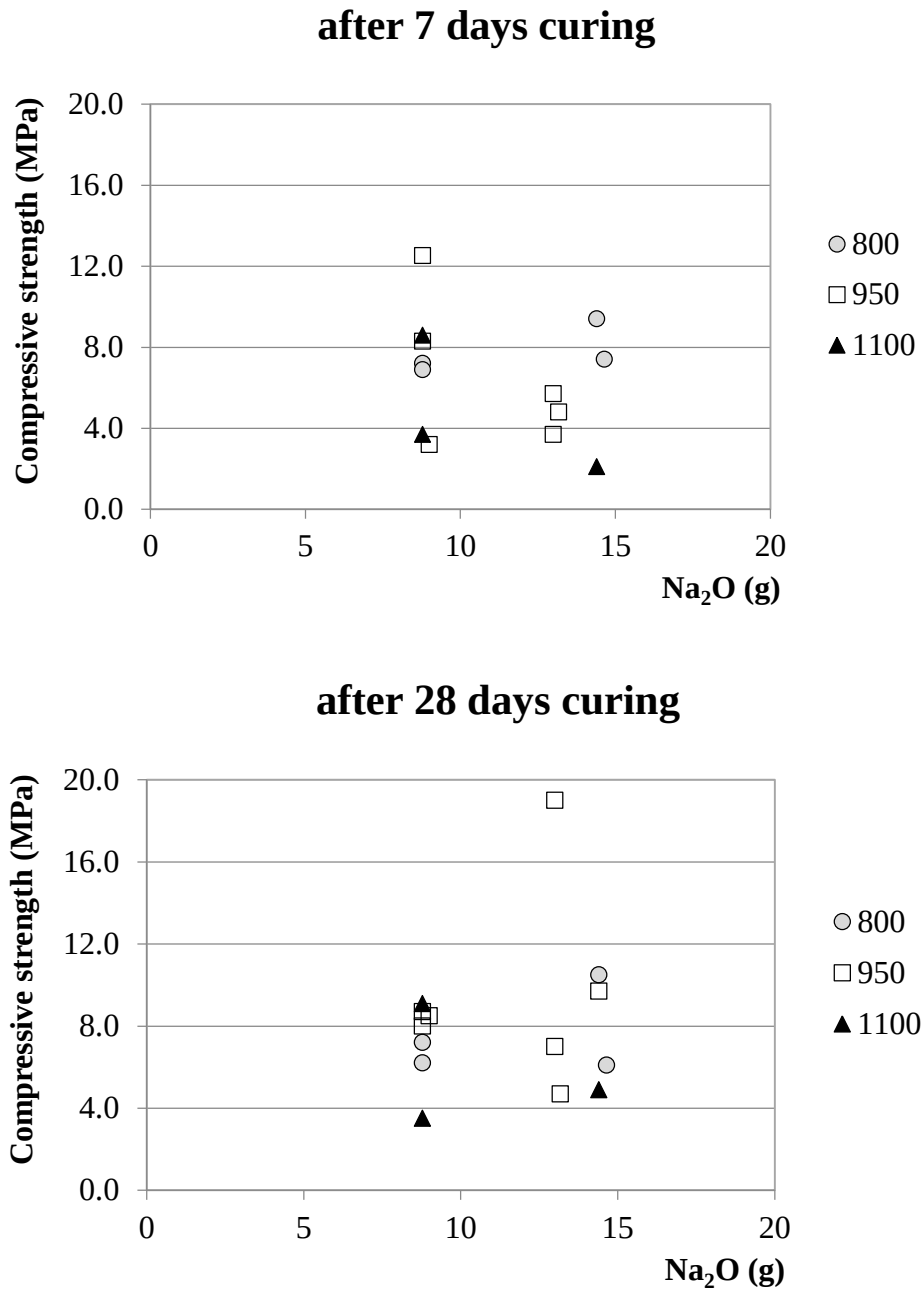

Figure 48 Effect of different temperatures of calcining (800, 950 and 1100°C) on the compressive strength of binders. The plotted mixes contain 10% and 20% $Ca(OH)_2$ and refer to testing after 7 and 28days of curing.

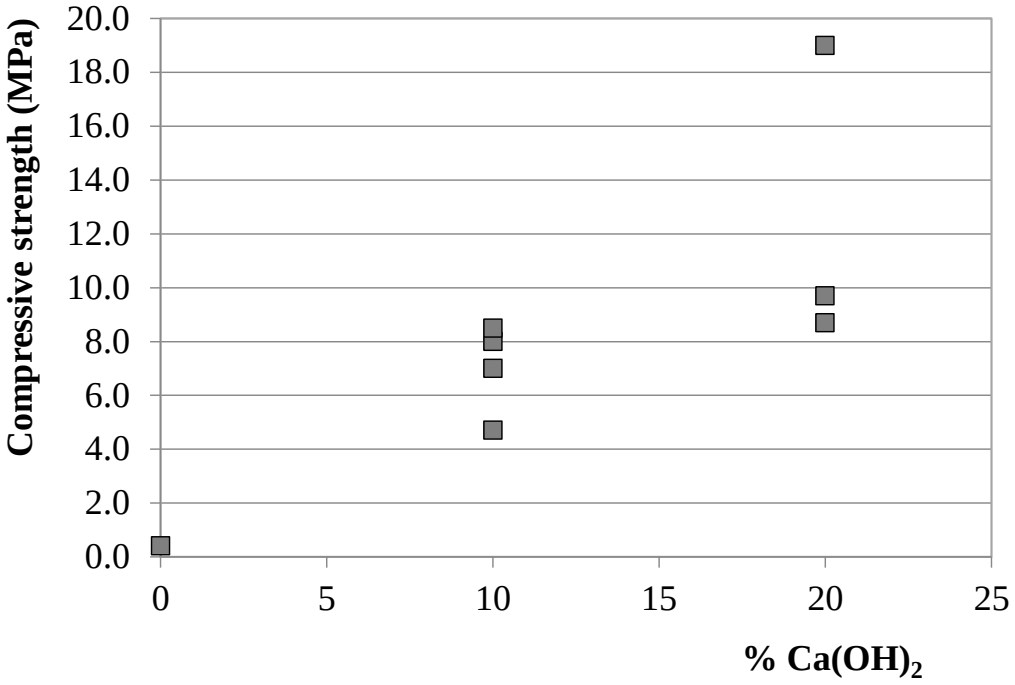

Figure 49 Effect of 28th day, for 0%, 10%, 20% $Ca(OH)_2$ content and are restricted to use of the 950°C calcine.

Inclusion of 20% $Ca(OH)_2$ complicates the results, where now the 950°C calcine showed higher strength than calcine of 800°C and calcine of 1100°C. Although the strength decreased from 12.5 to 8.7 from the 7th to the 28th day of curing, the results were considered that could be improved if using sodium silicate. However, the results for use of sodium silicate+NaOH and the same alkalinity were slightly lower. For use of sodium silicate+NaOH and higher alkalinity (13g of Na_2O) the results were strongly affected by the $Ca(OH)_2$ content. For 20% $Ca(OH)_2$, on the 28 days the highest achieved result is this set of tests is achieved, 19MPa. However, for 14g of Na_2O, 20% $Ca(OH)_2$ and increasing the water content from W_t/B=0.4 to 0.45 the strength achieved was about 10MPa. The increase of the water content was of interest in order to later incorporate sand and make mortars, as W_t/B=0.4 insufficient to develop mortars.

Figure 48 is a plot of the strength achieved after 7 and 28days of curing for calcines at 800, 950 and 1100°C, for 10% and 20% $Ca(OH)_2$ content (using Table 13-14). The highest achieved strength, although single points, belongs to the 950°C calcine. Generally, the 950°C and 800°C reach on average similar strength. The strength is not positively affected for increasing the alkalinity on day 7. However, on day 28 there the results are slightly improved for increase in the Na_2O.

Figure 49 refers to the results of the 28th day, for 0%, 10%, 20% $Ca(OH)_2$ content and are restricted to use of the 950°C calcine. The figure clearly shows an increasing trend for increasing $Ca(OH)_2$ content.

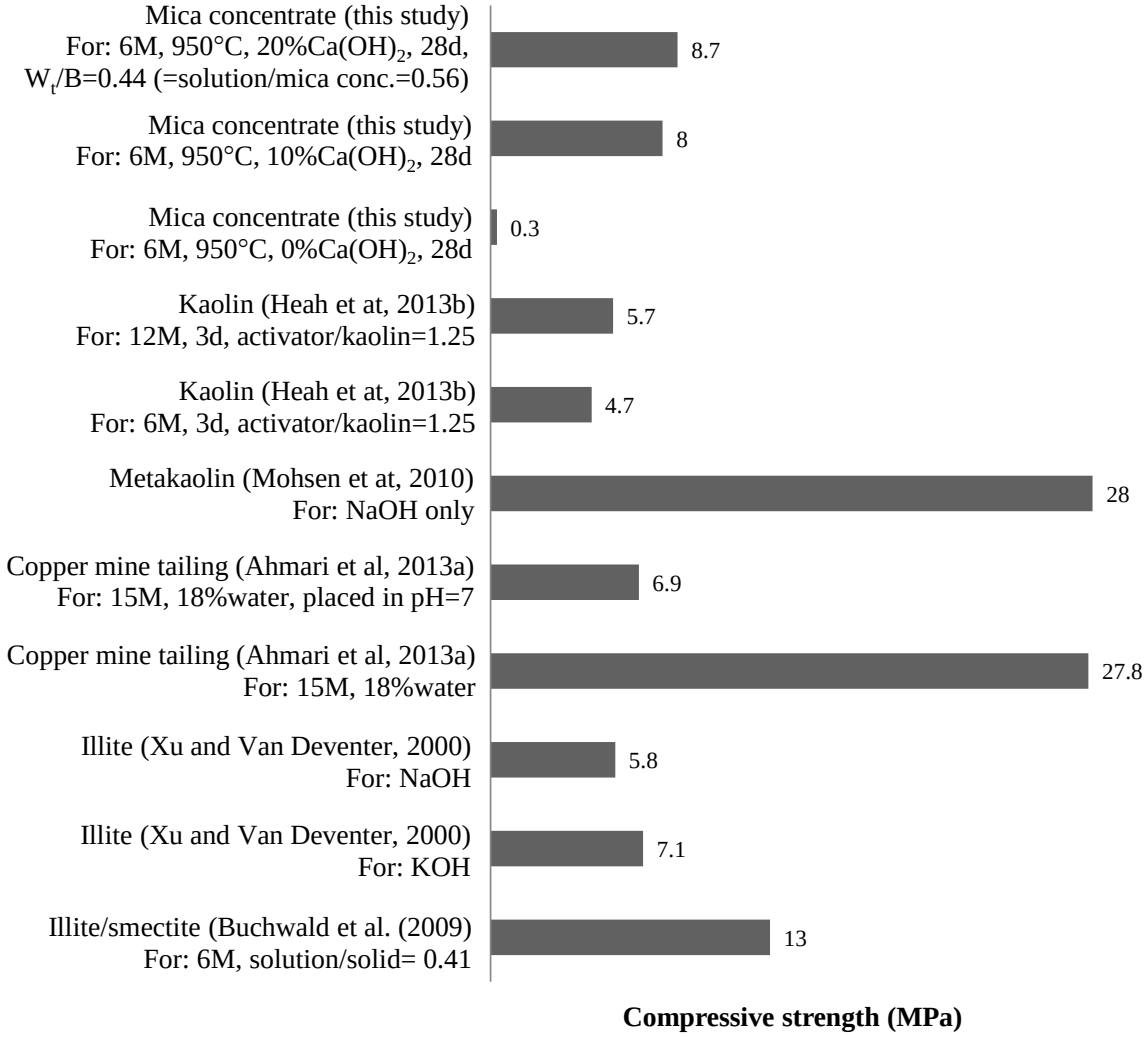

Figure 50 The performance of binder based on the 950°C calcine, for different levels of $Ca(OH)_2$ content and activation with 6M NaOH compared to other natural aluminosilicates studied by other authors, activated using only hydroxide and without inclusion of additions (like $Ca(OH)_2$ or blend of aluminosilicates).

Figure 50 is a comparison between the mica concentrate and other natural aluminosilicates, studies described in sections 2.7.3 and 2.7.4, where no additions have been used (like more aluminosilicates or $Ca(OH)_2$). Most of the other materials presented are activated using NaOH only solution. This figure highlights that the mica concentrate based on the conditions used here does not react at any state (calcined or unheated). Even kaolin and illite (unheated), which according to Figure 31 have poor performance as pozzolans in PC system, are more reactive than mica concentrate. Only by adding a 10%-20% of $Ca(OH)_2$, the compressive strength becomes comparable with the strength of the other materials.

The overall conclusion drawn from this set of tests is that there is a reaction happening but this does not result in a strong binder. It is seen that the mix design procedure used by Pacheco-Torgal is not suitable for these materials, even if the environmental impact fulfilled the goals of this current research project (discussed in Chapter 6) and that the reactivity of muscovite is low after calcining. This investigation rather confirms the results of pyrophyllite, where the 2:1 lattice is a barrier and the Si layer makes it difficult to access the five and four coordinated Al. For inclusion of $Ca(OH)_2$ and very low water content the strength of the binder is likely enough to develop unreinforced products, however taking into account the significant amount of aggregates in such products and as shown the quick decrease in strength for slightly higher water to binder ratio, manufacturing of such products would be challenging. The highest strength was achieved for 13g of Na_2O and low content of sodium silicate and it was of interest to assess the environmental impact of such a mix. As the MW would not be successful as a binder without other precursors, the options of other precursors were investigated.

4.3 GGBS series

4.3.1 Composition

First a short preliminary investigation was conducted, using 3 and 5g of Na_2O to activate 100g of slag, NaOH alone and sodium silicate of Ms=0.45-1.5. This amount of Na_2O is within the range of alkali content that other authors have used for slag (2.5%-8%, see some in Table 2 and Table 6). The range of Ms is also within the range of Ms commonly chosen for slag (Ms=0-2.00, in Table 2 and Table 6). It was decided that for 100g of GGBS, a minimum of 5g of Na_2O was needed for dissolution and adequate strength gain (over 50MPa to be similar to CEMI cement pastes). For clarity, Table 15 refers to the preliminary investigation mixes and shows their composition for 100g of GGBS and for W_t/B=0.40. The samples were cured at 20°C and were tested soon after they were demoulded.

Having decided the amount of Na_2O needed in the activator, four mixes of binders were prepared for Ms=0.45, 1.0, 1.25 and 1.50 by adjusting the use of NaOH and sodium silicate to observe the impact on strength and setting time. As mentioned earlier, the amount of water added is after deducting H_2O included in the solid form of NaOH and sodium silicate. The composition of the GGBS series of binders for 100g of slag is in Table 16, while the table also displays the overall SiO_2/Na_2O, SiO_2/Al_2O_3 molar ratios, assuming all the SiO_2 in the precursor is amorphous. While the Ms is the only variable in this table, it affects the quantities that constitute the alkaline solution and the given molar ratios. In practice all the mixes were mixed following the equivalent composition for 150g of GGBS as this provided sufficient material for the required testing.

Table 15 Trial mixes (preliminary results) for the alkali-activation of GGBS. Tested after being demoulded.

Mix	**(g) Na_2O / 100g of GGBS (therefore % to slag)**	**Ms**	**Strength (in MPa)**	**Comments for Mixing or Demoulding**
Use of Na_2SiO_3 & NaOH				
TrialA	5	0.45	39.58	-
TrialB		1	68.09	mainly green colour after curing
TrialC		1.5	61.73	deep green colour
TrialD	3	1	33.32	light green colour
TrialE		1.5	21.52	white, very thick paste.
Use of NaOH only				
TrialF	3	0	15.22	Denser pastes than the rest but more fluid than No.E.
TrialG	5	0	16.57	

Table 16 Composition (in g) of binders S1-S4 (S for Slag) based on 100g of GGBS.

	Mix	**Na_2O (g)**	**Ms**	**Precursor (g)**	**Na_2SiO_3 (g)**	**NaOH (g)**	**Binder (g)**	**W added (g) in solution**	**W_t/B**	**SiO_2/ Na_2O**	**SiO_2/ Al_2O_3**
GGBS series	S1	5	0.45	100	4.1	5.0	107.2	40.9	0.40	7.7	4.9
	S2	5	1.00	100	9.1	3.3	109.9	41.4	0.40	8.3	5.2
	S3	5	1.25	100	11.3	2.5	111.0	41.7	0.40	8.5	5.4
	S4	5	1.50	100	13.6	1.7	112.3	41.9	0.40	8.8	5.5

4.3.2 Curing conditions

The samples were cured at 20°C and ambient ~60% RH and demoulded one day after casting. After demoulding the samples were kept at 20°C and about 90% RH. It was noted that the high intensity and even distribution of the green colour of the samples is a positive indication for performance. This is consistent with previous observations of Brice et al. (2012) (section 2.4.2). Within days the green colour faded to light green/blue and white on the surface (contact with air) while inside it generally remained the same. Mixes S1-S4 contained the same amount of GGBS but only mixes S3 and S4 remained green inside and out (Figure 51).

Figure 51 (a) Mixing for 150g of GGBS using the small mixer, (b-c) Mix S1 is fluid while mix S3 already started setting. (d) Samples preparing for testing. Although all are green inside, only mix S3 and S4 turned completely green outside.

4.3.3 Setting time

The Vicat test was conducted under stable temperature and RH conditions (20°C, ~60% RH). The setting times can be found in Table 18. The initial setting time ranges from 5h to 25min which is considered marginal for casting (considering that 9minutes is the mixing process). Here, it is clear that an increase in the Ms accelerates setting time. As discussed in subsection 2.4.3.2, different studies have reported various results regarding the effect of Ms on setting time, but where there is a clear trend, it is decreasing. Therefore, here this trend is confirmed.

Table 17 Initial and Final setting time for the GGBS binder series.

		Setting time	
	Mix	**Initial**	**Final**
GGBS series	S1	5h	5h 20'
	S2	1h	1h 30'
	S3	35'	55'
	S4	25'	50'

4.3.4 Strength in compression

Figure 52 shows the strength in compression of the GGBS binder series after curing for 7 and 28 days. They all exhibited very high strength and the strongest binders had brittle fracture. On day seven the maximum strength was approximately 103MPa for both, Ms=1.0 and 1.25, and on the 28th day test a peak strength was noted for Ms=1.25 reaching 135MPa (30% increase). For Ms=1.0 the strength increased by 14%.

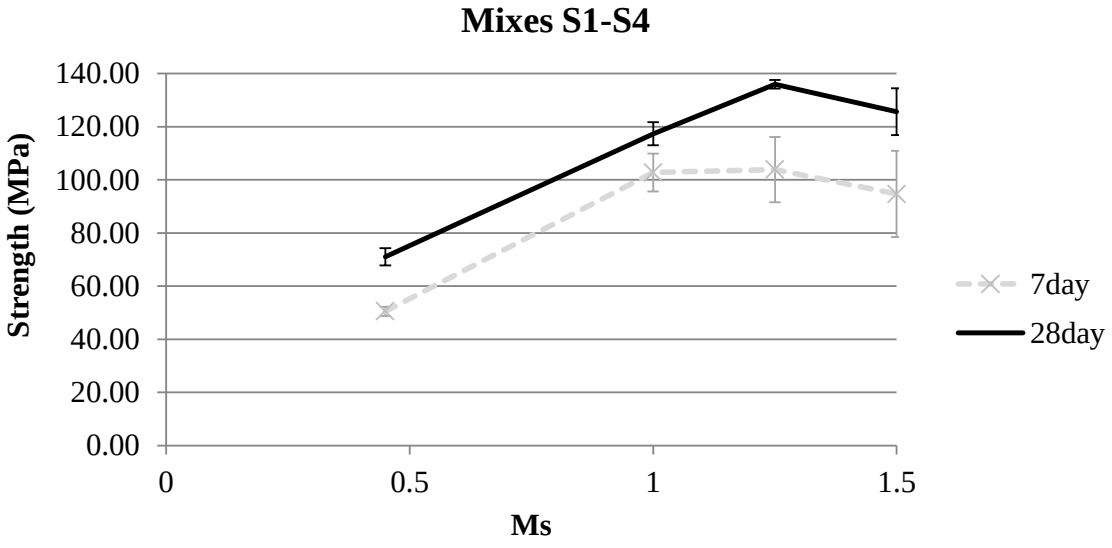

Figure 52 GGBS binder series: Compressive strength for increasing Ms on day 7 and 28.

The error bars in Figure 52 are calculated based on the performance of the triplicates tested and show one standard deviation. The error bars indicated small variance in standard error for most of the mixes with only mixes 3 and 4 having error greater than 10% of the value of strength for the 7 day test (12% and 17% error respectively). The mentioned percentages are an indication of the significance of the error with regard to the

average value of strength. For example, on day 7 for Ms=1.0 (mix S2), the error is about 7MPa but compared to the 103MPa of average strength, it is the 7/103= 6.8%.

4.3.5 XRD

The samples were ground (pulverized) and tested in XRD. The first XRD analysis ran soon after the 28 days and after having arrested hydration and carbonation. The resulting patterns had high levels of noise due to the use of capillary mode of the diffractometer (leading to diffraction on the glass of the capillary needle at low angles of 2θ) and are therefore not presented. Instead the analysis was repeated almost two years after mixing on the same samples which had been kept in sealed sample bags, in a dry place and in the presence of silica gel. The XRD analysis was performed using the Panasonic diffractometer, the step was 0.01° and step time 2s (Figure 53).

Apart from the disordered binder gel, the main reaction product in all samples was calcium silicate hydrate (noted CSH on the XRD pattern). There are small amount or traces of calcite ($Ca(CO)_3$) in most of the mixes indicating there was some carbonation. Different Ms ratios gave different additional peaks: mixes S1 and S2 show hydrotalcite ($Mg_6Al_2(CO_3)(OH)_{16}\cdot 4H_2O$), and mix S4 vaterite ($Ca(CO)_3$) which is a metastable phase of calcium carbonate. Mix S3 does not have any additional distinct crystalline phase.

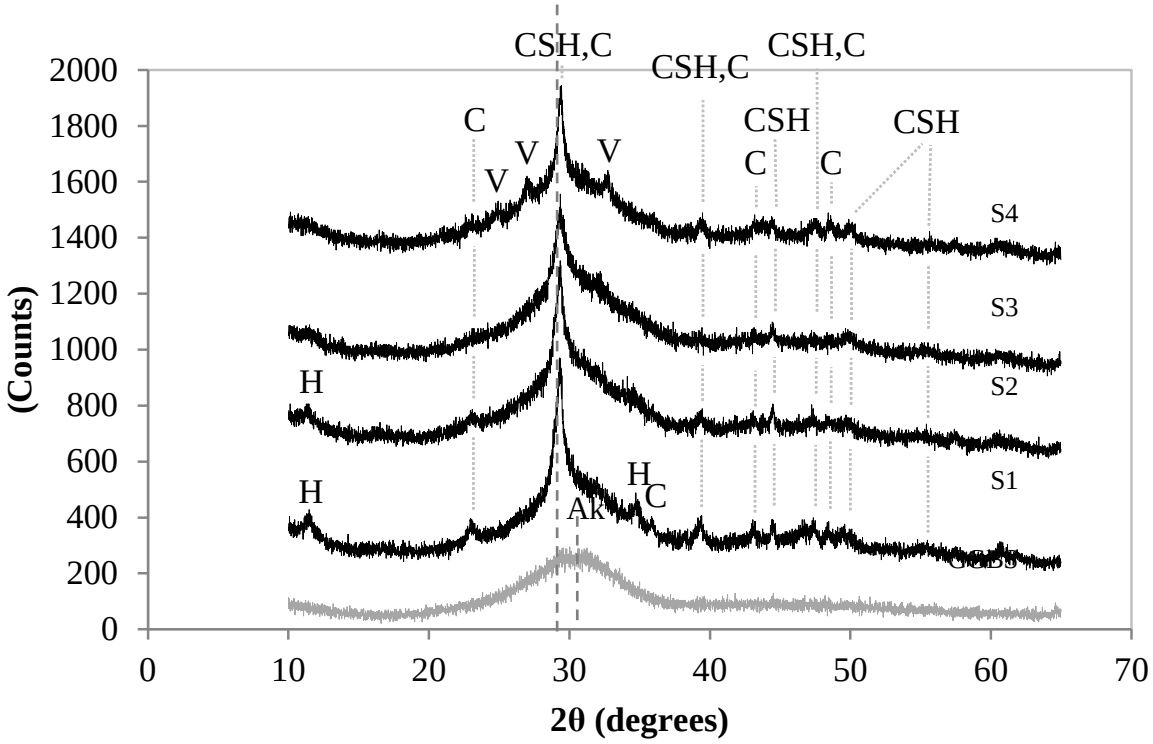

Figure 53 XRD patterns of mixes S1-S4. Where C=calcite, CSH=Calcium Silicate Hydrate, V=Vaterite, H=Hydrotalcite, Ak=Akermanite.

The unhydrated GGBS had shown no distinct peaks for impurities although there was a hint of calcite and akermanite ($Ca_2MgSi_2O_7$). As mentioned in section 2.4.2 when discussing about products in AAS, akermanite is related to the presence of hydrotalcite

after hydration (Haha et al., 2011, Wang and Scrivener, 1995, Richardson et al., 1994) and therefore it is reasonable that hydrotalcite could not be detected in all mixes. All the peaks correspond to products that have been previously reported. Regarding the presence of vaterite and calcite, these phases could be related to early stages of carbonation and small degree of carbonation during mixing of the samples, however with reference to the discussion in sections 2.4.2 and 2.4.5 it is understood that more work on understanding carbonation in AAM is needed. It is noted that while mixes S1-S4, as shown in Figure 53, could be considered aged and exposed to carbonation during the time left in the sample bags, instead of equivalent to the 28 days, the analysis is still useful for comparative purposes.

4.3.6 SEM

The settings for imaging in SEM were backscattered mode (BES signal), acceleration voltage 15kV, spotsize 60 and work distance 9-10. The samples had hydration and carbonation arrested at 28 days and were analysed in SEM/EDX five months later.

The binder matrices all have common characteristics in that they are highly amorphous with a number of undissolved particles of slag and microfissures, most of them have width less than 2μm. Although some of the microfissures may formed due to drying shrinkage during the hardening of the binder, it is most probable that they appeared during storage in the desiccator during sample preparation for scanning electron microscopy (SEM), as indicated previously by Palacios and Puertas (2011). This is in accordance with images taken using environmental scanning electron microscopy (ESEM) (Bernal et al., 2013, Haha et al., 2011) which requires minimal sample preparation as the samples in the images did not show severe microcracks. Such equipment does not exist in the University of Bath.

Sample ‘mix S2’ has striping on the slag particles. That shows that the preparation process was not completed in that the surface was not sanded and polished to the same level as the others. Generally, there are no obvious differences between the samples and the degree of dissolution of the slag looks similar.

4.3.7 Chemical identification of components

To ensure that the results of EDX are reliable, the system was calibrated using copper each time before running a new sample. This allowed spectra where the noise is relatively low. The fact that the samples were flat and polished enhanced the recovery of signal. Where quantitative chemical mapping was used, the set resolution was 512x384 (collecting signal from every point), for noise threshold equal to 1. Nine to eleven frames of scan ran for each sample analysed. Although the recording was in 512x384, the collection of spectra (during processing of the results) was done in lower resolution (what later is called square of 16x16 point spectra) to increase the reliability of outcome spectra.

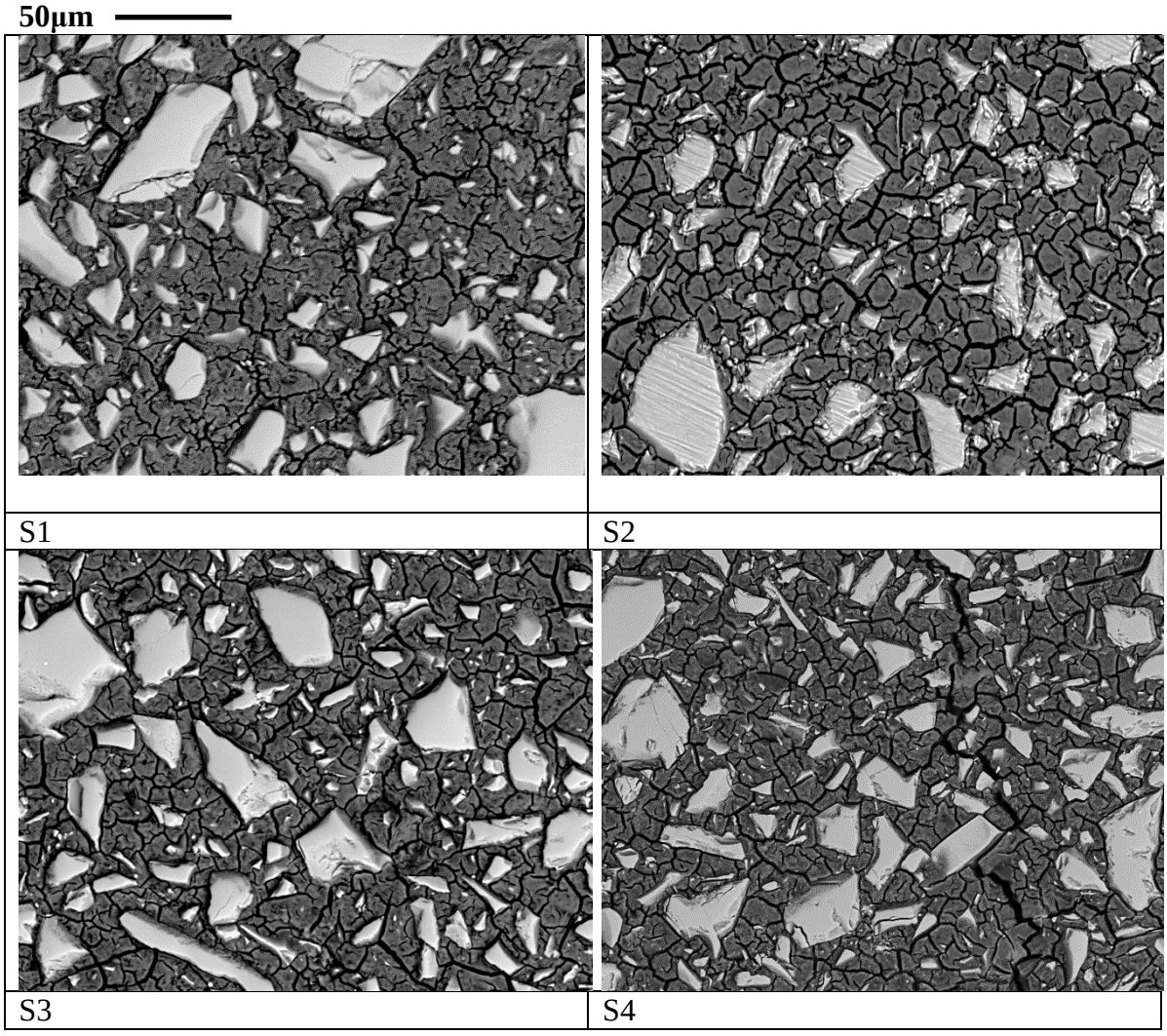

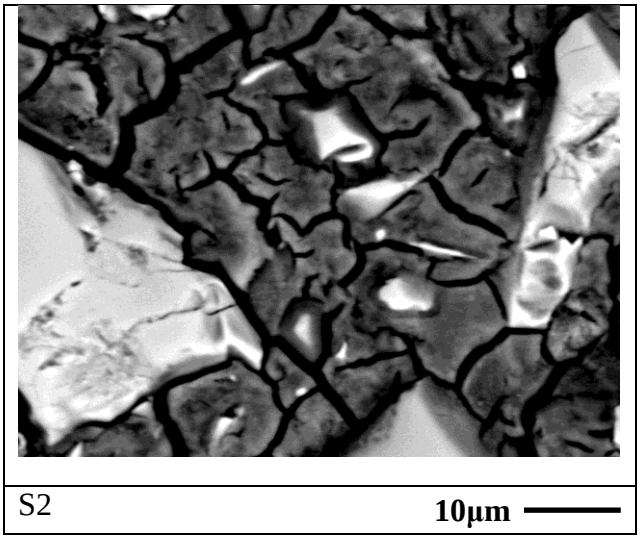

Figure 54 Backscattered electron images for the GGBS-based binders

Although care was taken to improve the quality of the chemical identification, EDX should be considered statistically over a number of points from each area of interest to

generate representative outcomes. For example, in Figure 55 (mix S2), ten points were taken from each area of interest to be analysed: the first area is the white parts which are suspected to be undissolved slag and the other is the cracked geopolymer matrix. Spectrum 10 (Figure 55) is representative of the GGBS chemical composition as provided by the XRF analysis. However in many of the undissolved GGBS particles, the presence of silicate is more intense than the presence of calcium (ex. spectrum 4, also in Figure 55). The spectra show traces of Mn, S, Na, K and Ti as expected. The undissolved particles of GGBS give similar spectra over all samples (mixes S1-S4) and for the 50/50 series.

According to the XRF in Table 11 the used GGBS has 13.07% Al_2O_3, which by stoichiometry is 6.9% atomic Al (calculated by multiplying with the mass percent of Al in Al_2O_3), 39.60% CaO which is 28.3% Ca, 16.4% Si and 5.1% Mg. Hence, theoretically, the atomic Ca/Si ratio of slag particles would be 1.72, the atomic Mg/Si would be 0.31 and Al/Si would be 0.42. However, the EDX analysis over a number of slag particles gave as average values: Ca/Si=0.98, Mg/Si=0.27 and Al/Si=0.46. Therefore, based on the discussion in section 2.4.2, the measured values of Ca/Si and Al/Si would be the upper limit of the equivalent ratios for the glassy product, while the Mg/Si of the product can be higher than the Mg/Si of the undissolved slag particles. The further discussion focuses on the matrix.

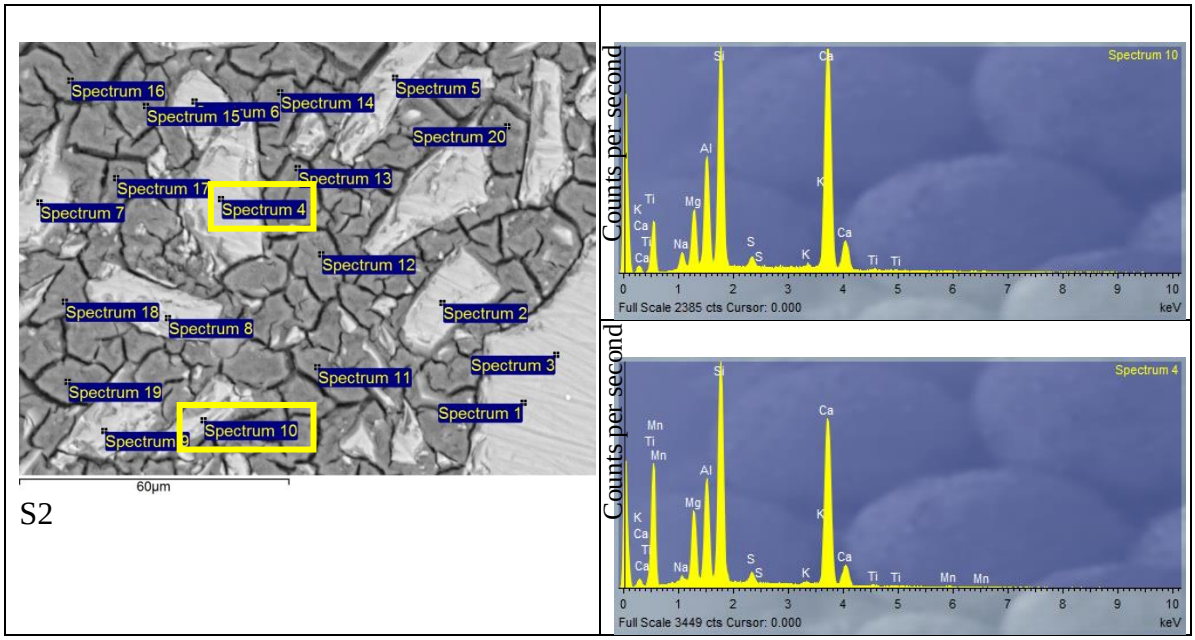

Figure 55 Point analysis. Spectras 10 and 11 refer to undissolved slag particles.

Figure 57 shows a reference image of an area of interest of mix S4 and chemical maps for Si, Na, Ca, Al, Mg and Fe. Please note that all these elemental maps show the atomic percentage and they were set to display in black areas which have elemental atomic concentration less than about 5%. The number at the right is the percentage of elemental concentration at the highest intensity on the map. The scale is 60µm. Looking briefly at the chemical maps it is clear that Na exists only in the matrix while Si exists in both,

mainly in slag particles but also in the gel. Ca is located mainly on the GGBS particles and around indicating there is some contribution of the Ca in the geopolymer binder (which is known from section 4.3.5., C-H-S is the main product). Some areas of the matrix are black in the Ca map, indicating Ca in these areas is lower than 5%. It also appears that Ca has been 'captured' in the microfissures as result of the sample preparation (material carried away). The particle in the centre is Fe and that is why it shows black in the other chemical maps.

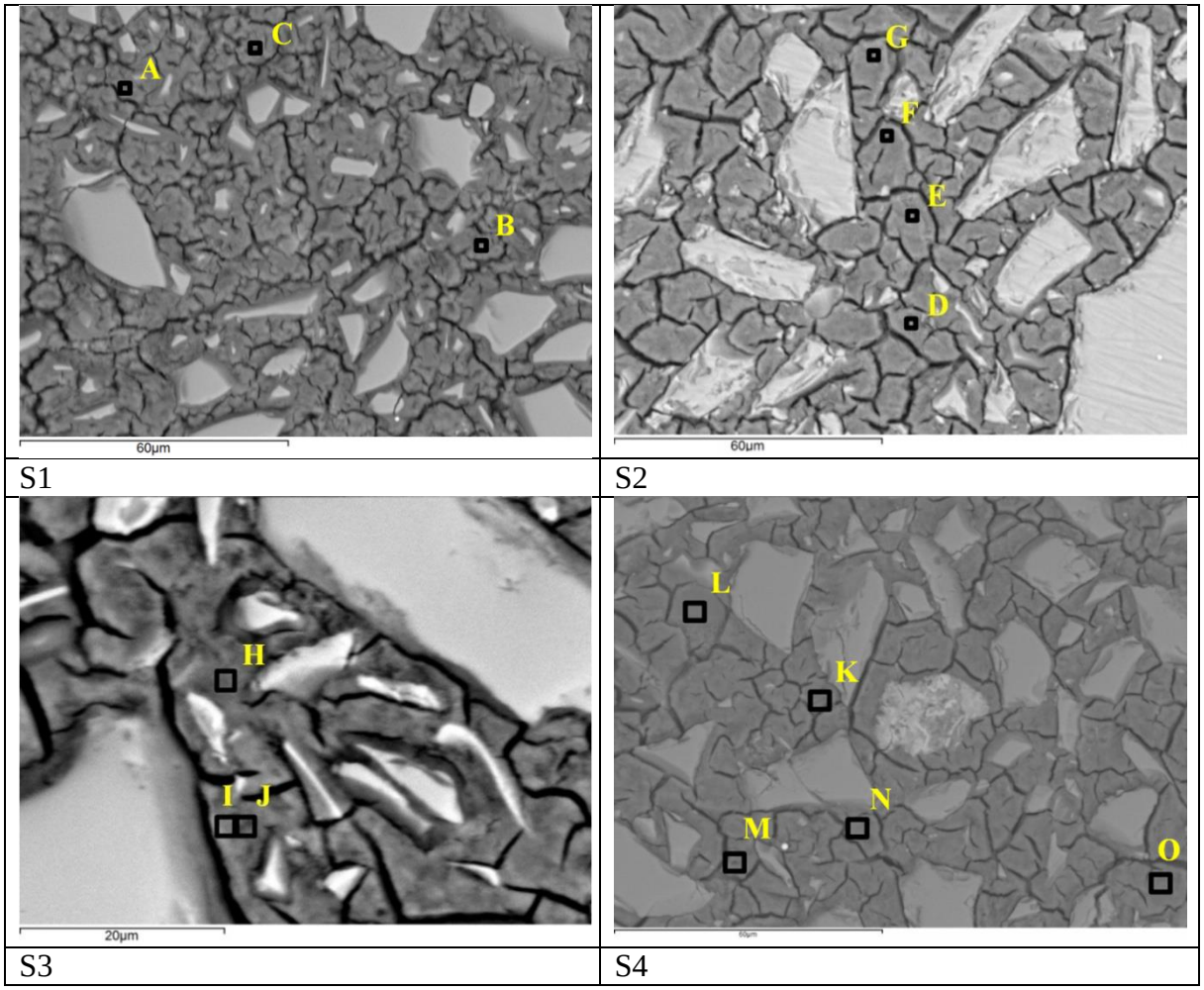

Figure 56 Points in matrix analysed in EDX for mixes S1-S4.

To understand the difference of Ms in the gel formation, the chemical composition of the geopolymer matrix in samples of mix S1-S4 was investigated. Figure 56 shows points on the matrix of mixes S1-S4 where data of elemental analysis have been collected. Mix S1 and S2 have been based on point analysis while mix S3 and S4 are based on high resolution maps and every point is an average of a square of 16x16 point spectra (where one point represents one pixel). Output from points A to O, is displayed in Figure 58, a plot of Mg/Si vs Al/Si. The dashed line is not calculated but only designed to show that the results fell in similar trend as shown for other AAS in Figure 19. The Mg/Ca equals to 0.11-0.97 and the Al/Si has a range of 0.27-0.50. Mix S1 has the highest

Al/Si ratio (in average) which is reasonable as the other mixes have higher soluble Si content. However, in average Al/Si ratio, no differences are seen between S2-S4. The Al/Si ratio agrees with the range of Al/Si ratio of Brough and Atkinson (2002) in Table 2, who used slag of similar chemical composition.

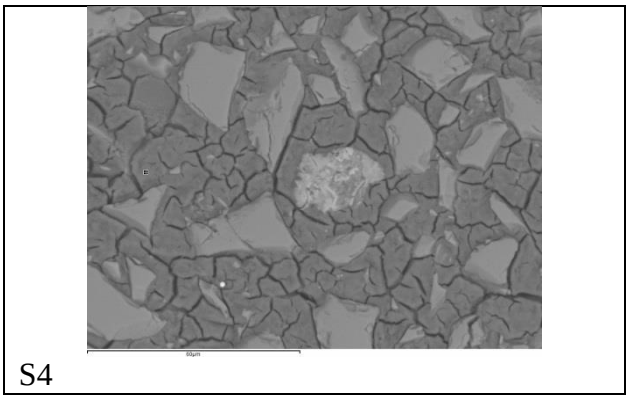

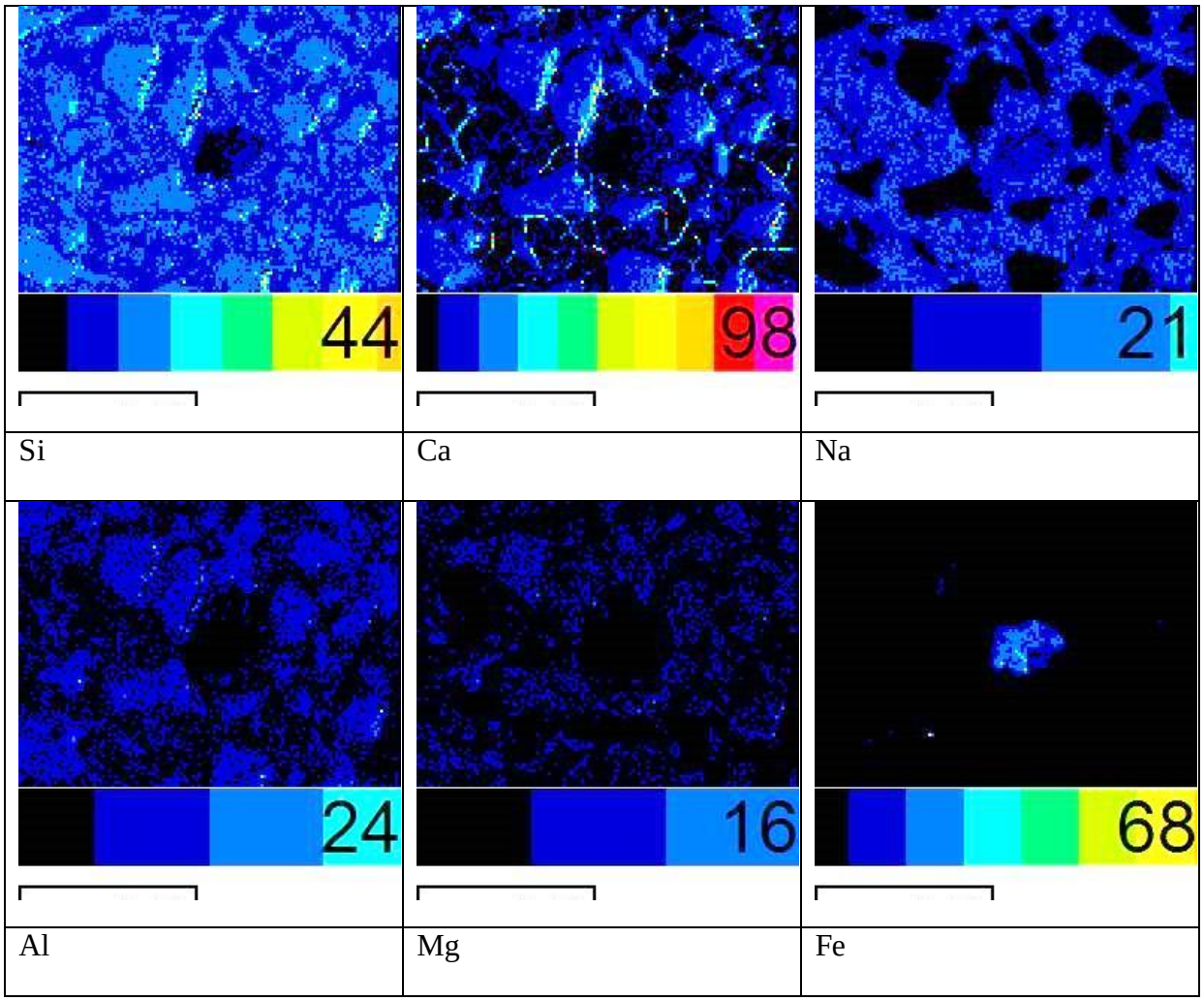

Figure 57 Chemical mapping on a selected area on a sample (mix S4).

The Ca/Si which is not graphically shown varied from 0.27-0.49 in all mixes. This is very low compared to the Ca/Si ratios reported by several authors in Table 2, while it is

low even compared to the range of Ca/Si reported by Brough and Atkinson (2002). The very low Ca/Si can be foreseen by Figure 57 where the black areas on the Ca map have higher than 5% Si content (on the Si map). Although the low Ca/Si generally can be due to carbonation (decalcification), here it is not considered to be the case: First, because the age of the samples was arrested on the 28th day. It is noted that the samples which were analysed in XRD had been kept pulverized in sample bags, so it is not the same with the samples analysed in SEM/EDX. Moreover, in the backscattered images shown above there is no indication that the matrix around the undissolved slag particles is decalcified, as found by Bernal et al. (2013) (section 2.4.5 and Table 4). Their backscattered images had different shade of grey around undissolved slag particles than the rest of the matrix, which is not seen here. After this remark, although differences between natural carbonation (mixes S1-S4) and accelerated carbonation (Bernal et al., 2013) could exist, it may be unsafe to attribute the particularly low Ca/Si ratio to carbonation. Seeing Figure 57 again, it is believed that the results were affected by material carried away, as Ca appears to be the only element captured in microfissures. To confirm this assumption, studies listed in Table 2, reporting high Ca/Si ratios were checked and it was seen that, although some show cracks on the microstructure of the samples (Puertas et al., 2004, Brough and Atkinson, 2002), none is damaged to the extent of the samples shown above. Gebregziabiher et al. (2015) and Haha et al. (2012) had no cracking on the analysed in SEM samples and from the three samples of Bernal et al. (2014) only one cracked, the one that shows the lowest Ca/Si ratio on Table 2. Therefore, it is likely that the low Ca/Si ratio is an error technically induced.

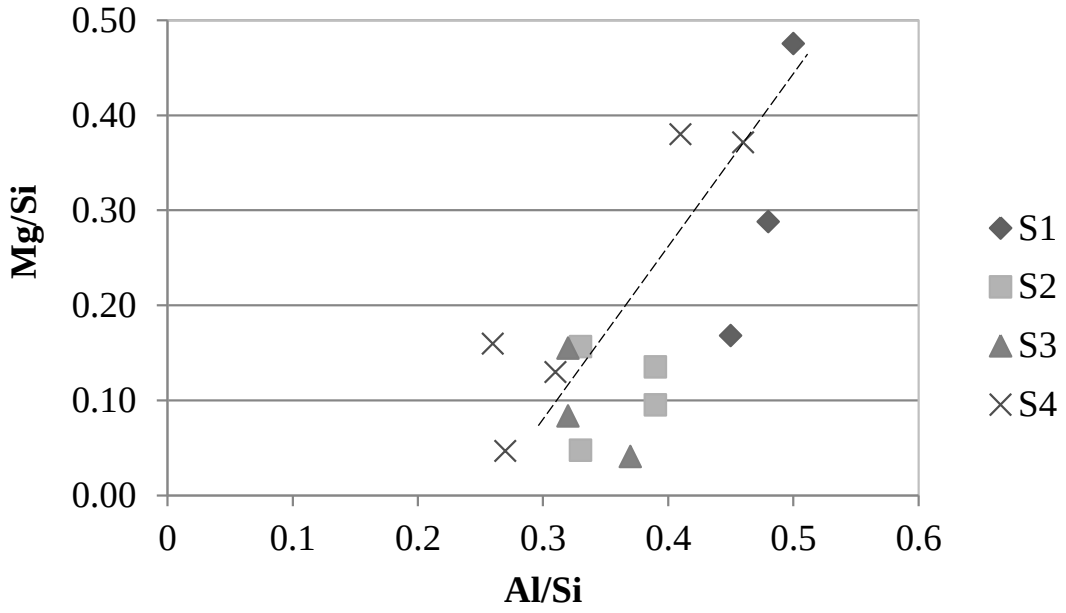

Figure 58 Atomic ratios Mg/Si vs Al/Si for the different GGBS-based pastes.

4.4 FA series

4.4.1 Composition

As seen in Table 3 the composition of FA can range considerably. The formulation of the FA series was based on the paper from Criado et al. (2007) who used FA of similar overall chemical composition to the used FA in this study, but with a higher content of silica. Details on the FA composition, formulation and products in their paper were presented in section 2.4.2 – Geopolymers. As mentioned in the same section, the FA of Criado et al. (2007) has same chemical composition with Fernández-Jiménez and Palomo (2005) in Table 3. Therefore, solution/ash ratio equal to 0.4 by weight was initially used and the right content of alkalis was searched around the value of 8% Na_2O per FA content. Hence, this investigation started with a preliminary test where fly ash was activated using 7 and 9g of Na_2O per 100g of FA, it was shown that the first formula was not enough to provide adequate strength in compression but the second had significantly higher strength, indicating dissolution was more complete. Therefore the experiment was designed for 9g of Na_2O per 100g of FA and five molar rates of SiO_2/Na_2O for the alkaline solution (Ms = 0.20, 0.45, 1.0, 1.25 and 1.50).

The composition of the FA series binders is shown in Table 18. The name of the mixes is composed of "FA" for indicating it is the FA-based binders of the chapter and a number, in continued numbering with the GGBS series. Note that there are two subseries. One had Solution/FA=0.4, where FA according to Table 18 is always 100g and 'Solution'=W+NaOH+Na_2SiO_3 (in g), therefore in contrast with the W_t in the equations of section 5.1, "solution" contains both the water and anhydrous part of the activator. While the Ms increases, the W (water added) is diminishing to have a constant Solution/FA ratio. This caused inconsistency in the fluidity of the generated pastes, with mix FA9 not having enough water to result into paste, that is why only four mixes were mixed for that series. To have pastes of similar workability, the other subseries was designed: a more fluid series where the $W_t/B=0.27$ (where W_t and B were calculated as shown in 4.1). Please note that mix FA5 is almost identical in both the sub-series. Therefore in Table 18, Ms and water content are the variables. As with the GGBS series, all the mixes were prepared following the equivalent composition for 150g of precursor.

4.4.2 Curing conditions

The FA series did not harden under ambient conditions and with reference to subsection 2.4.3.3, the specimens were oven cured till testing at 80°C to make sure that the temperature of the oven will not go above the 85°C, and ambient humidity. Samples were demoulded on day 1.

Table 18 Composition (in g) of binders FA5-FA9 based on 100g of FA.

								Water content					
	Mix	**Na_2O (g)**	**Ms**	**Precursor (g)**	**Na_2SiO_3 (g)**	**NaOH (g)**	**Binder (g)**	**W added (g) in solution**	**W_t/B**	**W added (g)**	**Solution /FA**	**SiO_2/Na_2O**	**SiO_2/Al_2O_3**
FA series	FA5	9	0.20	100	3.3	10.5	110.8	26.9	0.27	26.2	0.40	5.8	3.7
	FA6	9	0.45	100	7.3	9.1	112.9	27.0	0.27	23.6	0.40	6.1	3.8
	FA7	9	1.00	100	16.3	5.9	117.7	27.3	0.27	17.8	0.40	6.6	4.2
	FA8	9	1.25	100	20.4	4.5	119.9	27.4	0.27	15.1	0.40	6.9	4.3
	FA9	9	1.50	100	24.5	3.1	122.1	27.5	0.27	12.4	0.40	7.1	4.5

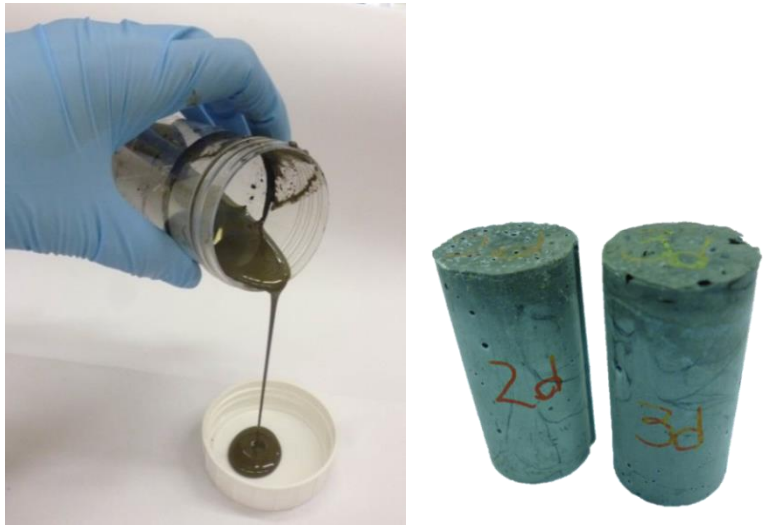

Figure 59 From the more fluid series (series with W_t/B=0.27). The samples formed bubbles on the free surface while hardening in the oven.

4.4.3 Setting time

The specimens were taken in the oven and were taken out every time that a reading for the Vicat test was due. The setting times of fly ash samples do not follow a linear trend for increasing Ms as shown in Figure 60, therefore do not confirm that increasing Ms accelerates the setting time (2.4.3.2). The drier sub-series showed a more regular (at least not increasing) trend for both the initial and final setting time. The workable paste had longer setting times compared to the drier sub-series. The testing of setting time with a sample which requires heat curing is problematic as the time for heat to penetrate the sample varies from the top of the sample (where the needle is placed) to the centre and the formation of a more reacted crust is possible. As a result, the values obtained provide an indication of relative performance of the mixes rather than results which can be compared to the GGBS series or PC based binders.

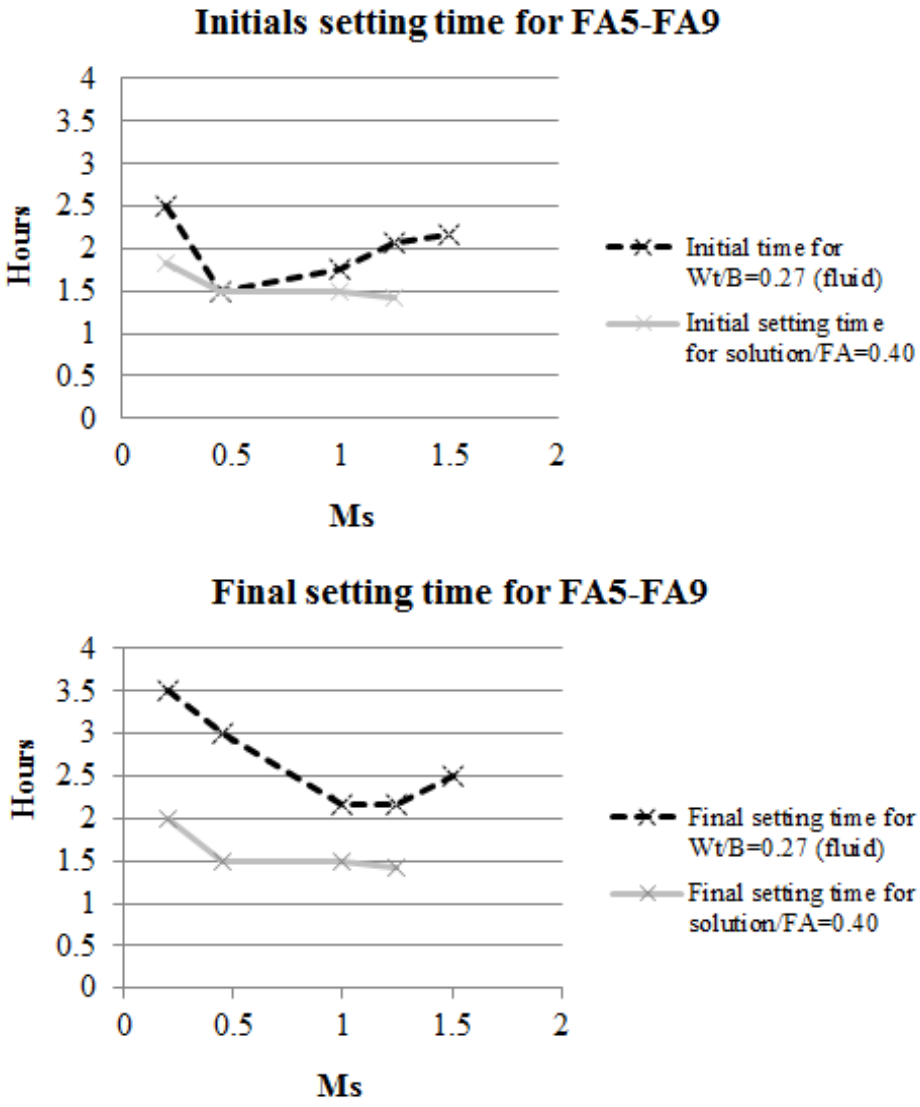

Figure 60 Plots of the initial and final setting time for the FA binder series, for $W_t/B=0.27$ (fluid pastes) and solution/FA=0.40 (drier pastes).

4.4.4 Strength in compression

The drier pastes (solution/FA=0.40) exhibit equal or better performance than the more fluid (W/B=0.27) based on Figure 61. Contrary to expectations, in most of the cases the strength only slightly increases or even drops over time. That issue was later attributed to the prolonged oven curing in dry conditions. The maximum strength achieved was 72MPa for Ms=1.0 on day 7. The same mix had a strength of 67MPa on day 28. The more fluid paste gave constant results about 30MPa for all the Ms which raises doubts as to whether proper activation of the FA was achieved. The standard errors on the graphs indicate high consistency in most of the mixes, with maximum error being a 13% of the strength (for FA7, solution/FA=0.4, day 28).

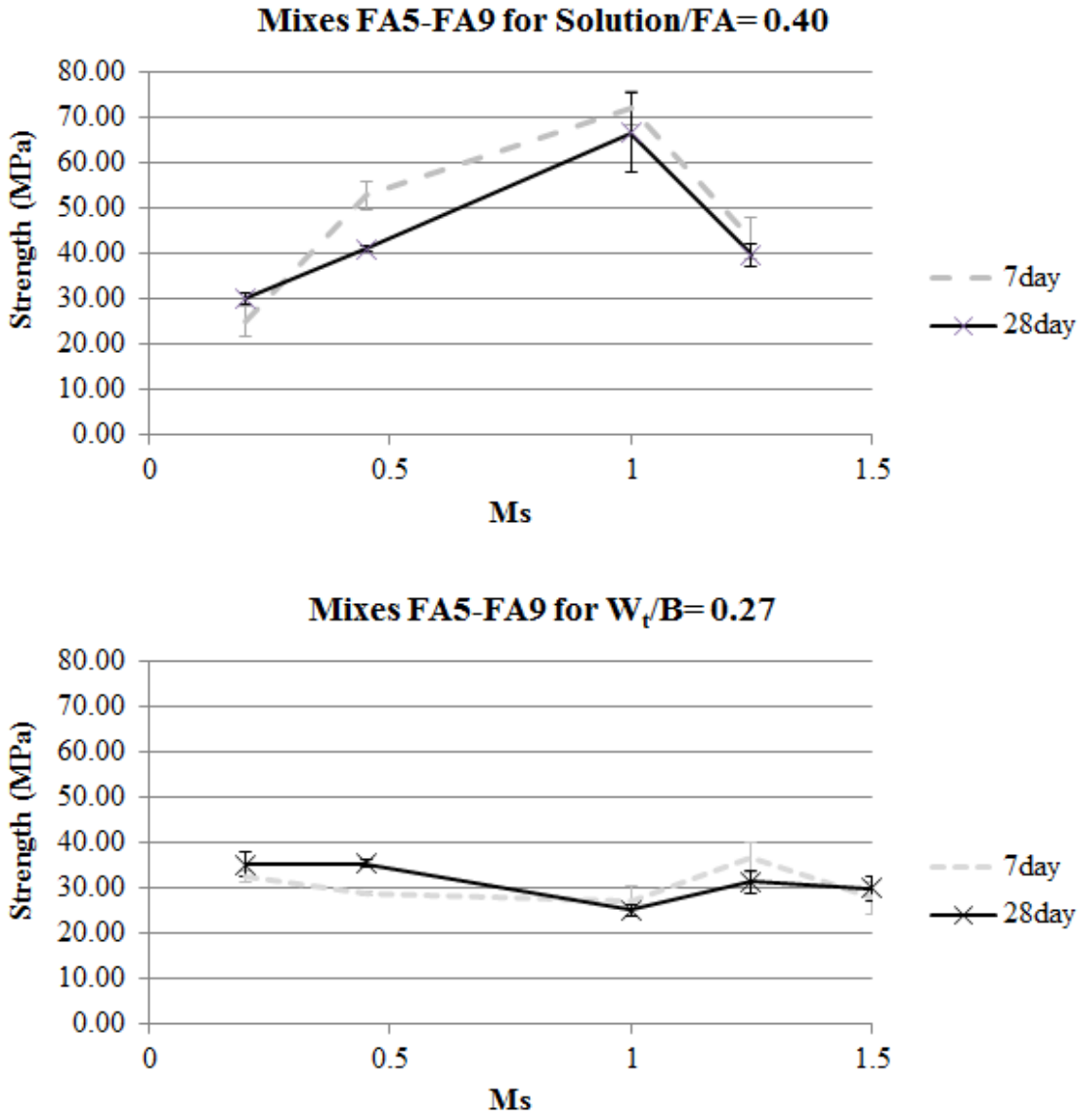

Figure 61 FA series, a) drier pastes (solution/FA=0.40), b) more fluid pastes (W_t/B=0.27): Compressive strength for increasing Ms on day 7 and 28.

4.4.5 XRD

The following figure displays the XRD patterns for mixes FA5-FA8 for Solution/FA=0.40 and mixes FA7-FA9 for W_t/B=0.27 (mixes FA5 and FA6 have little difference for the two water ratios). The X-ray powder diffraction pattern of FA is included for comparison and only peaks which are not common to all are noted on the graph. While FA shows it is a vitreous material by the presence of the halo at 2θ=20-35°, the products also have that feature at 25-40° which indicates the formation of aluminosilicate gel and remaining crystalline phases of FA after the alkali activation, all in accordance to what other authors have stated (section 2.4.2).

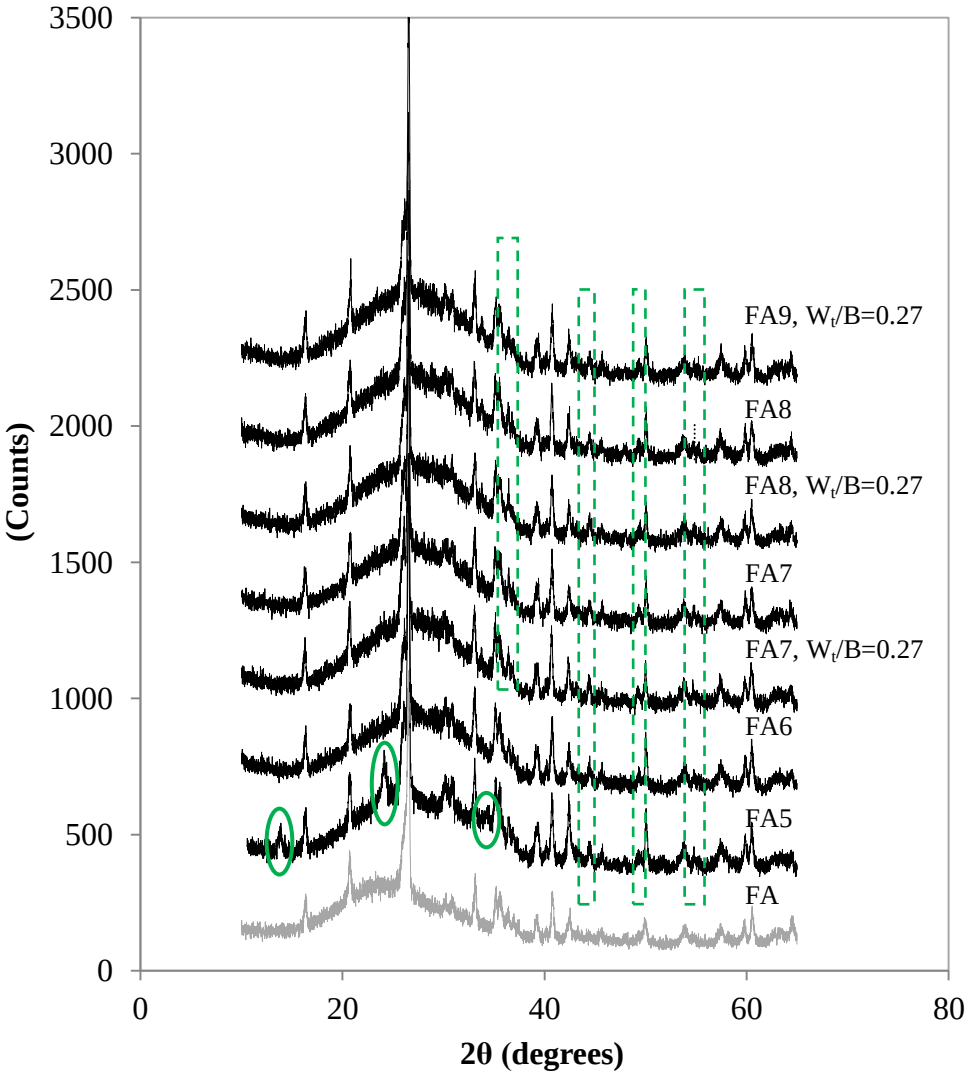

Figure 62 XRD patterns of mixes FA5-FA9. Minor differences for mixes FA6-FA9.

In Figure 62, it is observed that FA5 clearly formed a new crystalline phase, pointed on the figure, other than these associated with FA which is probably hydroxysodalite ($Na_4Al_3Si_3O_{12}OH$) (also seen in the FA products of Fernández-Jiménez and Palomo (2005)). At about 33.7° mixes FA7-FA9 have a weak crystalline product. Looking at the

American mineralogical database, the zeolite –which is assumed to incorporate Na- could not be identified. At about 44.4°, 49.3°, 54.8° all the samples show peaks.

It is interesting to point that FA7 and FA8 gave no distinguished differences for the two water contents, although according to the discussion in 2.4.2 higher water content would be expected to have higher crystallinity. It is believed that the difference in strength results from the change in porosity and the quality of the amorphous matrix rather than a difference in dissolution. It is reminded that substances with crystal size smaller than 8nm or with peaks less than 3% of the present crystalline substances, cannot be detected (Rees (2007), section 2.4.2). Although Rees (2007) mentioned that for samples of the same Na/Al and different Ms (as in this study), the XRD patterns will have the same location of peaks but different intensities, here the hydroxysodalite which occurs for the maximum NaOH content used (FA5) is not formed in the other samples. Criado et al. (2007) noted that zeolites can be converted in other, more stable zeolites over time.

4.4.6 SEM

Samples from mixes FA5-FA9 were analysed using the same settings as for the GGBS series. Unlike the slag-based samples, the preparation of FA-based samples did not cause extensive microcracks to the matrix, which has to do with the nature and the higher porosity of the material. The microstructure of FA series exhibits greater differences for the different Ms ratios and images are displayed in Figure 63 for different magnifications. FA9 looks more homogeneous than FA5 with more gel formed, although FA9 was slightly weaker than FA5 on day 28. The very bright particles in the images are iron oxides (raw FA contained 8.7% of Fe_2O_3). Resin could not fill the very small closed pores and cavities; where there is resin the colour is black. Cavities exist due to either water which evaporated later or gas pores or due to unreacted FA particles which sometimes pop out during polishing. The fact that FA5 is more crystalline than FA9 as seen in the XRD (Figure 62), can be confirmed by Figure 63.

4.4.7 Chemical identification of components

Figure 64 shows the points in matrix of different samples where EDX ran after 6months of curing but having arrested aging on day 28. The EDX confirmed that the dark-glassy areas in FA5 are resin (rich in carbon). Figure 65(a) shows where carbon is located and Figure 65 (b) shows where Na is located, indicating the matrix (although some Na is contained in FA particles too according to the XRF results). These images are not quantitative and are based on counts of the EDX. FA7 in Figure 64 and FA5 in high magnification in Figure 63, remind the findings of Fernández-Jiménez et al. (2005) who stated that the alkaline attack in FA-based mixes starts from one point on the sphere, expands inwards (in some cases there are inner spheres), and then the alkaline attack continues from inside and outside to the rest of the sphere, while part of the outer layer of the sphere may be intact under reaction product.

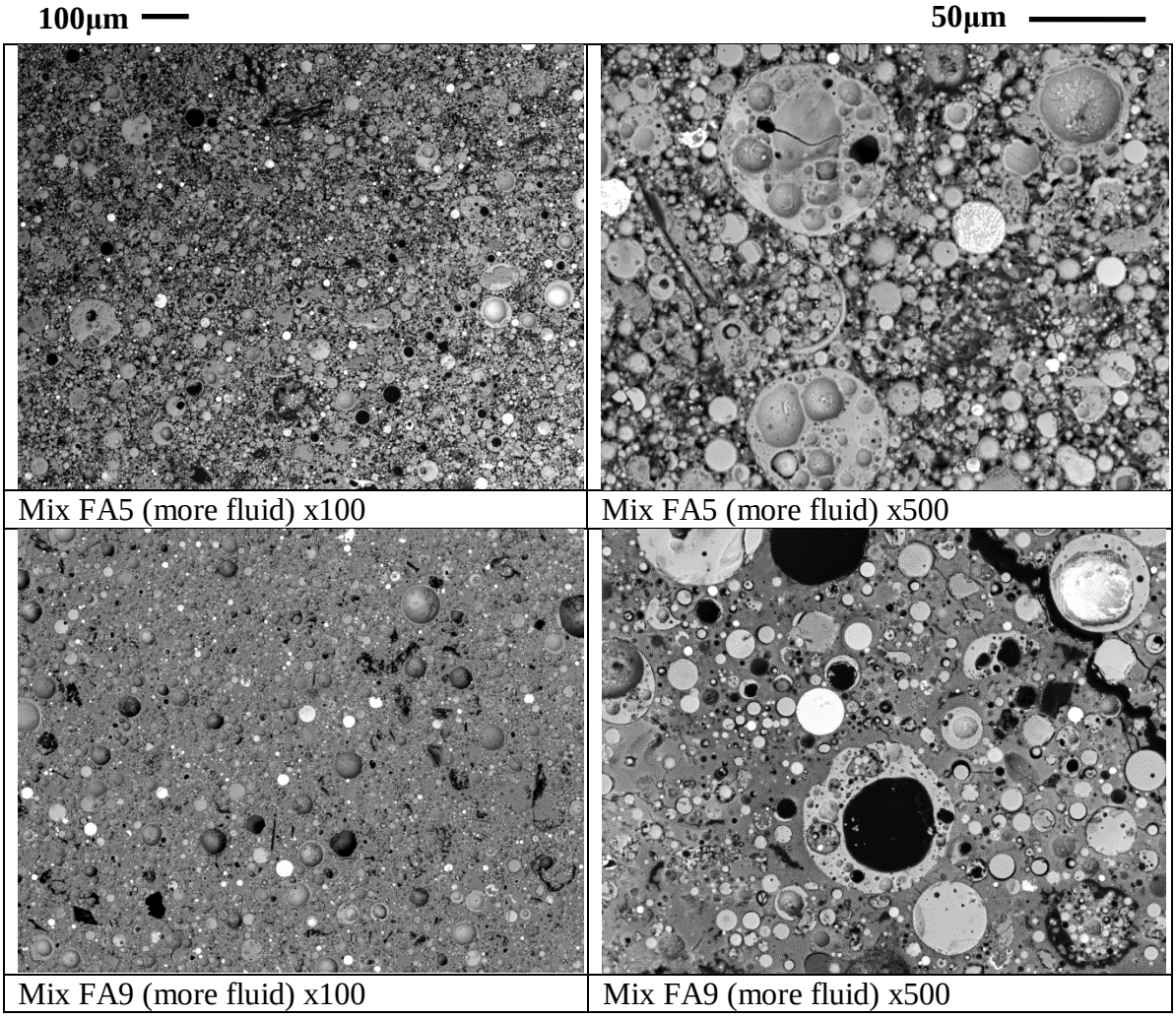

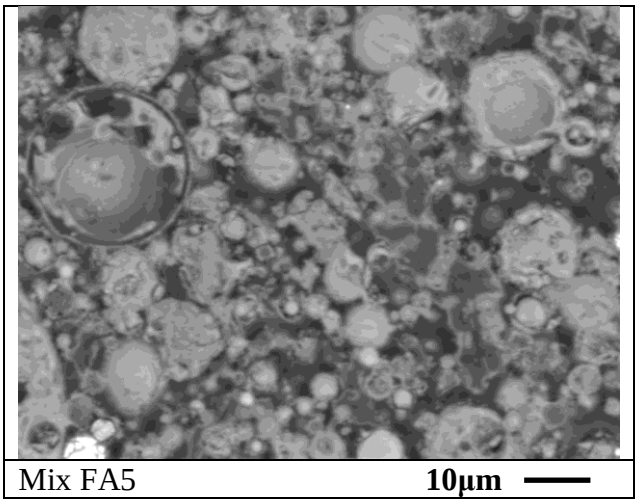

Figure 63 Backscattered electron images for the FA-based binders.

In Figure 64, the elemental analysis of FA5, FA7 and FA8 has been conducted based on point analysis while mix FA9 was based on high resolution maps (average of a square of 16x16 point spectra where one point represents one pixel). Mix FA7 is less porous than

FA5 and mixes FA8 and FA9 look even more homogeneous. Table 19 shows the atomic ratios of Si/Al for all the points above. The results are in the same range with the results of Fernández-Jiménez and Palomo (2005) for activation using sodium silicate (Table 3). Generally, in average there is an increasing trend between the FA5-FA7 and FA8-FA9, which should be due to the use of more silicate (section 2.4.2). It was not possible to acquire enough points of matrix on mix FA5 suitable for EDX, only area A.

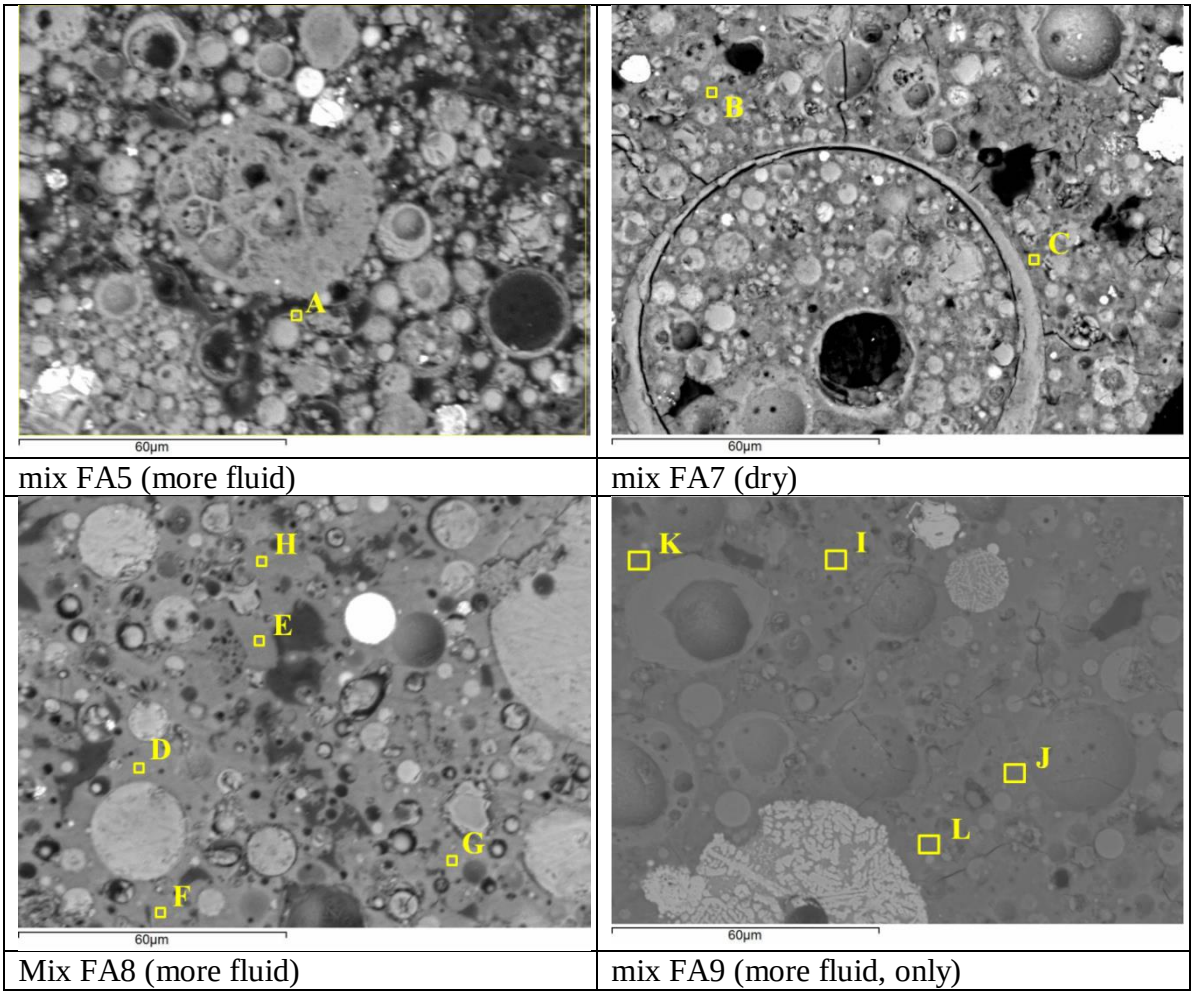

mix FA5 (more fluid)	mix FA7 (dry)
Mix FA8 (more fluid)	mix FA9 (more fluid, only)

Figure 64 Points in matrix analysed in EDX for mixes FA5-FA9.

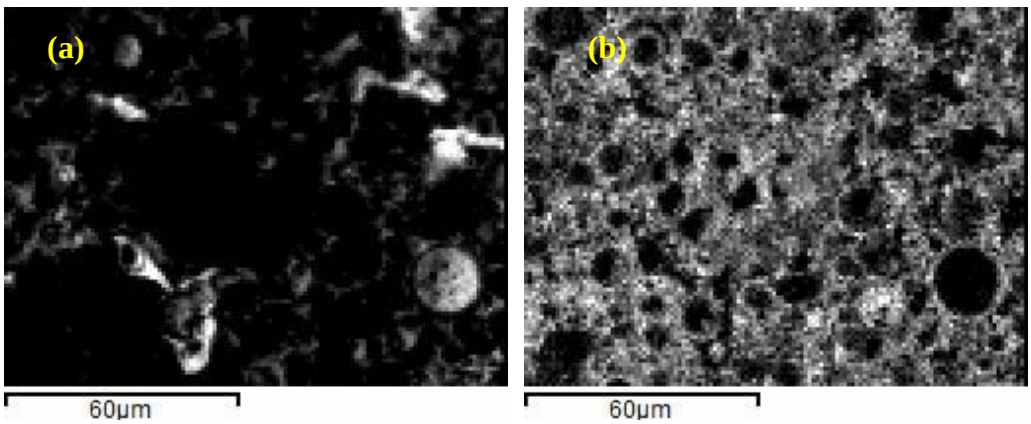

Figure 65 Mix FA5: detection of (a) Carbon, (b) Na.

Table 19 Results from EDX analysis for points (seen in Figure 63) on some of the FA-based binders.

		Si/Al
Mix FA5	A	2.23
Mix FA7	B	2.26
	C	3.67
Mix FA8	D	3.34
	E	3.20
	F	3.53
	G	1.88
	H	2.70
Mix FA9	I	3.73
	J	3.98
	K	3.71
	L	2.55

4.5 50/50 GGBS/FA series

4.5.1 Composition

The goal of the binary mix was to provide setting without heating, while minimising GGBS use which is more expensive and currently less available than FA as discussed in section 1.3. This series was decided to be based to a blend of 50% FA and 50% slag, for reasons discussed in subsection 2.4.3.1. Table 20 shows the composition of mixes for 5 and 7g of Na_2O in 100g of aluminosilicate and Ms=0.75, 1.00 and 1.25. Therefore, the variables on the table are the Na_2O content, the Ms and the W_t/B ratio which slightly ranges (from 0.35-0.37). This series has lower W_t/B ratio than the GGBS series due to the rheological properties of FA. The mixes were mixed following the equivalent composition for 150g of GGBS+FA.

Figure 66 Characteristic grey-green colour internally.

4.5.2 Curing conditions

The samples were cured at 20°C and high RH (~90%) and demoulded on day 2. They were kept in the same conditions after demoulding. The specimens had a dark colour but the areas that were properly activated had grey-green colour.

4.5.3 Setting time

The Vicat test was conducted in stable temperature and RH conditions (20°C, ~60% RH). The setting times can be found in Figure 67. The setting time was shorter than the FA series and usually slightly longer than the GGBS-based mixes. While the initial setting time had no clear trend, the final setting time for all samples was descending.

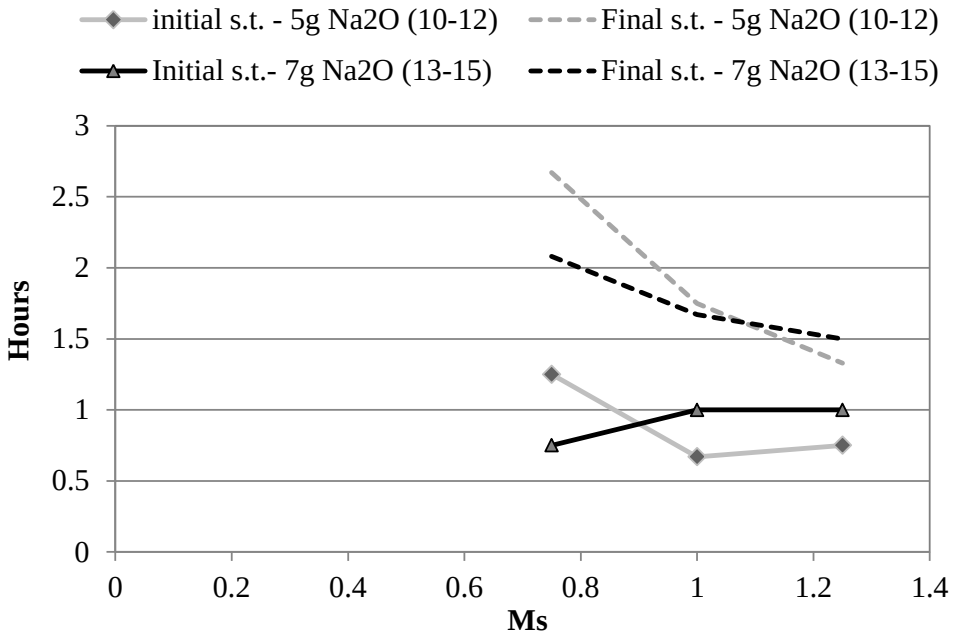

Figure 67 Plots of the initial and final setting time for the 50/50 binder series.

4.5.4 Strength

Figure 68 a) and b) show the strength of the 50/50 series' specimens in compression and the standard errors are noted. On the 7th day the strength is approximately the same for mixes 10-15 while on the 28th day the mixes 10-12 gave higher strength than mixes 13-15. This is surprising because, since generally FA needs higher alkalinity to be activated, it was assumed that the blend of GGBS/FA would also need more than 5g of Na_2O in the activator per 100g of precursor which was the case for the GGBS series.

Regarding the molar ratio of the activator, most of the specimens follow the trend of the previous series: there is a peak for Ms=1.00. The highest value is 71MPa on the 28 day for Ms=1.00 and use of 5g of Na_2O per 100g of GGBS and FA. This is about 60% of the 117MPa that the equivalent mix of the GGBS series reached and equal in strength to the FA series equivalent, before it lost strength (72MPa on day 7).

The errors are within a 10% of the strength values apart from the 28day test of mixes 12-15 in which case the error increases to 20%. Mixes 12 and 13 were repeated and the errors fell in the 10% range giving as average strength: 46 and 66MPa for the 7 day and 28 day respectively for mix12, 33 and 63MPa for day 7 and 28 of mix13. It was chosen to present the inconsistency in Figure 68 to point out that the small dimensions of the specimens but also the nature of the material introduces variation to the values of strength.

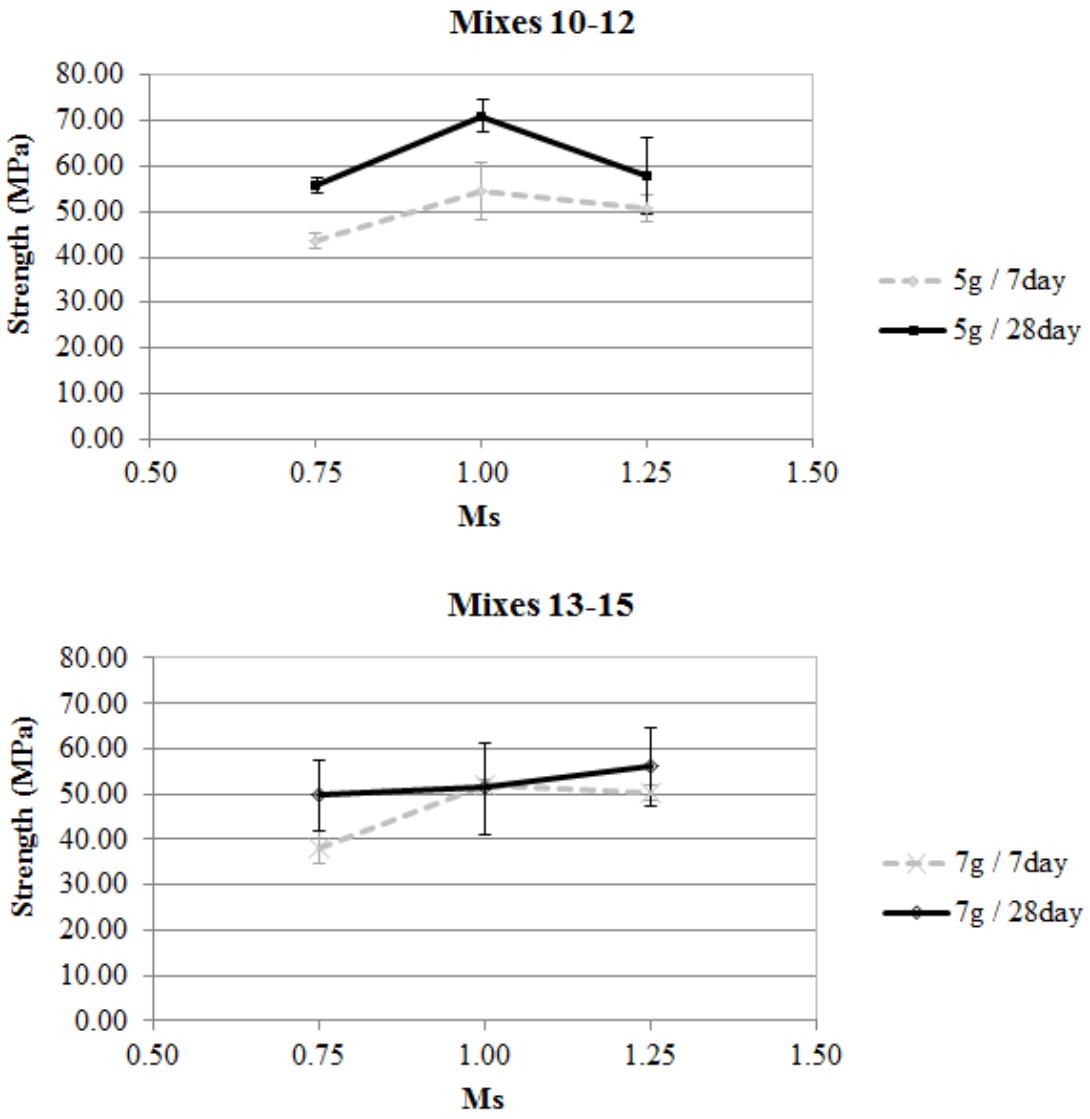

Figure 68 50/50 series: Compressive strength for increasing Ms on day 7 and 28.

Table 20 Composition (in g) of binders 10- 15 based on 50g FA+50g GGBS.

	Mix	Na_2O (g)	Ms	Precursor (g)	Na_2SiO_3 (g)	NaOH (g)	Binder (g)	W added (g) in solution	W_t/B	SiO_2/Na_2O	SiO_2/Al_2O_3
50/50 series	10	5	0.75	100	6.8	4.1	108.7	37.8	0.37	9.4	4.2
	11	5	1.00	100	9.1	3.3	109.9	37.5	0.36	9.7	4.4
	12	5	1.25	100	11.3	2.5	111.0	37.2	0.36	9.9	4.5
	13	7	0.75	100	9.5	5.7	112.1	36.9	0.36	7.0	4.4
	14	7	1.00	100	12.7	4.6	113.8	36.5	0.35	7.2	4.5
	15	7	1.25	100	15.9	3.5	115.5	36.1	0.35	7.5	4.7

4.5.5 XRD

Samples from mixes 10,11,12 and 14 were not embedded in acetone and ran in XRD on day 29 using the Bruker diffractometer for the range of 2θ=5-65°. Flatplate mode was used and the step changed to 0.016° for 0.3s. Although there is noise, the main crystalline phases are visible. Phases ascribed to FA including quartz, mullite and hematite are present and and C-S-H associated to the activation of the GGBS can also be noted (Figure 69). For all samples the intensity of diffraction is low and there is no evident difference between the different Ms or alkaline content used by the age of 29days.

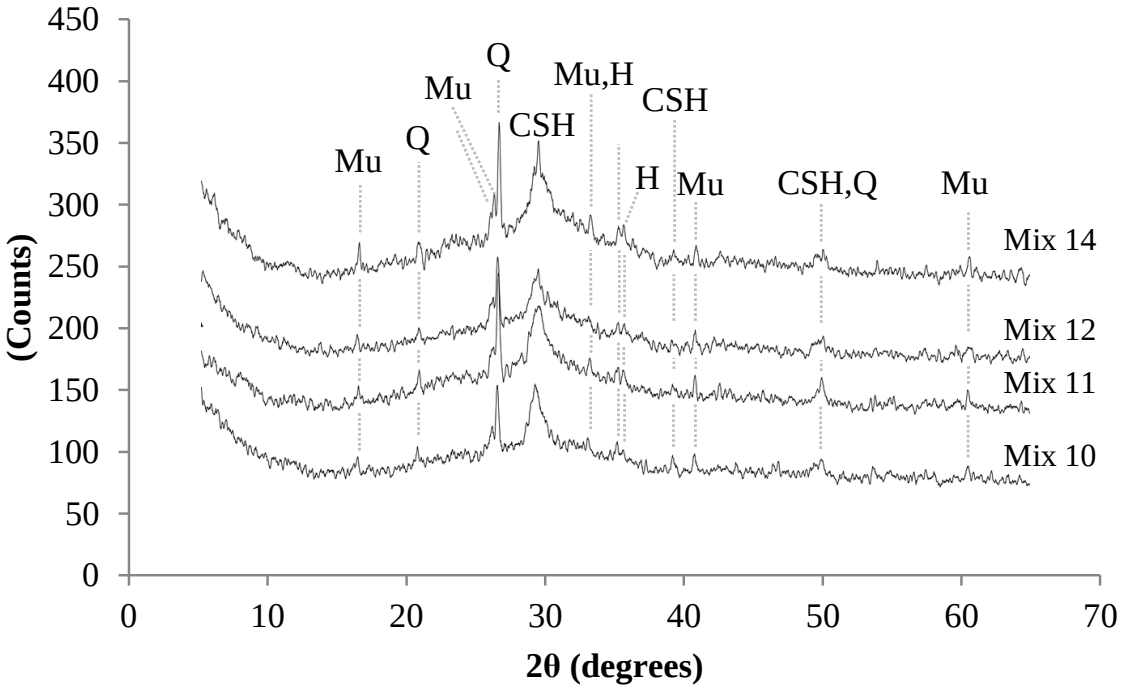

Figure 69 XRD patterns of the 50/50 series. Where H=Hematite, Mu=Mullite, Q=Quartz, CSH= Calcium Silicate Hydrate.

4.5.6 SEM

Samples from mixes 10,11,12 and 14 were left curing (no arrest of aging) and were tested in SEM 6 months later. The polished samples were covered in chromium (2nm) but as they were still charging in high vacuum, the analysis was conducted using low vacuum. The settings were: backscattered mode (BES signal), 15kV, spotsize 60, work distance 10mm, 1Pa. The dark areas which are not round could be resin which damaged the matrix during being impregnated or carbonated areas. The following images show the different mixes in increasing magnification:

- x100

100µm —

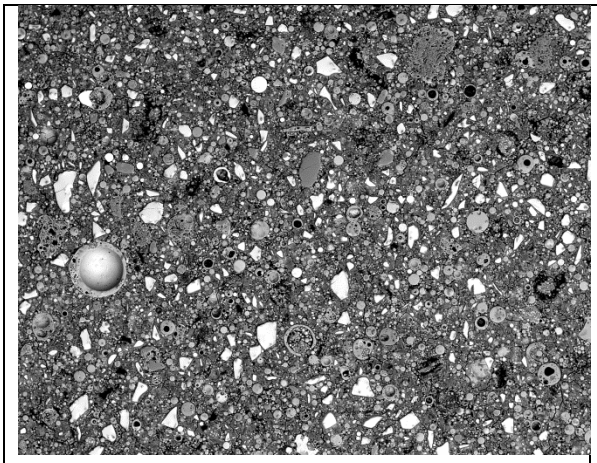	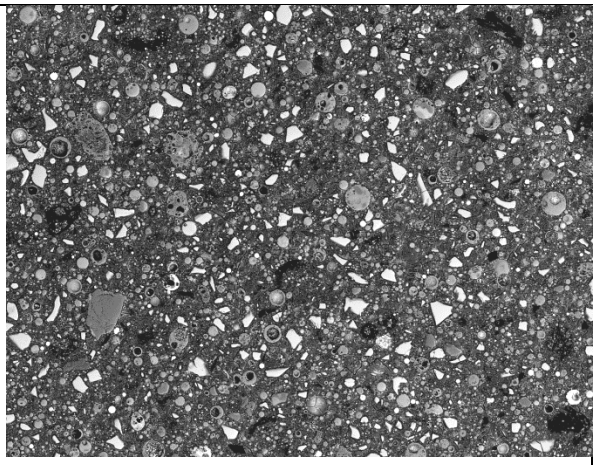
Mix 10	Mix 11
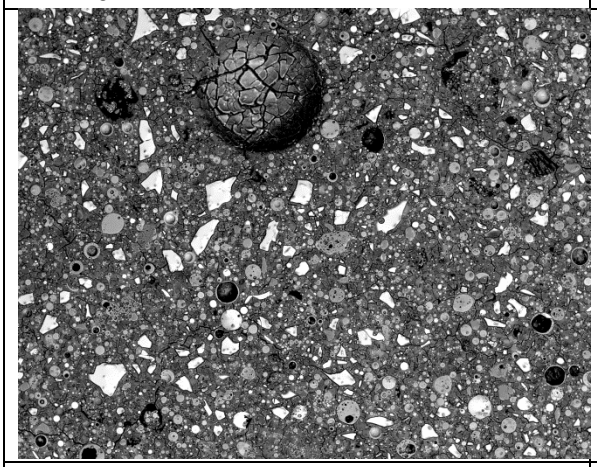	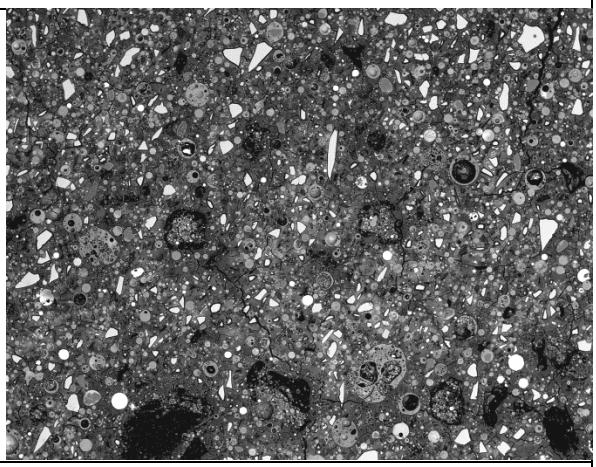
Mix 12	Mix 14

- x500

50µm

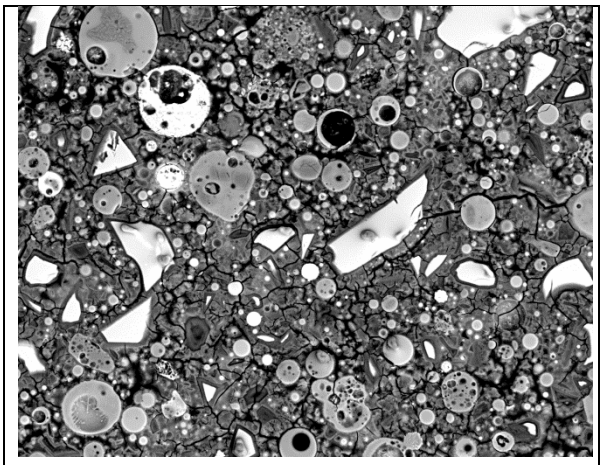	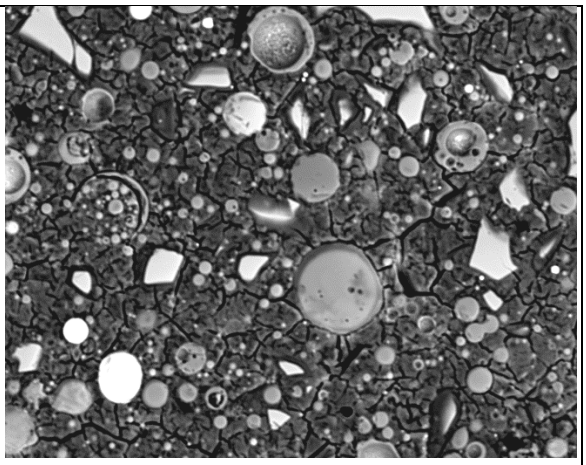
Mix 10	Mix 11
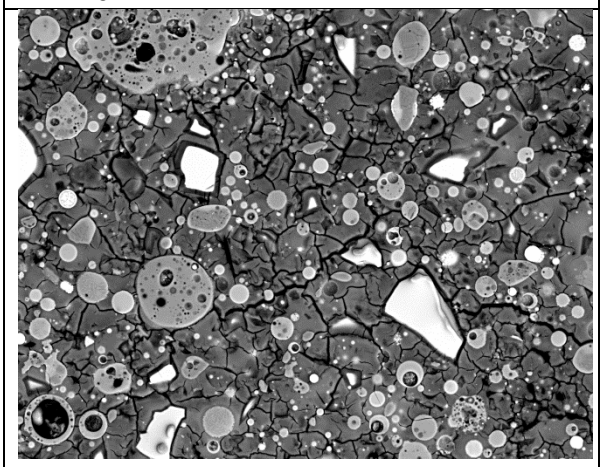	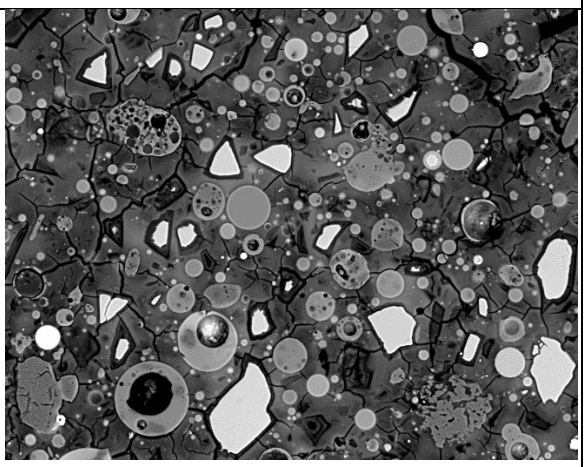
Mix 12	Mix 14

- x1000

10μm —

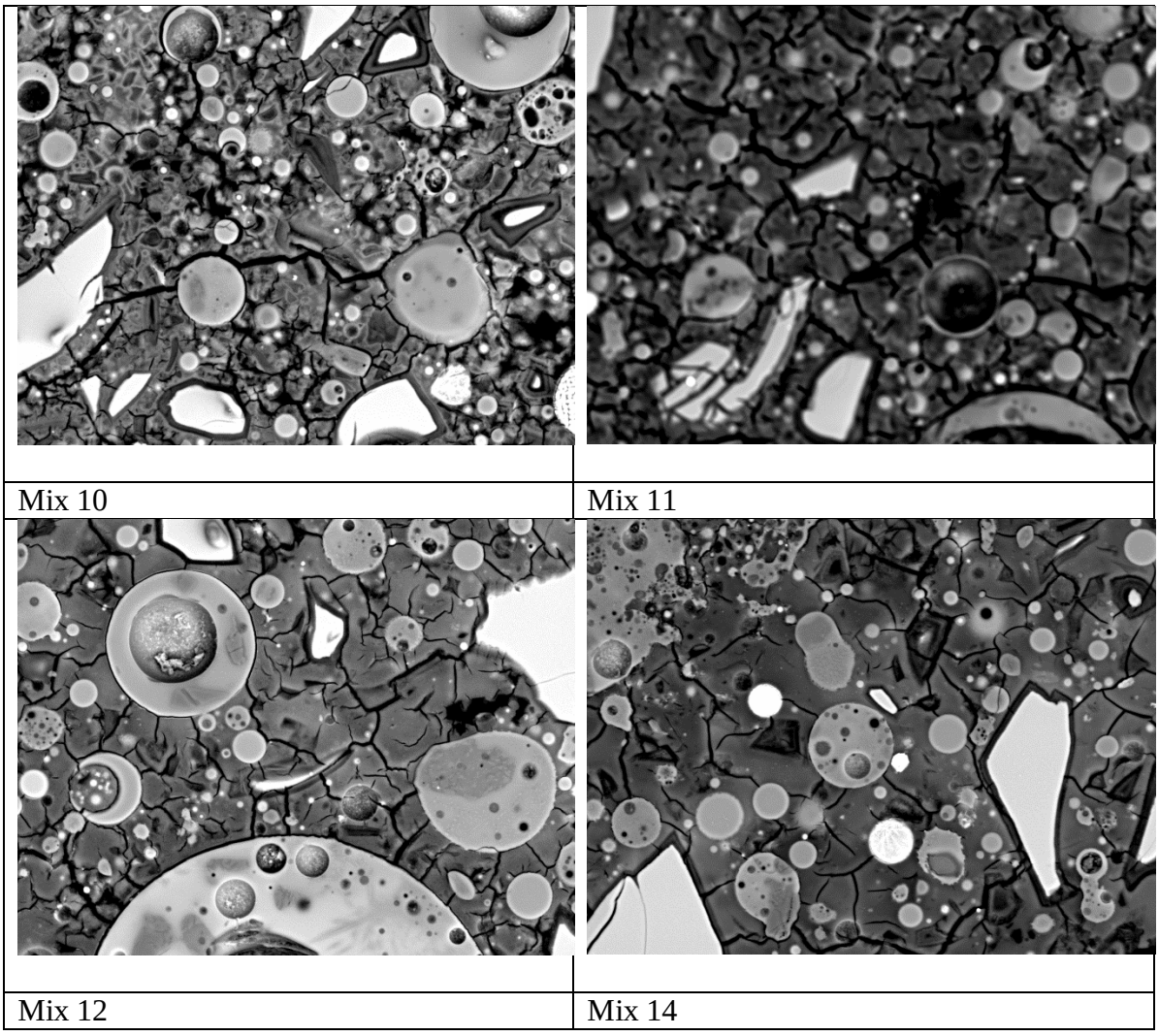

Figure 70 Backscattered electron images for the GGBS/FA-based binders.

The matrix of Mix 11 appears more reacted (fewer unreacted fly ash particles visible) than Mixes 10 and 12 which could justify why mix 11 showed optimum strength between the mixes activated using 5g of Na_2O. Mix 14 shows also good dissolution of FA and GGBS and large areas of gel only. In the highest magnification it is easy to see that mix 11 holds the densest 'net' of microfissures compared to mix 10 and 12, with similar density to the GGBS series (Figure 70). It is interesting to observe two shades of grey for the matrix of mix 14, visible in all scales, which indicates a heterogeneous mix.

4.5.7 Chemical identification of components

From the EDX (Figure 71, based on point analysis) it can be seen that the dark areas of the rims and marks of ongoing dissolution of slag particles, give different results than the rest of the matrix with the Al/Si atomic ratio significantly lower than the typical 0.14-0.37 which is observed in all the samples and the Al/Ca atomic ratio close to or higher than 1.

The matrix of Mix 10 has Ca/Si=0.70 which changes only in the newly polycondensed areas. The Ca/Si drops to 0.42 for Mix 11 while in Mix 12 it ranges from 0.21-0.60. During the analysis, it was obvious that the rims (spectrum J) had high Mg atomic percent and less Si, Al and Ca. Spectrum G gave very high Si content (Al/Si=0.14) and some Ca and Al, therefore completely different composition than that of spectrums I and H which contain half amount of Si and slightly higher Ca. In mix 14 we note differences between the dark (spectrums K,M, L, Ca/Si=0.61-0.65) and the clear areas (spectrums O,N, Ca/Si=0.71-0.73) of the matrix we observed earlier.

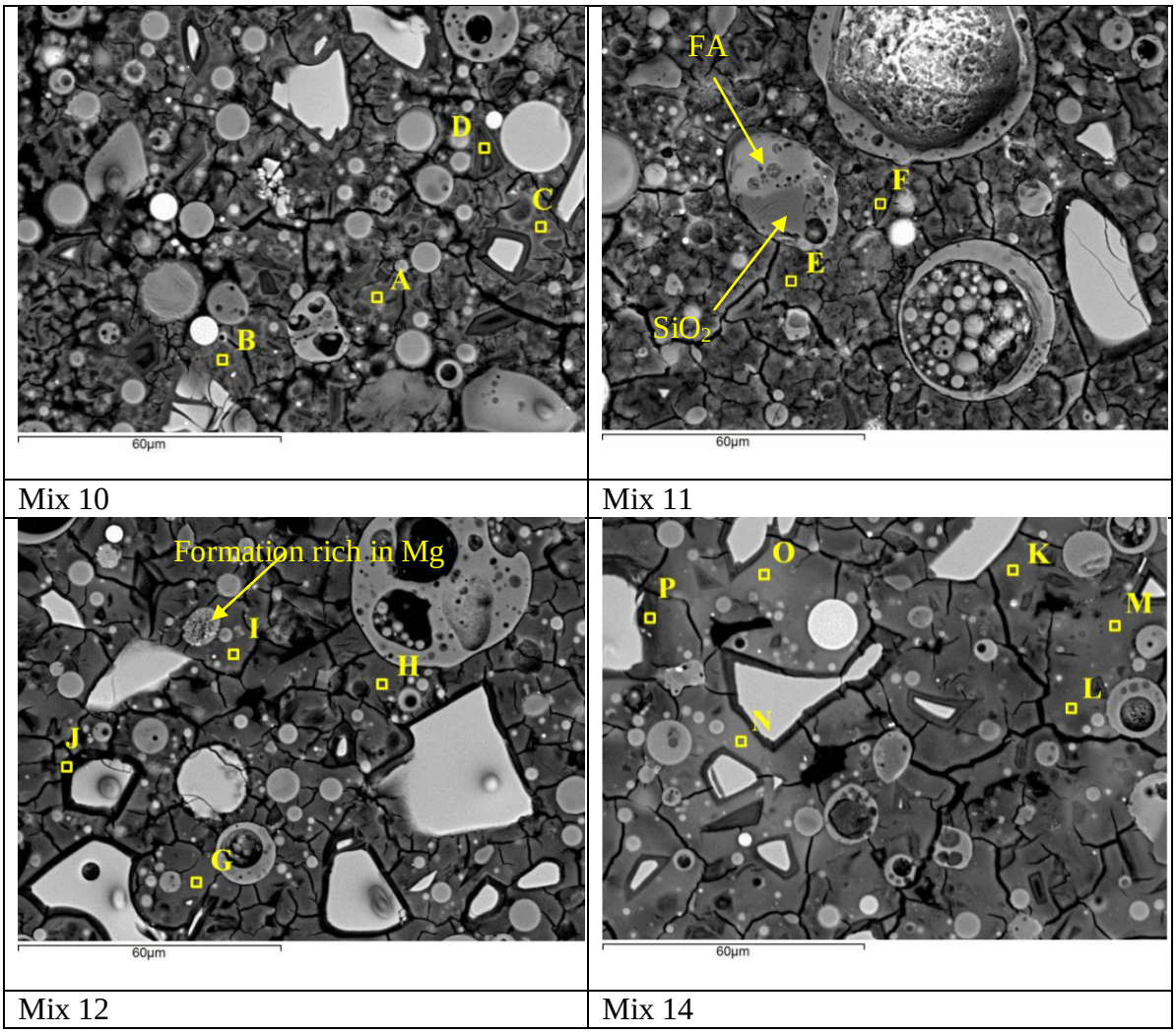

Figure 71 Points analysed in EDX for mixes 10-12 and 14. Samples after 6months of curing.

Compared with Table 4, the 50/50 blend used here (48%SiO_2, 18%Al_2O_3, 21%CaO, 5%MgO), is not similar in chemical composition to any of the blends used by other authors. Therefore, comparison is not advised. However in general, the matrix, excluding the dark areas, has Al/Si in the same range with the other authors. In Table 4 it is seen that Ca/Si and Al/Ca can largely range.

As the products here are based in a 50/50 blend it would be expected that the Ca/Si should be lower than the Ca/Si of the GGBS binder series (section 4.3.7). On the opposite the Ca/Si here is higher. It lowers for Mix 11 which has the densest net of microcracks as mentioned earlier. The higher Ca/Si ratio is likely due to the lower degree of damage of the sample.

Table 21 Elemental Analysis of points from Figure 71

		Ca/Si	Al/Ca	Al/Si
Mix 10	A	0.70	0.45	0.32
	B	0.59	0.84	0.50
	C	0.70	0.45	0.31
	D	0.70	0.90	0.63
Mix 11	E	0.42	0.89	0.37
	F	0.42	1.93	0.81
Mix 12	G	0.21	0.69	0.14
	H	0.60	0.44	0.27
	I	0.60	0.44	0.26
	J	0.44	1.84	0.81
Mix 14	K	0.61	0.47	0.28
	L	0.65	0.44	0.29
	M	0.67	0.44	0.29
	N	0.71	0.42	0.30
	O	0.73	0.36	0.26
	P	0.57	1.00	0.57

4.6 Conclusions of chapter

The calcined mica concentrate (optimum at 950°C) showed some potentials when alkali-activated with presence of $Ca(OH)_2$. Without presence of $Ca(OH)_2$, the results in compression were lower than 1MPa and the samples were unstable in water. It was therefore shown that calcined muscovite has some reactivity, but not enough to reach the performance suggested by Pacheco-Torgal et al. (2008,d). This observation agrees with the findings for pyrophyllite (MacKenzie et al., 2008) where the 2:1 lattice is a barrier and the Si layer makes it difficult to access the five and four coordinated Al.

Moreover, even with the presence of $Ca(OH)_2$ the strength was relatively low with the average below 10MPa. The highest strength achieved in the trials was 19MPa for $W_t/B=0.40$ and 20% $Ca(OH)_2$ on day 28. For such a water content, the later incorporation of aggregates in order to develop mortars may be ineffective. Moreover, from an environmental point of view, binders for which (1) energy and materials have to be spend

to produce mica concentrate from MW, (2) energy has to be spend to calcine the MW, (3) significant quantity of $Ca(OH)_2$ and alkalis (although low in sodium silicate) has to be added, in relation to the low compressive strength reached, are unlikely to fulfil the objectives of this study. Therefore it was decided not to continue in developing mortars using only MW as a precursor and binders based on slag and FA precursors were developed to use with the china clay waste.

The GGBS series was the strongest paste and reached over 100MPa while the FA and the 50/50 series varied from 30-70MPa. The FA series had lower strength for the more fluid mixes. As expected, the highest strengths were achieved for Ms=1.00-1.25. Based on Figure 52, Figure 61 and Figure 68, three mixes were selected as optimum, one for each binder series. These were then used to produce the test mortars: mix 3 (Ms=1.25) for the GGBS series, mix 7 for the FA series (Ms=1.00) and mix 11 for the 50/50 series (Ms=1.00). These mixes were then used with the china clay waste, as described in the following chapters.

Chapter 5: **Effect of china clay waste as filler in AA mortars**

This chapter presents the investigation on the effect of the china clay waste (here CCS, unheated MW, calcined MW is used) in AA mortars. A new, control series using Portland cement was introduced in order to observe if indeed aspects listed in 2.6.2 are valid and could lead to better mechanical performance. A paper on this topic was published in the Journal "ICE *Construction Materials*" and this paper is included in the Annex.

Control mortars using standard sand were cast for all the Ms ratios for the three binder series to develop an understanding as to whether the trend for increasing Ms remains the same and what is the magnitude of strength decrease that would be expected when proceeding from binders to mortars. In addition, test samples using the small fractions of china clay waste were cast using the optimum binder as selected in the previous chapter. The samples containing calcined MW were part of the pozzolanic index investigation described in 3.3. It should be noted that the binders here have different W_t/B ratios than in the previous chapter as the control mortars (using SS) would not incorporate extra water after the addition of the aggregate. Table 22 outlines all the possible combinations considered between binders from the previous chapter, plus the newly introduced PC series, and the different fillers. Where "x" is the selected-to-be-mixed mortars. Therefore as shown in the table, 12 mixes contain either CCS or MW or calcined MW (CMW) and 18 mixes contain standard sand (SS) or ground standard sand (GSS) (details in 3.1.3). The detailed mortar composition is shown later, in Table 24. The names of the mortar mixes in Table 24 are according to Table 22, "sand / number of binder mix that the mortar was based-on". For example, SS/ Mix13 is mortar based on binder 13 of the 50/50 series (therefore has same GGBS+FA and activator content but higher water content as increased W_t/B was used) and SS as aggregate.

Table 22 Outline of the mixed mortars.

	Binders															
Mortars	GGBS series				FA series					50/50 series						PC series
(Sands used:)	**S1**	**S2**	**S3***	**S4**	**FA5**	**FA6**	**FA7***	**FA8**	**FA9**	**10**	**11***	**12**	**13**	**14**	**15**	**PC16**
Standard sand (SS)	x	x	x	x	x	x	x	x		x	x	x	x	x	x	x
China clay sand (CCS)			x				x				x					x
Mica waste (MW)			x				x				x					x
Calcined Mica Waste (CMW)			x(1)				x(1)				x(2)					x(1)
Ground St.sand (GSS)			x				x				x					x

* Peak strength from binder series

(1) Calcined MW at 950°C

(2) Calcined MW at 1100°C

5.1 Methodology

The control mortars (all the mixes using SS) follow the BS EN 196-1:2005 and use a 'binder to aggregate' ratio (B/A) equal to 1:3 as specified in the standard. However, all the other mortar mixes incorporate a 'volume factor', reducing the proportion of sand used. This is because the finer sands have lower bulk density and fill the regular prismatic mould with less material than what is indicated in mass (g) in the standard and it was desirable to have the same quantity of binder in each sample, rather than the same ratio of binder to sand. Table 23 shows the mix ratios including the 'volume factors' which would result in the same mass of binder for each mould if constant water to binder ratio was used, regardless of sample density. This allowed a more realistic comparison of strengths. GSS (described in 3.1.3) was used as 'control' for the fine sands. Interestingly, although GSS and MW have almost the same particle size distribution, their different particle shape (due to different mineralogy) leads to different density and, consequently, different mixing ratios. The same happens with CCS and SS.

The calcined MW was used as part of the pozzolanic index investigation. It was heated at 950°C for 3hours for use in the GGBS, FA and PC series and at 1100°C for 3hours for use in the 50/50series. These temperatures are over the metakaolin-present state and as used in sections 3.3.3 and 4.2 they gave comparable results. They were therefore chosen to observe if they have the same behaviour when used as filler and whether they lead to matrix of special features.

The starting W_t/B ratio in mortars was 0.47 for the GGBS series (while for binders in Chapter 4 it was 0.4), 0.43 for the 50/50 series (for binders it was about 0.36) and 0.24-0.29 for the FA series (similar to the fluid FA binder series). For more details see Table 16, Table 18, Table 20 and Table 23. The W_t/B was increased so that the control mortars (using SS) would have acceptable workability, required for the manufacturing process, plus they would not incorporate extra water after the addition of the aggregate. The SS control mortar specimens make minimum use of water, especially in the case of FA series. To achieve similar workability for mortars using the other sands, it was necessary to increase the water content, therefore these mixes have higher W_t/B ratio than 0.47 or 0.43 or 0.24-0.29. That is due to the greater apparent water absorption of the waste compared to SS and particle size and shape (therefore increased surface area) of the waste and GSS. Even the CCS that had the same particle size distribution as the SS needed extra water which shows the impact of particle shape and mineralogy in surface area and water absorption. Figure 72 shows a CCS/S3 and a MW/S3 samples for no addition of extra water, for using as much paste as in SS/S3 (based on the composition table). The picture shows that that amount of paste was not enough to cover the sand particles. The two samples look "sandy" and show only a number of green spots (mainly on the CCS/S3 sample) where apparently, locally, the moisture was enough to allow the activation of slag.

For the new W_t/B ratios of the binders, the initial setting time of mix S3 was 40 minutes and the final setting time was 50 minutes. For mix FA7 the initial setting time

was 105 minutes and the final setting time was approximately 120 minutes. The initial setting time for the Portland cement paste was 245 minutes and the final setting time is 285 minutes (without immersion of the sample in water as the reference method in BS EN 196-3:2005 indicates).

The principle of ensuring the mixes had the same binder content per unit volume and the same workability was driven by the target applications which are unreinforced concrete blocks and roof tiles. For these applications the majority of the embodied CO_2 and material costs come from the binder used and fixing the binder content per unit volume (or per brick / roof tile) enables easy and realistic comparison of performance. As concrete blocks have a very high proportion of voids (Bastos et al., 2005), typical volumetric based concrete mix design procedures may not be applicable. However, due to the addition of extra water in the mixes there is some variation in the binder content of the different mixes which is shown in the compositional table in the Annex A.4 (equivalent of Table 24 but with mixes expressed in kg/m^3). The volume was measured in the lab using a plastic, commercial volumetric cylinder of 139ml capacity. Varying the water content to achieve the desired workability has certain limitations, in particular for alkali-activated materials where adding water reduces the concentration of the activator. These aspects are included in the discussion on the results.

Table 23 Mixing ratios of mortars by weight. Where "binder"= [GGBS or FA +anhydrous activator] or [cement (PC)]. Where "total water"= added water in the binder+ extra water in the mortar+ water bound the activator (=W_t).

Ratios of binder : total water : sand			Series based on:		
			GGBS or PC	FA	50/50
aggregate type	medium-fine	MW	1 : 0.65 : 2.3	1 : 0.55 : 2.3	1 : 0.60: 2.3
		CMW	1 : 0.65 : 2.3	1 : 0.55 : 2.3	1 : 0.60: 2.3
		GSS	1 : 0.60 : 2.6	1 : 0.40 : 2.6	-
	medium-coarse	CCS	1 : 0.60 : 3	1 : 0.50 : 3	1 : 0.55: 3
		SS	1 : 0.47 : 3	1 : [0.24÷0.29] : 3	1 : 0.43 :3

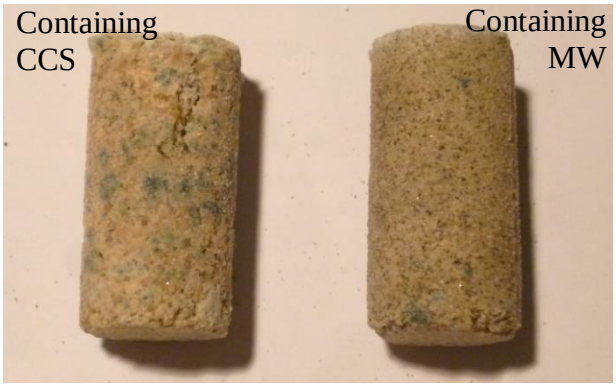

Figure 72 Texture of sand for trial mortars without enough water in the mix.

Table 24 Composition of mortars by weight (in g).

		Composition (in g)					
		First part of mixing (binder)				Second part (mortar)	
	Name of Mortar mix	GGBS (for the GGBS series) or FA (for the FA series) or GGBS+FA (for the 50/50) or Portland cement	W added	Na_2SiO_3 powder	NaOH pellets	Aggregate	Extra water
GGBS series	SS/ S1	100.0	48.5	4.1	5.0	321.5	-
	SS/ S2	100.0	49.1	9.1	3.3	329.7	-
	SS/ S3	100.0	49.4	11.3	2.5	333.1	-
	CCS/ S3	100.0	49.4	11.3	2.5	333.1	14.4
	MW / S3	100.0	49.4	11.3	2.5	255.4	20.0
	CMW (950°C)/ S3	100.0	49.4	11.3	2.5	255.4	20.0
	GSS/ S3	100.0	49.4	11.3	2.5	288.7	14.4
	SS / S4	100.0	49.7	13.6	1.7	336.8	-
FA series	SS / FA5	100.0	29.3	3.3	10.5	332.4	-
	SS / FA6	100.0	28.4	7.3	9.1	338.8	-
	SS / FA7	100.0	27.3	16.3	5.9	353.1	-
	CCS/ FA7	100.0	27.3	16.3	5.9	353.1	27.1
	M /FA7	100.0	27.3	16.3	5.9	270.7	33.0
	CMW (950°C)/ FA7	100.0	27.3	16.3	5.9	270.7	33.0
	GSS/ FA7	100.0	27.3	16.3	5.9	306.0	15.1
	SS / FA8	100.0	23.4	20.4	4.5	359.8	-
	SS / FA9	not mixed					
50/50 series	SS / Mix 10	100.0	44.5	6.8	4.1	326.0	-
	SS / Mix 11	100.0	44.5	9.1	3.3	329.7	-
	CCS/ Mix 11	100.0	44.5	9.1	3.3	326.7	13.0
	M / Mix 11	100.0	44.5	9.1	3.3	252.7	18.4
	CMW (1100°C)/ Mix 11	100.0	44.5	9.1	3.3	252.7	18.4
	SS / Mix 12	100.0	45.0	11.3	2.5	333.1	-
	SS / Mix 13	100.0	45.1	9.5	5.7	336.2	-
	SS / Mix 14	100.0	45.4	12.7	4.6	341.4	-
	SS / Mix 15	100.0	45.8	15.9	3.5	346.6	-
PC	SS / PC16	100.0	52.2	-	-	333.1	-
	CCS / PC16	100.0	52.2	-	-	333.1	14.4
	MW / PC16	100.0	52.2	-	-	255.4	20.0
	CMW(950°C)/ PC16	100.0	52.2	-	-	255.4	20.0
	GSS / PC16	100.0	52.2	-	-	288.7	14.4

Group of mortars based on common binder.

The mixing process was as following: Preparing the activator solutions separately and allowing to cool. When added together they were mixed for 30 seconds in the mixer and then the precursor was added. Mixing was first at slow speed and after 2 minutes at high speed, the binder was mixed for 5 minutes in total. Later, sand and any extra water was added (columns noted as "second part of mixing" on Table 24) before an additional 10 minutes of mixing. The same cylindrical moulds of 36mm height and 18mm diameter were used. The GGBS and 50/50 series were cured at room temperature and RH>90% and were demoulded on day 3. The FA series were cured at 80°C as they did not harden at room temperature as mentioned in the previous chapter.

For the Portland cement series mixing and curing were as specified in BS EN 196-1 but the moulds used were not the prismatic moulds specified but the cylindrical 36mm height and 18mm diameter moulds used for the other mixes. The binder: water: sand ratio was exactly the same as for the GGBS based series which is close to the standard mortar mix in EN 196-1 which has a binder : water : sand ratio of 1 : 0.5 : 3.

The full mix designs are presented in Table 24. The flow table test was conducted according to BS EN 1015-3 where relevant and it was used to ensure the workability of the different mixes were comparable. The alkali-activated series were tested in compression on days 7, 28, 90 and 180 while the Portland samples were tested only after 7 and 28 days curing. All test results are presented as the averages of three replicates. Samples of alkali-activated mortars after 6months of curing were taken for imaging in the SEM. There are images of fragments (not coated) and of polished samples (prepared as in Chapter 4). All were stored in desiccator before imaging and were tested in low vacuum.

5.2 GGBS series

5.2.1 Strength

Control specimens

Figure 73 shows the results of the mortar specimens using standard sand. The mortars show approximately half the strength of the equivalent binder (Chapter 4, Figure 52), with an increasing trend for increasing the Ms (while for the binders there was a peak in strength for Ms=1.25). For Ms=1.25 the strength is approximately 50MPa and rises to 70MPa after 90days of curing. Only one of the mortars reached just over 50MPa compressive strength on day 7 and there is a threshold at 80MPa for the 6-month strength. The decrease in strength after the 90^{th} day is not considered representative and this trend is not repeated later for the test specimens (Figure 74).

From the compositional table in Annex A.4 it is seen that SS/S1-SS/S3 had decreasing content of GGBS but the same Binder content (calculated as indicated in 4.1.1). SS/S4 has slightly higher Binder content. By Figure 73 it is shown that the performance of SS/S1-SS/S4 is different than the trend of the GGBS content, therefore not affected by

that. The results in Figure 73 are considered representative for mortars which have approximately the same Binder content.

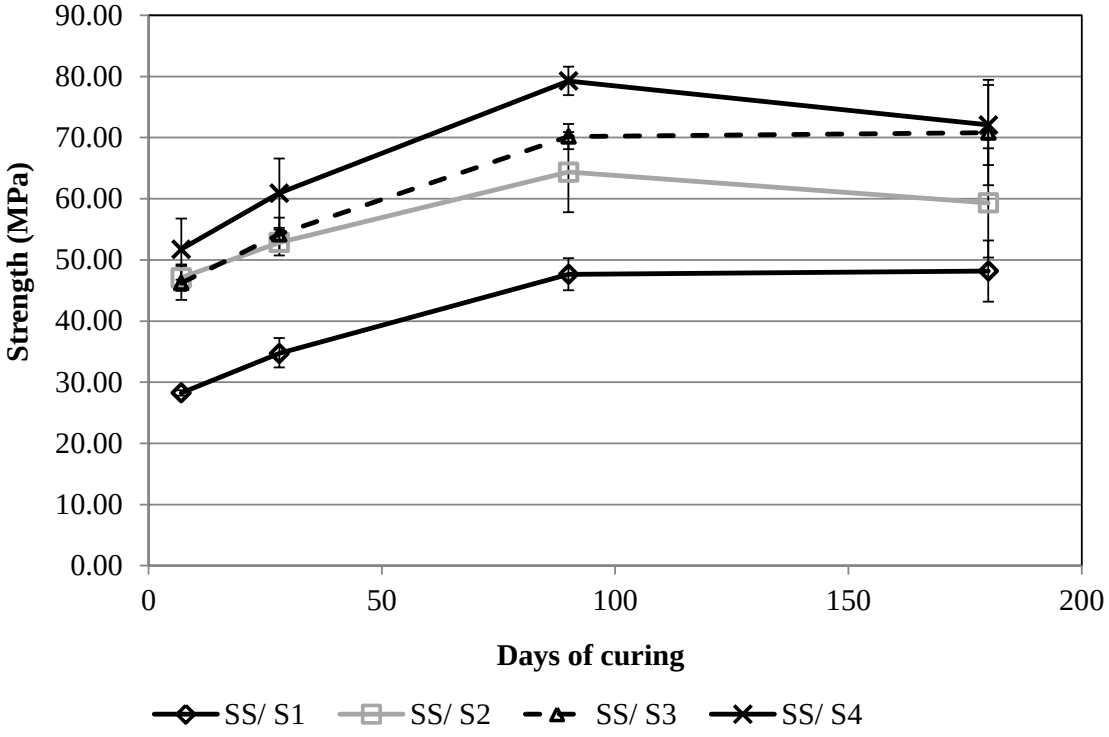

Figure 73 Strength development for mortars of the GGBS series using SS.

Effect of sand type

To facilitate comparison, the control mix SS/S3 is included in the graphs of this section too. For 'water to binder' ratio of 0.47 the control mix 3 has flow of 134mm in the flow table test which is between the limits of 120mm and 175mm in BS EN 1015-2. For an 'overall water to binder' ratio of 0.60, the mixes containing CCS and GSS had approximately the same flow (±10mm). The mix using MW had similar flow values of about 114mm.

The results of the compression tests of the GGBS series are presented in Figure 74. As expected all samples gain strength over time. As mentioned in Chapter 3, the CMW used was treated at 950°C for 3h. At 7 days all samples which had a higher water content to achieve a similar workability as the SS samples had low strength compared to the SS samples. The impact of high water content decays over time as geopolymerisation continues. As a consequence, the difference in strength between the CCS mortar and the SS control mortar decreased from the initial 29.6% on day 7 to 5.2% difference by 6 months. Generally medium-coarse aggregates produce mortars of higher strength than fine-medium aggregates as they have a lower surface area per unit volume. The CMW shows lower strength than MW at all ages indicating the calcination does not result in a strength increase through additional reactions with the activators.

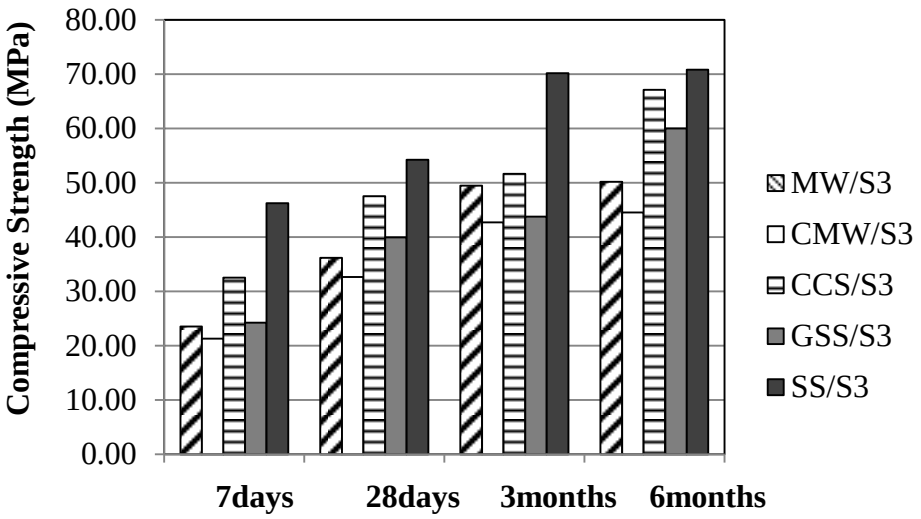

Figure 74 Strength development of mortars based on the same binder (S3) for the different types of aggregate.

From the compositional table in Annex A.4 it is seen that SS/S3, MW/S3 and GSS/S3 have approximately 500kg/m^3 Binder content and about 450kg/m^3 while CCS/S3 has lower Binder and GGBS content (470kg/m^3 and 424kg/m^3 respectively). Again it is noted that the mortars strength is not according to the Binder content, otherwise SS/S3, MW/S3 and GSS/S3 would have equal strength and CCS/S3 lower strength. Therefore the lower performance of the mortars containing MW and GSS compared to SS/S3 was due to the increased water content and was not affected by the Binder content. It is worth noting the case of CCS/S3 which reached the 6-month strength of the control mortar for lower binder content.

5.2.2 Imaging and Chemical identification of components

Images were taken using an optical microscope (Figure 75) to show difference in appearance between the MW and CMW samples. It is not clear in the pictures that the colour of the matrix is in the shades of green. The CM sample compared to the MW fragment contains orange-brown aggregate particles, probably due to the oxidation of Fe-bearing particles during calcination (Bouzidi et al., 2014).

Figure 76 shows BEC images of the SS, MW, CMW and CCS samples. The binder matrices in all geopolymer samples have common characteristics: highly amorphous, with a number of undissolved particles of slag and microfissures. The SS sample (Figure 76,a) has thicker and more distinct microfissures than the samples with higher water content, MW and CCS (Figure 76,b and c). The more rough particle surface for the CCS compared with the SS (Figure 76, c and a) provides an explanation why a higher water content was required with the CCS to achieve a similar workability to the SS. Figure 76,d belongs to the CCS mix and shows in high magnification the vitreous nature of the matrix while the different intensity of grey indicates the progressive dissolution of slag particles. Mica mineral particles could be detected during the SEM analysis. Comparing fractions

with polished sections is not possible therefore, the images in Figure 76 cannot be compared to the microstructure of the binders seen in section 4.3.7.

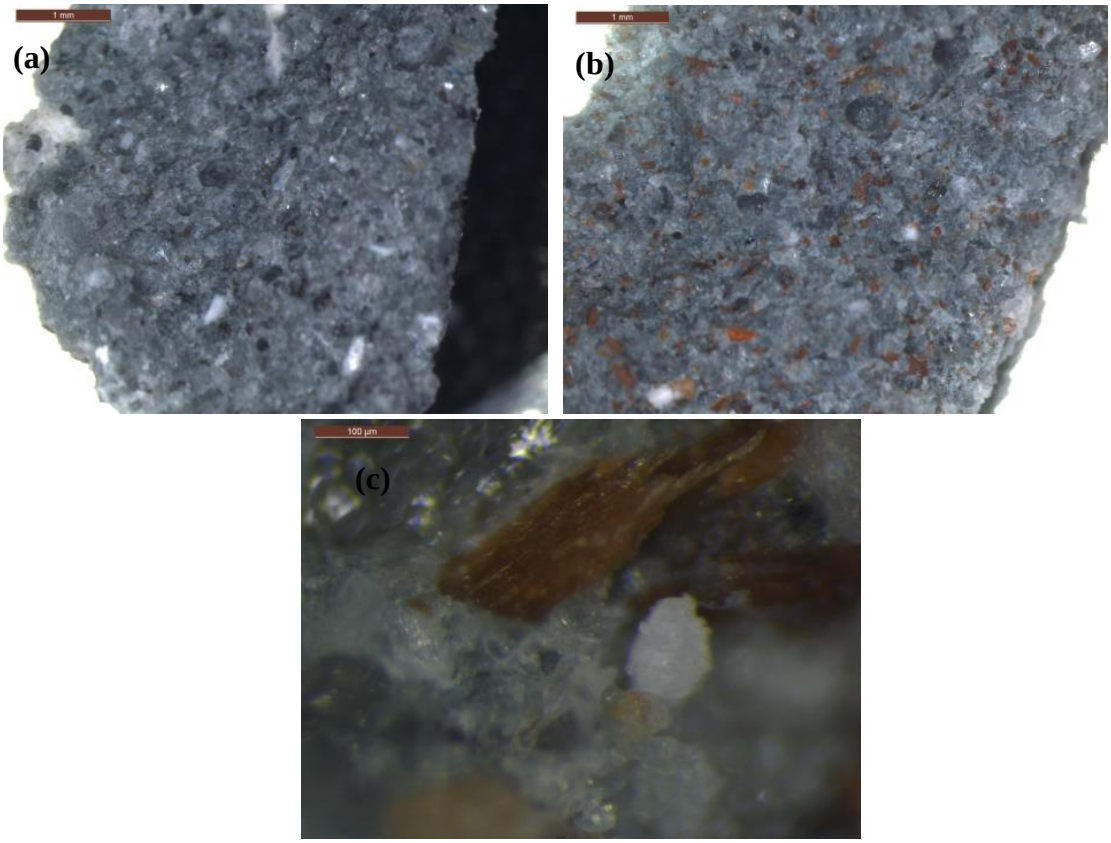

Figure 75 Pictures of fragments using an optical microscope. a) MW, b) and c) CMW

Figure 77 shows in low magnification the MW and CMW polished samples and Figure 78 shows all mortars and points of interest which were analysed in EDX. The point analysis focuses on the matrix near the mica particles, both next to the basal surfaces and edges, comparing to other areas of the matrix and comparing the mortars between them as different elemental composition would indicate possible dissolution of the mica mineral.

The SEM and EDX analysis showed that in the calcined state, the mica particle is delaminated. That can be seen in Figure 78,d where the mica particle has its layers separated and slightly bent. In Figure 77 the detected mica mineral particles (highlighted in yellow) are often partially fractured and thinner due to the delamination and therefore harder to detect than in the MW sample. It is noted that the magnification in Figure 77 is set to observe the aggregates and the general layout of the mortars, therefore microstructure of the matrix cannot be seen. The mica particles were detected based on its features (elongated shape, layers. See Table 7) and confirmed by EDX. Delamination of mica particles is likely to lead to increased water absorption as the total surface area of the aggregate is increased. This is confirmed by the manufacture of the CMW mortar which appeared drier.

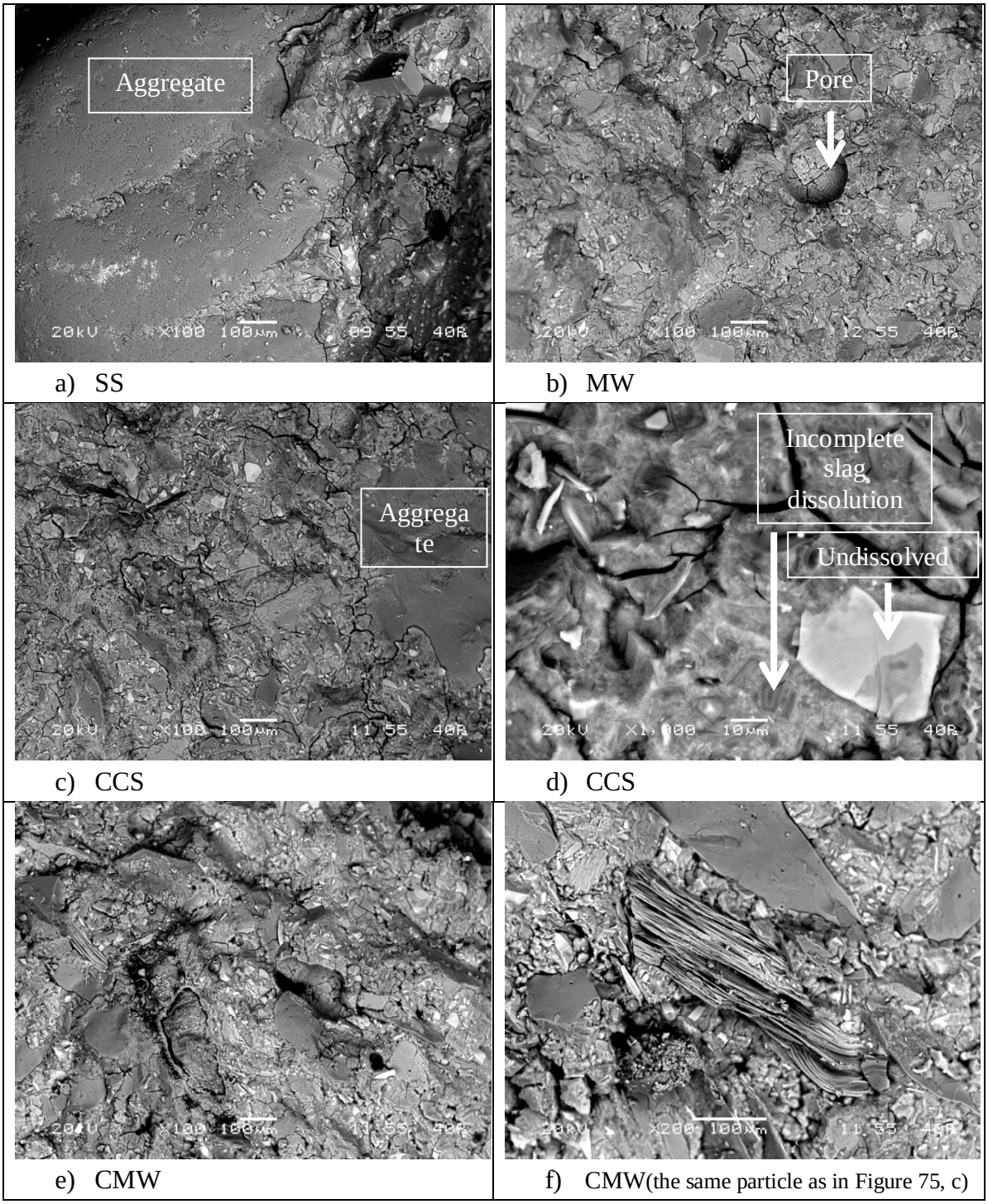

a) SS b) MW

c) CCS d) CCS

e) CMW f) CMW(the same particle as in Figure 75, c)

Figure 76 Backscattered electron composition (BEC) Images from fragments after six months curing.

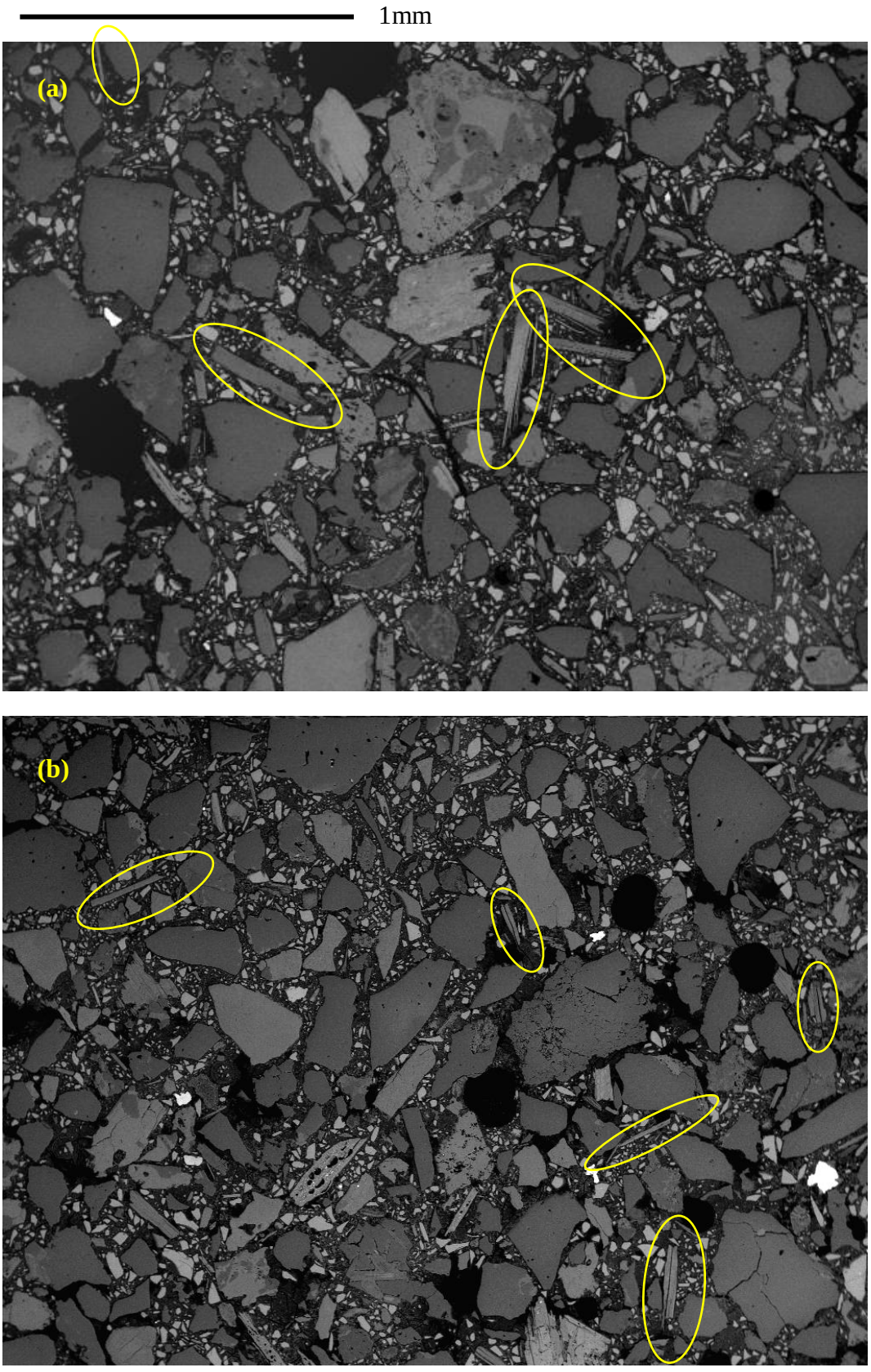

Figure 77 BEC for polished samples a) MW, b) CMW. Mica particles are pointed.

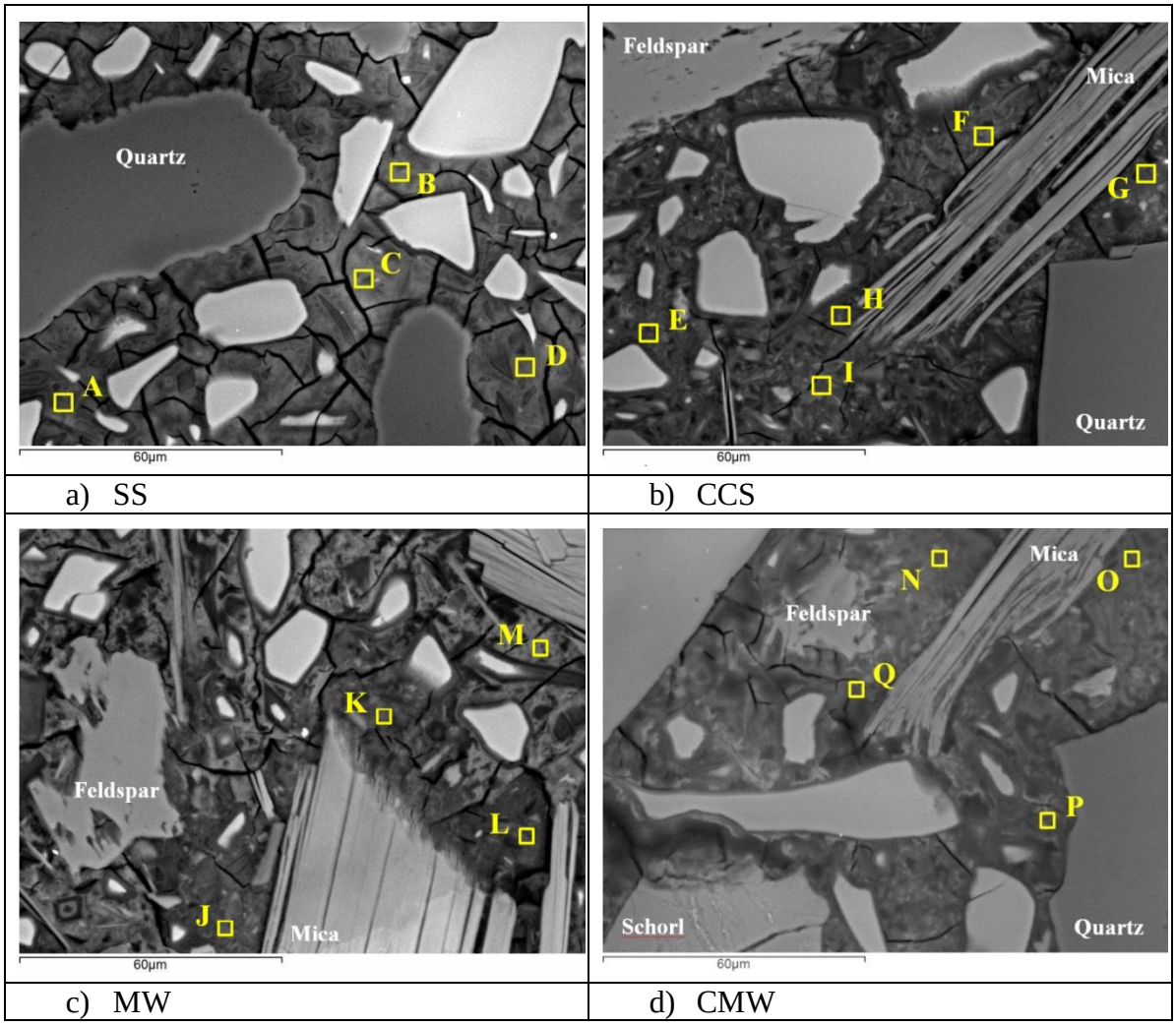

Figure 78 EDX in polished samples.

The elemental analysis conducted was based on high resolution maps. Figure 79 presents the Al/Si vs Ca/Si of different points of the binder, indicated on Figure 78. Every point is an average of a square of 16x16 point spectra (where one point represents one pixel). Features of objects which intersect with the polished surface can be seen, however what underlies the polished surface but is still in the interaction volume of the microanalysis probe, cannot be seen. The exact value in μm^3 depends on the density of the material where the beam falls. Increasing the surface for data collection was necessary in order to increase the strength of the signal and reliability of the outcome EDS pattern. However, this induces variation in the values and a degree of uncertainty.

Considering the work of Zhang and Bailey (1998b), Oelkers et al. (2008) and Kuwahara (2008) (section 2.5.2) Figure 78,b-d could possibly indicate reactivity at the edges of the muscovite sheets. However, the elemental analysis did not confirm this. As it can be seen in Figure 79, the CCS and MW samples showed higher variation in the Ca/Si and/or Al/Si atomic ratios than the SS and CMW samples. In average, the Al/Si ratio for the SS and CMW samples is 0.25, while the CCS and MW samples have higher average ratio of about 0.30-0.34. Compared to the Al/Si of the S3 binder (section 4.3.7) these

values are slightly lower. The Ca/Si ratio of all mortars is between 0.35-0.65 while the Ca/Si ratio of the S3 binder was 0.36-0.49. It is noted that since the mortars have higher water content it is not expected to find the same values as with the S3 binder.

The most important outcome from the EDX analysis is that, the samples which showed the greatest consistency, the CMW and SS, have in average the same values of Ca/Si and Al/Si. Therefore, there is no indication for dissolution of the mica particles from the CMW, as there would be some contribution to Al. This observation is confirmed by the fact that the elemental analysis showed for the H, I, K, L points (edges of mica particles) and F, G, J, Q, O (points close to the basal planes) not apparent differences.

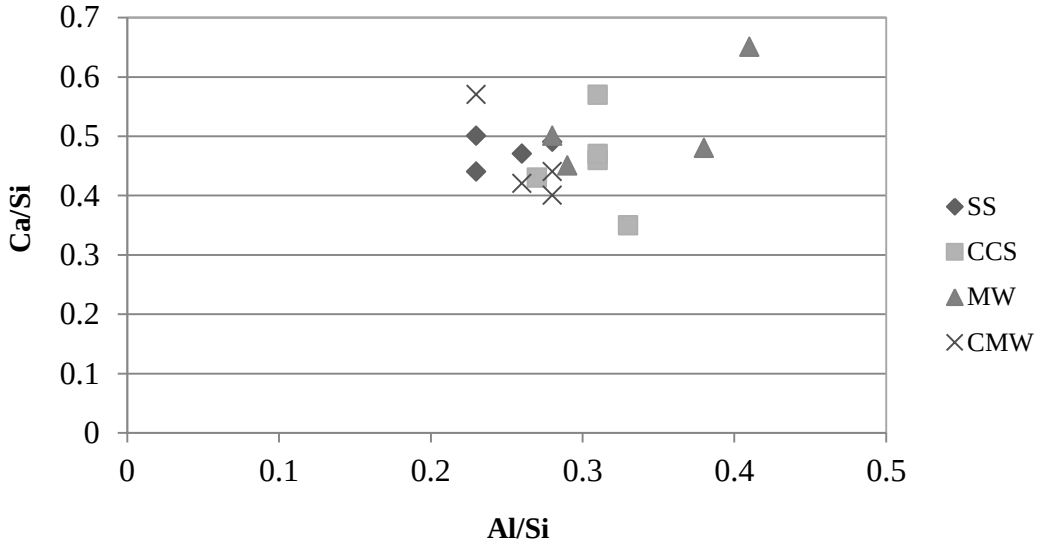

Figure 79 Atomic ratios Ca/Si vs Al/Si for points A-Q as shown in Figure 78, which correspond to SS, CCS, MW and CMW mortars.

5.3 FA series

5.3.1 Strength

Control specimens

Figure 80 shows the results of the mortar specimens using standard sand. Although the mixes were based on the workable paste (W_t/B=0.27, mixes 5 and 8 contain +2 and -4g of W for each 100g of precursor) in the flow table test they did not deform sufficiently to make the test valid (flow value of 103mm). Their texture could be described as 'dry/sticky' in the sense that the mixes do not feel completely dry (texture of sand) but viscous, retaining their shape in the flow table test.

While the FA binders had strength in the range of 30-70MPa (Figure 61), the mortars are in the range of 20-50MPa with the strength increasing for increasing Ms. Contrary to

expectations, in most of the cases the strength only slightly increases or even drops over time. That issue was later attributed to the prolonged oven curing in dry conditions.

Based on the compositional table in the Annex A.4, SS/FA5-SS/FA8 have decreasing content of GGBS per cubic meter and varying Binder content. However their performance is steadily increasing for increasing Ms, independently of the Binder content.

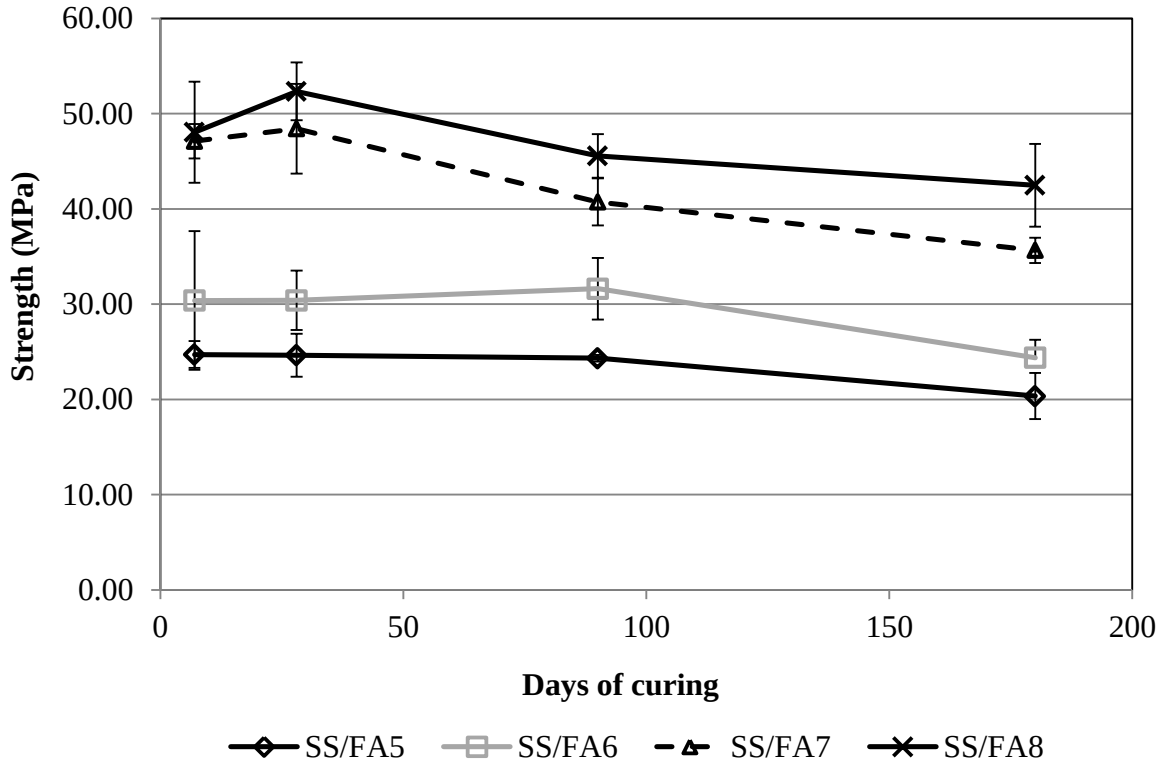

Figure 80 Strength development for mortars of the FA series using SS.

Effect of sand type

The FA series visually appeared very dry/sticky in spite of having relatively high water content. All these mixes were too dry/sticky to accurately test using the flow table and this demonstrates the problem of transferring standard tests and mix designs developed for PC binders to alternate binders.

The results of FA mortars were disappointing: the mortars did not typically gain strength over time and all apart from the SS control mortar showed extremely low strength. Due to the poor performance testing with all other than the SS stopped after 28 days. To understand why the test mortars (higher water / binder ratio than SS) achieved such low strengths, the SS control mortar was repeated with an increased water content, so that the binder : water : sand ratio was 1 : 0.55 : 3 (not included in the figures above). This produced a mix which was too fluid and this resulted in segregation of the sand and binder, a trend not noted with the finer sands. The specimens were tested after 7 days and the strength was 9.66 MPa which indicates it is most likely the extra water required to

obtain the desired workability which reduced the strength of the mortar as it may have reduced the concentration of the activator to a point where precursor dissolution was limited. Therefore, without use of a water reducing admixture, use of a significantly higher B:A ratio or increased activator content, it is unlikely that the strength of the alkali-activated FA mortar using the china clay waste will improve. Increasing the activator content or B:A ratio will result in an increase in cost and environmental impact which would defeat the aim of the research. As a result, the research into to the FA mortars was not taken further but an investigation of the reason for the poor performance was carried out using microscopy.

Some contribution to the detrimental decrease of strength may be attributed to the lower Binder content of MW/FA7 and CCS/FA7 (Annex A.4) compared to GSS/FA7. However the extent of the decrease in strength is such that would not be justified only by the binder content.

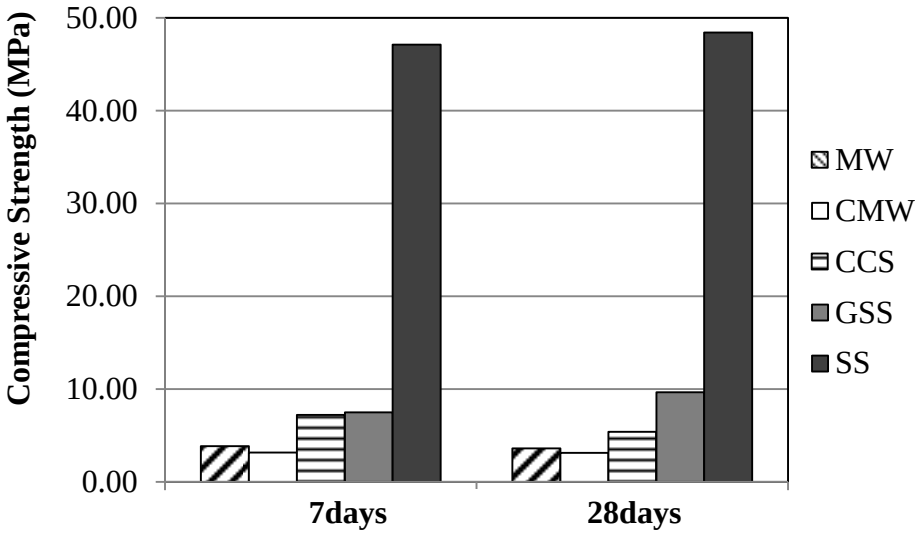

Figure 81 Strength development of mortars based on the same binder (FA7) for the different types of aggregate.

5.3.2 Imaging

Under an optical microscope (Figure 82), it is obvious that the matrix of CCM is porous and looks poor compared to SS. Figure 83 shows BEC images of the MW and SS samples. The topography of the MW sample is not glassy, is inhomogeneous and the aggregate can easily be detected behind the loosely structured fly ash particles which shows limited dissolution when used with the MW sand. The binder with the SS sand is largely amorphous and dense indicating dissolution and formation of a geopolymeric structure. The completely different nature of the binders is shown even more intensively in high magnification (Figure 83, c and d). The lack of dissolution may be because the increased water required for the M samples resulted in a lower concentration activator which limited dissolution, indicating the difficulty of extrapolating binder results to

mortars for alkali-activated geopolymers. This justified the initial decision to limit future research into using FA only as a precursor.

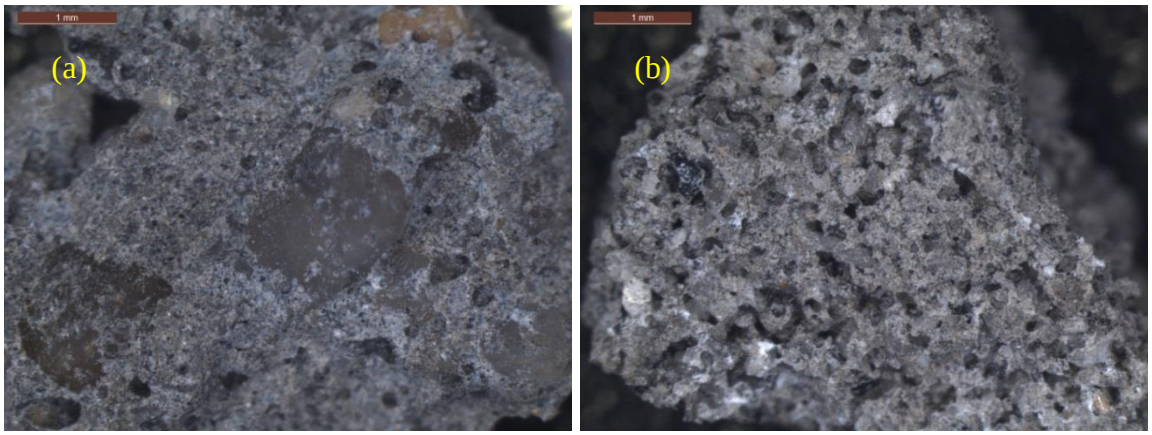

Figure 82 Pictures of fragments using an optical microscope. a) SS and b) CCM mixes.

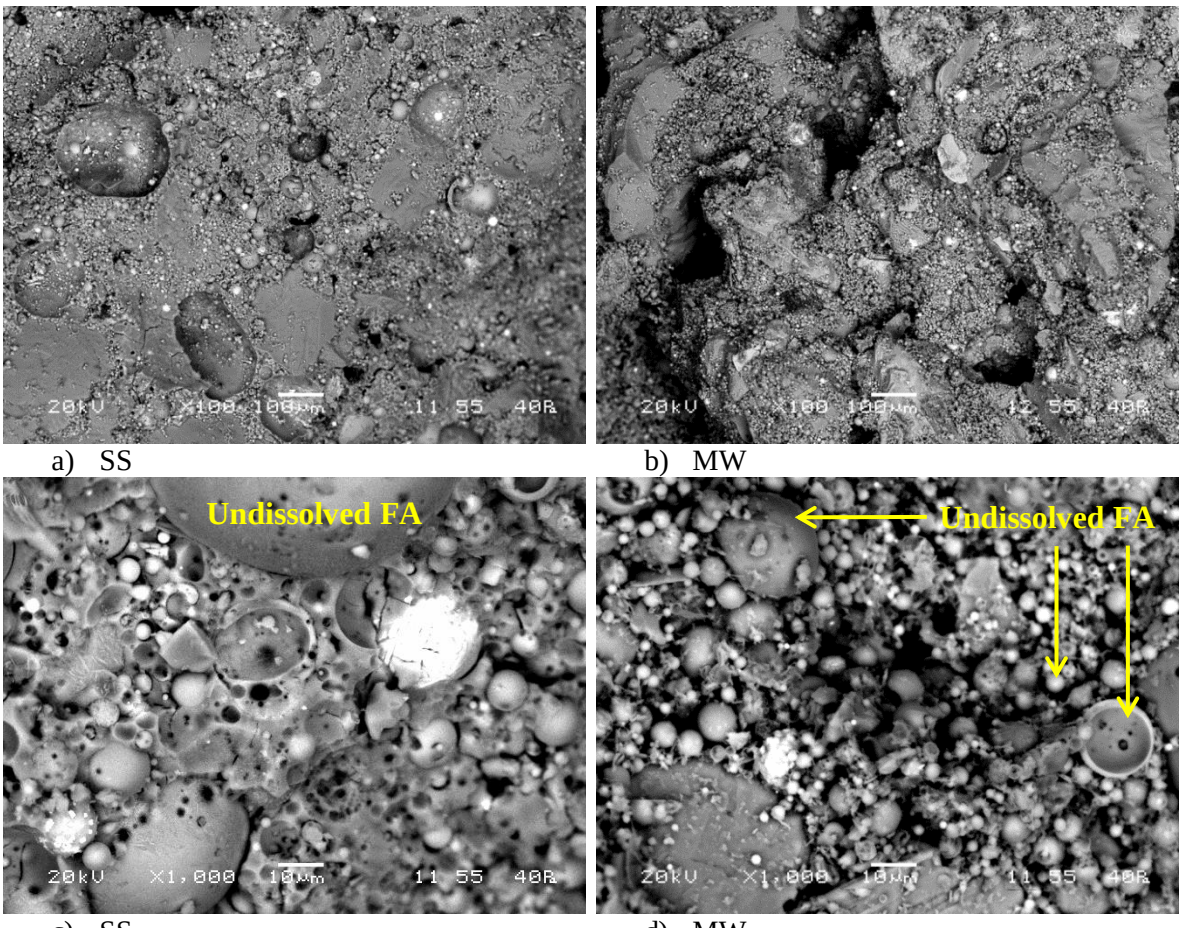

a) SS b) MW

c) SS d) MW

Figure 83 Fragments of mortars from the FA series

5.4 50/50 GGBS/FA series

5.4.1 Strength

Control specimens

Figure 84 shows the results of the mortar specimens using standard sand. The strength is increasing over time. As in the binders of the 50/50 series, the mortars show no significant difference till the 28th day for increasing the alkalinity (mixes 10-12 and 13-15) but after 3months of curing the mixes of the highest alkalinity (mixes 13-15) reach higher strength. In addition, increasing the Ms from 0.75 to 1.25 has positive impact on strength. Based on the compositional table in Annex A.4, all the control mortars have approximately the same binder content (507kg/m^3) therefore the results in Figure 84 are fully representative of the tailored mixes.

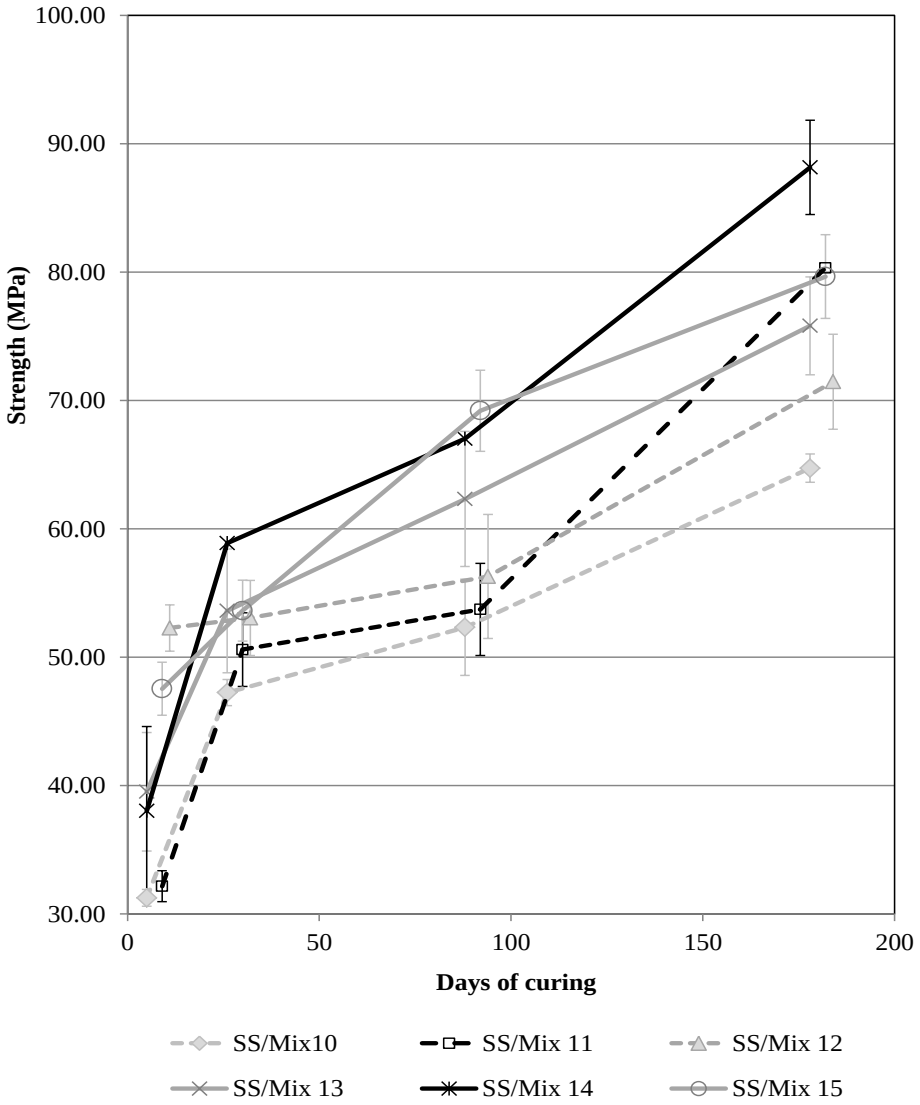

Figure 84 Strength development for mortars of the 50/50 series using SS. All the values correspond to 7, 28, 90 and 180 days of curing although they are slightly moved to have more clarity with the error bars.

Effect of sand type

In addition to the MW, SS and CCS used for the other series, the CMW used was heated at 1100°C for 3h. At that temperature some minerals sintered and a ball mill had to be used to ensure there were no lumps of minerals. After the ball mill a sieve of 1mm nominal size was used and only material passing the sieve was used for the mixes. For a 'water to binder' ratio of 0.43, the SS mix had flow of 186mm in the flow table test. For an 'overall water to binder' ratio of 0.55 the CCS mix had 138mm flow and for a ratio of 0.60, the MW mix had 116mm while the CMW had 105mm flow. The differences in strength did not follow the trend for the varying binder content (Annex A.4).

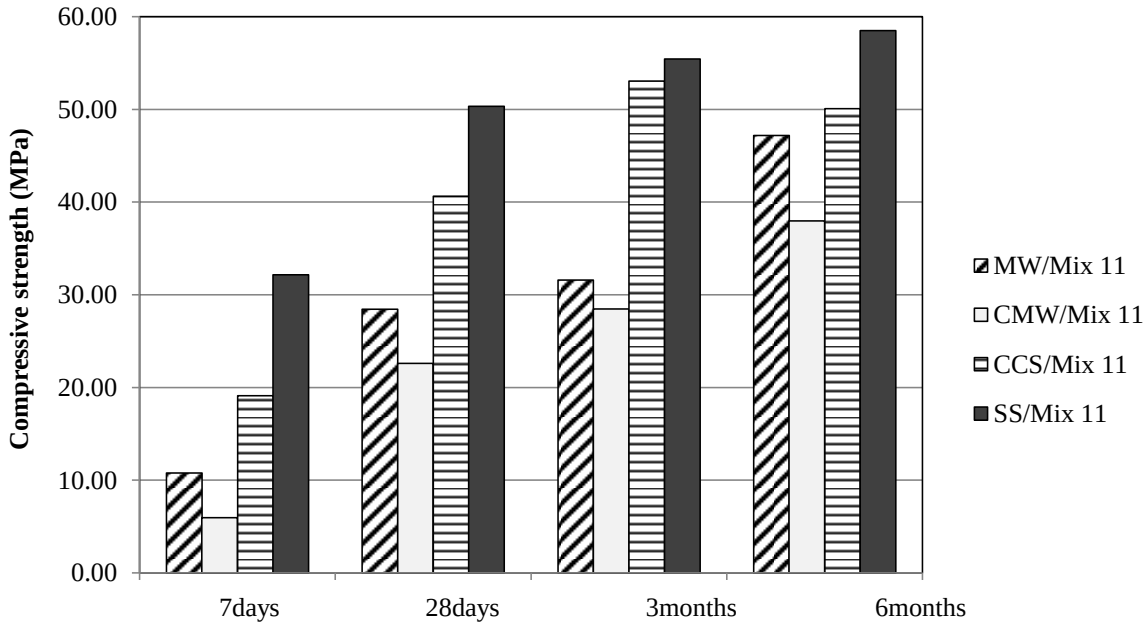

Figure 85 Strength development of mortars based on the same binder (Mix 11) for the different types of aggregate.

5.4.2 Imaging and Chemical identification of components

Figure 86 is backscattered images of polished sections. In yellow are particles that are suspected to be mica (confirmed with EDX). Mica particles could not be easily detected in the CMW sample which is in accordance to the findings of the XRD for calcined mica concentrate at 1100°C. This indicates there is no muscovite at this temperature and it has been transformed into other phases. In low magnification, Figure 87 shows that the MW and CMW are not very dense. The gaps are not air bubbles or water filled pores as they do not have round shape and may be due to damaging during the preparation of the samples for SEM. The samples were not coated and were tested directly in low vacuum. The settings used are: BEC, 20kV, work distance 10, spot size 53, 20Pa. For the

elemental analysis, copper was used for calibration. The point analysis is based again on chemical maps.

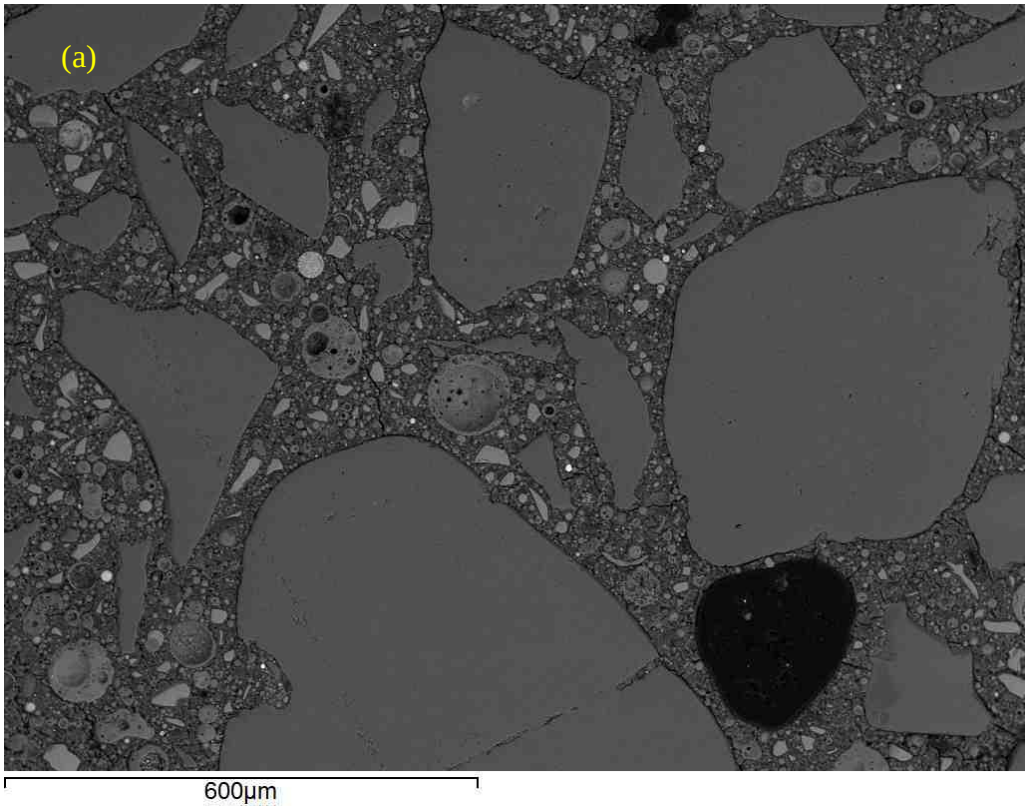

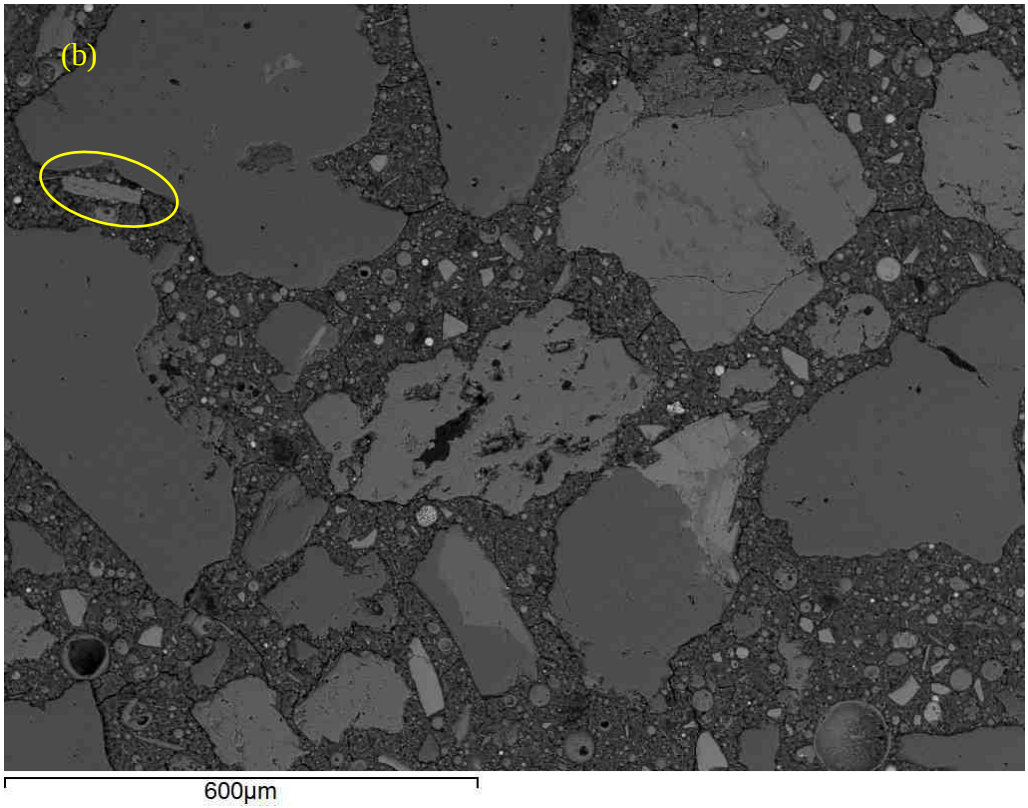

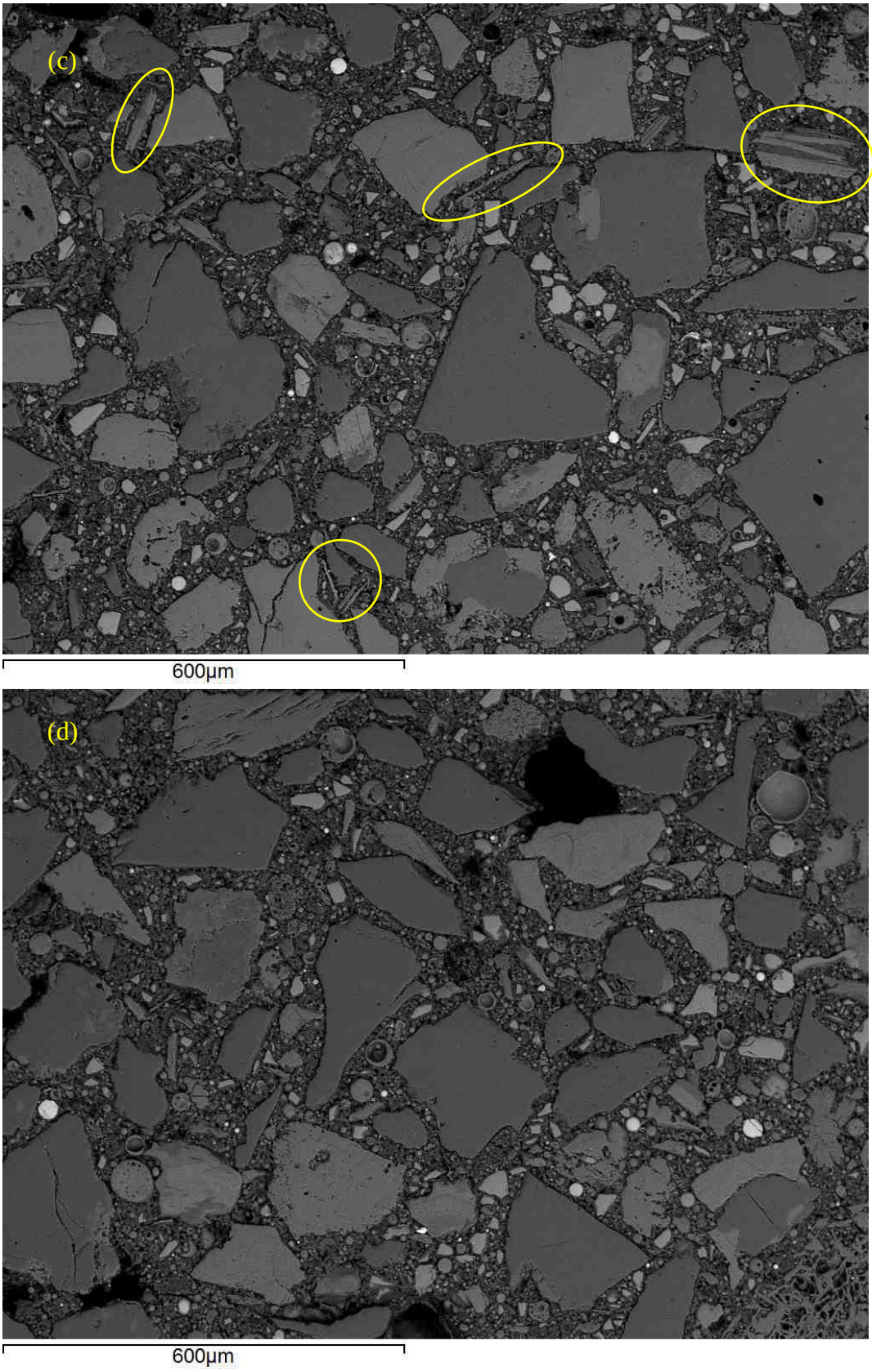

Figure 86 Polished sections of the 50/50 series mortars. a) SS, b) CCS, c) MW, d) CM.

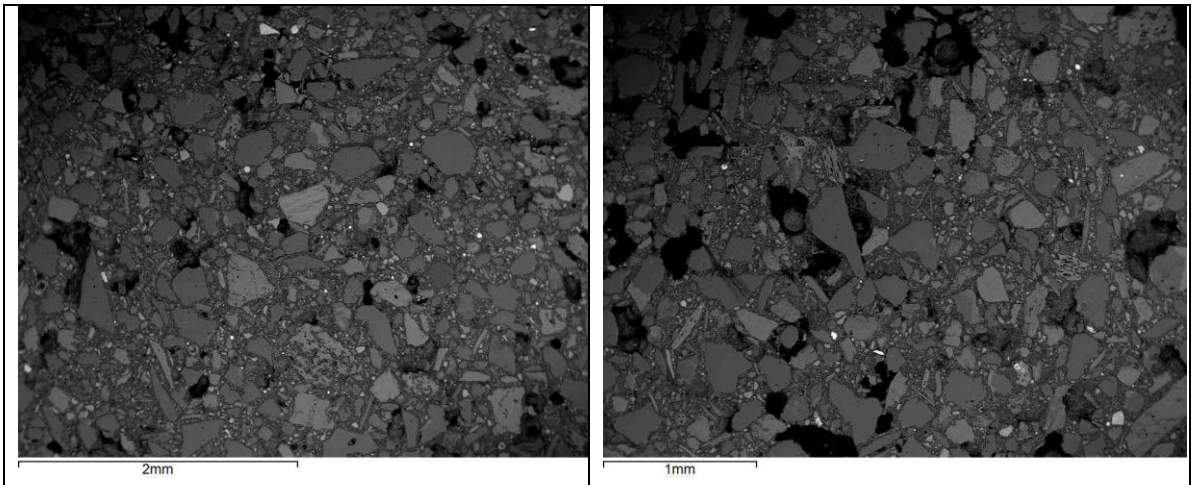

MW | CMW

Figure 87 Particle packing and porosity in MW and CMW mortars.

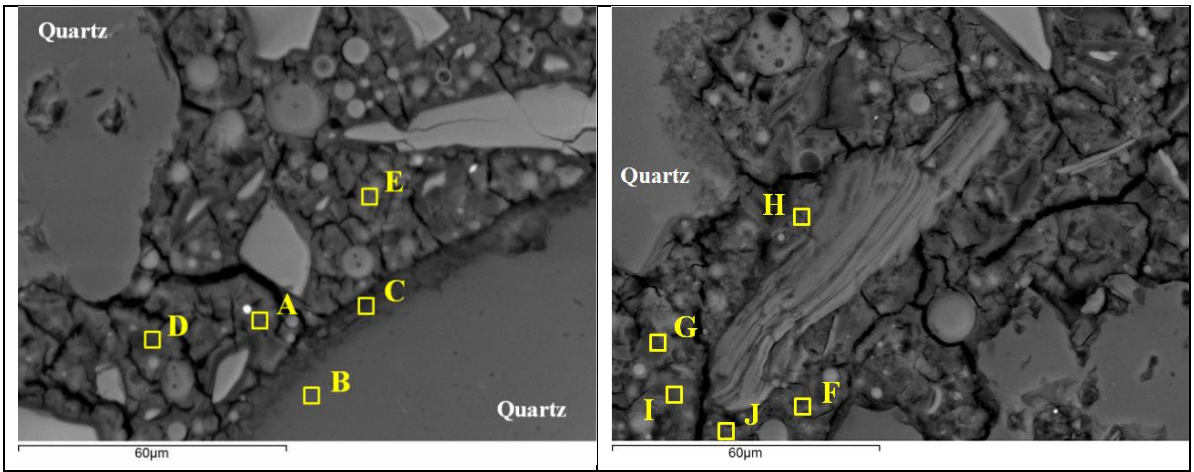

a) SS

b) CCS

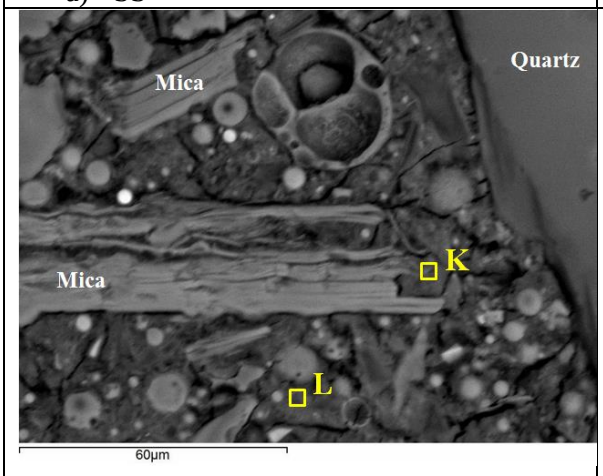

c) MW

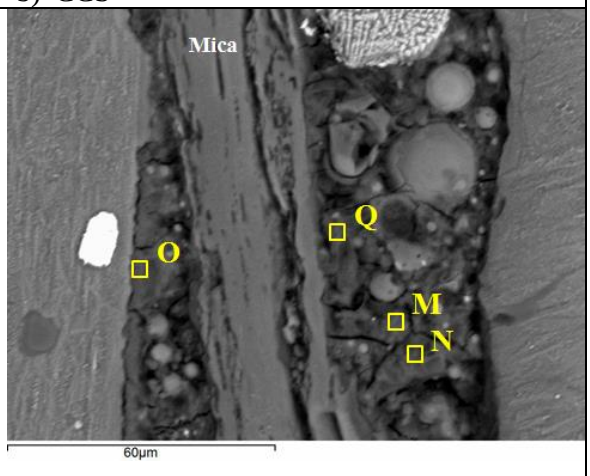

d) CMW, remaining mica particle, half altered.

Figure 88 Areas for EDX analysis in the 50/50 series.

Based on the EDX analysis, the mortar using SS shows there is good adhesion between aggregate-matrix with point C being part of the matrix (although it has zero Ca, Al/Si=0.10 therefore lower than the average Al/Si of the matrix but higher than the Al/Si=0.01 of point B which belongs to quartz – in reality there is no Al in quartz but the EDX showed traces). The fact that the adjacent crack (which is due to sample preparation) did not occur at the interfacial zone demonstrates the good adhesion.

Excluding points B and C, the values of the mortars are different from the values of binder 11(Table 21) with Ca/Si significantly lower and Al/Ca ratio higher even for the SS sample. Please note that quartz (therefore SS) has no Al to contribute to the dissolution. That leads to the conclusion that the dissolution in the mortars was probably different from the reaction degree in binder 11. The mortars between them have the same Ca/Si atomic ratios (0.17-0.26) and similar Al/Ca and Si/Al ratios. There is no obvious difference in the elemental analysis between MW and CMW samples, therefore no indication that the CMW contributes extra to geopolymerisation.

Table 25 EDX on the 50/50 series mortars (see Figure 88).

		Ca/Si	Al/Ca	Al/Si
SS	A	0.21	1.80	0.37
	B			0.01
	C	0.04	2.59	0.10
	D	0.22	1.93	0.43
	E	0.23	1.40	0.33
CCS	F	0.19	2.25	0.42
	G	0.17	1.68	0.28
	H	0.20	2.59	0.51
	I	0.26	2.20	0.57
	J	0.20	2.27	0.45
MW	K	0.16	2.47	0.40
	L	0.20	2.68	0.53
CMW	M	0.19	2.52	0.47
	N	0.23	2.04	0.47
	O	0.21	2.54	0.53
	Q	0.24	1.97	0.47

Also, comparing points next to the basal surface of mica mineral particles (points Q,H) and points next to the edge of these particles (points K,J,I) there is again no obvious difference. Other authors have proved different reactivity of the basal surface and edges of muscovite but if there is dissolution of mica here, this is minimal to the extent which cannot be detected by the EDX.

5.5 PC series

Figure 89 shows the mixes with Portland cement mortar. For the specific Portland based cement used, the values of strength are of the order of 20-30 MPa. Although all mixes increased in strength over time, as expected with PC based mixes, the ratio of strength between the mixes does not vary significantly on day 7 and 28. CCS performs as well as the control mortars and MW has less than 8% difference to the strongest mixes, GSS and SS, on day 28.

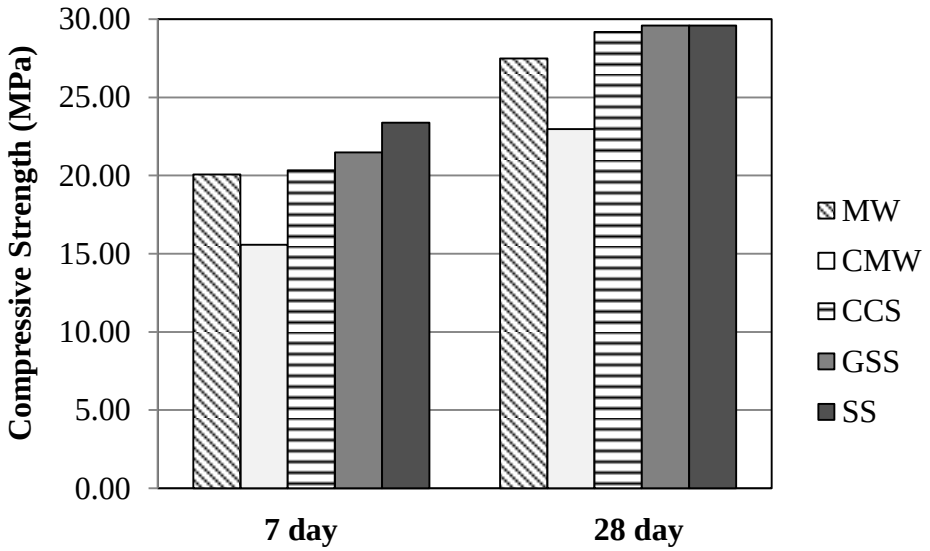

Figure 89 Strength development of mortars based on the same PC binder for the different types of aggregate.

5.6 Discussion

Through the materials used, it is not possible to effectively distinguish the effect of micas and kaolin on the strength of the mixes. Previous work by Fernandes et al. (2007) has shown replacing silica sand by up to 20% kaolin has limited effect on the compressive strength of PC based mixes. As this 20% kaolin content is much higher than that of the materials used for this research (approximately 4-8% as shown in Table 9) and as micas have been shown to affect PC based concrete mixes at much lower contents (Fookes and Revie, 1982), this discussion has focussed on the effect of mica rather than kaolin on the compressive strength of the material.

As the FA based alkali-activated binders performed so poorly and because this was demonstrated to be related to the water:binder ratio, rather than the aggregate type, these mortars are excluded from this discussion. The discussion is therefore focussed on the PC, alkali-activated slag (AAS) binders 50/50 GGBS/FA based binders. For the mixes of different water content but of adjusted aggregate content (incorporating the ‘volume factors’), Portland cement binders resulted in mortars of similar strength while the alkali-

activated based mortars showed greater diversity, justifying the initial assumptions that behaviour would be different.

Data on the effect of mica content on the compressive strength of PC based cements were obtained from Fookes and Revie (1982) (section 2.7.4) and the data on the effect of water:binder ratio on the compressive strength of both PC and AAS concretes was obtained from Yang et al. (2012a). The work by Fookes and Revie represents mixes with different mica contents which have similar workability and different water:binder ratios as used for this study, but a limitation of the previous study by Fookes and Revie is that the binder content per unit volume was different as the different volume factors were not accounted for. The work by Yang was based on concrete mixes with the same volume of water per unit volume concrete, so as the water: binder ratio increased, the binder content per unit volume of concrete also decreased. This work was also focussed on calcium hydroxide / sodium silicate based AASs rather than the sodium hydroxide / sodium silicate based ASSs used here.

Figure 90 and 91 show the data for this study along with that from Fookes and Revie and Yang et al. The data are shown as a percentage reduction in compressive strength from a reference case with no mica for each mix design. The data shown for Yang et al. does not include mica content but rather represents the reduction in compressive strength as the water:binder ratio increases from the baseline case with no mica (GSS and SS for the medium-fine and medium-coarse gradings), to the case with 9% mica (CCS and MW respectively).

As shown in Figure 90 for the medium-fine sand, the strength reduction with increased mica content or water:binder ratio for both the AAS and PC mortars is considerably lower than that indicated by the work of Fookes and Revie or Yang et al. This is most likely because the authors of both these previous studies varied the binder content per unit volume by not accounting for volume factors or by fixing the volume of water (rather than the volume of binder) in the mixes. As the mica flakes have a higher bulking factor than the more cubic quartz used for the ground standard sand, not accounting for bulking would result in a decreased binder content per unit volume as the mica content was increased which would lead to a reduction in strength. This demonstrates the importance of considering bulking when investigating different aggregates and of maintaining the same binder content per unit volume when considering the water:binder ratio. This is a particularly important consideration when attempting to manufacture low-impact PC or AAS concretes where the binder provides the greatest contribution to impact.(Habert et al., 2011)

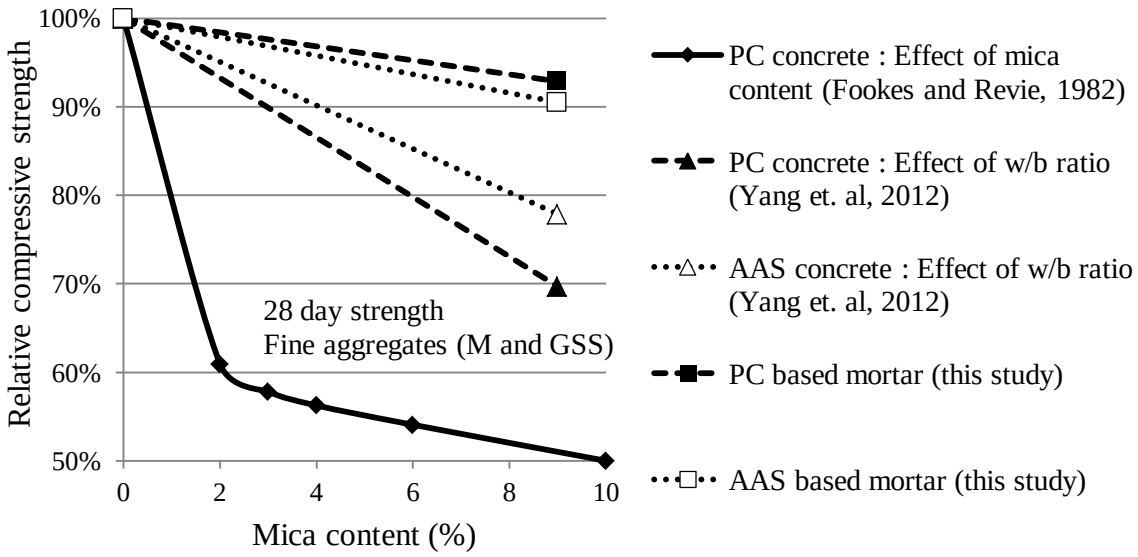

Figure 90 Reduction of strength for increasing content of mica mineral for fine materials.

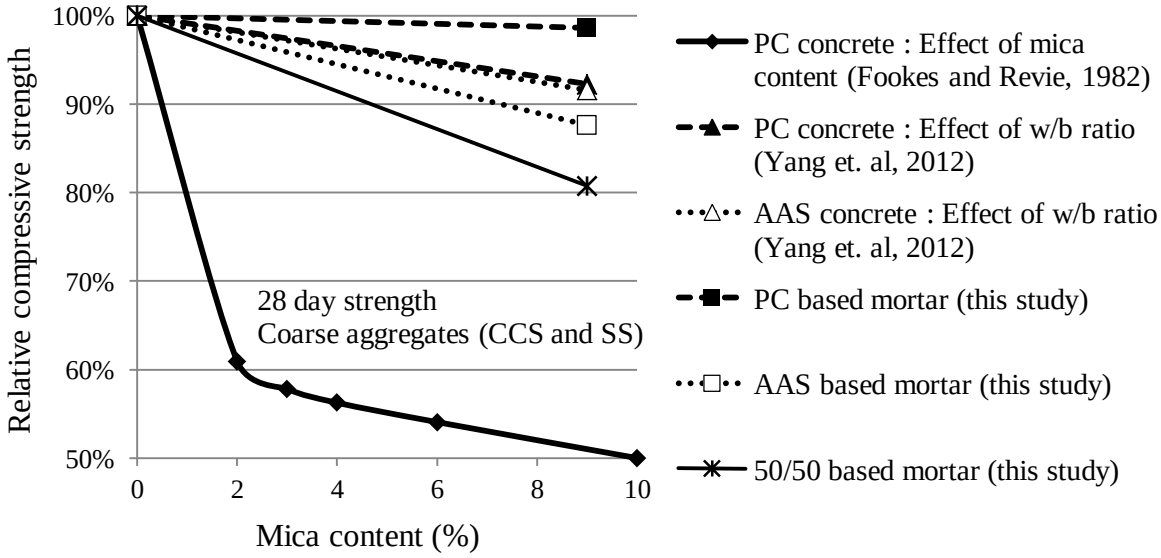

Figure 91 Reduction of strength for increasing content of mica mineral for coarse materials.

As shown in Figure 91 for the medium-coarse sand, the strength reduction with increased mica content or water:binder ratio for both the AAS and PC mortars is again much lower than that predicted by Fookes and Revie (1982) and is generally close or lower than the strength reduction which can be attributed to the increase in water:binder ratio (Yang et al., 2012a).

5.7 Conclusions of chapter

The CMW calcined at both 950°C and 1100°C gave lower strength that the MW specimens. The high water demand of the china clay waste has a negative impact on strength for Portland cement and geopolymer binders, but this effect varies depending on the specific mix design. Some variation in the binder content was not significant.

The china clay waste performed poorly with FA based geopolymer binders and this was largely attributed to the high water content required for mixing. It is unlikely that these mixes could be used unless an effective plasticizer is incorporated in the mixture or/and the mix is redesigned for higher alkalinity or higher ratio of B:A, but this will increase environmental impacts and costs.

The use of fine china clay waste in slag based alkali-activated cement is possible and there is potential for optimisation. The samples incorporating china clay waste initially develop strength slowly but in the long term they tend to approach the strength of the control mortars with quartzitic sand. In particular, based on the results of compression testing after 6 months, samples with china clay sand of standardised particle distribution have the same strength as samples with standard sand. The reduction in strength with increased water content to obtain the required workability with these waste materials is not as high as expected from previous research. Although the use of the waste does result in strength decreases compared with the control sand, an overall environmental and cost benefit may result through use of this waste material.

Using the china clay waste with Portland cement appears to have very little strength reduction compared to standard sand. This is contrary to previous research which indicated larger strength reductions with increasing binder contents. This previous research was based on mixes which did not account for the increase in volume for the waste material, which provided a net decrease in binder content per unit volume. This aspect of different bulking or volume factors must be accounted for if an accurate assessment of different wastes is to be undertaken.

Although the MW stream is finer than materials typically used as aggregate in cementitious products, it may provide adequate strength for certain applications without the high energy crushing process required for the production of sand from coarser china clay waste streams. The durability of these materials should be assessed before use.

Chapter 6: **Effect of china clay waste as aggregate in AA concrete and comparative environmental impact**

Based on the most successful binder and mortar mixes described in the previous sections, a GGBS series and a 50/50 GGBS/FA series of alkali-activated concrete mixes were produced while Portland cement concrete was used as a control series. The design of the mixes was based on gradually replacing primary sand with china clay waste. By this means it was possible to assess the order of strength reduction which should be expected when using stent, china clay sand and MW. Further optimizing of the mixes to form a specific product which would allow direct production of the targeted unreinforced uses did not take place as it was considered product development rather than fundamental research and was therefore out of the scope of this research project.

As the goal was to produce concrete blocks and tiles with lower impacts than existing PC based products, an environmental evaluation of the concrete was performed. The SimaPro life cycle assessment software was used to determine the environmental impact of the mixes. The impacts were compared with mixes from literature and the viability of geopolymer technology versus Portland cement based products was finally discussed.

6.1 Methodology for Concrete making

6.1.1 Composition and Design of the mixes

The BRE guide for concrete mixes (Teychenné et al., 1997) was used to design the concrete mixes even though this methodology was designed for conventional cast concrete applications and not specifically for unreinforced concrete blocks. Unreinforced concrete block mix designs are typically proprietary mixes based on available materials and Manufacturing technology.

The design was based on the following requirements:

- The impact of all forms of the waste should be assessed, including MW.
- The mix should be of low workability and strength as the target application was unreinforced building products, including blocks.
- The design should be driven by lowering the environmental impact while still meeting existing performance standards for dense concrete blocks.

By setting these requirements, it was accepted that:

- The total particle distribution of the aggregates serves research purposes and it does not represent the optimum aggregate composition for product manufacture. Although the BRE guide suggests a functional total particle distribution based on technical requirements (max particle size, uncrushed/crushed aggregate, free-water/cement ratio, proportion of fine aggregate and targeted flow), the optimization of the mix (good aggregate

packing complying with application, the potential need for alteration of the grading of the coarse aggregate and sand, maximum strength) is achieved progressively after trials and this was out of the scope of this study.

- The cement content should be as low as possible to minimize environmental impact. That would possibly be the worst case scenario in terms of mechanical strength and durability.

The mix was initially designed for minimum workability: 0-10mm slump (class S1, conducted in accordance to BS EN 12350-2:2009 ; classes defined in BS EN 206:2013). The maximum particle size of the coarse aggregate was set at 10mm, which is common in concrete blocks. The water to cement ratio (W_t/C) was set at 0.47 resulting in 383kg/m^3 Portland cement and 180kg/m^3 water. According to the fineness of the CCS 0/4 and MW, the guide indicated that the fine aggregates should be a 32% of the total aggregates. From that amount, half was CCS 0/4 and half MW. Based on these percentages (68% stent, 16% CCS and 16% MW), the curve "for the concrete mixes (mix D)", shown in Figure 92, was calculated (for the detailed calculations see Annex A.3).

Figure 93 shows the different aggregate composition used to investigate the impact of the china clay waste in AAC concrete. Control mix A contains only primary aggregate (NS2, NS1 and NS, presented in subsection 3.1.4). Mix D contains only forms of the waste. To investigate the impact of the different forms of the waste in the mix, the primary aggregate was gradually replaced with forms of the waste. Because of the variation in particle size between NS2, NS1, NS and stent, CCS 0/4 and M respectively (Figure 92) there is a slight variation in the particle size distribution of the aggregate combination for concrete, seen in Figure 92 (as "for the concrete mixes (mix A)" and "for the concrete mixes (mix D)"). The aggregates were used dry, rather than saturated surface dry, as this is the typical process in concrete block production (Mineral Products Association, 2013).

Once the composition of the Portland concrete was decided, the AAC mixes had to be designed. To mix equivalent AAC mixes the binder was calculated as equal in weight (563kg/m^3) and the aggregate composition did not change. The GGBS concrete series and the 50/50 concrete series were based on the pastes of the mortars, mixes 3 and 11, which were simply adjusted to the required 563kg/m^3. Therefore as in mortars, when referring to W_t/B, "B" is calculated as shown in section 4.1.1 and includes the anhydrous activator.

Table 25 shows the breakdown of the PC, GGBS and 50/50 series concrete mixes which is based on the design described above, targeting 0-10mm slump for PC. The table refers to 50% sodium hydroxide solution and a 50% sodium silicate solution (chemicals described in 3.1.7) and where "H_2O", tap water added.

Table 26 Composition of the PC, GGBS and 50/50 series for the initial design which is based on $W_t/B=0.47$ and 0-10mm slump (for PC). Where B= GGBS or FA + anhydrous activator. Where $W=H_2O$+water in the alkaline solutions.

	kg/m^3		
Constituents	PC series	GGBS series	50/50 series
Portland	383.0		
GGBS		344.9	174.3
FA			174.3
NaOH solution		17.2	23.0
Na_2SiO_3 solution		78.0	63.4
H_20	180.0	122.9	127.9
NS2 or Stent	1249.2	1249.2	1249.2
NS1 or CCS	293.9	293.9	293.9
NS or M	293.9	293.9	293.9
W_t/B (or Cement)	0.47	0.47	0.47
B (or Cement)	383.0	383.0	383.0

6.1.2 Mixing and testing

As would be expected for 0-10mm slump, the trial mixes showed very poor workability. In the case of the 50/50 concrete series, due to the rheological properties of FA in concrete, the mixes were significantly more workable. Although dry mixes were initially aimed, it was realized that this fact when combined with the gap graded particle size distribution of the total aggregate (Figure 92), gave samples with high variability in compressive strength. This may be because the process in commercial concrete block manufacturing plants uses high levels of mechanically applied compression, sometimes with added vibration, in order to densify the samples, an option which was not available in the laboratory environment. It was therefore decided to add extra water to reach 70-80mm in the slump test (falling in class S2 although the design was for Slump class 1). It should also be noted that in the case of AAC when there is insufficient water, the samples do not properly harden, probably because of poor dissolution of the precursor, which is one of the required steps in the geopolymerisation process.

The binder was mixed separately for 5 minutes in a small mortar mixer (Automix Controls model 65-L0006/AM) and then added to the coarse aggregate in a pan mixer. The already blended fines and sand were then added. The last ingredient to be added was the extra water required for workability. The pan mixer was run for approximately 5 minutes until a homogeneous mix was formed. If the slump was less than 70-80mm the material would be further mixed with more water for 1 minute. The fresh concrete was cast in 100mm cubic moulds, compacted in four layers each receiving 25 blows. The specimens were demoulded on day 2. The alkali-activated concrete cubes cured at 20°C

and 60% relative humidity while the Portland concrete series cured in a water tank according to the BS EN 12390-2:2009. Triplicate specimens were used for every test, as for that number of specimens the consistency in the results was noted to be satisfying. The specimens were tested in compression after 7, 28 and 90 days.

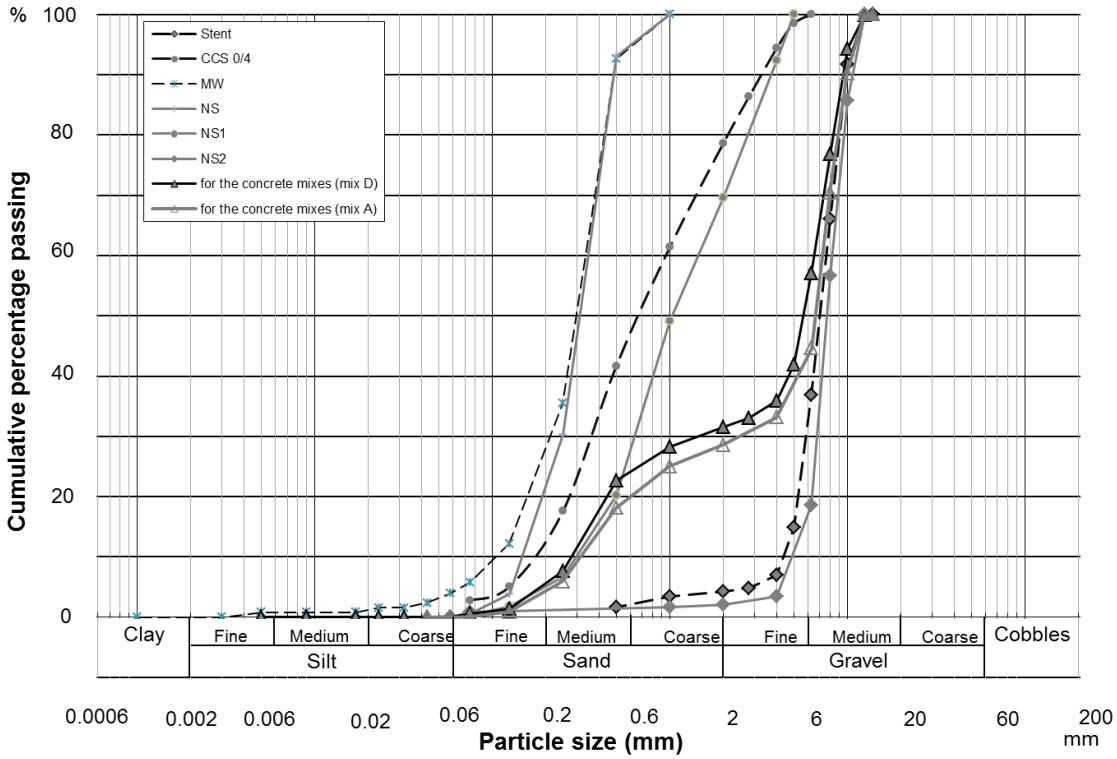

Figure 92 Particle distribution of the coarse aggregate, sand and fines used in this study, as raw materials and combined.

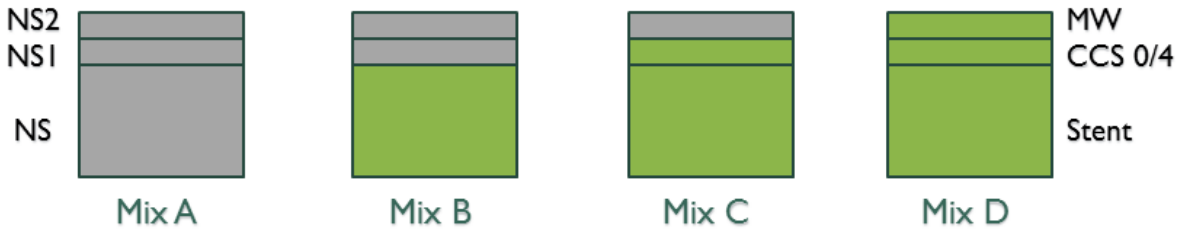

Figure 93 Aggregate composition for mix A,B,C and D.

Because of adding extra water to the mixes during mixing, the overall water to binder ratio (W_t/B) increased above 0.47 (the initially planned ratio, as Table 25) and subsequently, there was some variation in volume for different mixes. The volumes of all the mixes were measured using a 100mm cubic mould and the extra water used was also recorded. Following, the details of Table 25 were personalized for every mix and are displayed in Table 27. It should be noted that Table 27 reports the overall water content

(including the extra). The table shows that for all series, the binder or PC content in mix A is about 380kg/m^3 and for mixes B, C and D it is gradually reduced to about 360-365kg/m^3, a decrease due to addition of extra water.

6.1.3 Required tests

In terms of the targeted applications, the following tests are indicated in standards:

- BS EN 490:2011 gives the specifications for concrete roofing tiles and wall cladding. It displays the range of acceptable dimensions, mass and specifies the performance by requiring:
    - The value of transverse strength. Depending on the type of tile (interlocking or non-interlocking, flat or profiled) and geometrical characteristics the average minimum required transverse strength value F_{min} ranges from 550-2000N on the 28^{th} day. This is a function of the final product rather than material as it will vary by changing thickness. It has also been shown that the ratio of flexural to compressive strength of geopolymer concrete is similar to that for PC based concretes (Provis and van Deventer, 2014)
    - Water impermeability (according to BS EN 491:2011) This is a function of product thickness so was not included, although research has shown that geopolymer concretes can have lower water absorption and permeability than PC based concretes (discussed later). This testing was therefore not included.
    - Resistance to freeze-thaw (the only durability test required, according to BS EN 491:2011). After 25 cycles of freeze-thaw the specimens are inspected for breakage or cracks and tested again for water impermeability and transverse strength. This issue is discussed in more detail later but this aspect was not included in testing.
    - Test of nib support (applies only to a formed-final product so was not included)
    - To be class A1 and $A1_{FL}$ (classification in 2000/147/EC) for fire performance. In this case, since the there is no coating and the material is inorganic, there is no need for testing according to EU Commission Decision 2000/553/EC.
    - To be free of release of dangerous substances. There are no dangerous substances in geopolymer cement. If the composition is not appropriate then there could be issues of alkaline leaching but no problem occurs for well formulated binders.

Table 27 The actual concrete mixes, including extra water for slump 70-80mm.

	kg/m^3			
Constituents	Mix A	Mix B	Mix C	Mix D
Portland	380.0	360.0	363.0	359.3
H_20	200.8	232.6	239.7	237.7
NS2	1239.6			
NS1	291.7	276.3		
NS	291.7	276.3	278.6	
Stent		1174.4	1184.0	1172.0
CCS			278.6	275.8
M				275.8
* W_t/C	0.53	0.65	0.66	0.66
GGBS			329.0	329.0**
*H_20			172.9	172.9**
NaOH solution			16.5	16.5**
Na_2SiO_3 solution			74.4	74.4**
NS2				
NS1				
NS			280.4	
Stent			1191.6	1191.6**
CCS			280.4	280.4**
M				280.4**
* W_t/B			0.62	
B			365.3	
GGBS	174.6	167.5	167.5	165.6
FA	174.6	167.5	167.5	165.6
*H_20	137.6	148.3	149.9	161.7
NaOH solution	23.0	22.1	22.1	21.9
Na_2SiO_3 solution	63.5	61.0	61.0	60.3
NS2	1251.3			
NS1	294.4	282.5		
NS	294.4	282.5	282.5	
Stent		1200.4	1200.5	1186.9
CCS			282.5	279.3
M				279.3
* W_t/B	0.49	0.54	0.54	0.58
B	383.7	368.1	368.1	364.0

* including the extra water added

** No data on the extra water added. Assumed to be the same with GGBS series-mix C.

- EN 771-3:2011 provides the specifications for aggregate concrete masonry units (in this case dense aggregates are of interest). The necessary characteristics to describe and design such a unit are the dimensions, configuration and compressive strength. Since geopolymer concrete is expected to have much higher strength than a common concrete unit, it is possible for the unit to incorporate voids. Furthermore:
    - The gross density should also be stated and it can be used for evaluation of thermal insulation. The density of the mixed concrete is presented in the following sections.
    - There is no need for testing the fire performance as there is no organic content in the material as with the roofing tile applications.
    - Water absorption by capillarity and freeze-thaw resistance should be tested if the units are designed to apply to surfaces exposed to weather. As mentioned earlier, free-thaw is discussed later and was not tested. Comparative data on water absorption by capillarity are included later in this chapter.
    - Water vapour permeability is needed for external elements and the required value of water vapour diffusion coefficient(μ) is given in BS EN 1745:2012 based on the net dry density of the material. For dense aggregate concrete unit of 2300-2400kg/m^3, μ=50/150.
    - For units intended to be used in elements subject to structural requirements the moisture movement has to be declared. The test should be undertaken after optimizing the mix, to characterize the final product.
    - Shear and flexural bond strength with mortar should be tested for relevant applications. This is a function of the final product and of the mortar used and not the material, and this testing should be undertaken once final products are developed.

The issue of freeze-thaw was noted for both concrete roof tiles and concrete blocks. As noted in Chapters 2 and 3, stent and the china clay sand comply with existing aggregate standards. Grading, petrological and chemical information and list of results from tests indicated in BS EN 12620:2002+A1:2008 ("*Aggregates for concrete*") can be found in Chapter 3 and the Annex. They were therefore considered suitable for use in concrete. The same Standard, when referring to the durability of aggregates for concrete, mentions that when the water absorption of the aggregate is not greater than 1% then the aggregate is considered resistant to freeze-thaw attack. The Standard also states that aggregates with higher absorption frequently offer adequate resistance. The water absorption of the waste ranges from 1% to 1.5% and although the maximum is slightly above the standard (1%), it is unlikely that the aggregates will be susceptible to freeze-thaw, particularly as they have been successfully used in a number of concrete applications (see 2.2) where freeze thaw testing was required.

While the freeze-thaw resistance appears in both Standards, it was decided not necessary to conduct the test as there is adequate information in literature that well-formed geopolymer concrete (in terms of binder composition and binder/aggregate ratio) would have good performance as explained in section 2.4.5. As the aggregates have been successfully used in applications where freeze-thaw testing was required and as data in the scientific literature have shown that geopolymer concretes have good freeze-thaw resistance, it was determined that no testing was required at this stage, although testing on any final products is recommended.

6.1.4 Strength in compression

The compressive strength of the samples is summarized in Figure 94. The standard errors of the mean which are noted on the columns are of small scale which indicated the reliability of the results. The mixes reached strength in the same range of compressive strength achieved by other authors (Bernal et al., 2012a, Collins and Sanjayan, 1999), 30-60MPa on the 28th day of curing. The work of Bernal et al. (2012a) is discussed in sections 2.4.3.1, 2.4.5 and 2.7.3. GGBS mixes by Collins and Sanjayan (1999) contain GGBS of very similar composition to the GGBS used in this study (SiO_2 35.04%, Al_2O_3 13.91%, CaO 39.43%, MgO 6.13%) and their concrete mix design was based on 347kg/m^3 GGBS and free water/binder=0.5, therefore similar values to the ones used. Pictures of cross-sections of concrete cubes after testing in compression on day 7 and 90, cut using saw, can be seen in Figure 97 and are discussed in 6.1.5.

Compared to the control specimens (mix A) all the test specimens had lower compressive strength, as expected from the results with the mortars. The results in general show a common trend: a decrease in strength with increasing use of stent and CCS (mixes B and C), even though these materials meet the specification for secondary aggregates and are broadly used. There is a further decrease in strength for the use of MW (mix D). It is worth noting that while on day 7 the performance of the PC and the AAC series is similar, on the 28th and 90th day the AAC series has gained significantly more strength compared to the slightly improved Portland series. Only mix D from the 50/50 series remains low, as low as its equivalent mix from the Portland series.

According to Figure 94, mix D from the GGBS series could replace mix A of the Portland series as from the 28th day and onwards it shows equivalent strength. After the 28th day, mixes B and C of the 50/50 series also approach the strength of mix A of the Portland series. In other words, the use of stent, CCS and even MW is not prohibitive in terms of mechanical strength and mixes with similar compressive strength can be obtained. This initial study indicates that it is possible to use AAS with the coarser forms of china clay waste and obtain higher strengths than what would be obtained with a PC based binder and virgin aggregates. Optimising the aggregate grading, binder content and water/binder ratio will most likely result in even higher compressive strengths. For the GGBS series, even the detrimental effect of the MW on compressive strength can be overcome with strengths comparable to that of the PC based series with virgin aggregates, but this would have to be shown for more general cases by conducting further research.

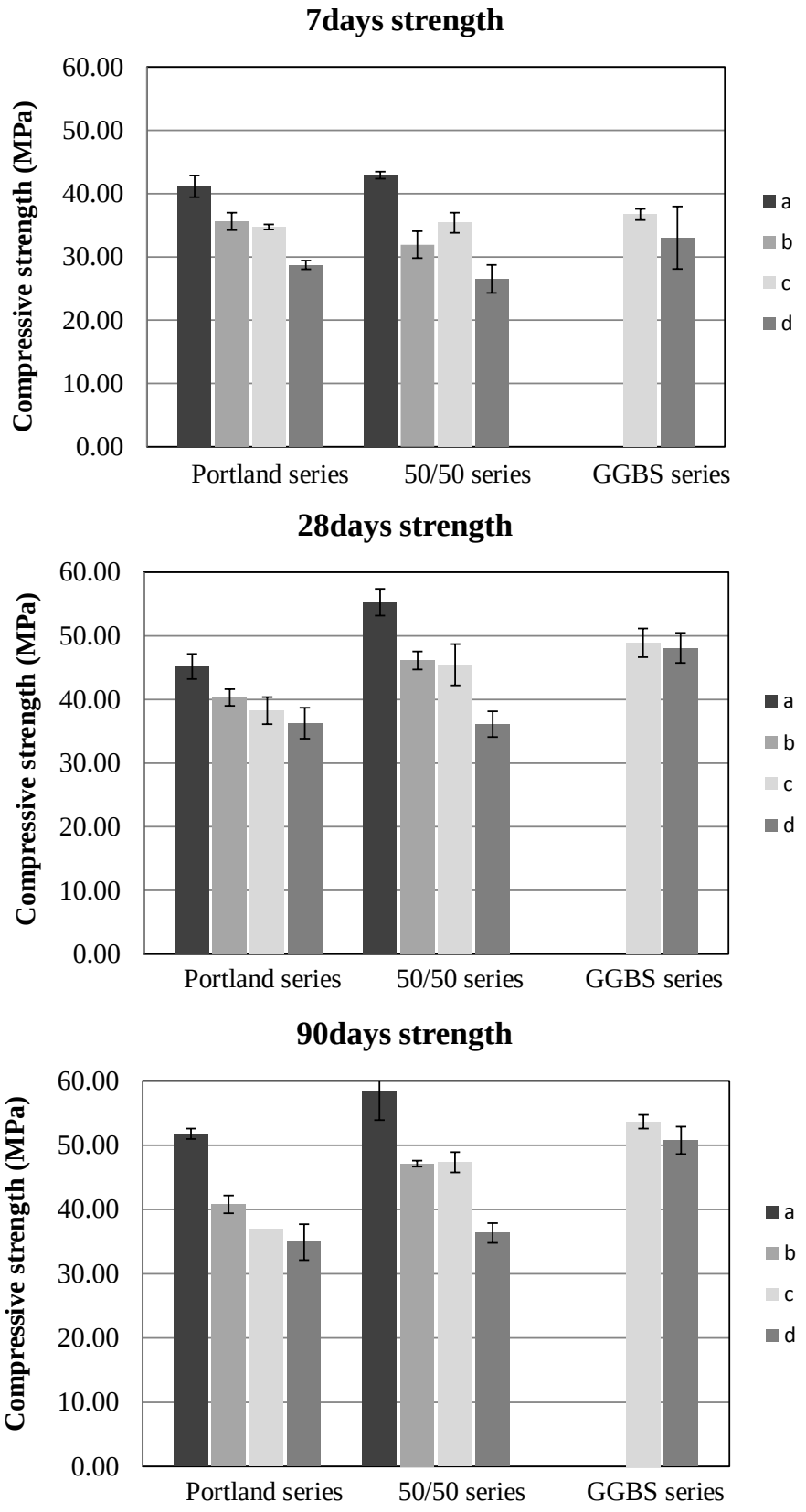

Figure 94 Comparison of strength for the different series and aggregate combination in different ages.

The bulk density of the specimens on day 28 is: 2365 and 2310kg/m^3 for PC mixes A and D respectively, 2438 and 2295kg/m^3 for the 50/50 mixes A and D respectively and 2347kg/m^3 for mix D of the GGBS series. Unlike the gross density (described in EN 772-13:2000) the measurement of the bulk density does not include drying of the samples and the calculation is based on the bulk volume of the specimen. The bulk densities are consistent with the exhibited compressive strength of the specimens.

From Figure 95 it could be suggested that the high ratios of water to Binder (or PC) affected the AAC more than the Portland series. The 50/50 series shows as average from all the ages of testing: 20% decrease from mix A to mixes B and C and an extra 17% decrease for mix D. For the Portland mixes, mixes A and B have 15% difference, the addition of CCS (mix C) gives an extra 5% decrease and the use of MW (mix D) a further 8% decrease.

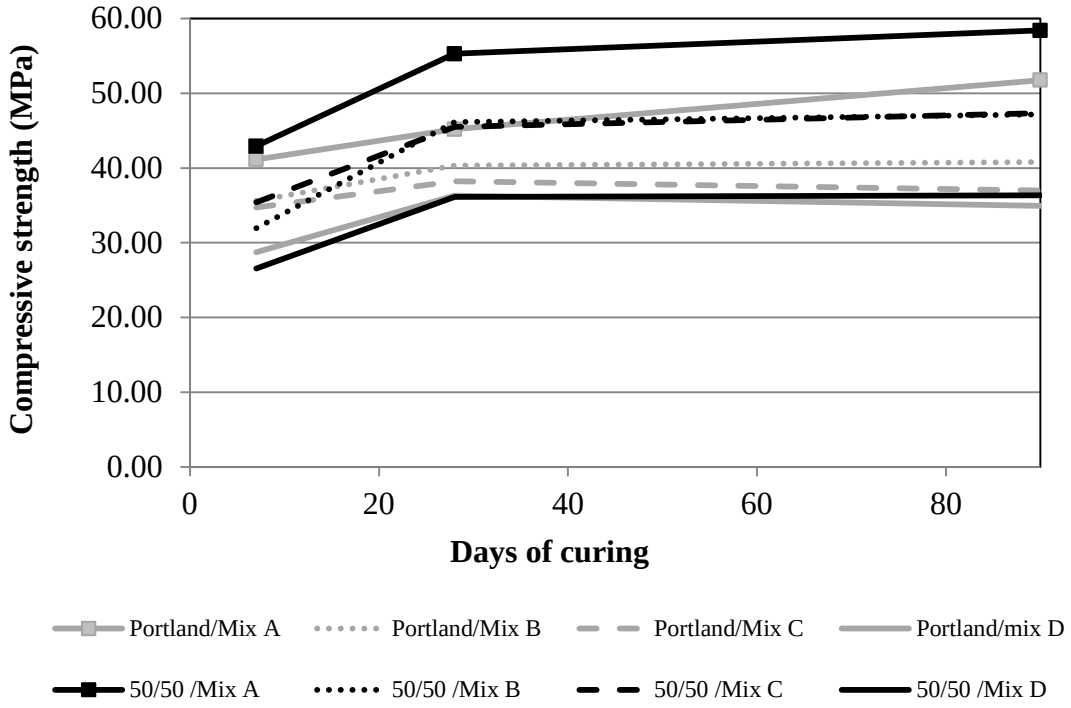

Figure 95 Strength development for the 50/50 and Portland series.

6.1.5 Observations

By visual observation of the pictures in Figure 96 and 97, it is seen that the presence of coarse aggregate is dominant in all the mixes. Mixes A and B are more homogeneous and show better packing than mixes C and D where the small particle size aggregates (CCS, MW, NS) is not easily detected. This may be related to the lower performance of these mixes in compression. Where stent is used (mixes B,C,D), in either the GGBS or 50/50 series, there are areas which differ in colour (noted in yellow on Figure 96). This shows inhomogeneous mixing (without implying presence of soluble phases) and it is likely due to the higher water content in these mixes compared to mix A and the higher water

absorption of stent which affects the water absorbed and gathered around an aggregate particle which could weaken locally the binder. This again can possibly have a role to the lower performance achieved of these mixes.

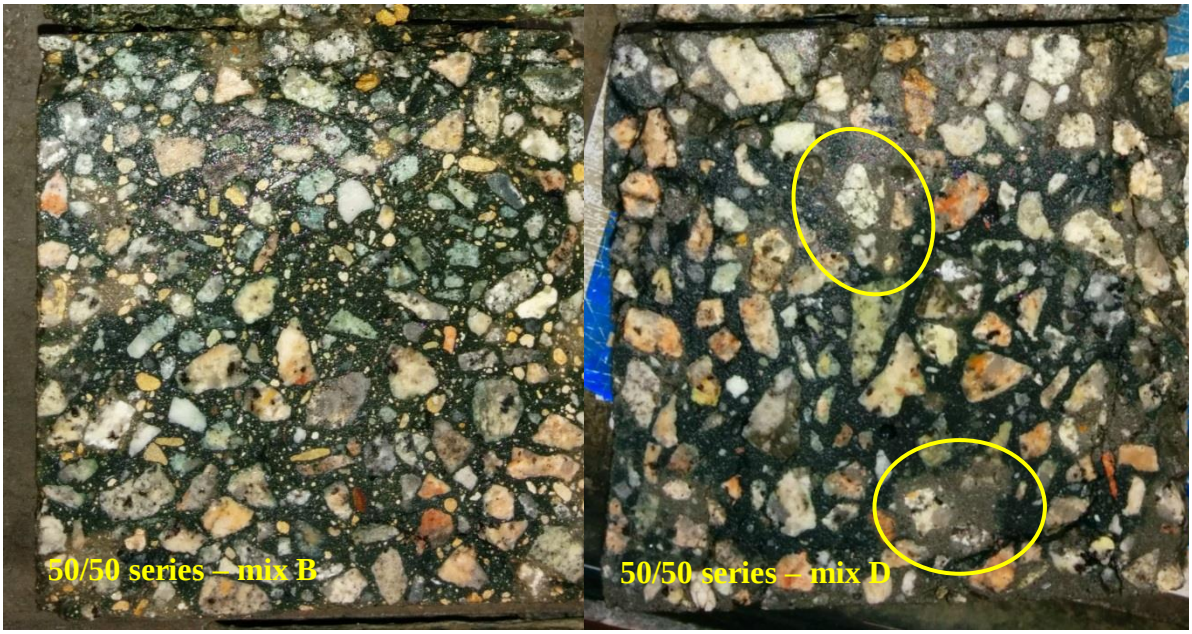

Figure 96 Cut sections after 7 days of curing. In yellow, areas of binder of different colour.

Light grey coloured stains were observed in the hardened AAC which disappeared over time (Figure 98). There are no stains in mix A of the GGBS and 50/50 series, either in any mix of the Portland series. It is suspected that this is because of agglomerates of finer particles which did not have enough time to be separated and be equally distributed in the mix during mixing and they weaken the binder locally. Clay agglomerates are generally categorized as deleterious material for concrete in Forde and Institution of Civil (2009) and it is explained that this is due to the reduced abrasion of the paste on the coarse aggregate and due to the shrinkage of particles during drying which might leave cavities. However, as the Portland series did not have any apparent effect it is suggested that the stain is related to higher absorption of water locally, which can be highly detrimental for AAM, and may be related to some extent of reaction with the lesser minerals.

The hypothesis that agglomerates cause the stains can be confirmed using SEM/EDX. Three samples were taken from AAC cubes. It should be highlighted that the samples were taken from the first set of cubes which were dry, did not give good consistency and are not presented elsewhere in this chapter (Figure 99-102). Phyllosilicate particles can be observed in all the fragments (Figure 99-100). There is also high inhomogeneity: presence of crystals (Figure 99), parts of properly developed matrix (Figure 101) and, in the case of samples from a slag-based cube which were drier than the 50/50 series, there is high amount of undissolved slag particles.

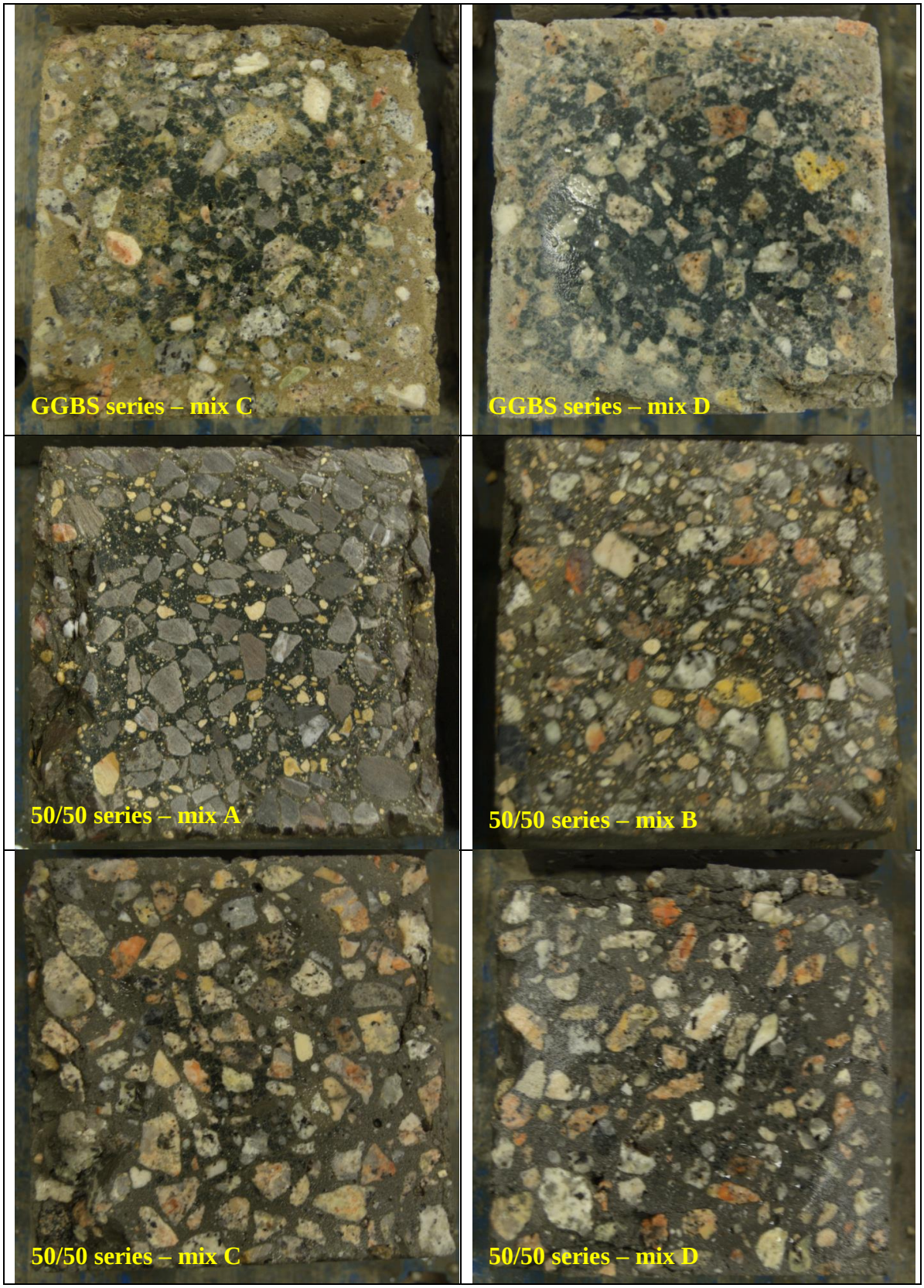

Figure 97 Cut sections after 3months of curing

The coefficient of water absorption due to capillary action was tested after three months of curing for two specimens. The test ran according to BS EN 771-3 and BS EN

772-11, however the samples were not oven dried – instead the Portland sample was left to dry under the same conditions as the 50/50 series sample for thirty days. That drying method was selected because, according to what was discussed at section 2.4.5, it is not clear if drying AAM (especially AAS) at 100°C causes changes in concrete or if applying different drying temperatures to PC and AAM affects the later comparison. The measured values were:

- 50/50 series mix C: 93 g/(m^2s)
- Portland series mix D: 58 g/(m^2s)

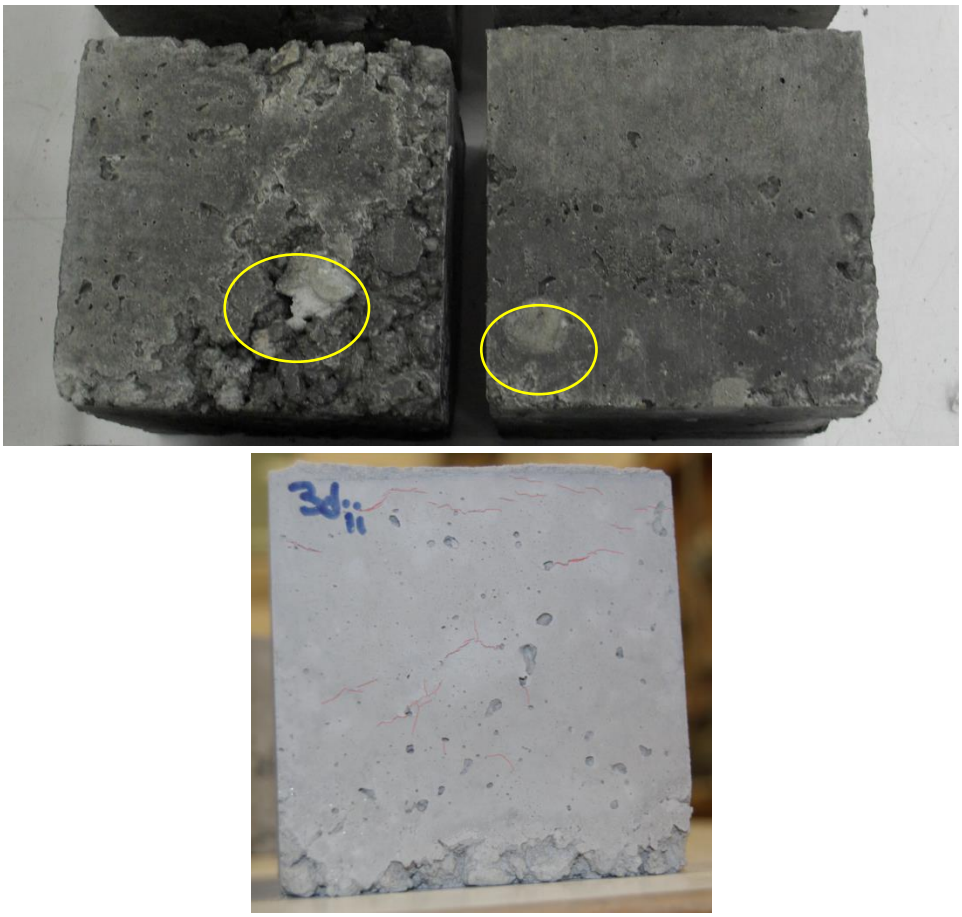

Figure 98 Stains of the 50/50 series on day 28 (outlined in yellow) and the same series after 3months of curing where the stain is not visible anymore.

Therefore the specimen of the 50/50 series has greater capillary sorptivity than the Portland series mix D, an unfavorable result which shows that the sorptivity does not necessarily follow the trend of the strength (as shown on Figure 95, 50/50 series mix C has up to 10MPa greater strength than Portland series mix D). The result is in contrast to many authors (see 2.4.5) who have reported lower capillary sorptivity in AAM than PC. This is reasonable considering the low content of FA+slag used together with the extra water added as it leads to lower quality concrete. From section 2.4.5 it was observed that only robust AAC (high content of precursor, low water/binder ratio and/or significantly

higher strength that PC) could excel the resistance in sorptivity and water permeability of PC. In any case the capillary sorptivity should be tested for the optimized mix as the extra water in the mix is of crucial importance.

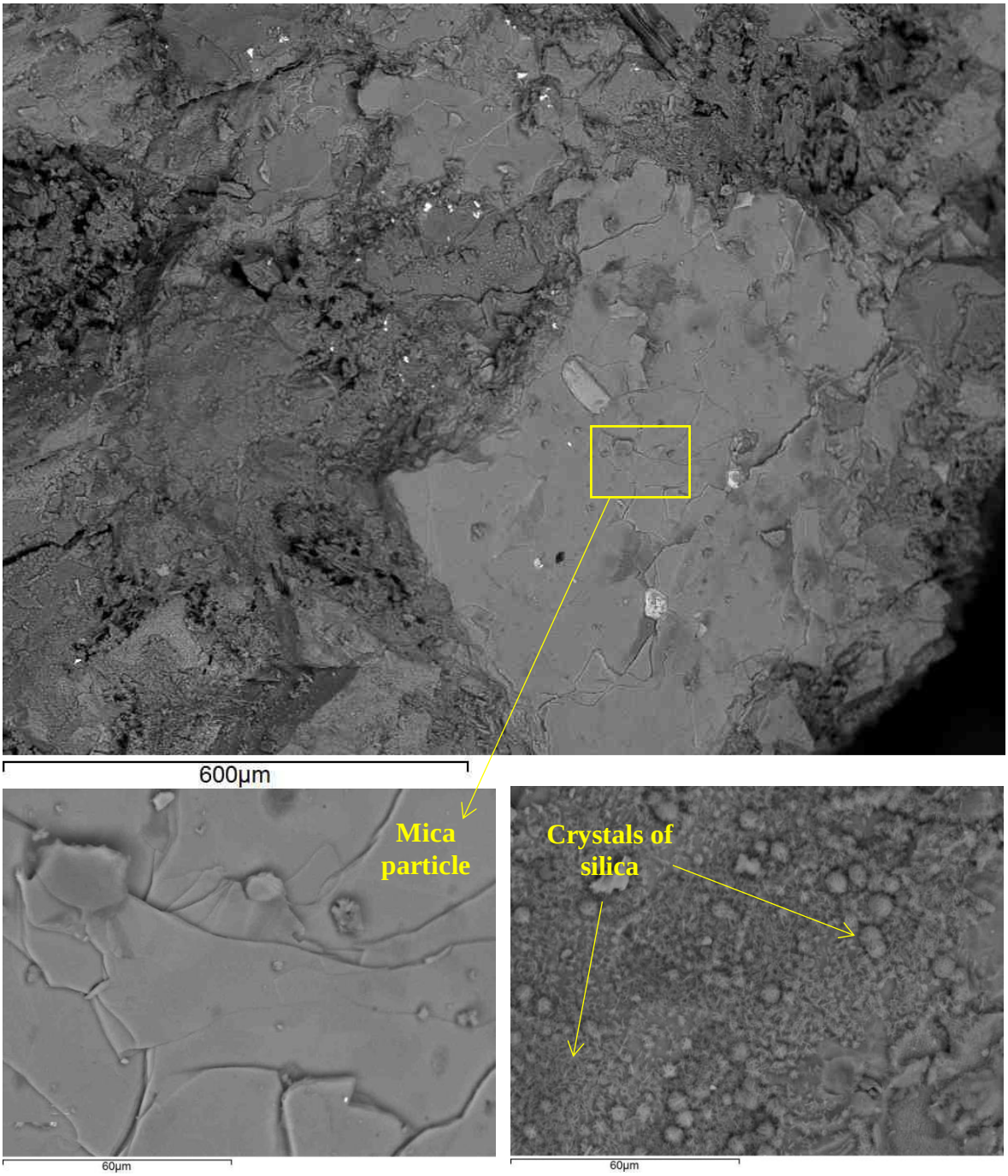

Figure 99 Microstructure of the stain area - Crystals of silica.

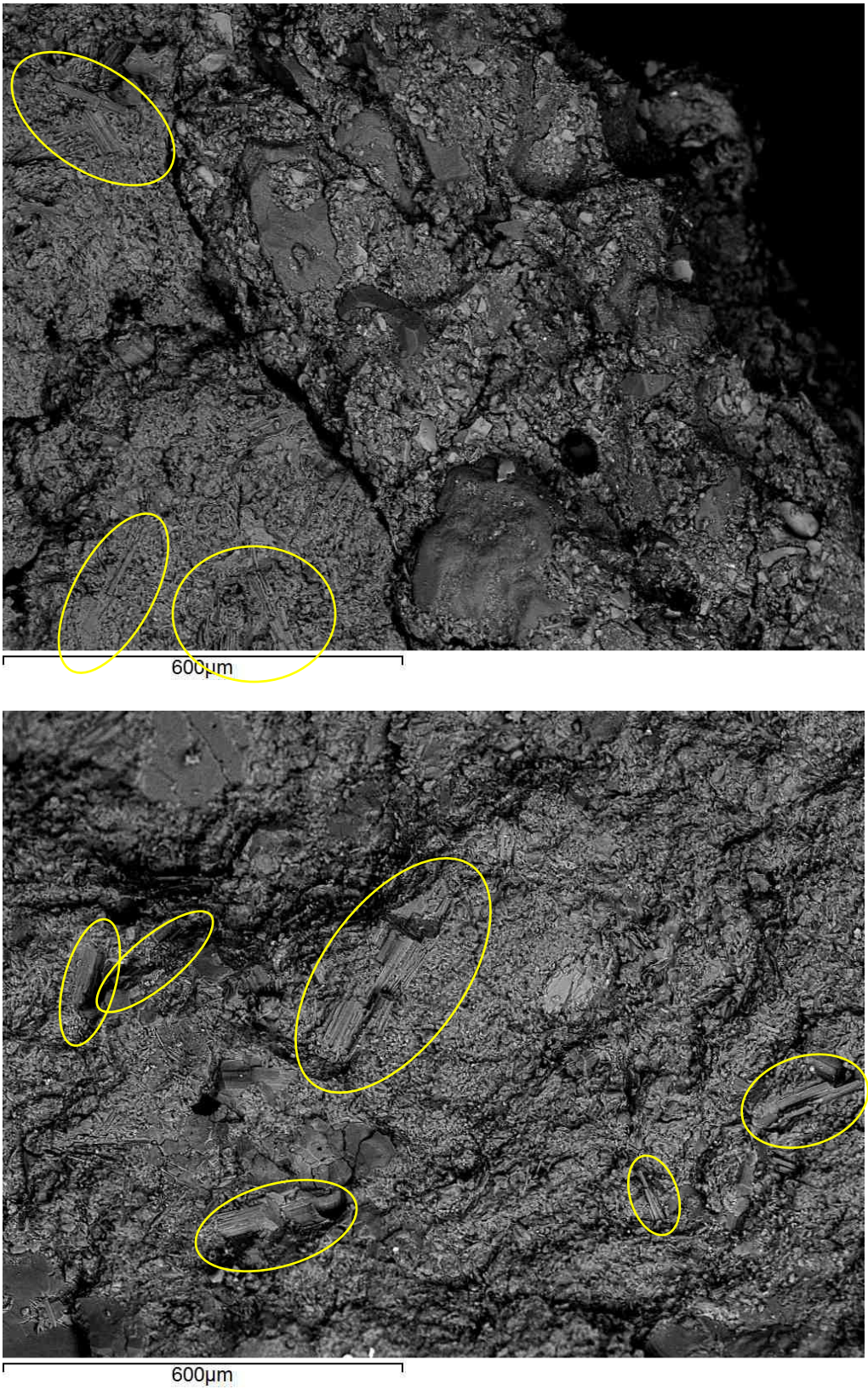

Figure 100 Microstructure of the stain area - High presence of phyllosilicate particles.

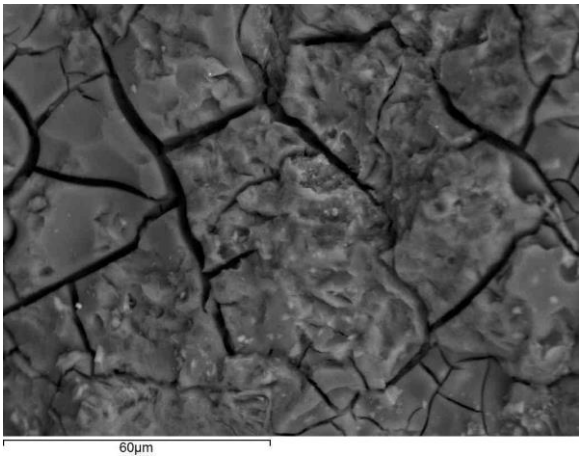

Figure 101 Microstructure of the stain area – Geopolymeric matrix.

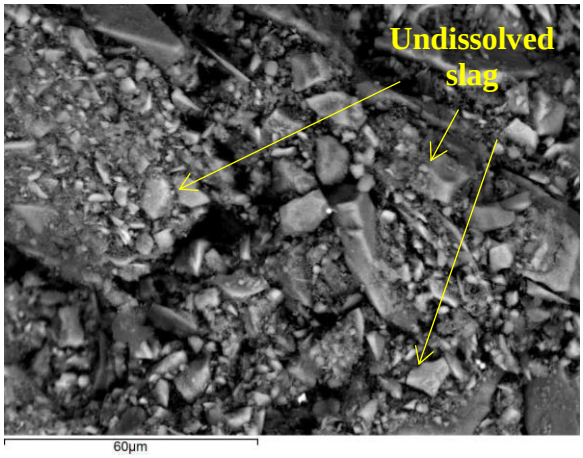

Figure 102 Microstructure of the stain area – Area poorly dissolved (notice: image refers to first set of cubes, dry mixes

It is noted that there is decrease of strength for the use of stent. Stent as mentioned in Chapter 1 is unaltered granite, however the rock might be exposed on some extent of weathering. Based on the discussion in 2.6.2 and the fact that the china clay waste comprises largely quartz (Table 9), mixes A and B in terms of aggregate mineralogy, would be expected to give equal strength. Therefore this suggests that stent decreased the strength of the unit due to the increased need in water and less likely due to the mechanical degradation during weathering.

The results above and information from the literature have shown that it is possible to obtain GGBS based geopolymer concretes containing china clay waste with similar or improved technical performance to that of PC based concretes containing virgin aggregates, for potential future use in concrete blocks or roofing tiles. In order to meet the overall aims of the project, it is necessary to investigate whether these new mixes have a reduced environmental impact over the currently used PC based mixes.

6.2 Environmental Impact

6.2.1 Methodology

The assessment of the environmental impact was conducted using SimaPro. In this software, materials and processes are listed for their impact in different environmental categories based on different databases. For this study, the latest Ecoinvent database (Kellenberger and Althaus, 2003) was used for sodium hydroxide, the different types of sodium silicate (based on Fawer et al. (1999)), tap water, gravel, sand, lime and calcination (see Table 29). The values for slag, FA and cement were taken from Chen et al. (2010) who, as discussed in 2.4.6, used three types of allocation for GGBS and FA in their environmental analysis. The input values are presented in Table 29. The ten environmental categories which are displayed according the CML (Center of

Environmental Science of Leiden University) method, have been introduced in section 2.4.6.

The output was calculated as a multiplication between the values presented in Table 29 and the relevant quantities in Table 27. In the case of AAC the activator had to be calculated based on the active substance as indicated in the Ecoinvent code of practice (Weidema et al., 2009). In particular:

- The sodium hydroxide used (50% solution) is calculated by multiplying the impact values with half the quantity indicated in the Table 27 which refers to the solid NaOH used.
- The sodium silicate used (in solid it has Ms=2.0 with approximately 20% H_2O) is calculated by multiplying the impact values of "*Sodium silicate, hydrothermal liquor, 48% in H_2O*" (Table 29) with 0.4(=0.5x0.8) times the quantity of sodium silicate solution shown in Table 27. Where "0.5" refers to the 48% H_2O and "0.8" is an additional reduction to reach the anhydrous substance of sodium silicate, as the particular solid used contained a 20% H_2O.
- The code of practice states that "*the amount of the solvent required in addition to the active substance is already included in the inventory of the dissolved chemicals*". Therefore the 50% NaOH solution is not included in calculating the impact of water. From sodium silicate only the extra water of 20% (in the solid) is included. The value for tap water was calculated based on the following equation:

  (H_2O + 0.2 x Na_2SiO_3 solution) x Impact

6.2.2 Assessment of the environmental impact

The output of the concrete mixes is presented in Figure 103 to ease comparison, instead of being presented in tables equivalent to the input tables (Table 29). This figure shows mixes A and D for PC, GGBS and 50/50 series, although mix A from the GGBS series has not been mixed. For the different environmental categories under study, the mix which had the maximum impact was noted as the 100%. This way it can easily be detected the environment saving that is offered by the other mixes. The figure is based on calculations using economic allocation of GGBS and FA, which as discussed in section 2.4.6 is the most reasonable of the three allocations. As shown, using the waste instead of primary sand offers only a slight advantage, ranging from 1% to 15% in all series of concrete (GGBS, PC, 50/50). The geopolymeric binders significantly decrease the global warming potential compared with the PC based mixes, on average by 68%. Likewise the impact of ozone layer depletion and eutrofication is decreased. However, other impact categories including abiotic depletion, acidification, photochemical oxidation and everything that involves toxicity are increased for the geopolymer based mixes. It should be mentioned that the figure shows ratios and the absolute values of areas with toxicity in PC are very low.

For the AAC, the values calculated for the different allocations follow the same trend: *"no allocation*" shows the lowest impact and then follows the "*economic allocation*" and "*mass allocation*" with high impact. That is shown in Figure 104 which refers to pastes, not concrete, based on 1kg of PC/ GGBS/ Tungsten waste with $Ca(OH)_2$/ Mica concentrate with $Ca(OH)_2$. The anhydrous activator for the alkali-activated pastes and the water content of all pastes was encountered on top in the calculation. In specific, Figure 104 assessed the impact of:

- A PC paste of 1kg PC and 400g water (W/C=0.40).
- AAS based on mix S3 as shown in Table 16, where the water to binder ratio is 0.40, but the paste was scaled to 1kg of GGBS.
- Mix B3 in Table 14, where water to binder is 0.40, but the paste was scaled to 1kg of mica concentrate+$Ca(OH)_2$. Mix B3 was chosen as it was the mix that gave the highest strength on the 28 days (19MPa).
- The TMWM paste had water to binder equal to 0.43 (as calculated in the Annex A.2 based on Pacheco-Torgal et al. (2008,d)) and was scaled to 1kg of TMWM+$Ca(OH)_2$.

The figure has as baseline the PC binder, as the 100% of environmental impact in all the environmental categories under study. It is noted that the vertical axis is exponential. Therefore, as example, for the fresh water aquatic ecotoxicity where the AAS has the most aggravating impact, AAS based on 1kg GGBS has from 4 to 45 times greater impact than the equivalent PC paste (ranges depending to the allocation considered). In the same figure, the mix from Pacheco-Torgal et al. (2008,d) described in section 2.7.4 shows equal or higher impact than PC, further justifying the decision not to use this approach to binder design. The impact of the mica concentrate-based paste offers advantage over PC in eutrophication and the global warming potential. It is noted that the calcining at 950°C is encountered in Figure 104 but any impact from the processing of the MW to produce the mica concentrate was not included. The impact for the AAS has lower global warming potential, ozone layer depletion and eutrophication for no allocation and economic allocation. No allocation shows as well lower abiotic depletion, acidification and photochemical potential. However, for mass allocation all the areas are disadvantageous for the GGBS-based binder, but as mentioned in section 2.4.6, the use of mass allocation is questionable when determining environmental impact. The paste based on mica concentrate has similar impact, in most of the environmental categories, to the AAS for economic allocation of the GGBS. It is worth noting that although the mica concentrate-based paste has lower sodium silicate content than the AAS, its impact is relatively high as it is activated using a higher-in-alkalis solution than AAS (13g versus 5g of Na_2O).

The assessment also includes the work of Bernal et al. (2011) (see 2.4.5) for comparison as it is considered a good example of ranging the robustness of concrete (in terms of strength, water absorption and carbonation) according to the binder content. This study used GGBS content close to the minimum binder content of Bernal et al. (2011)

(300 kg/m^3), the relatively least robust design. Therefore it is of interest to observe how the environmental impact would range for a higher in performance product. Figure 105 shows how the environment impact of concrete would be affected for an increase of slag content, from the current 329kg/m^3 to 400kg/m^3. Although the design of Bernal et al. (2011) has been discussed in 2.4.5, the exact composition of concrete is not displayed here. The Portland and GGBS series in Figure 105 are calculated based on mix A. Economic allocation was used for the GGBS and Bernal et al mix. Portland concrete is again presented as a baseline. It is seen that although the difference between 329kg/m^3 to 400kg/m^3 binder content is small, it is enough to bring the level of eutrophication and ozone layer depletion to the same level as PC. Therefore, for a more robust AAS concrete mix, the environmental superiority of this material would be limited to only lower GWP than the Portland series. Bernal et al. (2011) in Figure 105 is also included in later comparisons (Table 28, Figure 106, Figure 107).

Table 28 summarizes the strength and the GWP, calculated and presented in absolute values, for mixes A and D of this study. The table also shows the "*CO_2 intensity*" (C_i) and "*binder intensity*" (B_i) based on the methodology suggested by Damineli et al. (2010) (see section 2.4.6) where $B_i = B/f_c$ and $C_i = C_e/f_c$. In practice, the lower the values of B_i and C_i, the more efficient the design is, as actually B_i and C_i represent the binder needed and the carbon emissions for 1MPa of strength. By comparing mixes A and D of the same series in Table 28, it is noted that more effective is the use of primary aggregate (in terms of both, B_i and C_i). It is also considered arbitrary to use the B_i to compare OPC to AAC: while in PC the cementitious material is the CEM I used, in AAC the cementitious material includes the anhydrous activator. However, this is an assumption and other authors could consider the cementitious material to be only the GGBS/other aluminosilicate. So conclusions here were based on C_i. Moreover, in Table 28 GGBS mix D, 50/50 mix A and AAC based on 400kg/m^3 are the most and equally, effective, with the lowest CO_2 intensity. Therefore, it is important to notice that the AA slag offers the lowest CO_2 emissions, even when using higher amount of binder.

Would the environmental advantage of the AAC over PC remain if an optimized PC concrete design, using additives, was used? To answer this question, the work of Yang et al. (2014) was employed (9209 concrete mixes, see 2.4.6) and used to illustrate comparatively the results from Table 28. First, it was necessary to compare how the values of the Portland series of this study correlate with C_i values from the Portland designs that Yang et al. (2014) processed, as the GWP database they used is different. In their case, Portland has higher CO_2 emissions than the value taken in this study (0.9310 instead of 0.7733kg CO_2 eq in Table 29). It is shown that the PC values from this study are in the bottom (the most efficient) of the statistical sample. Yang et al. (2014) who elaborated mix designs of all possible combinations between PC, FA, slag and silica fume, found that the most efficient binder, therefore the best case scenario environmentally, is PC mixed with both, slag and FA. Figure 107 shows where the values of AAC stand compared to PC mixed with slag and FA. Using again the bottom values of the "*Portland+FA+GGBS concrete*" sample, it is shown that the AAC maintains the environmental preeminence marginally.

Table 28 Relating the GWP to strength: Carbon emission intensity (C_i) and binder intensity (B_i) of mixes from this study and Bernal et al. (2011).

			CO_2 (*), in kg CO_2 eq	28d stength, in MPa	B_i	C_i
Portland series Mix A	(this study)	●	300.7	45.19	8.41	6.65
Portland series Mix D	(this study)	▲	277.9	36.3	9.90	7.66
GGBS series Mix A	(this study)		98.4	-	-	-
GGBS series Mix D	(this study)	▲	87.5	48.1	7.59	1.82
50/50 series Mix A	(this study)	●	105.4	55.3	6.94	1.91
50/50 series Mix D	(this study)	▲	93.6	36.1	10.08	2.59
AAC based on 300kg/m^3 GGBS	Bernal et al, 2011	●	102.2	50.0	7.02	2.04
AAC based on 400kg/m^3 GGBS	Bernal et al, 2011	●	133.3	70.0	6.68	1.90
AAC based on 500kg/m^3 GGBS	Bernal et al, 2011	●	164.4	75.0	7.80	2.19

(*) where slag used in the calculation, it is based on economic allocation

6.3 Potential for optimization

BS EN 771-3 does not specify the ratio of binder to aggregate for blocks. The mixes used had a ratio of 1:4.8 and had much higher strength than the strength of common aggregate concrete units; the currently suspended BS 5628-3:2005 stated that for durable masonry the aggregate concrete block should have density ≥1500kg/m³, or to use dense aggregate which complies to BS EN 12620, or to have compressive strength of at least 7.3N/mm³. Although the water to binder ratio used is generally high, especially for the mixes which incorporate china clay waste, it is expected that the GGBS and 50/50 series would be durable enough to be used in masonry since the strength requirement is not high. This would, however, need to be determined for specific products incorporating these materials.

While the grading of the aggregates has to be refined before using the mixes under study in products, it was considered useful to refer to a study by Burciaga-Díaz et al. (2013) to facilitate further research and manufacturers who would prefer to use lower binder to aggregate ratio for blocks. In this study mortars of aggregate to binder ratio equal to 1:8 and 1:10 were mixed using 0.3 water content in the binder paste and saturated sand. The sand used had particle size less than 5mm. Using a vibro-processing machine, the mortar was pressed into bricks reaching up to 20MPa compressive strength. No results are reported regarding shrinkage and strength is reported till day 28, but this research indicates that it should be possible to produce products with the required properties and lower binder content.

Table 29 Input values for the environmental assessment: The impact of materials and processes in several environmental categories (from Kellenberger and Althaus (2003). The cement, GGBS, FA values from Chen et al. (2010)).

Impact category	Unit	Sodium hydroxide, 50% in H_2O	Sodium silicate, 37% in H_2O	Sodium silicate, 48% in H_2O	Sodium silicate, spray powder 80%	Cement, unspecified	Tap water	Brick	Gravel, crushed	Sand
Abiotic depletion	10^{-7} kg Sb eq	82093.18	72203.54	58299.72	128128.71	14706.28	9.40	11828.41	296.19	168.18
Acidification	10^{-7} kg SO_2 eq	53735.47	52157.84	34394.00	54484.14	10676.31	5.52	5476.23	231.24	149.69
Eutrophication	10^{-8} kg PO_4 eq	40485.25	49483.42	29963.13	47908.49	15993.03	5.94	6708.34	407.70	290.06
Global warming	10^{-4} kg CO_2 eq	11210.10	11436.42	7776.61	16362.78	7732.59	1.55	2197.24	43.58	24.67
Ozone layer depletion	10^{-11} kg CFC-11 eq	6881.51	8819.77	5768.80	14719.50	2144.09	1.16	1583.12	45.25	27.86
Human toxicity	10^{-5} kg 1,4-DB eq	47825.81	80345.71	49379.26	86199.53	4270.42	6.99	2974.54	296.08	171.74
Fresh water aquatic ecotox.	10^{-5} kg 1,4-DB eq	12016.21	21202.39	18391.94	24323.87	491.29	4.00	455.38	66.12	32.20
Marine aquatic ecotox.	10^{-2} kg 1,4-DB eq	23769.05	33185.06	24112.89	36068.95	1944.00	4.40	1836.58	79.41	39.43
Terrestrial ecotoxicity	10^{-6} kg 1,4-DB eq	23311.11	8961.67	12042.81	15434.89	1134.26	1.50	235.88	31.16	12.05
Photochemical oxidation	10^{-8} kg C_2H_4	23166.41	24333.81	16344.74	28063.60	4069.09	6.51	3999.62	104.26	56.08

(Part 1/2. Table continued in next page)

					Fly Ash			Granulated Blast Furnace Slag		
Impact category	Unit	Lime, hydrated, loose	Lime, hydrated, packed	Heat, natural gas, at industrial furnace	No allocation	Mass allocation	Economic allocation	No allocation	Mass allocation	Economic allocation
Abiotic depletion	10^{-4} kg Sb eq	17.21	17.65	6.10	2.02	195.00	17.90	2.88	121.00	17.10
Acidification	10^{-5} kg SO_2 eq	64.84	68.49	5.41	3.32	1920.00	160.00	34.60	485.00	89.10
Eutrophication	10^{-6} kg PO_4 eq	69.26	79.62	6.10	4.94	1060.00	91.20	10.50	677.00	91.10
Global warming	10^{-3} kg CO_2 eq	755.98	766.13	71.32	5.26	2510.00	210.00	16.90	1250.00	167.00
Ozone layer depletion	10^{-9} kg CFC-11 eq	52.20	52.70	8.71	3.35	24.30	5.07	4.11	24.50	6.57
Human toxicity	10^{-3} kg 1,4-DB eq	16.02	24.11	9.81	1.58	501.00	55.15	8.24	399.00	55.60
Fresh water aquatic ecotox.	10^{-4} kg 1,4-DB eq	25.36	52.39	2.60	1.76	317.00	27.60	19.20	2010.00	260.00
Marine aquatic ecotox.	kg 1,4-DB eq	5.45	12.08	3.55	3.21	4950.00	409.00	11.10	578.00	64.83
Terrestrial ecotoxicity	10^{-5} kg 1,4-DB eq	20.47	24.90	2.54	1.68	44.80	38.30	14.20	335.00	53.10
Photochemical oxidation	10^{-6} kg C_2H_4	127.29	129.29	4.88	1.93	662.00	56.00	15.90	839.00	116.00

(Part 2/2)

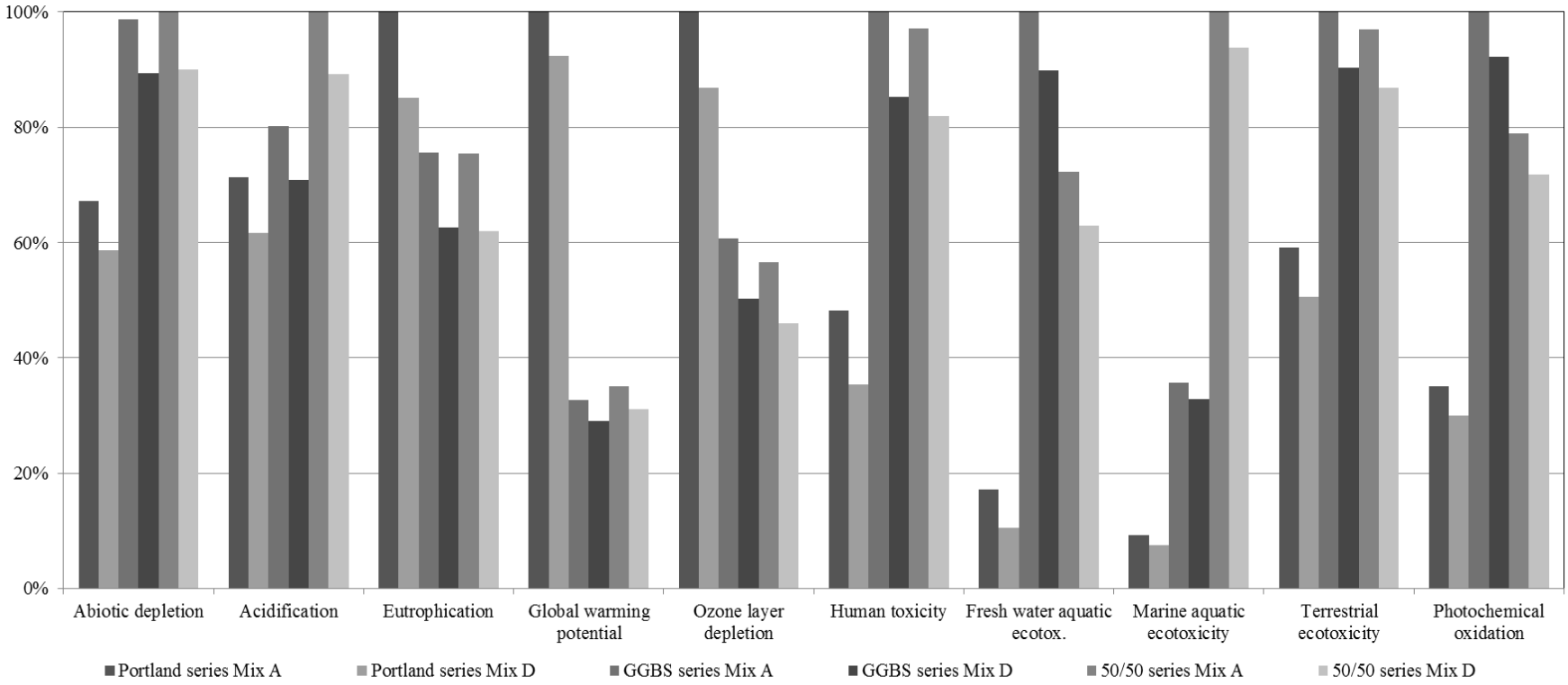

Figure 103 Comparative environmental impact for mixes A and D of the designed concrete series (Economic allocation for GGBS and FA).

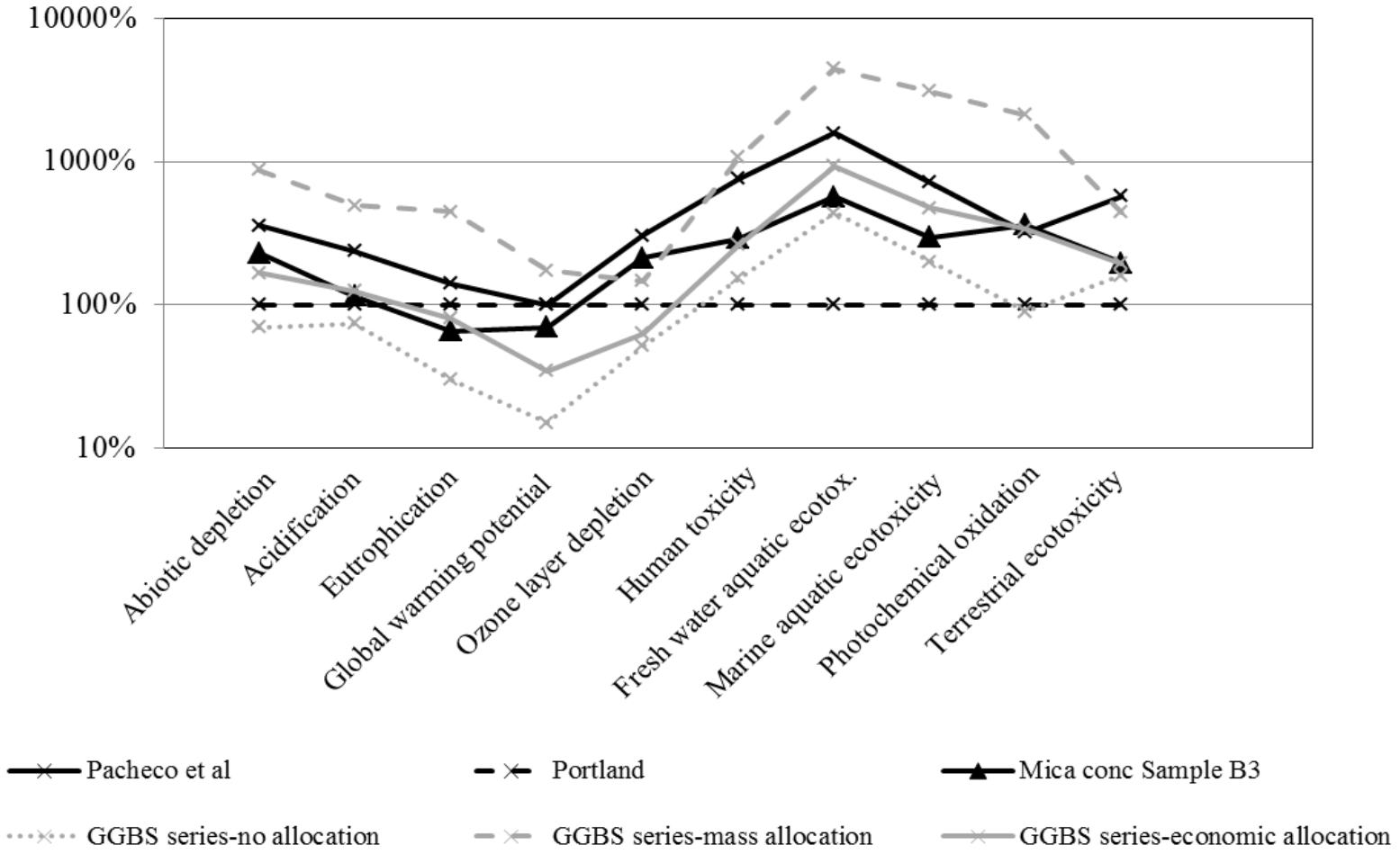

Figure 104 Comparison of the environmental impact of pastes based on 1kg of cement/precursor and water to binder (or cement) ratio approx. 0.40. The shown GGBS series is calculated based on binder S3 (but scaled to reach 1kg of GGBS).

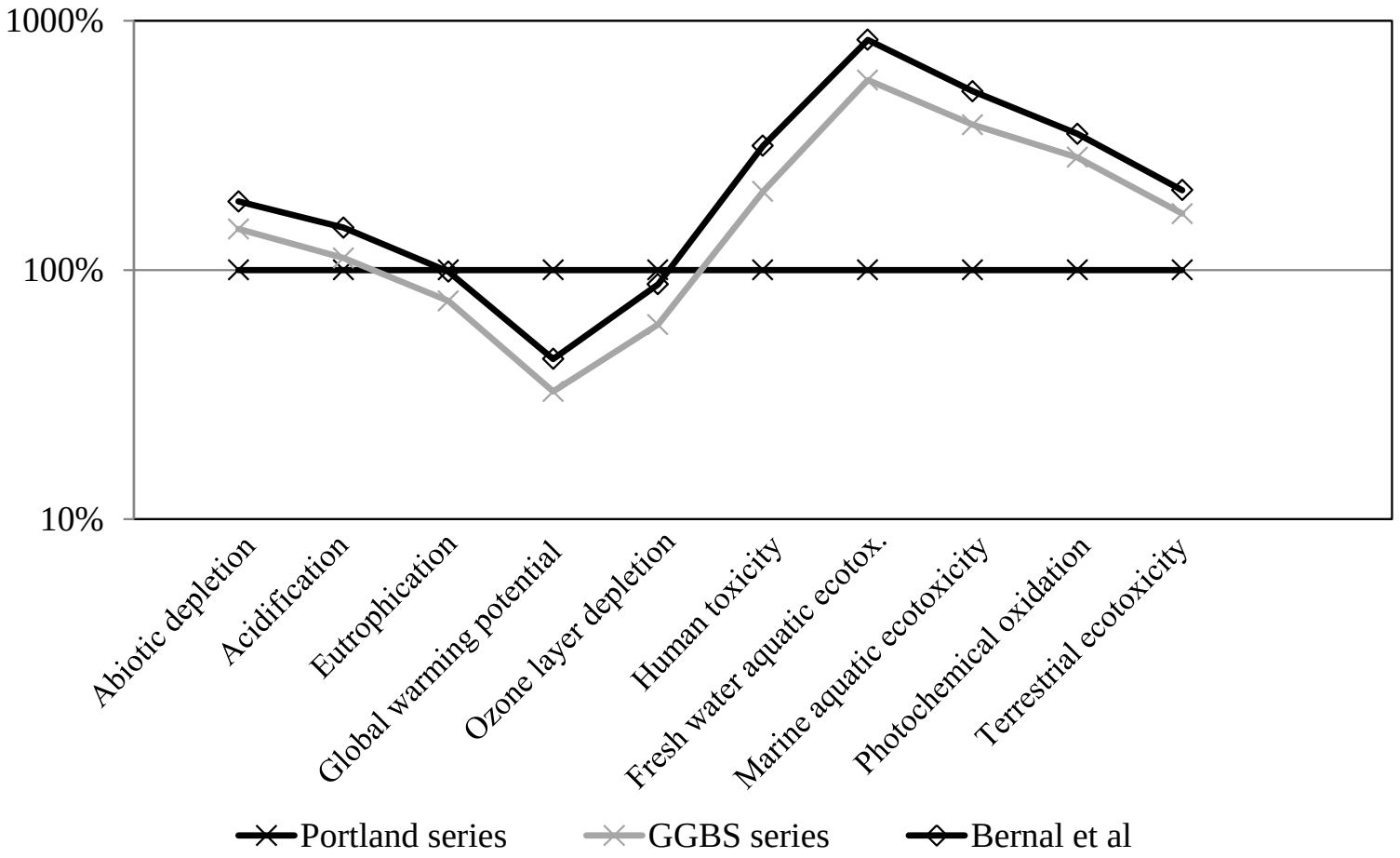

Figure 105 Comparison of the environmental impact between PC concrete based on 380kg/m^3 PC and AA concrete based on 329kg/m^3 and 400kg/m^3 slag (GGBS series and Bernal et al respectively). Calculated for economic allocation of slag.

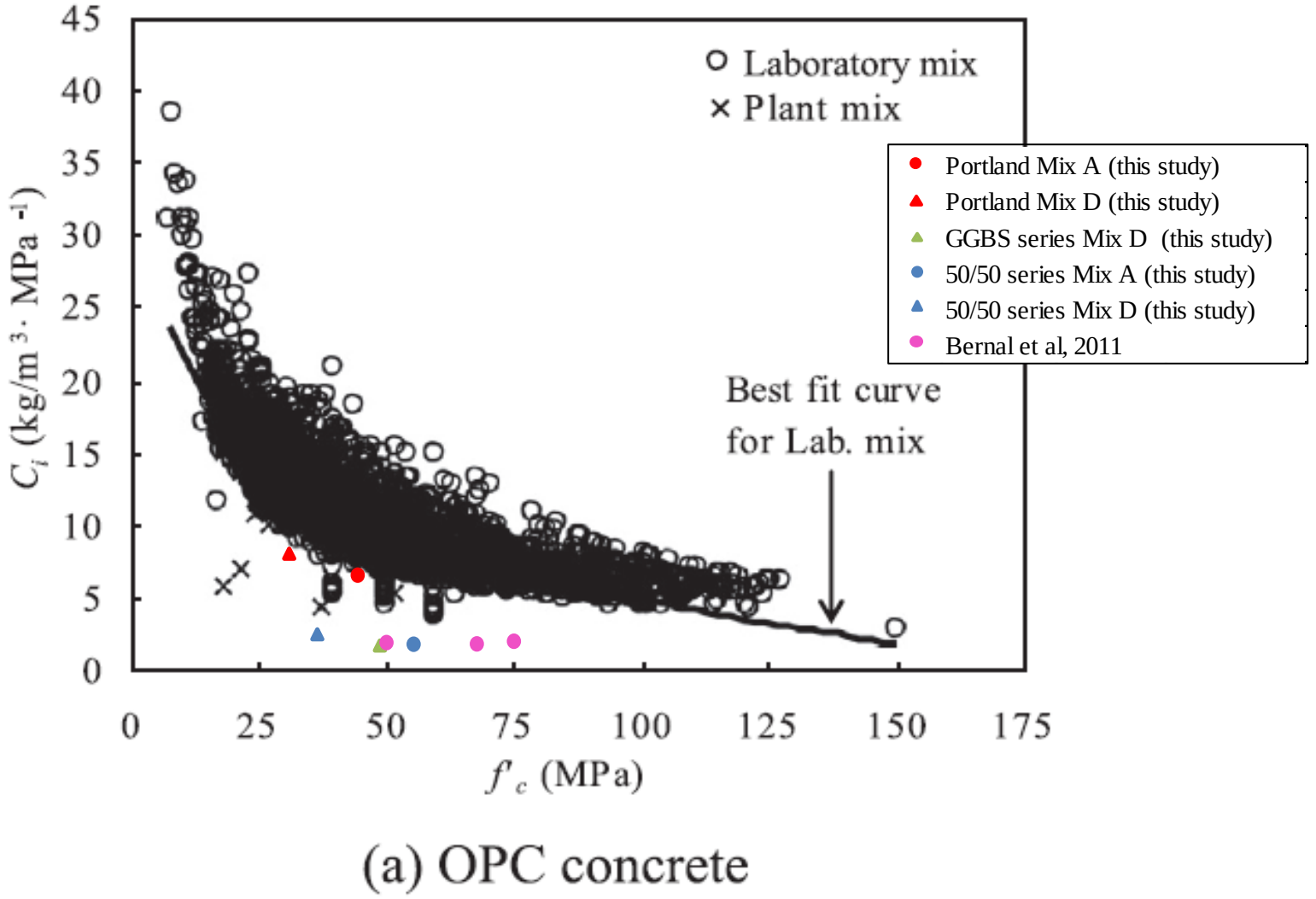

Figure 106 Comparing the Ci of AAC with OPC mixes. Data added in a graph by Yang et al. (2014)

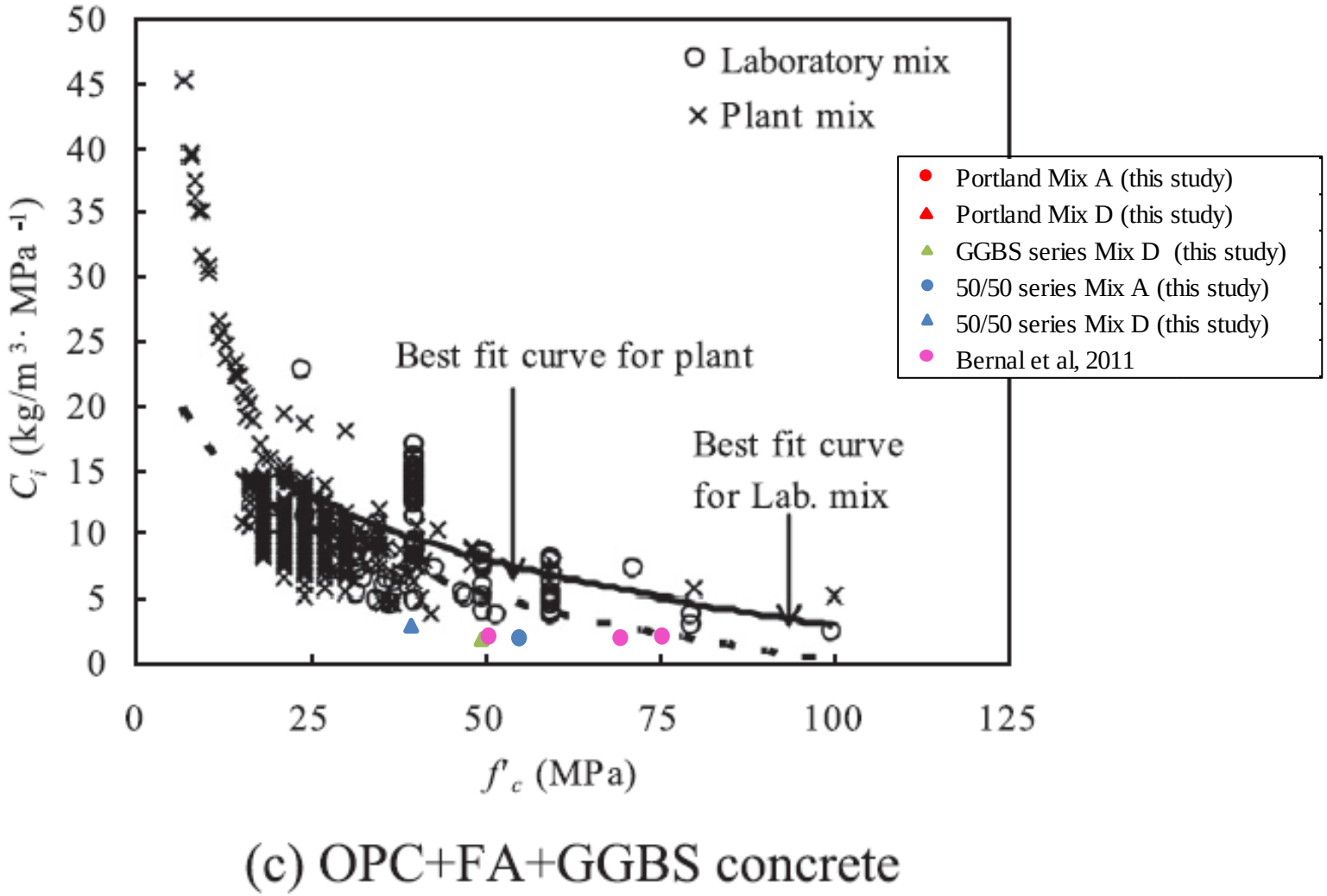

Figure 107 Comparing the Ci of AAC with OPC+FA+GGBS mixes. Data added in a graph by Yang et al. (2014)

6.4 Conclusions of chapter

Primary aggregate was gradually replaced by china clay waste in AAC and Portland control mixes and the following conclusions have been made:

- The reported overall water content is higher for increasing percentage of waste, trying to keep constant slump of 70-80mm. This slump is higher than the slump typically used for concrete blocks, but was necessary for consistent strengths. The process for manufacturing blocks may have to be modified if the mixes presented here are to be used, but this should be done in conjunction with a commercial block manufacturer using their high energy compaction processes.
- For such high water contents, but not higher than those used in mortars, the compressive strength followed again a decreasing trend: a 20% decrease for use of stent and CCS and additional decrease for use of MW that was observed to be higher in the case of the 50/50 series (17%) than to Portland (8%).
- The AA concrete had stains for use of stent which disappeared over time. The stains were attributed to agglomerates of fine particles.
- As in the scientific literature AAM are reported to be superior than Portland in freeze-thaw and the specifications for blocks and tiles have low requirement in strength (before and after the durability test) it is expected that china clay waste would be successful replacement of primary aggregate in geopolymeric concrete.
- It is observed that the CO_2 emissions for the production of the designed AAC mixes is 1/3 the carbon emission of the Portland equivalent mixes and AA slag using china clay waste can replace Portland using primary aggregate. However, other environmental categories, especially those related to toxicity, are significantly influenced in negative way.
- For lower binder: aggregate ratios the environmental benefit would be higher and this should be considered in future work. This would require a test programme of optimizing mixes and would be linked to product development.

Chapter 7: **Conclusions and future work**

7.1 Conclusions

The following conclusions were made in response to the initial aims of this study, highlighted in section 1.4:

1) The results showed that the china clay waste is unlikely to be suitable as precursor for cost-effective and low impact AA binders.

First, it was shown that the finest fraction of the waste, the MW, which was initially considered to have potentials due to its fineness (max particle size just over 0.5mm) and mica mineral content, consists mostly of inert minerals and it does not show pozzolanic properties. The MW was used unheated and calcined because from the literature review it was shown that mica particles in the waste could be reactive when muscovite is dehydroxylated; A case equivalent to transforming kaolin into the reactive metakaolin. It was therefore believed that the dehydroxylated mica particles could improve the microstructure of the mortar by enhancing the ITZ, taking also into account that the AA binders are based on aluminosilicates. However, either the CMW was reactive. This conclusion was made based on the performance of CMW in the activity index test according to BS EN 450-1:2012 and the poor performance of CMW compared to MW, as aggregate in GGBS and/or FA-based AA cement mortars. On a microscopic level there were no indications of dissolution of the mica particles in these mortars.

Moreover, it was observed that the dehydroxylated mica mineral from Cornwall shows some reactivity when in contact with an alkaline activator but not sufficient to result in a strong binder. The optimum temperature was 950°C. The study focused on the investigation of the pozzolanic index of mica mineral by using and processing a mica-rich material (mica concentrate, 74% in mica mineral). Requirements for natural mineral based geopolymers were partially satisfied (XRD showed some amorphous content at elevated temperature, calcined material exceeded the pozzolanic criteria based on BS EN 450-1:2012) but based on literature some indications which were initially positive were finally considered uncertain (aluminum in four coordination). Even kaolin and illite (unheated) which have poor performance as pozzolans in PC system, were more reactive than mica concentrate on its own right (kaolin, illite and mica concentrate activated using NaOH). Only addition of hydrated lime in the natural mineral based mix enhanced the properties of the hardened material. The highest reached strength was 19MPa on the 28 days and was obtained for low water to binder ratio (equal to 0.40) and 20% $Ca(OH)_2$. This strength is likely enough to develop unreinforced products, however the environmental impact of the binder was assessed to have limited advantage over

PC. It is unlikely that it would maintain that advantage after taking into account the energy and materials needed for processing the MW into mica concentrate. It was also observed that the compressive strength would drop quickly for raising the water to binder ratio from 0.40 to 0.45.

It was also shown that the mix design procedure used by Pacheco-Torgal et al. (2008,d) was not suitable for the mica concentrate, even if the environmental impact fulfilled the goals of this current research project. The investigation rather confirmed the results of pyrophyllite, where the 2:1 lattice is a barrier and the Si layer makes it difficult to access the five and four coordinated Al.

2) MW and fine sand (sand 0/4 tested in this study) from china clay extraction can be used in AA cement mortars based on GGBS and 50% GGBS/50% FA. The effect of using the fine fractions of the waste had a detrimental effect on FA-based geopolymer mortar.

However, it is noted that the high water demand of the waste resulted in lower strength of the test samples compared to the strength of control samples using standard sand. Also, the impact of water appears greater in AA binders than in the equivalent Portland based systems. Over time the impact of extra water in mixes was reduced in the case of AA binders. To understand the order of strength for mortars using MW and for the given raw materials and binder formulation used: CEM I 52.5N Portland system gave 27MPa on day 28 (approx. 90% of the strength of the control mix using standard sand on that day), GGBS series gave 36MPa on day 28 (approx. 66% of the AA GGBS control mix) and 50MPa after 6months of curing (approx. 71% of the control mix), 50/50 series gave 29MPa (approx. 58% of the 50/50 control mix) and 48MPa after 6months of curing (approx. 82% of the control mix on that day). Therefore, based on these values, the GGBS and 50/50 series show equivalent or improved compressive strength than the PC series. The reduction for using MW as aggregate was lower compared to previous research. This previous research was based on mixes which did not account for the increase in volume for muscovite used as aggregate, which provided a net decrease in binder content per unit volume.

It is noted, that the viscosity of the optimum FA-based paste which was used for making mortars, made it difficult to incorporate highly absorbent sands and worked well only when using standard sand. It is possible that an activator with lower SiO_2 content, to lower the viscosity, or higher ratio of binder to sand could provide reasonable strength for use of the fine fractions of the waste. However, based on the results for FA-based binders it is seen that for the given raw FA and activators containing lower SiO_2 the strength easily drops to 30MPa (low strength for an AA binder) for fluid mixes. On the other hand, from an environmental point of view it is not advised to increase the binder to sand ratio, especially since there are other mixes (GGBS-based and 50/50-based) which can provide higher strength with lower alkalinity and environmental impact. To conclude, the FA-based binder

incorporating fine fractions of the waste could possibly work if formulated differently but is still not suggested as a precursor.

3) In terms of strength it is possible to use all waste streams in manufacturing of geopolymeric block or roof tiles. However, the mix designs used are not necessarily appropriate for such products and they should be optimized. Durability should be tested for any final, optimized products (dimensions for roof tiles needed).

The results of the concrete mixes showed that reductions in strength should be expected for a similar binder content: for the current design there was a 20% decrease for use of stent and sand and an additional decrease for use of MW. It was observed to be higher in the case of the 50/50 series (17%) than to Portland (8%). It was also shown that GGBS series of concrete using the waste as aggregate could achieve strength approximately equal to the strength of PC concrete using virgin aggregates.

As in the scientific literature AAM are reported to be superior than Portland in freeze-thaw and the specifications for blocks and roof tiles have low requirement in strength (which applies before and after the durability test) it is expected that china clay waste would be a successful replacement of primary aggregate in AA cement concrete block and roof tiles. However, the coefficient of water absorption due to capillary action showed that the 50/50 series had greater capillary sorptivity than the Portland series. This was an unfavorable result and in contrast to a number of previous studies. Previous studies referred to robust AAC, meaning high content of precursor, low water/binder ratio and/or significantly higher strength that PC. The trend in this study was attributed to the lower quality of concrete due to addition. It is expected that this would not be an issue in an optimized mix/product which would require minimum water content.

It should be noted that there were stains observed in the AA cement concrete when using stent. These were attributed to agglomerates of leftover kaolin, mica and generally very fine particles combined with the fact that the water absorbed by these agglomerates locally weakened the alkali-activated binder. As Portland is not equally susceptible to water, there were no stains observed in the Portland specimens. If this issue cannot be resolved in the optimized mix of the AA concrete, it is considered likely that material might be locally scaled from the stains during freeze-thaw. This is unlikely to affect the overall strength, but may influence visual appearance.

4) For the current concrete design and based on economic allocation for GGBS and FA, there is a 2/3 decrease in the carbon emissions for use of alkali-activated series compared to Portland mixes with similar binder contents. There is also marginal benefit in eutrophication and ozone layer depletion. Using a lower binder to aggregate ratio in the optimized mix/product would lead to even lower values in these environmental categories. Using the standard environmental impact categories in the CML 2001 method, the positive impact of replacing primary

aggregate by forms of the china clay waste is minimal, but this does not include cost or socio-economic factors such as the visual impact of the waste heaps.

The environmental assessment considered also the carbon emissions of the concrete mixes in regard to their strength, by calculating the carbon emission intensity (C_i). According to this factor, it was shown that the advantage of AAM over PC in global warming potential is indisputable; however, compared to the more advanced technology PC systems (including slag and FA) the advantage is limited.

On the other hand, the other environmental categories in the CML 2001 methods, especially these related to toxicity, are influenced negatively when replacing PC based concrete with AA based concretes of similar binder content. A decision regarding the implementation of AA blocks and roof tiles using china clay waste in Cornwall and elsewhere should take that effect into consideration. Attention should be drawn to the different allocations for GGBS and FA, as they have a large impact on the environmental impact. The economic allocation shows mid values compared to the extremes of no allocation and mass allocation, and is considered representative which is why most of the calculations are based on it.

7.2 General remarks and Future work

The laboratory tests showed that alkali-activated pastes are a ”dynamic” type of cement as they easily reach high strength and they continue gaining strength over time while PC does not significantly increase its strength over the 28th day of curing. However, their strength and properties are easily affected by a number of parameters. The current research showed how the composition of AA pastes was tailored based to the chemistry of the given precursors and the same process has to be done for every new batch of GGBS and FA. It was also observed that for the small-dimension-mortar-specimens, the curing conditions were of crucial importance (constant, high relative humidity needed), while for larger specimens (concrete cubes) changes in the curing conditions were less important. By extension, large specimens are likely better for repeatable tests.

Products made with well formulated binders and using an optimum ratio of binder to aggregate will show not only high strength but good overall properties. This means that the extra water added when replacing the primary aggregate with waste forms will most likely negatively affect the other mechanical properties (flexural strength, water absorption, carbonation). However, this is not a barrier for implementation of blocks and roof tiles which have low requirements for mechanical strength, allowing optimization of the binder to aggregate ratio for further favourable environmental impact.

Future work should focus to the following:

- Finding a successful superplasticizer. Stent, sand and MW would give much higher strengths when used in alkali-activated mortar and concrete if less water was added.

- Optimization of the concrete mix. That includes decisions on the max particle size needed for the targeted applications, optimization of the particle size distribution of the total aggregate, including the bulking or volume factors for the different forms of the waste, adjustment of the quantities of material in $1m^3$ for using extra water and decision regarding the optimum manufacturing conditions (pressure applied, trial dimensions). The work of Burciaga-Díaz et al. (2013) is helpful for a first look in blocks with low ratio of AA binder to aggregate, although it is reminded that no results were reported regarding shrinkage and strength was only reported up to day 28.
- Resolving the issue of stains on concrete for use of stent. It is suggested that using soaked aggregates for mixing might help so that the agglomerates which cause the problem will be dissolved during mixing and equally distributed in the mix.
- Once an optimized, final mix concrete design is reached, durability issues should be addressed. For blocks: Water absorption by capillarity and freeze-thaw resistance should be tested. Moisture movement has also to be declared for the product. For roof tiles: resistance to freeze-thaw and water impermeability. A suitable mix design is expected to be able to produce products which meet the required durability properties.
- The cost and broader issues (such as socio-economic factors) should be investigated, as these will be a part in the success of the Cornwall Eco-town.

References

AGARWAL, S. K. 2006. Pozzolanic activity of various siliceous materials. *Cement and Concrete Research,* 36**,** 1735-1739.

AHMARI, S. & ZHANG, L. 2013a. Durability and leaching behavior of mine tailings-based geopolymer bricks. *Construction and Building Materials,* 44**,** 743-750.

AHMARI, S. & ZHANG, L. 2013b. Utilization of cement kiln dust (CKD) to enhance mine tailings-based geopolymer bricks. *Construction and Building Materials,* 40**,** 1002-1011.

ALLABY, M. 2008. *A Dictionary of Earth Sciences,* Oxford, Oxford University Press.

ALLEN, A. J., THOMAS, J. J. & JENNINGS, H. M. 2007. Composition and density of nanoscale calcium-silicate-hydrate in cement. *Nat Mater,* 6**,** 311-316.

ANGELICA, R. 2006. Possible uses of kaolin wastes and transformed materials from the Amazon region (northern Brazil) for environmental applications. *Chinese Journal of Geochemistry,* 25**,** 25-25.

ARELLANO-AGUILAR, R., BURCIAGA-DÍAZ, O., GOROKHOVSKY, A. & ESCALANTE-GARCÍA, J. I. 2014. Geopolymer mortars based on a low grade metakaolin: Effects of the chemical composition, temperature and aggregate:binder ratio. *Construction and Building Materials,* 50**,** 642-648.

AZEREDO, G. & DINIZ, M. 2013. Self-compacting concrete obtained by the use of kaolin wastes. *Construction and Building Materials,* 38**,** 515-523.

BAILEY, S. W. 1984. *REVIEWS IN MINERALOGY. VOLUME 13: MICAS*.

BAKHAREV, T., SANJAYAN, J. G. & CHENG, Y. B. 2000. Effect of admixtures on properties of alkali-activated slag concrete. *Cement and Concrete Research,* 30**,** 1367-1374.

BAKHAREV, T., SANJAYAN, J. G. & CHENG, Y. B. 2001. Resistance of alkali-activated slag concrete to carbonation. *Cement and Concrete Research,* 31**,** 1277-1283.

BARLOW, S. G. & MANNING, D. A. C. 1999. Influence of time and temperature on reactions and transformations of muscovite mica. *British Ceramic Transactions,* 98**,** 122-126.

BASTOS, A. M., SOUSA, H. & MELO, A. F. 2005. Methodology for the Design of Lightweight Concrete with Expanded Clay Aggregate. *TMS Journal,* 23**,** 73-84.

BBC. 2012. *St Austell's eco town project 'on hold'* [Online]. Available: http://www.bbc.co.uk/news/uk-england-cornwall-20606304 [Accessed 04/ 08/ 2014].

BEAUDOIN, J. J. 1983. Properties of portland cement paste reinforced with mica flakes. *Cement and Concrete Research,* 13**,** 153-160.

BERNAL, S. A., MEJÍA DE GUTIÉRREZ, R., PEDRAZA, A. L., PROVIS, J. L., RODRIGUEZ, E. D. & DELVASTO, S. 2011. Effect of binder content on the performance of alkali-activated slag concretes. *Cement and Concrete Research,* 41**,** 1-8.

BERNAL, S. A., MEJÍA DE GUTIÉRREZ, R. & PROVIS, J. L. 2012a. Engineering and durability properties of concretes based on alkali-activated granulated blast furnace slag/metakaolin blends. *Construction and Building Materials,* 33**,** 99-108.

BERNAL, S. A., PROVIS, J. L., BRICE, D. G., KILCULLEN, A., DUXSON, P. & VAN DEVENTER, J. S. J. 2012b. Accelerated carbonation testing of alkali-activated

binders significantly underestimates service life: The role of pore solution chemistry. *Cement and Concrete Research,* 42**,** 1317-1326.
BERNAL, S. A., PROVIS, J. L., WALKLEY, B., SAN NICOLAS, R., GEHMAN, J. D., BRICE, D. G., KILCULLEN, A. R., DUXSON, P. & VAN DEVENTER, J. S. J. 2013. Gel nanostructure in alkali-activated binders based on slag and fly ash, and effects of accelerated carbonation. *Cement and Concrete Research,* 53**,** 127-144.
BERNAL, S. A., SAN NICOLAS, R., MYERS, R. J., MEJÍA DE GUTIÉRREZ, R., PUERTAS, F., VAN DEVENTER, J. S. J. & PROVIS, J. L. 2014. MgO content of slag controls phase evolution and structural changes induced by accelerated carbonation in alkali-activated binders. *Cement and Concrete Research,* 57**,** 33-43.
BFTINTERNATIONAL 2011. Geopolymer binders: Ecological and economic analyses of geopolymer concrete mixes for external structural elements. *CONCRETE TECHNOLOGY | BETONTECHNOLOGIE*.
BGS 2009. Kaolin - Mineral Planning Factsheet. British Geological Survey.
BGS 2011. World mineral production 2005-2009. *In:* SURVEY), B. B. G. (ed.). Keyworth, Nottingham.
BORGES, P. H. R., FONSECA, L. F., NUNES, V. A., PANZERA, T. H. & MARTUSCELLI, C. C. 2014. Andreasen particle packing method on the development of geopolymer concrete for civil engineering. *Journal of Materials in Civil Engineering,* 26**,** 692-697.
BOUZIDI, N., SIHAM, A., CONCHA-LOZANO, N., GAUDON, P., JANIN, G., MAHTOUT, L. & MERABET, D. 2014. Effect of chemico-mineralogical composition on color of natural and calcined kaolins. *Color Res. Appl.,* 39**,** 499–505.
BRE 2010a. BRE Wales and South. Building Research Establishment Ltd.
BRE. 2010b. *News November 2010: Clay Country, Cornwall. (Image: Pilot Scheme / West Carclaze & Baal)* [Online]. Available: http://www.eco-development-group.org/news.html [Accessed 05/ 09/ 2012].
BRICE, D. G., DUXSON, P., KILCULLEN, A. R. & VAN, D. J. S. J. 2012. Settable composition comprising slag. Google Patents.
BROEKMANS, M. A. T. M. 2002. *The alkali-silica reaction: mineralogical and geochemical aspects of some Dutch concretes and Norwegian mylonites.* PhD Thesis (217), University of Utrecht.
BROUGH, A. R. & ATKINSON, A. 2002. Sodium silicate-based, alkali-activated slag mortars: Part I. Strength, hydration and microstructure. *Cement and Concrete Research,* 32**,** 865-879.
BSI 1999. BS EN 1015-2: Methods of test for mortar for masonry. Bulk sampling of mortars and preparation of test mortars.
BSI 2002. BS EN 12620:2002+A1:2008: Aggregates for concrete.
BSI 2005a. BS EN 196-1: Methods of testing cement. Determination of strength.
BSI 2005b. BS EN 196-3: 2005+A1: 2008: Methods of testing cement - Part 3: Determination of setting times and soundness.
BSI 2006a. BS 8500-1:2006+A1:2012: Concrete. Complementary British Standard to BS EN 206-1. Method of specifying and guidance for the specifier.
BSI 2006b. BS 8500-2:2006+A1:2012: Concrete. Complementary British Standard to BS EN 206-1. Specification for constituent materials and concrete.
BSI 2009. BS EN 12350-2: Testing fresh concrete. Slump-test.
BSI 2011a. BS EN 491: Concrete roofing tiles and fittings for roof covering and wall cladding. Test methods.

BSI 2011b. BS EN 771-3: Specification for masonry units. Aggregate concrete masonry units (dense and lightweight aggregates).
BSI 2011c. BS EN 772-11: Methods of test for masonry units. Determination of water absorption of aggregate concrete, autoclaved aerated concrete, manufactured stone and natural stone masonry units due to capillary action and the initial rate of water absorption of clay masonry units.
BSI 2012. BS EN 1745: Masonry and masonry products. Methods for determining thermal properties.
BSI 2013a. BS EN 206: Concrete. Specification, performance, production and conformity.
BSI 2013b. BS EN 1097-6: Tests for mechanical and physical properties of aggregates. Determination of particle density and water absorption.
BUCHWALD, A., HOHMANN, M., POSERN, K. & BRENDLER, E. 2009. The suitability of thermally activated illite/smectite clay as raw material for geopolymer binders. *Applied Clay Science,* 46**,** 300-304.
BURCIAGA-DÍAZ, O., DÍAZ-GUILLÉN, M. R., FUENTES, A. F. & ESCALANTE-GARCIA, J. I. 2013. Mortars of alkali-activated blast furnace slag with high aggregate:binder ratios. *Construction and Building Materials,* 44**,** 607-614.
CAI, L., WANG, H. & FU, Y. 2013. Freeze–thaw resistance of alkali–slag concrete based on response surface methodology. *Construction and Building Materials,* 49**,** 70-76.
CEMEX. 2012. *Fly Ash Products. CEMEX 450 S.* [Online]. Available: http://www.cemex.co.uk/fly-ash-products.aspx [Accessed May 29 2012].
CHEN, C., HABERT, G., BOUZIDI, Y., JULLIEN, A. & VENTURA, A. 2010. LCA allocation procedure used as an incitative method for waste recycling: An application to mineral additions in concrete. *Resources, Conservation and Recycling,* 54**,** 1231-1240.
CHERIAF, M., ROCHA, J. C. & PÉRA, J. 1999. Pozzolanic properties of pulverized coal combustion bottom ash. *Cement and Concrete Research,* 29**,** 1387-1391.
CHI, M. & HUANG, R. 2013. Binding mechanism and properties of alkali-activated fly ash/slag mortars. *Construction and Building Materials,* 40**,** 291-298.
CHINDAPRASIRT, P., DE SILVA, P., SAGOE-CRENTSIL, K. & HANJITSUWAN, S. 2012. Effect of SiO2 and Al2O3 on the setting and hardening of high calcium fly ash-based geopolymer systems. *Journal of Materials Science,* 47**,** 4876-4883.
CHRISTIE, T., THOMPSON, B. & BRATHWAITE, B. 2007. Mineral Commodity Report 20 - Clays. Institute of Geological and Nuclear Sciences.
COLLINS, F. & SANJAYAN, J. G. 1999. Effects of ultra-fine materials on workability and strength of concrete containing alkali-activated slag as the binder. *Cement and Concrete Research,* 29**,** 459-462.
CONCRETE INSTITUTION OF AUSTRALIA 2011. Z16 - Geopolymer Recommended Practice Handbook.
CRIADO, M., FERNÁNDEZ-JIMÉNEZ, A., DE LA TORRE, A. G., ARANDA, M. A. G. & PALOMO, A. 2007. An XRD study of the effect of the SiO_2/Na_2O ratio on the alkali activation of fly ash. *Cement and Concrete Research,* 37**,** 671-679.
DAMINELI, B. L., KEMEID, F. M., AGUIAR, P. S. & JOHN, V. M. 2010. Measuring the eco-efficiency of cement use. *Cement and Concrete Composites,* 32**,** 555-562.
DAVIDOVITS, F., DAVIDOVITS, J., DAVIDOVITS, M. & DAVIDOVITS, R. 2012. Geopolymer cement of the calcium ferro-aluminosilicate polymer type and production process. Google Patents.

DAVIDOVITS, J. 1991. Geopolymers - Inorganic polymeric new materials. *Journal of Thermal Analysis,* 37**,** 1633-1656.
DAVIDOVITS, J. 2005. Geopolymer chemistry and sustainable development. The poly(sialate) terminology: a very useful and simple model for the promotion and understanding of green-chemistry. In: Proceedings of 2005 geopolymere conference.
DAVIDOVITS, J. 2011. *Geopolymer Chemistry and Applications,* Saint-Quentin, France.
DAVIDOVITS, J. & DAVIDOVICS, M. 1988. Geopolymer: room-temperature ceramic matrix for composites. *Ceramic engineering science proceedings,* 9**,** 835-842.
DE LARRARD, F. & BELLOC, A. 1999. The influence of the aggregate on the compressive strength of concrete. *Bulletin des Laboratoires des Ponts et Chaussees***,** 41.
DE PAIVA GOMES NETO, D., CONCEIÇÃO, H., LISBOA, V. A. C., DE PAIVA SANTANA, R. S. & BARRETO, L. S. 2014. Influence of granitic aggregates from Northeast Brazil on the alkali-aggregate reaction. *Materials Research,* 17**,** 51-58.
DE VARGAS, A. S., DAL MOLIN, D. C. C., VILELA, A. C. F., SILVA, F. J. D., PAVÃO, B. & VEIT, H. 2011. The effects of Na2O/SiO2 molar ratio, curing temperature and age on compressive strength, morphology and microstructure of alkali-activated fly ash-based geopolymers. *Cement and Concrete Composites,* 33**,** 653-660.
DEVINEAU, K., DEVOUARD, B., VILLIERAS, F., FAURE, F., DEVIDAL, J. L. & KOHLER, A. 2006. Evolution of product phase assemblages during thermal decomposition of muscovite under strong disequilibrium conditions. *American Mineralogist,* 91**,** 413-424.
DEWAR, J. 1963. *Effect of mica in the fine aggregate on the water requirement and strength of concrete.* Technical Report TRA/370. Slough, UK: Cement and Concrete Association.
DONATELLO, S., TYRER, M. & CHEESEMAN, C. R. 2010. Comparison of test methods to assess pozzolanic activity. *Cement and Concrete Composites,* 32**,** 121-127.
DOUGLAS, E. & BRANDSTETR, J. 1990. A preliminary study on the alkali activation of ground granulated blast-furnace slag. *Cement and Concrete Research,* 20**,** 746-756.
DOWNS, R. T. & HALL-WALLACE, M. 2003. American Mineralogist Crystal Structure Database. *The American Mineralogist*
DURAN ATIŞ, C., BILIM, C., ÇELIK, O. & KARAHAN, O. 2009. Influence of activator on the strength and drying shrinkage of alkali-activated slag mortar. *Construction and Building Materials,* 23**,** 548-555.
DUXSON, P., FERNÁNDEZ-JIMÉNEZ, A., PROVIS, J. L., LUKEY, G. C., PALOMO, A. & DEVENTER, J. S. J. 2007a. Geopolymer technology: the current state of the art. *Journal of Materials Science,* 42**,** 2917-2933.
DUXSON, P., FERNÁNDEZ-JIMÉNEZ, A., PROVIS, J. L., LUKEY, G. C., PALOMO, A. & VAN DEVENTER, J. S. J. 2007b. Geopolymer technology: The current state of the art. *Journal of Materials Science,* 42**,** 2917-2933.
DUXSON, P., PROVIS, J. L., LUKEY, G. C., MALLICOAT, S. W., KRIVEN, W. M. & VAN DEVENTER, J. S. J. 2005. Understanding the relationship between geopolymer composition, microstructure and mechanical properties. *Colloids and Surfaces A: Physicochemical and Engineering Aspects,* 269**,** 47-58.

DUXSON, P., PROVIS, J. L., LUKEY, G. C. & VAN DEVENTER, J. S. J. 2007c. The role of inorganic polymer technology in the development of 'green concrete'. *Cement and Concrete Research,* 37**,** 1590-1597.

ECO-DEVELOPMENTGROUP. 2012. *Clay Country, St Austell* [Online]. Available: http://www.eco-development-group.org/exemplars/clay-country-st-austell.html [Accessed 31/ 08 2012].

ECOBOND 2007. Characterisation of Mineral Wastes, Resources and Processing tecnologies - Integrated waste management for the production of construction material.

EIPPCB 2012. Manufacture of Glass. *Industrial Emissions Directive (2010/75/EU).*

FAWER, M., CONCANNON, M. & RIEBER, W. 1999. Life cycle inventories for the production of sodium silicates. *International Journal of Life Cycle Assessment,* 4**,** 207-212.

FERNANDES, V. A., PURNELL, P., STILL, G. T. & THOMAS, T. H. 2007. The effect of clay content in sands used for cementitious materials in developing countries. *Cement and Concrete Research,* 37**,** 751-758.

FERNÁNDEZ-JIMÉNEZ, A. & PALOMO, A. 2003. Characterisation of fly ashes. Potential reactivity as alkaline cements. *Fuel,* 82**,** 2259-2265.

FERNÁNDEZ-JIMÉNEZ, A. & PALOMO, A. 2005. Composition and microstructure of alkali activated fly ash binder: Effect of the activator. *Cement and Concrete Research,* 35**,** 1984-1992.

FERNÁNDEZ-JIMÉNEZ, A., PALOMO, A. & CRIADO, M. 2005. Microstructure development of alkali-activated fly ash cement: a descriptive model. *Cement and Concrete Research,* 35**,** 1204-1209.

FERNÁNDEZ-JIMÉNEZ, A., PALOMO, J. G. & PUERTAS, F. 1999. Alkali-activated slag mortars: Mechanical strength behaviour. *Cement and Concrete Research,* 29**,** 1313-1321.

FERNÁNDEZ-JIMÉNEZ, A. & PUERTAS, F. 2003. Effect of activator mix on the hydration and strength behaviour of alkali-activated slag cements. *Advances in Cement Research,* 15**,** 129-136.

FERNÁNDEZ-JIMÉNEZ, A., PUERTAS, F., SOBRADOS, I. & SANZ, J. 2003. Structure of Calcium Silicate Hydrates Formed in Alkaline-Activated Slag: Influence of the Type of Alkaline Activator. *Journal of the American Ceramic Society,* 86**,** 1389-1394.

FLURY, K. & FRISCHKNECHT, R. 2012. Life Cycle Assessment of Rock Wool Insulation. Uster: ESU-services Ltd., fair consulting in sustainability.

FOOKES, P. G. 1980. An introduction to the influence of natural aggregates on the performance and durability of concrete. *Quarterly Journal of Engineering Geology and Hydrogeology,* 13**,** 207-229.

FOOKES, P. G. & REVIE, W. A. 1982. Mica in concrete- a case history from Eastern Nepal. *Concrete (Journal of the Concrete Society),* 16**,** p. 12-16.

FORDE, M. C. & INSTITUTION OF CIVIL, E. (eds.) 2009. *ICE manual of construction materials. Volume I. Fundamentals and theory, Concrete, Asphalts in road construction, Masonry,* London: Thomas Telford.

FORDER, I. 1971. An examination of the properties of some concreting sands in the South West of England. Section 4: Some effects of mica in concrete mixes. Slough, UK,: Cement and Concrete Association.

GARTNER, E. 2004. Industrially interesting approaches to "low-CO2" cements. *Cement and Concrete Research,* 34**,** 1489-1498.

GARTNER, E. M. & MACPHEE, D. E. 2011. A physico-chemical basis for novel cementitious binders. *Cement and Concrete Research,* 41**,** 736-749.
GEBREGZIABIHER, B. S., THOMAS, R. & PEETHAMPARAN, S. 2015. Very early-age reaction kinetics and microstructural development in alkali-activated slag. *Cement and Concrete Composites,* 55**,** 91-102.
GLUKHOVSKY, V. 1959 Soil silicates. Gosstroyizdat. 154pp.
GOEDKOOP, M., OELE, M., DE SCHRYVER, A. & VIEIRA, M. 2008. SimaPro Database Manual. Methods library PRé Consultants.
GOMES, K. C., ROCHA, B. D., FERREIRA, D. T. A., LIRA, E. C., TORRES, S. M., DE BARROS, S. R. & BARBOSA, N. B. 2012. Activation alkaline waste kaolin for fabrication of building blocks. *Key Engineering Materials.*
GRIDI-BENNADJI, F. & BLANCHART, P. 2007. Dehydroxylation kinetic and exfoliation of large muscovite flakes. *Journal of Thermal Analysis and Calorimetry,* 90**,** 747-753.
GUGGENHEIM, S., CHANG, Y. H. & KOSTER VAN GROOS, A. F. 1987. Muscovite dehydroxylation: high-temperature studies. *American Mineralogist,* 72**,** 537-550.
HABERT, G. 2013. Assessing the environmental impact of conventional and 'green' cement production. *Eco-Efficient Construction and Building Materials: Life Cycle Assessment (LCA), Eco-Labelling and Case Studies.*
HABERT, G., D'ESPINOSE DE LACAILLERIE, J. B. & ROUSSEL, N. 2011. An environmental evaluation of geopolymer based concrete production: reviewing current research trends. *Journal of Cleaner Production,* 19**,** 1229-1238.
HAHA, M. B., LOTHENBACH, B., LE SAOUT, G. & WINNEFELD, F. 2011. Influence of slag chemistry on the hydration of alkali-activated blast-furnace slag — Part I: Effect of MgO. *Cement and Concrete Research,* 41**,** 955-963.
HAHA, M. B., LOTHENBACH, B., LE SAOUT, G. & WINNEFELD, F. 2012. Influence of slag chemistry on the hydration of alkali-activated blast-furnace slag - Part II: Effect of Al2O3. *Cement and Concrete Research,* 42**,** 74-83.
HAMMOND, G. P. & JONES, C. I. 2008. Embodied energy and carbon in construction materials. *Proceedings of the ICE - Energy,* 161**,** 87-98.
HARDJITO, RANGAN, D. A. & VIJAYA 2005. Development and properties of low-calcium fly ash-based geopolymer concrete. Curtin University.
HARDJITO, D., CHEAK, C. C. & LEE, C. H. 2008. Strength and Setting Times of Low Calcium Fly Ash-based Geopolymer Mortar. *Modern Applied Science,* 2**,** 3-11.
HE, C., MAKOVICKY, E. & OSBÆCK, B. 1994. Thermal stability and pozzolanic activity of calcined kaolin. *Applied Clay Science,* 9**,** 165-187.
HE, C., MAKOVICKY, E. & OSBÆCK, B. 2000. Thermal stability and pozzolanic activity of raw and calcined mixed-layer mica/smectite. *Applied Clay Science,* 17**,** 141-161.
HEAH, C. Y., KAMARUDIN, H., AL BAKRI, A. M. M., BINHUSSAIN, M., LUQMAN, M., NIZAR, I. K., RUZAIDI, C. M. & LIEW, Y. M. 2013a. Influence of oxide molar ratios on kaolin geopolymers. *Advanced Science Letters,* 19**,** 3588-3591.
HEAH, C. Y., KAMARUDIN, H., BAKRI, A. M. M. A., BINHUSSAIN, M., LUQMAN, M., NIZAR, I. K., RUZAIDI, C. M. & LIEW, Y. M. 2011a. Effect of Curing Profile on Kaolin-based Geopolymers. *Physics Procedia,* 22**,** 305-311.
HEAH, C. Y., KAMARUDIN, H., MUSTAFA AL BAKRI, A. M., BNHUSSAIN, M., LUQMAN, M., KHAIRUL NIZAR, I., RUZAIDI, C. M. & LIEW, Y. M. 2013b. Kaolin-based geopolymers with various NaOH concentrations. *International Journal of Minerals, Metallurgy and Materials,* 20**,** 313-322.

HEAH, C. Y., KAMARUDIN, H., MUSTAFA AL BAKRI, A. M., LUQMAN, M., KHAIRUL NIZAR, I. & LIEW, Y. M. 2011b. Potential application of kaolin without calcine as greener concrete: A review. *Australian Journal of Basic and Applied Sciences,* 5**,** 1026-1035.
HEALTHPROTECTIONAGENCY 2009. Radon and Public Health: Report of the Independent Advisory Group on Ionising Radiation (RCE-11).
HEATH, A., PAINE, K., GOODHEW, S., RAMAGE, M. & LAWRENCE, M. 2013. The potential for using geopolymer concrete in the UK. *Proceedings of the ICE - Construction Materials,* 166**,** 195-203.
HELLER-KALLAI, L. & LAPIDES, I. 2007. Reactions of kaolinites and metakaolinites with NaOH-comparison of different samples (Part 1). *Applied Clay Science,* 35**,** 99-107.
HENDERSON, N. & ASBRIDGE, T. 2006. Using china clay waste in sprayed concrete. *Proceedings of the ICE - Waste and Resource Management,* 159**,** 29 –38.
HIGHWAYS AGENCY, W. A., SCOTTISH EXECUTIVE AND THE DEPARTMENT OF THE ENVIRONMENT FOR NOTHERN IRELAND 2004. Design Manual for Roads and Bridges: Volume 7, Section 1, Part 2, HD 35/04 Conservation and use of secondary and recycled materials.
HIGHWAYS AGENCY 2008. A30 Bodmin to Indian Queens Improvement.
HILDEBRANDO, E. A., ANDRADE, C. G. B., ROCHA JUNIOR, C. A. F. D., ANGÉLICA, R. S., VALENZUELA-DIAZ, F. R. & NEVES, R. D. F. 2014. Synthesis and characterization of zeolite NaP using kaolin waste as a source of silicon and aluminum. *Materials Research,* 17**,** 174-179.
HILLIER, S. 2000. Accurate quantitative analysis of clay and other minerals in sandstones by XRD: comparison of a Rietveld and a reference intensity ratio (RIR) method and the importance of sample preparation. *Clay Minerals,* 35**,** 291-302.
HMREVENUE&CUSTOMS. 2015. *Guidance: Rates and allowances: Aggregates Levy* [Online]. HM Revenue & Customs. Available: https://www.gov.uk/government/publications/rates-and-allowances-aggregates-levy/rates-and-allowances-aggregates-levy [Accessed April 1st 2015].
HOUNSI, A. D., LECOMTE-NANA, G. L., DJÉTÉLI, G. & BLANCHART, P. 2013. Kaolin-based geopolymers: Effect of mechanical activation and curing process. *Construction and Building Materials,* 42**,** 105-113.
HUANG, F. H., ZHOU, Z. H. & CHENG, X. 2013. Properties of waste-based geopolymer building blocks. *Applied Mechanics and Materials.*
HUSSIN, A. & POOLE, C. 2011. Petrography evidence of the interfacial transition zone (ITZ) in the normal strength concrete containing granitic and limestone aggregates. *Construction and Building Materials,* 25**,** 2298-2303.
IMERYS 2012. Mica brochure. Cornwall.
IPCC 2014. Chapter 10: Industry. *Working Group III – Mitigation of Climate Change.*
ISABELLA, C., LUKEY, G., XU, H. & VAN DEVENTER, J. S. J. 2005. The effect of aggregate particle size on formation of geopolymeric gel. *2003 ECI Conference on Advanced Materials for Construction of Bridges, Buildings and Other Structures III.*
ISMAIL, I., BERNAL, S. A., PROVIS, J. L., HAMDAN, S. & VAN DEVENTER, J. S. J. 2013a. Drying-induced changes in the structure of alkali-activated pastes. *Journal of Materials Science,* 48**,** 3566-3577.
ISMAIL, I., BERNAL, S. A., PROVIS, J. L., SAN NICOLAS, R., BRICE, D. G., KILCULLEN, A. R., HAMDAN, S. & VAN DEVENTER, J. S. J. 2013b.

Influence of fly ash on the water and chloride permeability of alkali-activated slag mortars and concretes. *Construction and Building Materials,* 48**,** 1187-1201.
JANG, J. G., LEE, N. K. & LEE, H. K. 2014. Fresh and hardened properties of alkali-activated fly ash/slag pastes with superplasticizers. *Construction and Building Materials,* 50**,** 169-176.
KASHANI, A., PROVIS, J. L., QIAO, G. G. & VAN DEVENTER, J. S. J. 2014. The interrelationship between surface chemistry and rheology in alkali activated slag paste. *Construction and Building Materials,* 65**,** 583-591.
KELLENBERGER, D. & ALTHAUS, H.-J. 2003. Life Cycle Inventories of Building Products. Final report ecoinvent. EMPA - Swiss Centre for Life Cycle Inventories.
KELLENBERGER, D., ALTHAUS, H.-J., JUNGBLUTH, N., KÜNNIGER, T., LEHMANN, M. & THALMANN, P. 2007. Life Cycle Inventories of Building Products. ecoinvent report No. 7, v2.0. . EMPA Dübendorf, Swiss Centre for Life Cycle Inventories, Dübendorf, CH,.
KHAN, S. U., NURUDDIN, M. F., AYUB, T. & SHAFIQ, N. 2014. Effects of different mineral admixtures on the properties of fresh concrete. *The Scientific World Journal,* 2014.
KIM, Y. Y., LEE, B. J., SARASWATHY, V. & KWON, S. J. 2014. Strength and durability performance of alkali-activated rice husk ash geopolymer mortar. *Scientific World Journal,* 2014.
KOMLJENOVIĆ, M., BAŠČAREVIĆ, Z. & BRADIĆ, V. 2010. Mechanical and microstructural properties of alkali-activated fly ash geopolymers. *Journal of Hazardous Materials,* 181**,** 35-42.
KONG, D. L. Y. & SANJAYAN, J. G. 2010. Effect of elevated temperatures on geopolymer paste, mortar and concrete. *Cement and Concrete Research,* 40**,** 334-339.
KOSTICK, D. S. 2011. Mineral Commodity Summaries 2011 - Soda Ash: U.S. Geological Survey, 198 p.
KULIFFAYOVÁ, M., KRAJČI, L., JANOTKA, I. & ŠMATKO, V. 2012. Thermal behaviour and characterization of cement composites with burnt kaolin sand. *Journal of Thermal Analysis and Calorimetry,* 108**,** 425-432.
KUWAHARA, Y. 2008. In situ observations of muscovite dissolution under alkaline conditions at 25-50 °C by AFM with an air/fluid heater system. *American Mineralogist,* 93**,** 1028-1033.
KWAN, A. K. H., NG, P. L. & HUEN, K. Y. 2014. Effects of fines content on packing density of fine aggregate in concrete. *Construction and Building Materials,* 61**,** 270-277.
LASKAR, A. I. & BHATTACHARJEE, R. 2013. Effect of plasticizer and superplasticizer on rheology of fly-ash-based geopolymer concrete. *ACI Materials Journal,* 110**,** 513-518.
LAVANGARE, V. H., KULKARNI, G. S. & SAWANT, A. B. 2014. Experimental Study of Partial Replacement of Fine Aggregate with Waste Material from China Clay Industries. *International Journal of Research in Engineering and Science* 2**,** 18-22.
LAW, D. W., ADAM, A. A., MOLYNEAUX, T. K., PATNAIKUNI, I. & WARDHONO, A. 2014. Long term durability properties of class F fly ash geopolymer concrete. *Materials and Structures/Materiaux et Constructions,* 48**,** 721-731.

LEEMANN, A. & HOLZER, L. 2005. Alkali-aggregate reaction—identifying reactive silicates in complex aggregates by ESEM observation of dissolution features. *Cement and Concrete Composites,* 27**,** 796-801.

LI, X. 2012. Study on performances of concrete with high content of mica in stone powder. *水力发电学报,* 31**,** 211-215.

LIEW, Y. M., KAMARUDIN, H., MUSTAFA AL BAKRI, A. M., LUQMAN, M., KHAIRUL NIZAR, I. & HEAH, C. Y. 2011. Investigating the possibility of utilization of kaolin and the potential of metakaolin to produce green cement for construction purposes-A review. *Australian Journal of Basic and Applied Sciences,* 5**,** 441-449.

LLOYD, R. R., PROVIS, J. L., SMEATON, K. J. & VAN DEVENTER, J. S. J. 2009. Spatial distribution of pores in fly ash-based inorganic polymer gels visualised by Wood's metal intrusion. *Microporous and Mesoporous Materials,* 126**,** 32-39.

LOTFY, A., KARAHAN, O., OZBAY, E., HOSSAIN, K. M. A. & LACHEMI, M. 2015. Effect of kaolin waste content on the properties of normal-weight concretes. *Construction and Building Materials,* 83**,** 102-107.

MACKENZIE, K. J. D., BROWN, I. W. M., CARDILE, C. M. & MEINHOLD, R. H. 1987. The thermal reactions of muscovite studied by high-resolution solid-state 29-Si and 27-AI NMR. *Journal of Materials Science,* 22**,** 2645-2654.

MACKENZIE, K. J. D., BROWN, I. W. M., MEINHOLD, R. H. & BOWDEN, M. E. 1985a. OUTSTANDING PROBLEMS IN THE KAOLINITE-MULLITE REACTION SEQUENCE INVESTIGATED BY **2**9Si AND **2**7Al SOLID-STATE NUCLEAR MAGNETIC RESONANCE: I, METAKAOLINITE. *Journal of the American Ceramic Society,* 68**,** 293-297.

MACKENZIE, K. J. D., BROWN, I. W. M., MEINHOLD, R. H. & BOWDEN, M. E. 1985b. Thermal Reactions of Pyrophyllite Studied by High-Resolution Solid-state 27Al and 29Si Nuclear Magnetic Resonance Spectroscopy. *Journal of the American Ceramic Society,* 68**,** 266-272.

MACKENZIE, K. J. D., KOMPHANCHAI, S. & VAGANA, R. 2008. Formation of inorganic polymers (geopolymers) from 2:1 layer lattice aluminosilicates. *Journal of the European Ceramic Society,* 28**,** 177-181.

MAIA, A. Á. B., ANGÉLICA, R. S., DE FREITAS NEVES, R., PÖLLMANN, H., STRAUB, C. & SAALWÄCHTER, K. 2014. Use of 29Si and 27Al MAS NMR to study thermal activation of kaolinites from Brazilian Amazon kaolin wastes. *Applied Clay Science,* 87**,** 189-196.

MAIA, A. A. B., ANGÉLICA, R. S. & NEVES, R. F. 2011. Use of industrial kaolin waste from the Brazilian Amazon region for synthesis of zeolite A. *Clay Minerals,* 46**,** 127-136.

MAKANI, A. 2014. Analytical Estimate of the Mechanical Behavior of Rock: Granitic Aggregates. *Arabian Journal for Science and Engineering,* 39**,** 3651-3663.

MARJANOVIĆ, N., KOMLJENOVIĆ, M., BAŠČAREVIĆ, Z., NIKOLIĆ, V. & PETROVIĆ, R. 2015. Physical–mechanical and microstructural properties of alkali-activated fly ash–blast furnace slag blends. *Ceramics International,* 41**,** 1421-1435.

MARSH, B. 2006. One Coleman street - A case study in the use of secondary materials in concrete. *ICT Yearbook 2006-2007* The Institute of concrete technology (ICT), p. 45-55.

MARSH, B. 2007. One Coleman Street - a case study in the use of secondary materials in concrete. *The Structural Engineer, p. 35-37.*

MASSAZZA, F. 2003. 10 - Pozzolana and Pozzolanic Cements. *In:* HEWLETT, P. C. (ed.) *Lea's Chemistry of Cement and Concrete (Fourth Edition).* Oxford: Butterworth-Heinemann.
MAZZUCATO, E., ARTIOLI, G. & GUALTIERI, A. 1999. High temperature dehydroxylation of muscovite-2M1: A kinetic study by in situ XRPD. *Physics and Chemistry of Minerals,* 26**,** 375-381.
MCGUIRE, E. 2012. *Examining the viability of geopolymer concrete. Carbon dioxide emissions and key attributes.* Master of Architecture, The University of Melbourne.
MCKEOWN, D. A., BELL, M. I. & ETZ, E. S. 1999. Vibrational analysis of the dioctahedral mica: 2M1 muscovite. *American Mineralogist,* 84**,** 1041-1048.
MCLELLAN, B. C., WILLIAMS, R. P., LAY, J., VAN RIESSEN, A. & CORDER, G. D. 2011. Costs and carbon emissions for geopolymer pastes in comparison to ordinary portland cement. *Journal of Cleaner Production,* 19**,** 1080-1090.
MEHTA, P. K. 1984. Mineral admixtures. *In:* RAMACHANDRAN, V. S. (ed.) *Concrete Admixtures Handbook.* USA: Noyes Publications.
MEHTA, P. K. 1987. Natural pozzolans. *In:* MALHORTA, V. M. (ed.) *Supplementary Cementing Materials for Concrete. Canadian Government Publishing Center.* Ottawa: Materials for Concrete. Canadian Government Publishing Center.
MEINHOLD, R. H., MACKENZIE, K. J. D. & BROWN, I. W. M. 1985a. Thermal reactions of kaolinite studied by solid state 27-AI and 29-Si NMR. *Journal of materials science letters,* 4**,** 163-166.
MEINHOLD, R. H., MACKENZIE, K. J. D. & BROWN, I. W. M. 1985b. THERMAL REACTIONS OF KAOLINITE STUDIED BY SOLID STATE 27-Al AND 29-Si NMR. *Journal of Materials Science Letters,* 4**,** 163-166.
MELLADO, A., CATALÁN, C., BOUZÓN, N., BORRACHERO, M. V., MONZÓ, J. M. & PAYÁ, J. 2014. Carbon footprint of geopolymeric mortar: Study of the contribution of the alkaline activating solution and assessment of an alternative route. *RSC Advances,* 4**,** 23846-23852.
MENEZES, R., FARIAS, F., OLIVEIRA, M. F., SANTANA, L. N. L., NEVES, G. A., LIRA, H. L. & FERREIRA, H. C. 2009a. Kaolin processing waste applied in the manufacturing of ceramic tiles and mullite bodies. *Waste Management and Research,* 27**,** 78-86.
MENEZES, R. R., BRASILEIRO, M. I., GONÇALVES, W. P., SANTANA, L. N. D. L., NEVES, G. A., FERREIRA, H. S. & FERREIRA, H. C. 2009b. Statistical design for recycling kaolin processing waste in the manufacturing of mullite-based ceramics. *Materials Research,* 12**,** 201-209.
MENEZES, R. R., BRASILEIRO, M. I., SANTANA, L. N. L., NEVES, G. A., LIRA, H. L. & FERREIRA, H. C. 2008a. Utilization of kaolin processing waste for the production of porous ceramic bodies. *Waste Management and Research,* 26**,** 362-368.
MENEZES, R. R., FERREIRA, H. S., NEVES, G. A., LIRA, H. D. L. & FERREIRA, H. C. 2005. Use of granite sawing wastes in the production of ceramic bricks and tiles. *Journal of the European Ceramic Society,* 25**,** 1149-1158.
MENEZES, R. R., NETO, H. G. M., SANTANA, L. N. L., LIRA, H. L., FERREIRA, H. S. & NEVES, G. A. 2008b. Optimization of wastes content in ceramic tiles using statistical design of mixture experiments. *Journal of the European Ceramic Society,* 28**,** 3027-3039.
MINERAL PRODUCTS ASSOCIATION 2013. Learning text Part 05: Brick and block production.

MINERALS ZONE. 2012. *The formation of china clay, Production and Uses* [Online]. Minerals Zone. Available: http://www.mineralszone.com/minerals/china-clay.html [Accessed 15/ 08/ 2012].
MINERALSZONE. 2014. *Mica - Industrial applications* [Online]. Available: http://www.mineralszone.com/minerals/mica.html [Accessed 3 March 2014].
MOHSEN, Q. & MOSTAFA, N. Y. 2010. Investigating the possibility of utilizing low kaolinitic clays in production of geopolymer bricks. *Ceramics - Silikaty,* 54**,** 160-168.
MYERS, R. J., BERNAL, S. A., SAN NICOLAS, R. & PROVIS, J. L. 2013. Generalized Structural Description of Calcium–Sodium Aluminosilicate Hydrate Gels: The Cross-Linked Substituted Tobermorite Model. *Langmuir,* 29**,** 5294–5306.
NAJAFI KANI, E., ALLAHVERDI, A. & PROVIS, J. L. 2012. Efflorescence control in geopolymer binders based on natural pozzolan. *Cement and Concrete Composites,* 34**,** 25-33.
NEMA, M., JAIN, R. & GROVER, R. K. 2014. Use of china clay waste in semi dense bitumenous concrete. *International Journal of Engineering & Science Research,* 4**,** 602-612.
NEMATOLLAHI, B. & SANJAYAN, J. 2014a. Effect of different superplasticizers and activator combinations on workability and strength of fly ash based geopolymer. *Materials and Design,* 57**,** 667-672.
NEMATOLLAHI, B. & SANJAYAN, J. 2014b. Efficacy of available superplasticizers on geopolymers. *Research Journal of Applied Sciences, Engineering and Technology,* 7**,** 1278-1282.
OELKERS, E. H., SCHOTT, J., GAUTHIER, J.-M. & HERRERO-RONCAL, T. 2008. An experimental study of the dissolution mechanism and rates of muscovite. *Geochimica et Cosmochimica Acta,* 72**,** 4948-4961.
OH, J. E., MONTEIRO, P. J. M., JUN, S. S., CHOI, S. & CLARK, S. M. 2010. The evolution of strength and crystalline phases for alkali-activated ground blast furnace slag and fly ash-based geopolymers. *Cement and Concrete Research,* 40**,** 189-196.
OLYMPIC DELIVERY AUTHORITY (ODA) 2009. Sustainable design and construction update. November 2009 ed.
ONS 2014. Mineral extraction in Great Britain 2012. Business Monitor PA1007. London: Office for National Statistics. Department for Communities and Local Government.
PACHECO-TORGAL, F., ABDOLLAHNEJAD, Z., CAMÕES, A. F., JAMSHIDI, M. & DING, Y. 2012. Durability of alkali-activated binders: A clear advantage over Portland cement or an unproven issue? *Construction and Building Materials,* 30**,** 400-405.
PACHECO-TORGAL, F., CASTRO-GOMES, J. & JALALI, S. 2008. Alkali-activated binders: A review: Part 1. Historical background, terminology, reaction mechanisms and hydration products. *Construction and Building Materials,* 22**,** 1305-1314.
PACHECO-TORGAL, F., CASTRO-GOMES, J. & JALALI, S. 2010. Durability and environmental performance of alkali activated tungsten mine waste mud mortars. *J Mater Civ Eng ASCE,* 22**,** 897-904.
PACHECO-TORGAL, F., CASTRO-GOMES, J. P. & JALALI, S. 2008,b. Investigations on mix design of tungsten mine waste geopolymeric binder. *Construction and Building Materials,* 22**,** 1939-1949.

PACHECO-TORGAL, F., CASTRO-GOMES, J. P. & JALALI, S. 2008,d. Investigations of tungsten mine waste geopolymeric binder: Strength and microstructure. *Construction and Building Materials,* 22**,** 2212-2219.
PACHECO-TORGAL, F., LOURENCO, P. B., LABRINCHA, J. A. & KUMAR, S. (eds.) 2014. *Eco-efficient Masonry Bricks and Blocks: Design, Properties and Durability*.
PACHECO-TORGAL, F., MOURA, D., DING, Y. & JALALI, S. 2011. Composition, strength and workability of alkali-activated metakaolin based mortars. *Construction and Building Materials,* 25**,** 3732-3745.
PACHECO-TORGAL, F. C.-G., JOÃO; JALALI, SAID 2008,a. Properties of tungsten mine waste geopolymeric binder. *Construction and Building Materials,* 22**,** 1201-1211.
PACHECO-TORGAL, F. C.-G., JOÃO; JALALI, SAID 2008,c. Investigations about the effect of aggregates on strength and microstructure of geopolymeric mine waste mud binders. *Cement and Concrete Research,* 37**,** 933-941.
PACHECO TORGAL, F., CASTRO-GOMES, J. P. & JALALI, S. Geopolymeric Binder Using Tungsten Mine Waste: Preliminary Investigation. *In:* DAVIDOVITS, J., ed. World Congress Geopolymer 2005, 2005a.
PACHECO TORGAL, F., GOMES, J. P. C. & SAID, J. 2005b. Tratamento térmico das lamas residuais das minas da Panasqueira : influencia do tempo e da temperatura de calcinação. *Conferência Engenharia 2005 – Inovação e Desenvolvimento: actas.* Covilhã: Universidade da Beira Interior.
PALACIOS, M., HOUST, Y. F., BOWEN, P. & PUERTAS, F. 2009. Adsorption of superplasticizer admixtures on alkali-activated slag pastes. *Cement and Concrete Research,* 39**,** 670-677.
PALACIOS, M. & PUERTAS, F. 2004. Stability of superplasticizer and shrinkage-reducing admixtures in high basic media. *Materiales de Construccion,* 54**,** 65-86.
PALACIOS, M. & PUERTAS, F. 2005. Effect of superplasticizer and shrinkage-reducing admixtures on alkali-activated slag pastes and mortars. *Cement and Concrete Research,* 35**,** 1358-1367.
PALACIOS, M. & PUERTAS, F. 2011. Effectiveness of mixing time on hardened properties of waterglass-activated slag pastes and mortars. *ACI Material Journal,* V.108**,** 73-78.
PALOMO, A., GRUTZECK, M. W. & BLANCO, M. T. 1999. Alkali-activated fly ashes: A cement for the future. *Cement and Concrete Research,* 29**,** 1323-1329.
PALOMO, A., MACIAS, A., BLANCO, M. T. & PUERTAS, F. 1992. Physical, chemical and mechanical characterisation of geopolymers. *Proceedings of the Ninth International Congress on the Chemistry of Cement.*
PAN, Q., SHI, C. L. & ZHU, B. 2014. Effect of aminosulphonate based superplasticizer on the properties of slag pastes. *Advanced Materials Research.*
PART, W. K., RAMLI, M. & CHEAH, C. B. 2015. An overview on the influence of various factors on the properties of geopolymer concrete derived from industrial by-products. *Construction and Building Materials,* 77**,** 370-395.
PÉREZ-MAQUEDA, L. A., BLANES, J. M., PASCUAL, J. & PÉREZ-RODRÍGUEZ, J. L. 2004. The influence of sonication on the thermal behavior of muscovite and biotite. *Journal of the European Ceramic Society,* 24**,** 2793-2801.
PÉREZ-RODRÍGUEZ, J. L., PASCUAL, J., FRANCO, F., JIMÉNEZ DE HARO, M. C., DURAN, A., RAMÍREZ DEL VALLE, V. & PÉREZ-MAQUEDA, L. A. 2006. The influence of ultrasound on the thermal behaviour of clay minerals. *Journal of the European Ceramic Society,* 26**,** 747-753.

PHAIR, J. W., VAN DEVENTER, J. S. J. & SMITH, J. D. 2000. Mechanism of polysialation in the incorporation of zirconia into fly ash-based geopolymers. *Industrial and Engineering Chemistry Research,* 39**,** 2925-2934.
PROVIS, J. L. & BERNAL, S. A. 2014. Geopolymers and related alkali-activated materials. *Annual Review of Materials Research.*
PROVIS, J. L., MYERS, R. J., WHITE, C. E., ROSE, V. & VAN DEVENTER, J. S. J. 2012. X-ray microtomography shows pore structure and tortuosity in alkali-activated binders. *Cement and Concrete Research,* 42**,** 855-864.
PROVIS, J. L. & VAN DEVENTER, J. S. J. (eds.) 2014. *Alkali Activated Materials. State-of-the-Art Report, RILEM TC 224-AAM.*
PUERTAS, F., FERNÁNDEZ-JIMÉNEZ, A. & BLANCO-VARELA, M. T. 2004. Pore solution in alkali-activated slag cement pastes. Relation to the composition and structure of calcium silicate hydrate. *Cement and Concrete Research,* 34**,** 139-148.
PUERTAS, F., PALACIOS, M., MANZANO, H., DOLADO, J. S., RICO, A. & RODRIGUEZ, J. C-A-S-H gels formed in alkali-activated slag cement pastes. Structure and effect on cement properties and durability. MATEC Web of Conferences, 2014.
PUERTAS, F., PALACIOS, M. & VÁZQUEZ, T. 2006. Carbonation process of alkali-activated slag mortars. *Journal of Materials Science,* 41**,** 3071-3082.
PUERTAS, F., PALOMO, A., FERNÁNDEZ-JIMÉNEZ, A., IZQUIERDO, J. D. & GRANIZO, M. L. 2003. Effect of superplasticisers on the behaviour and properties of alkaline cements. *Advances in Cement Research,* 15**,** 23-28.
PURNELL, P. & BLACK, L. 2012. Embodied carbon dioxide in concrete: Variation with common mix design parameters. *Cement and Concrete Research,* 42**,** 874-877.
RASHAD, A. M. 2013. Alkali-activated metakaolin: A short guide for civil Engineer-An overview. *Construction and Building Materials,* 41**,** 751-765.
RASHAD, A. M. 2015. Metakaolin: Fresh properties and optimum content for mechanical strength in traditional cementitious materials - A comprehensive overview. *Reviews on Advanced Materials Science,* 40**,** 15-44.
REES, C. A. 2007. *Mechanisms and kinetics of gel formation in geopolymers.*
REN, X., ZHANG, L., RAMEY, D., WATERMAN, B. & ORMSBY, S. 2014. Utilization of aluminum sludge (AS) to enhance mine tailings-based geopolymer. *Journal of Materials Science,* 50**,** 1370-1381.
RICHARDSON, I. G., BROUGH, A. R., BRYDSON, R., GROVES, G. W. & DOBSON, C. M. 1993. Location of Aluminum in Substituted Calcium Silicate Hydrate (C-S-H) Gels as Determined by 29Si and 27Al NMR and EELS. *Journal of the American Ceramic Society,* 76**,** 2285-2288.
RICHARDSON, I. G., BROUGH, A. R., GROVES, G. W. & DOBSON, C. M. 1994. The characterization of hardened alkali-activated blast-furnace slag pastes and the nature of the calcium silicate hydrate (C-S-H) phase. *Cement and Concrete Research,* 24**,** 813-829.
ROCHA, J. & KLINOWSKI, J. 1990. 29Si and 27Al magic-angle-spinning NMR studies of the thermal transformation of kaolinite. *Physics and Chemistry of Minerals,* 17**,** 179-186.
RODRIGUEZ-NAVARRO, C., CULTRONE, G., SANCHEZ-NAVAS, A. & SEBASTIAN, E. 2003. TEM study of mullite growth after muscotive breakdown. *American Mineralogist,* 88**,** 713-724.
SABIR, B. B., WILD, S. & BAI, J. 2001. Metakaolin and calcined clays as pozzolans for concrete: a review. *Cement and Concrete Composites,* 23**,** 441-454.

SÁNCHEZ-SOTO, P. J., DEL CARMEN JIMÉNEZ DE HARO, M., PÉREZ-MAQUEDA, L. A., VARONA, I. & PÉREZ-RODRÍGUEZ, J. L. 2000. Effects of dry grinding on the structural changes of kaolinite powders. *Journal of the American Ceramic Society,* 83**,** 1649-1657.

SCHMITZ, S., PAULINI, I., SIEGFRIED, A., CLAUDIA, M., BUNGE, T., MAHRENHOLZ, P., EGGERS, H.-H., MATTERN, K., FRITZ, K., NEITZEL, H., GEORGI, B., RAUERT, C., GOTTLOB, D., REICHE, J., HENSELING, K.-O., SPRANGER, T., KALMBACH, S., STEINHÄUSER, K., KÖHN, M., SUMMERER, S., LANDGREBE, J., TIEDEMANN, A. & LOHRER, W. 1999. Valuation as an element of life cycle assessments: German Federal Environmental Agency method for impact indicator standardization, impact category grouping (ranking), and interpretation in accordance with ISO 14042 and 14043. Berlin: German Federal Environment Agency.

SCRIVENER, K. & GARTNER, E. 1987. Microstructural gradients in cement paste around aggregate particles. *Mater Res Soc,* 114.

SHAFIQ, N., NURUDDIN, M. F., KHAN, S. U. & AYUB, T. 2015. Calcined kaolin as cement replacing material and its use in high strength concrete. *Construction and Building Materials,* 81**,** 313-323.

SHI, C. 1996. Strength, pore structure and permeability of alkali-activated slag mortars. *Cement and Concrete Research,* 26**,** 1789-1799.

SHI, C. & FERNÁNDEZ-JIMÉNEZ, A. 2006. Stabilization/solidification of hazardous and radioactive wastes with alkali-activated cements. *Journal of Hazardous Materials,* 137**,** 1656-1663.

SHI, C., KRIVENKO, P. V. & ROY, D. 2006. *Alkali-Activated Cements and Concretes,* Taylor & Francis.

SHI, C., WU, Y., RIEFLER, C. & WANG, H. 2005. Characteristics and pozzolanic reactivity of glass powders. *Cement and Concrete Research,* 35**,** 987-993.

SHVARZMAN, A., KOVLER, K., GRADER, G. S. & SHTER, G. E. 2003. The effect of dehydroxylation/amorphization degree on pozzolanic activity of kaolinite. *Cement and Concrete Research,* 33**,** 405-416.

SIDDIQUE, R. & KLAUS, J. 2009. Influence of metakaolin on the properties of mortar and concrete: A review. *Applied Clay Science,* 43**,** 392-400.

SILVA, I., CASTRO-GOMES, J. & ALBUQUERQUE, A. 2010. Evaluation of the stability of waste-based geopolymeric artificial aggregates for wastewater treatment processes under different curing conditions. *Advances in Science and Technology* 69**,** 86-91.

SILVA, I., CASTRO-GOMES, J. P. & ALBUQUERQUE, A. 2012. Effect of immersion in water partially alkali-activated materials obtained of tungsten mine waste mud. *Construction and Building Materials,* 35**,** 117-124.

SIMS, I. & BROWN, B. 2003. 16 - Concrete Aggregates. *In:* HEWLETT, P. C. (ed.) *Lea's Chemistry of Cement and Concrete (Fourth Edition).* Butterworth-Heinemann. Oxford, UK. p. 907-1015.

SLADE, R. C. T. & DAVIES, T. W. 1989. The mechanism of kaolinite dehydroxylation followed by high resolution 27Al and 29Si NMR. *Colloids and Surfaces,* 36**,** 119-125.

SMITH, R. A., SOWERBY, C., KNAPMAN, D., MYALL, D., MAY, J., LEWIS, R., BAMFIELD, B. & FOX-DAVIES, T. 2005. Feasibility of china clay secondary aggregate use.

SOLOMON, S. 2007. Climate Change 2007: the Physical Science Basis: Contribution of Working Group I to the Fourth Assessment Report of the Intergovernamental Panel on Climate Change. Cambridge, UK

SPERINCK, S., RAITERI, P., MARKS, N. & WRIGHT, K. 2011. Dehydroxylation of kaolinite to metakaolin-a molecular dynamics study. *Journal of Materials Chemistry,* 21**,** 2118-2125.

STENGEL, T. R., J.; HEINZ D. 2009. Life cycle assessment of geopolymer concrete - what is the environmental benefit? *Concrete Solutions 09,* Concrete Institute of Australia, Luna Park, Sydney, Australia**,** p. Paper 6a–4.

SUFIAN BADAR, M., KUPWADE-PATIL, K., BERNAL, S. A., PROVIS, J. L. & ALLOUCHE, E. N. 2014. Corrosion of steel bars induced by accelerated carbonation in low and high calcium fly ash geopolymer concretes. *Construction and Building Materials,* 61**,** 79-89.

SUN, P. & WU, H.-C. 2013. Chemical and freeze–thaw resistance of fly ash-based inorganic mortars. *Fuel,* 111**,** 740-745.

SURANA, M. S. & JOSHI, S. N. 1990. Estimating reactivity of pozzolanic materials by a spectrophotometric method. *Advances in Cement Research,* 3**,** 81-83.

TEYCHENNÉ, D. C., FRANKLIN, R. E. & ERNTROY, H. C. 1997. Design of normal concrete mixes. Second Edition ed.: Building Research Establishment (BRE).

THURLOW, C. 2005. *China clay from Cornwall and Devon - The modern china clay industry,* St Austell, UK.

TIRONI, A., TREZZA, M. A., SCIAN, A. N. & IRASSAR, E. F. 2013. Assessment of pozzolanic activity of different calcined clays. *Cement and Concrete Composites,* 37**,** 319-327.

TURNER, L. K. & COLLINS, F. G. 2013. Carbon dioxide equivalent (CO2-e) emissions: A comparison between geopolymer and OPC cement concrete. *Construction and Building Materials,* 43**,** 125-130.

UL HAQ, E., PADMANABHAN, S. K. & LICCIULLI, A. 2014. In-situ carbonation of alkali activated fly ash geopolymer. *Construction and Building Materials,* 66**,** 781-786.

VAN DEVENTER, J., PROVIS, J., DUXSON, P. & BRICE, D. 2010. Chemical Research and Climate Change as Drivers in the Commercial Adoption of Alkali Activated Materials. *Waste and Biomass Valorization,* 1**,** 145-155.

VAN DEVENTER, J. S. J., PROVIS, J. L. & DUXSON, P. 2012. Technical and commercial progress in the adoption of geopolymer cement. *Minerals Engineering,* 29**,** 89-104.

VAN JAARSVELD, J. G. S., VAN DEVENTER, J. S. J. & LORENZEN, L. 1997. The potential use of geopolymeric materials to immobilise toxic metals: Part I. Theory and applications. *Minerals Engineering,* 10**,** 659-669.

VAN JAARSVELD, J. G. S., VAN DEVENTER, J. S. J. & LUKEY, G. C. 2002. The effect of composition and temperature on the properties of fly ash- and kaolinite-based geopolymers. *Chemical Engineering Journal,* 89**,** 63-73.

VAN JAARSVELD, J. G. S., VAN DEVENTER, J. S. J. & SCHWARTZMAN, A. 1999. The potential use of geopolymeric materials to immobilise toxic metals: Part II. Material and leaching characteristics. *Minerals Engineering,* 12**,** 75-91.

VANCE, K., AGUAYO, M., OEY, T., SANT, G. & NEITHALATH, N. 2013. Hydration and strength development in ternary portland cement blends containing limestone and fly ash or metakaolin. *Cement and Concrete Composites,* 39**,** 93-103.

WANG, H., LI, H. & YAN, F. 2005. Synthesis and mechanical properties of metakaolinite-based geopolymer. *Colloids and Surfaces A: Physicochemical and Engineering Aspects,* 268**,** 1-6.
WANG, J. W. & CHENG, T. W. 2003. Production geopolymer materials by coal fly ash. *7th International Symposium on East Asian Resources Recycling Technology*. Tainan, Taiwan.
WANG, Q., LI, N., WU, C. P. & SUI, Z. T. 2009. Research on adaptability of slag-based geopolymer with superplasticizer. *Key Engineering Materials.*
WANG, S.-D., PU, X.-C., SCRIVENER, K. L. & PRATT, P. L. 1995. Alkali-activated slag cement and concrete: a review of properties and problems. *Advances in Cement Research,* 7**,** 93-102.
WANG, S. D. & SCRIVENER, K. L. 1995. Hydration products of alkali activated slag cement. *Cement and Concrete Research,* 25**,** 561-571.
WATANABE, T., SHIMIZU, H., NAGASAWA, K., MASUDA, A. & SAITO, H. 1987. 29Si- and 27Al-MAS/NMR study of the thermal transformations of kaolinite. *Clay Minerals,* 22**,** 37-48.
WEIDEMA, B., HISCHIER, R., ALTHAUS, H.-J., BAUER, C., DOKA, G., DONES, R., FRISCHKNECHT, R., JUNGBLUTH, N., NEMECEK, T., PRIMAS, A. & WERNET, G. 2009. Code of Practice. Ecoinvent report No. 2. St. Gallen: Swiss Centre for Life Cycle Inventories.
WEIL, M. 2009. *Life-cycle analysis of geopolymers. Geopolymers, Structure, Processing, Properties and Applications*.
WEISMANN, A. 2011. *RE: Clayworks.*
WHITE, C. E., PERANDER, L. M., PROVIS, J. L. & VAN DEVENTER, J. S. J. 2011. The use of XANES to clarify issues related to bonding environments in metakaolin: a discussion of the paper S. Sperinck et al., "Dehydroxylation of kaolinite to metakaolin-a molecular dynamics study," J. Mater. Chem., 2011, 21, 2118-2125. *Journal of Materials Chemistry,* 21**,** 7007-7010.
WHITE, C. E., PROVIS, J. L., PROFFEN, T., RILEY, D. P. & VAN DEVENTER, J. S. J. 2010. Density functional modeling of the local structure of kaolinite subjected to thermal dehydroxylation. *Journal of Physical Chemistry A,* 114**,** 4988-4996.
WINNEFELD, F., LEEMANN, A., LUCUK, M., SVOBODA, P. & NEUROTH, M. 2010. Assessment of phase formation in alkali activated low and high calcium fly ashes in building materials. *Construction and Building Materials,* 24**,** 1086-1093.
WRAP. 2004. *Use of china clay sand as fine aggregate in pre-mixed concrete Structural & Non-Structural applications* [Online]. Available: http://aggregain.wrap.org.uk/case_studies/2676_use_of_chin.html [Accessed 16-08-2013].
WRAP. 2012. *China Clay Sand and Stent* [Online]. Available: http://aggregain.wrap.org.uk/specifier/materials/china_clay_sand.html, [Accessed 16/ 08/ 2012].
WU, K.-R., CHEN, B., YAO, W. & ZHANG, D. 2001. Effect of coarse aggregate type on mechanical properties of high-performance concrete. *Cement and Concrete Research,* 31**,** 1421-1425.
WYPYCH, G. 2010. Handbook of Fillers (3rd Edition). ChemTec Publishing.
XING, J. Q., ZHAN, S. L. & LI, X. Y. 2014. Effect of mica content in stone powder of manufactured sand on performance of cement mortar. *Advanced Materials Research.*
XU, H., PROVIS, J. L., VAN DEVENTER, J. S. L. & KRIVENKO, P. V. 2008. Characterization of Aged Slag Concretes. *ACI Material Journal,* 105**,** 131-139.

XU, H. & VAN DEVENTER, J. S. J. 2000. The geopolymerisation of alumino-silicate minerals. *International Journal of Mineral Processing,* 59**,** 247-266.
XU, H. & VAN DEVENTER, J. S. J. 2002. Microstructural characterisation of geopolymers synthesised from kaolinite/stilbite mixtures using XRD, MAS-NMR, SEM/EDX, TEM/EDX, and HREM. *Cement and Concrete Research,* 32**,** 1705-1716.
YANG, K.-H., CHO, A.-R. & SONG, J.-K. 2012a. Effect of water–binder ratio on the mechanical properties of calcium hydroxide-based alkali-activated slag concrete. *Construction and Building Materials,* 29**,** 504-511.
YANG, K. H., JUNG, Y. B., CHO, M. S. & TAE, S. H. 2014. Effect of supplementary cementitious materials on reduction of CO2 emissions from concrete. *Journal of Cleaner Production*.
YANG, K. H., SONG, J. K. & SONG, K. I. 2013. Assessment of CO 2 reduction of alkali-activated concrete. *Journal of Cleaner Production,* 39**,** 265-272.
YANG, T., YAO, X., ZHANG, Z. & WANG, H. 2012b. Mechanical property and structure of alkali-activated fly ash and slag blends. *Journal of Sustainable Cement-Based Materials and Design,* 1**,** 167-178.
ZABALZA BRIBIÁN, I., VALERO CAPILLA, A. & ARANDA USÓN, A. 2011. Life cycle assessment of building materials: Comparative analysis of energy and environmental impacts and evaluation of the eco-efficiency improvement potential. *Building and Environment,* 46**,** 1133-1140.
ZHAN, B. J. & POON, C. S. 2015. Study on feasibility of reutilizing textile effluent sludge for producing concrete blocks. *Journal of Cleaner Production,* 101**,** 174-179.
ZHANG, J. & SCHERER, G. W. 2011. Comparison of methods for arresting hydration of cement. *Cement and Concrete Research,* 41**,** 1024-1036.
ZHANG, Z., WANG, H., ZHU, Y., REID, A., PROVIS, J. L. & BULLEN, F. 2014. Using fly ash to partially substitute metakaolin in geopolymer synthesis. *Applied Clay Science,* 88–89**,** 194-201.
ZHANG, Z. Z. & BAILEY, G. W. 1998a. Reactivity of basal surfaces, steps and edges of muscovite: an AFM study. *Clays and Clay Minerals,* 46**,** 290-300.
ZHANG, Z. Z. & BAILEY, G. W. 1998b. Reactivity of basal surfaces, steps and edges of muscovite; an AFM study. *Clays and Clay Minerals,* 46**,** 290-300.

ANNEX A

A.1. Specification for Coarse Aggregate (Stent 4/10) and Sand (CCS 0/4)

AGGREGATE INDUSTRIES

Moorcroft Laboratory
Moorcroft Quarry
Billacombe
Plymouth
DEVON
PL9 8AT

AGGREGATE PROPERTIES DATA SHEET

Unit :-	LITTLEJOHN
Address :-	Cocksbarrow
	Carthew
	St Austell
	CORNWALL PL26 8XT
Telephone :-	01726 852145

Type of Deposit :-	Igneous
Aggregate Size :-	Coarse Aggregate
Aggregate Type :-	Granite
Aggregate Colour :-	White (generally)
ASR Classification :-	LOW

MECHANICAL/PHYSICAL PROPERTIES	BS Ref.	Result	Frequency	Date of Test	Report No.
Apparent Relative Density	BS EN 1097-6	2.67 Mg/m³	1 / Year	24-Apr-13	STR 318643
S.S.D. Relative Density	BS EN 1097-6	2.61 Mg/m³	1 / Year	24-Apr-13	STR 318643
Oven Dry Relative Density	BS EN 1097-6	2.57 Mg/m³	1 / Year	24-Apr-13	STR 318643
Water Absorption (%)	BS EN 1097-6	1.4%	1 / Year	24-Apr-13	STR 318643
Aggregate Abrasion Value	BS EN 1097-8	4.2	1 / Year	01-Nov-13	STR 345214
Water Soluble Chloride salt Content	BS EN 1744-1	<0.001%	2 Years	12-Nov-12	STR 303044
Water Soluble Sulfate Content SO_4	TRL 447 Test 1	28mg/l	1 / Year	25-Oct-13	STR 345215
Acid Soluble Sulfate Content SO_3	TRL 447 Test 2	<0.01%	1 / Year	25-Oct-13	STR 345216
Total Sulphur Content	BS EN 1744-1	<0.1%	1 / Year	24-Oct-13	STR 345217
Total Potential Sulfate Content	TRL 447 Test 4	<0.03	1 / Year	25-Oct-13	STR 345218
pH Value	BS 1377 : 1990	9.9	1 / Year	23-Oct-13	STR 345219
Calcium Carbonate Content Equivalent	BS EN 196-21: 1989	3.08%	2 Years	13-Nov-12	STR 303045
Carbon Dioxide Content	BS EN 196-21: 1994	1.35%	2 Years	13-Nov-12	STR 303045
Micro Deval Coefficient	BS EN 1097-1	13	2 / year	01-Nov-13	STR 345220
Los Angles Coefficient	BS EN 1097-2	29	2 / year	01-Nov-13	STR 345221
Drying Shrinkage	BS EN 1367-4	0.020%	5 years	01-May-13	STR 318646
Petrographical Examination	BS EN 932-3: 1997	YES	3 Years	09-Nov-12	STR 303043
Alkaline Silica Reaction - ASR		LOW		01-Aug-09	280536-001
Magnesium Sulphate Soundness Value	BS EN 1367-2	17	2 Years	08-Nov-12	STR 303046
Oxidisable Sulfides Content SO_4	TRL 447	<0.01%	1 / Year	25-Oct-13	STR 345222
Loss on Ignition	BS EN 1744-1	2.10%	1 / Year	23-Oct-13	STR 345225
Resistance to Thermal Shock	BS EN 1367-5	1.5	1 / Year	05-Nov-13	STR 345223
Affinity to Bituminous Binders	prEN 12697-11:2000	0%	1 / Year	25-Oct-13	STR 345224
Mass of lightweight contaminators	BS EN 1744-1	N/A	1 / Year		
Polished Stone Value	BS EN 1097-8	64		29-Sep-08	G13939/M38559

Type 1	OMC	BS 812 - 124	7.6%	1 / Year	31-Oct-13	STR 345231
	Max Dry Density	BS 812 - 124	2.18	1 / Year	31-Oct-13	STR 345231
	Plastic Limit	BS 1377 - 2	Non Plastic	1 / Year	28-Oct-13	STR 345232
	Frost Heave	BS 812 -124	8.2mm	1 / Year	05-Nov-13	STR 345229

All tests carried out by UKAS approved Laboratory unless denoted by *.

OTHER INFORMATION :-	
	For Bardon Aggregates

AGGREGATE INDUSTRIES

Moorcroft Laboratory
Moorcroft Quarry
Billacombe
Plymouth
DEVON
PL9 8AT

AGGREGATE PROPERTIES DATA SHEET

Unit :-	LITTLEJOHN
Address :-	Cocksbarrow
	Carthew
	St Austell
	CORNWALL PL26 8XT
Telephone :-	01726 852145

Type of Deposit :-	Igneous
Aggregate Size :-	Fine Aggregate
Aggregate Type :-	Granite
Aggregate Colour :-	White (generally)
ASR Classification :-	LOW

MECHANICAL/PHYSICAL PROPERTIES	BS Ref.	Result	Frequency	Date of Test	Report No.
Apparent Relative Density	BS EN 1097-6	2.68 Mg/m³	1 / Year	17-Oct-13	STR 343020
S.S.D. Relative Density	BS EN 1097-6	2.67 Mg/m³	1 / Year	17-Oct-13	STR 343020
Oven Dry Relative Density	BS EN 1097-6	2.66 Mg/m³	1 / Year	17-Oct-13	STR 343020
Water Absorption (%)	BS EN 1097-6	1.1%	1 / Year	17-Oct-13	STR 343020
Water Soluble Chloride salt Content	BS EN 1744-1	<0.001%	2 Years	11-Oct-13	STR 343033
Water Soluble Sulfate Content SO_4	BS EN 1744-1	<10mg/l	1 / Year	11-Oct-13	STR 343021
Acid Soluble Sulfate Content SO_3	BS EN 1744-1	0.01%	1 / Year	11-Oct-13	STR 343022
Total Sulphur Content	BS 1377 : 1990	<0.1	1 / Year	10-Oct-13	STR 343023
Total Potential Sulfate Content	BS 1377 : 1990	<0.03	1 / Year	11-Oct-13	STR 343024
pH Value	BS 1377 : 1990	9.1	1 / Year	11-Oct-13	STR 343025
Calcium Carbonate Content	BS EN 196-21: 1993	0.96%	2 Years	17-Oct-13	STR 343034
Carbon Dioxide Content	BS EN 196-21: 1994	0.42%	2 Years	17-Oct-13	STR 343034
Mean Organic Content	BS 1377 : 1990	N/A	N/A		
Drying Shrinkage	BS EN 1367-4		5 Years		
Petrographical Examination	BS EN 932-3: 1997	YES	3 Years	09-Nov-12	STR 303043
Alkaline Silica Reaction - ASR		LOW		01-Aug-09	280536-001
Methylene Blue (MB) Value	BS EN 933-9	0.50g/kg	2 / Year	09-Oct-13	STR 343028
Sand Equivalent (SE) Value	BS EN 933-8	78.0	2 / Year	15-Oct-13	STR 343029
Oxidisable Sulfides Content SO_4	TRL 447	<0.01%	1 / Year	11-Oct-13	STR 343026
Neutralizing Value			1 / Year		
Loss on Ignition	BS EN 1744-1	1.60%	1 / Year	09-Oct-13	STR 343027
Mass of lightweight contaminators	BS EN 1744-1	<0.1%	1 / Year	09-Oct-13	STR 343030
Humus Content	BS EN 1744-1	Negative Test	1 / Year	09-Oct-13	STR 343031
Relative Strengh of aggregate mortar	BS EN 1744-1	100%	1 / Year	07-Nov-13	STR 343032
Change in stiffening time	BS EN 1744-1	0	1 / Year	07-Nov-13	STR 343032

OTHER INFORMATION :-

For Bardon Aggregates

A.2. Related to section 4.2

- ***Calculations for design according to Pacheco-Torgal et al (2008,d)***

  Based on the material that Pacheco et al, 2008 used, the activator has the following breakdown:

71.43g of Na_2SiO_3 solution (*) is: (*) 8.6% Na_2O, 27.8% SiO_2, 0.4% Al_2O_3, 63.2% H_2O.	6.14 g Na_2O 19.86 g SiO_2 0.29 g Al_2O_3 45.14 g H_2O
And 28.57g NaOH solution of 24M(*) is: (*)24M=24mol NaOH in 1L =24mol* molecular weight of NaOH (=40g/mol) =960g NaOH in 1L of solution In the lab 96g of NaOH were dissolved till the volume of a beaker would be filled up to 100ml. It was shown that 100ml of solution= 158g of solution = 96g of NaOH+ 62g H_2O. However in such a concentrated solution the full dissolution of NaOH was not achieved.	Approx. 13.45 g Na_2O 15.12 g H_2O
Therefore the activator as overall has:	19.59 g Na_2O 19.86 g SiO_2 60.26 g H_2O 0.29 g Al_2O_3

That shows that the activator had 19.59g Na_2O and molar ratio of SiO_2/Na_2O= (19.89/ 60.083)/ (19.59/ 61.9786)= 1.05.
Therefore for their mix: W_t/B = 60.36/(19.59+19.86+0.29+100) = 0.43

- ***Calculations for design according to Davidovits, 2011.***

Assuming that all the calcined mica concentrate is amorphous, the amount of SiO_2 and Al_2O_3 that would be expected to participate in the reactions is (based on the XRF analysis, Table 10):

	Weight in 100g of mica concentrate (in g)	Reactive material in calcined mica concentrate (in g) (contains % of the LOI)	Molecular weight (g/mol) *	Reactive material in calcined mica concentrate (in mol)
SiO_2	51.59	46.66	60.08	0.777
Al_2O_3	30.80	33.23	101.96	0.326

*Atomic weight of Al=26.9815, Si=28.085, O=15.999 u (1u equivalent to 1g/mol).

Based on that an example of formulating a mix of calc. mica concentrate as if it was MK is given. The outcome numbers here are not displayed in tables in order to describe the breakdown of calculations. Calculations like the following take place later for the formulation of the binders but the composition of the binders will be presented in tables, skipping presenting the calculations related to chemistry which were preceded. Therefore it is good to see for once the chemistry analytically.

The molecular weights of the chemical formulas of interest are necessary:

Na_2O	61.979g/mol
NaOH	39.9968g/mol
H_2O	18.015 g/mol

If in a mix of 100g precursor (calc. mica concentrate) the overall molar ratios needed for the mix was Na_2O/SiO_2=0.28, SiO_2/Al_2O_3=4, H_2O/Na_2O=17, then the amount of NaOH and Na_2SiO_3 needed would be:

SiO_2/Al_2O_3=4 → $(SiO_{2\ in\ activator})/Al_2O_3$= 4-0.777/0.326= 1.62 → $SiO_{2\ in\ activator}$= 1.62*0.326=0.527mol or 0.527mol*60.08g/mol= 31.67g

The purchased Na_2SiO_3 (solid) has 53.5% SiO_2 , 27.05% Na_2O and 19.45% H_2O.
It takes: 31.67g/53.5%= 59.2g of Na_2SiO_3 to have the required 31.67g of SiO_2 in the activator.

Out of that: 27.05%*59.2g= 16.01g or (16.01g)/(61.979g/mol)= 0.26mol is Na_2O.
So far the molar Na_2O/SiO_2=0.26/(0.527+0.777)= 0.199 and needs to be increased to reach the required 0.28. That will happen by adding NaOH. The amount of Na_2O needed from NaOH is: (0.527+0.777)*0.28-0.26= 0.1067mol

According to the balance equation $Na_2O+H_2O \rightarrow 2NaOH$:
0.1067mol of Na_2O= 2*0.1067mol NaOH= 0.2134mol or 0.2134mol*39.997g/mol= 8.5g NaOH

H_2O/Na_2O=17 → H_2O= 17*(0.26+0.1067)= 6.234mol or 6.234mol*18.015 g/mol=112.3g. In practice, that amount of water (which corresponds to 100g of precursor) might be too much and result in a quite watery binder.

For this mix the molar ratio of Na_2O/Al_2O_3= (0.26+0.1067)/ 0.326= 1.12 and total mass of alkali would is Na_2O= (0.26+0.1067)mol*61.979g/mol= 22.7g.

The calculations end up in very high content of alkali, even greater than the amount of Na_2O that Pacheco-Torgal et al (2008,d) used. Even if the mix had Na_2O/SiO_2=0.28 and SiO_2/Al_2O_3=3.5, we would need 40.9g of Na_2SiO_3 and 11.3g of NaOH. From these two components alone we get:

53.5%*40.9=21.88g or 21.88g/(60.08g/mol)= 0.36mol of SiO_2
27.05%*40.9+77.48%*11.3= 19.82g or 19.82g/(61.979g/mol)= 0.32mol of Na_2O
19.45%*40.9+22.52%*11.3=10.50g or 10.50/(18.015 g/mol)= 0.58mol of H_2O,

where the SiO_2 and Na_2O content is similar to Pacheco-Torgal et al (2008,d). (77.48% is the Na_2O in NaOH. It is calculated from their molecular weights as: 61.979/(2*39.9968) and 22.52% is the rest in the NaOH molecule, the H_2O)

However, as mentioned before, it is arbitrary to consider reactive all the SiO_2 and Al_2O_3 in the calcined mica concentrate since the XRD does not indicate equivalent amount of amorphous material as in metakaolin

A.3. Tables of calculation for particle size distribution of the concrete mixes

(Related to Figure 92)

Sieve (mm)	Material passing (%)			
	MW	CCS	Stent	For concrete mixes (mix D) (*)
14	100.00	100.00	100.00	100.00
12.5	100.00	100.00	99.90	99.93
10	100.00	100.00	91.70	94.36
8	100.00	100.00	66.00	76.88
6.3	100.00	100.00	36.80	57.02
5	100.00	98.50	14.90	41.89
4	100.00	94.40	7.00	35.86
2.8	100.00	86.40	4.80	33.09
2	100.00	78.60	4.30	31.50
1	100.00	61.40	3.50	28.20
0.5	92.65	41.70	1.65	22.62
0.25	35.50	17.60	0.00	8.50
0.125	12.20	5.10	0.00	2.77
0.075	5.80	2.80	0.00	1.38
0.058	3.96	0.00	0.00	0.63
0.043	2.38	0.00	0.00	0.38
0.032	1.58	0.00	0.00	0.25
0.023	1.58	0.00	0.00	0.00
0.017	0.79	0.00	0.00	0.00
0.009	0.79	0.00	0.00	0.00
0.005	0.79	0.00	0.00	0.00
0.003	0.00	0.00	0.00	0.00

(*) Calculated as [0.68*(stent passing)+0.16*(CCS passing)+0.16*(MW passing)]

Sieve (mm)	Material passing (%)			
	NS2	NS1	NS	For concrete mixes (mix A) (**)
12.5	100.00			100.00
10	85.69			90.27
8	56.59			70.48
6.3	18.54	100.00		44.61
4	3.47	92.45		33.15
2	2.08	69.65		28.56
1	1.72	49.13	100.00	25.03
0.5		20.25	93.05	18.13
0.25		6.77	30.27	5.93
0.125		1.75	3.87	0.90
0.075	0.80	0.27	0.55	0.13
0.058	0.00	0.11	0.00	0.02
0.043	0.00	0.00	0.00	0.00

(**) Calculated as [0.68*(NS2 passing)+0.16*(NS1 passing)+0.16*(NS passing)]

A.4. Tables of mortar mixes in kg/m^3

		Composition (in kg/m^3)					
	Mortar mix	GGBS (for the GGBS series) or FA (for the FA series) or GGBS+FA (for the 50/50)	W added+Extra water	Na_2SiO_3 powder	NaOH pellets	Aggregate	Binder
GGBS series	SS/ S1	472.0	228.9	19.4	23.6	1517.6	505.9
	SS/ S2	460.2	226.0	41.9	15.2	1517.3	505.7
	SS/ S3	452.3	223.4	51.1	11.3	1506.7	502.3
	CCS/ S3	423.9	270.4	47.9	10.6	1411.9	470.7
	MW/ S3	449.9	312.2	50.8	11.2	1149.0	499.6
	GSS/ S3	453.1	289.1	51.2	11.3	1308.1	503.1
	SS / S4	455.8	226.5	62.0	7.7	1535.2	511.7
FA series	SS / FA5	458.2	135.6	15.1	48.1	1523.0	507.6
	SS / FA6	450.3	127.9	32.9	41.0	1525.6	508.5
	SS / FA7	447.9	122.3	73.0	26.4	1581.5	527.2
	CCS/ FA7	409.4	223.5	66.7	24.2	1445.6	481.9
	MW/ FA7	426.9	257.4	69.6	25.2	1155.6	502.4
	GSS/ FA7	(*)					
	SS / FA8	435.6	101.9	88.9	19.6	1567.2	522.3
	SS / FA9	not mixed					
50/50 series	SS / Mix 10	467.9	208.2	31.8	19.2	1525.2	508.3
	SS / Mix 11	462.3	205.7	42.1	15.3	1524.2	508.0
	CCS/ Mix 11	434.1	249.6	39.5	14.3	1431.1	477.0
	MW / Mix 11	442.8	278.5	40.3	14.6	1119.0	486.6
	SS / Mix 12	458.5	206.3	51.8	11.5	1527.2	509.1
	SS / Mix 13	451.5	203.6	42.9	25.7	1517.9	506.0
	SS / Mix 14	444.5	201.8	56.4	20.4	1517.4	505.8
	SS / Mix 15	438.8	201.0	69.8	15.4	1520.9	506.9

(*) No data of volume (therefore the conversion from grams to kg/m^3 cannot be done)

A.5. Checks of stoichiometry

According to the ideal composition of minerals noted in Table 5, their main oxide composition is:

	Al_2O_3	SiO_2	K_2O	FeO
Muscovite $KAl_2(Si_3Al)O_{10}(F,OH)_2$	38.4%	45.2%	11.8%	
Quartz SiO_2		100.0%		
Kaolinite $Al_2Si_2O_5(OH)_4$	39.5%	46.6%		
Orthoclase $KAlSi_3O_8$	18.3%	64.8%	16.9%	
Schorl $NaFe^{2+}{}_3Al_6(BO_3)_3Si_6O_{18}(OH)_4$	29.0%	34.2%		20.5%

According to Table 8, the TMWM has 16.66% Al_2O_3, 53.48% SiO_2 and 7.65% K_2O. The TMWM was stated to contain muscovite and quartz, without mentioning any impurities. Assuming that muscovite is the only Al-containing phase in TMWM:

- The contained muscovite in TMWM is:

  $100\% \frac{16.66\%}{38.4\%} = 43.4\%$

  It should be noted that if the check is conducted using K_2O, instead of Al_2O_3, muscovite is 64.8%. However, in that case the Al in the TMWM is not enough. Therefore, muscovite is 43.4% (and there are probably impurities).

- The contained quartz is:

  53.5% − (43.4% x 45.2%) = 33.9%

- There is an amount of remaining phases: 100% − (43.4% + 33.9%) = 22.7%

According to Table 9, mica concentrate contains 17% kaolinite, 74% mica and 9% quartz. Assuming mica to be entirely muscovite:

- 74% muscovite is: 74% x 38.4% = 28.42% Al_2O_3
  And, 74% x 45.2% = 33.45% SiO_2 and 74% x 11.8% = 8.74% K_2O.
- 17% kaolinite adds: 17% x 39.5% = 6.7% Al_2O_3 and 7.9% SiO_2.
- 9% quartz: 9% SiO_2.

In total, the calculation shows:

- 35.12% Al_2O_3 (=28.42%+6.7%)

- 50.34% SiO_2 (=33.45%+7.9%+9%), which are values close to the values in Table 10 for mica concentrate.

Using the same process, the MW was calculated to comprise 13.84% Al_2O_3 and 75.80% SiO_2, again close to the values in Table 10 for MW.

Published papers

(1) ZOGRAFOU, A., HEATH, A. & WALKER, P. 2014. China clay waste as aggregate in AA cement mortars. Proceedings of the ICE - Construction Materials, 1-11.

(2) ZOGRAFOU, A., HEATH, A. & WALKER, P. 2015. Reuse of Waste from the South West of England in Alkali-Activated Cement Concrete. Key Engineering Materials, 629-630, 449-454.